Modulation of myocardial creatine transporter levels and the effects of gene regulation and post-translational modification on its function

Liam M. Sebag-Montefiore

BSc (Hons)

A thesis submitted in partial fulfilment of the requirements for the degree of Doctor of Philosophy

Hilary 2012

Christ Church

Department of Cardiovascular Medicine

Wellcome Trust Centre for Human Genetics

University of Oxford

Declaration of own work

This D.Phil. thesis is entirely my own work unless otherwise indicated. It has not been submitted, either wholly or substantially, for another degree of this University, or for a degree at any other institution. Any assistance from colleagues or collaborators has been appropriately acknowledged.

Abstract

Heart failure (HF) is a common, disabling and deadly condition that causes high rates of morbidity and mortality worldwide. It is widely recognised that the failing heart is energy-starved, and that restoring energy homeostasis is a promising approach towards improving cardiac output. This thesis aims to address the role of energetics in the failing heart, by focussing on modulation of the creatine transporter (CrT). Creatine (Cr), together with the phosphocreatine shuttle, plays a vital role in maintaining energy supplies via ATP in times of high energy demand. Key to the regulation of intracellular [Cr] is the CrT, a Na^+ and Cl^- - dependent membrane transporter. Previous CrT genetic mouse models include a knockout model, found to still express cardiac CrT, and a cardiac-specific CrT overexpressing (OE) model with large variations in myocardial [Cr] between animals and Cr levels high enough to cause spontaneous hypertrophy. To overcome the shortfalls of this CrT-OE model, a novel *in vivo* model of temporal inducible expression of CrT is described, using a cardiac-specific tetracycline inducible (Tet-On) system. Ten transgenic lines (RCT) were created with a construct containing the *CrT*-HA (*CrT* cDNA with an haemagglutinin epitope tag), following successful doxycyline-inducibility *in vitro*. Eight lines showed germline transmission, with LV CrT OE achieved in an individual mouse that displayed double LV [Cr] compared to WT. Issues with the inducer line (rtTA) were ruled out by its use in the creation of a luciferase overexpressing mouse line; all mice tested demonstrated LV luciferase expression in response to doxycycline feeding. The failure to overexpress CrT could be attributed to position or copy number dependent suppression, or to position effect variegation in the case of the single OE mouse obtained.

Subsequent work focussed on regulatory pathways *in vitro* in a cell line of mouse fibroblasts stably overexpressing CrT-HA. Post-translational modifications (PTMs) had been previously suggested to regulate CrT activity. Two *N*-linked glycosylation sites exist, in addition to the putative phosphorylation sites. Inhibition of glycosylation by tunicamycin led to decreased CrT activity, reflected by decreased Cr uptake capacity. Strategies to confirm the presence of phosphorylation were employed, including isolation of CrT-HA by immunoprecipitation and subsequent LC-MS / MS analysis to identify PTMs. Although the presence of CrT was confirmed in 5 different sized species- one previously unreported- inadequate sequence coverage prevented identification of any PTM sites. Tyrosine phosphorylation was not detected using a phosphospecific antibody on immunopurified CrT-HA.

Candidate signalling pathways *in vitro* were then investigated to elucidate CrT regulation, namely the IGF-1R signalling pathway. This study included a cardiomyocyte-like mouse cell line (HL-1) in addition to 3T3-CrT-HA. Exposure of cells to extracellular insulin, growth hormone and IGF-1 led to increased Cr uptake of 125% - 300% of normal. Pharmacological inhibition of the downstream kinases PKA and PKC reduced the effect of insulin and GH, while PMA, sapintoxin (STX) and Gö 6976 induced CrT activity. The mammalian target of rapamycin (mTOR) is also a candidate regulator of CrT, as incubation with rapamycin decreased Cr uptake in 3T3-CrT-HA.

Finally, a targeted approach on transcription factors in the 5'UTR region of mouse CrT identified HEY1 as a highly conserved site. In siRNA experiments, HEY1 was found to exert a mild effect on CrT activity, suggesting that regulation at the transcriptional level merits further investigation. Together, this work has provided novel insights into the modulation of CrT *in vitro*, identifying molecular and pharmacological targets in a known therapeutic signalling pathway. Further work could potentially develop these findings by identifying candidate compounds that would increase CrT activity, potentially in a tissue-specific manner.

Acknowledgements

This section has been surprisingly difficult to complete. Having finished the rest of the thesis, I thought that acknowledgements would be very straightforward, but I was wrong, owing to the huge number of people deserving thanks. Therefore, please accept my apologies if I have omitted to mention anyone who should have been included.

Thanks must first go to Professor Stefan Neubauer, as well as the Department of Cardiovascular Medicine and Professor Hugh Watkins, for providing me with this opportunity. My time in the Neubauer Group has been an enjoyable one. Professor Neubauer, along with Sevasti Zervou, have been exceptionally supportive supervisors, for which I am extremely grateful. Thanks particularly to Sevi for providing so much help throughout with correcting drafts. Additionally, Craig Lygate has been generous with taking time to proof-read this thesis, and facilitating my time away from other lab duties when necessary for writing-up. Kimmo Makinen deserves a special mention too, for his help and enthusiasm in the 'early days', which along with Imre Hunyor, made the lab an exciting place to be. That certainly did not change following their departure, and thanks must go to everyone else in the Group who has had to tolerate me on a daily basis for a very long time. The long-suffering Phil, unfortunate enough to have to sit directly opposite me in the lab, has found himself in the firing-line of bad humour and nonsensical comments on a regular basis. To his credit, he has tolerated me, and provided much support throughout his time here. Tanmoy has also been extremely helpful and supportive throughout his time in the lab, and has kept me in order with threats of physical violence when appropriate. Debra, despite her reputation, has not 'decked' me yet, even though I have tried my hardest to provoke her with rudeness and bad jokes. Thank you for sparing me (and for helping with aspects of the work that I was less than keen on!). Thanks also to Kiterie, for various help and support, and also taking repeated 'Allo 'Allo-style jokes so well. Finally, to Dunja, for stimulating political conversations, and a recently discovered mutual love of the art of HPLC. Outside the Neubauer lab, lab manager James Brown has gone beyond the call of duty, helping with too many things to mention. Thanks also to Phil Townsend, Richard Wade-Martins, and Barbara Casadei. Ben Davies very kindly gave his time to review part of the thesis, as well as providing a professional transgenics service throughout the project. Great thanks must also go to Richard Copley, and Benedikt Kessler for their invaluable input.

It goes without saying that without my family, none of this would have been possible, including those who are unfortunately no longer with us. My parents have been wonderful. Even though they are so far away, I feel that I have had more love and support from them than many who live closer together would have received. This is despite extremely difficult circumstances. My regret is that I haven't been able to visit more often over the past few years. Needless to say, that will be changing. My grandparents have also been wonderful, and are still there for me through difficult times (even though they really deserve a rest!). The same goes for my in-laws, who have always managed to make me smile.

Finally, to my wife Justina, my son Reuben, and the little girl we have yet to meet. Without your unstinting love and support, there is simply no way I that I could have managed throughout this period. I am so grateful, and so lucky to have you. I can't tell you how much I am looking forward to spending more time together. That said, I feel quite a backlog of housework beckoning.

Table of contents

Declaration of own work 2
Abstract 3
Acknowledgements 4
Table of contents 5
List of Figures 12
List of tables 15
Abbreviations 16
Chapter 1 Introduction 20
1.1.Creatine and the Creatine Transporter 20
1.1.1. Creatine and creatine metabolism 20
1.1.2. Biosynthesis of creatine 20
1.1.3. Degradation of creatine 21
1.1.4. Cellular creatine uptake and the Creatine Transporter 22
1.1.5. The *CrT* gene 23
1.1.6. Expression of *CrT* 24
1.1.7. The CrT, a saturable Na^+ and Cl^- -dependent membrane protein 25
1.1.8. Putative structure of the CrT 27
1.1.9. CrT isoforms 29
1.1.10. CrT regulation and expression during development 30
1.1.11 CrT regulation by post-translational modification 31
1.2. The role of creatine in myocardial energetics and the phosphotransfer systems- synthesis of high-energy phosphates 31
1.2.1. Adenosine triphosphate 31
1.2.2. Hydrolysis of ATP and $\Delta G_{\sim ATP}$ 32
1.2.3. Creatine kinase and the creatine kinase reaction 33
1.2.4. The phosphocreatine shuttle 34
1.2.5. Adenylate kinase 36
1.3. Heart failure 37
1.4. The role of energetics in heart failure 38
1.5. Models of altered cardiac phosphotransfer 40
1.5.1. Creatine transporter overexpression (CrT-OE) model 41
1.5.2. CrT knockout model 48
1.5.3. β-GPA models of chronic creatine depletion 48
1.5.4. Loss-of-function models targeting the synthesis of creatine 49
1.5.4.1. GAMT knockout 49

1.5.4.2. AGAT knockout 50
1.5.5. Other models targeting cardiac phosphotransfer 50
1.5.5.1. Creatine kinase-deficient mice 50
1.6. Research aims and objectives 51
Chapter 2. General Materials and Methods 54
2.1. Introduction 54
2.1.1. Software 54
2.1.2. Chemical suppliers 54
2.2. Cell culture, cell lines and transfections 55
2.2.1. Cell lines 55
2.2.1.1. NIH 3T3 Tet-Off 55
2.2.1.2. 3T3-CrT-HA 55
2.2.1.3. HEK293T 55
2.2.1.4. HL-1 Cardiomyocytes 55
2.2.2. General maintenance of cell lines 55
2.2.2.1. NIH 3T3 Tet-off, 3T3-CrT-HA and HEK293T cells 55
2.2.2.2. HL-1 cardiomyocytes 56
2.2.3. Transient cell transfections 57
2.2.4. Stable cell transfections 57
2.2.5. RNA isolation from adherent cells *in vitro* 58
2.2.6. Storage of cells 58
2.2.7. Seeding 6- and 24-well tissue culture plates for creatine uptake assays and transfections 58
2.3 Radiolabelled-creatine uptake assays 59
2.4 Immunofluorescence microscopy and immunocytochemistry 60
2.5 Animal tissues 60
2.5.1. Mice 60
2.5.2 Harvesting of cardiac tissue 61
2.5.3.Nucleic acid extraction 61
2.5.3.1.Purification of genomic mouse DNA from ear biopsy 61
2.5.3.2.Purification of genomic mouse DNA from tail biopsy 62
2.5.3.3.RNA isolation from animal tissue 62
2.6. Polymerase chain Reaction (PCR) 63
2.6.1. Real-time quantitative PCR (qRT-PCR) 63
2.6.1.1. One-step qRT-PCR 63
2.6.1.2. Quantification of qRT-PCR results 63
2.6.2. Polymerase Chain Reaction (PCR) of genomic or plasmid DNA 63
2.6.2.1. PCR primers and probes 64
2.7 Southern gel preparation 65

2.7.1. Southern hybridisation 66
2.8 DNA Manipulation and Molecular Cloning 67
2.8.1 Plasmid DNA 67
2.8.2 Small-scale preparation of plasmid DNA (Miniprep) 67
2.8.3. Restriction endonuclease digestion 68
2.8.4. DNA agarose gel electrophoresis 68
2.8.5. Purification of DNA from agarose gels 68
2.8.6. Phenol:chloroform extraction method and ethanol precipitation of DNA 69
2.8.7. Linearising DNA vectors prior to ligation and cloning 69
2.8.8. Ligation of DNA fragments 70
2.8.9. Large-scale production of plasmid DNA (Maxiprep) 70
2.8.10. DNA Sequencing 70
2.9. Protein expression studies 71
2.9.1. Protein extraction from cell lines and mouse tissue 71
2.9.1.1. Determination of protein concentration 72
2.9.2. SDS polyacrylamide gel electrophoresis (SDS-PAGE) 72
2.9.3. Immunoblotting 72
2.10. Biochemical measurements 73
2.10.1. HPLC determination of creatine levels 73
Chapter 3. Cardiac-specific overexpression of the Creatine Transporter *in vivo*.. Generation of an inducible ..... murine model… 74
3.1. Introduction 74
3.1.1. Limitations of existing models of Creatine Transporter overexpression 75
3.1.2. The Cre/*lox*P system for conditional knockouts 77
3.1.3. The tetracycline-inducible system 78
3.1.4. Potential unwanted effects of the doxycycline and the tetracycline-inducible system in the heart 79
3.1.5. Tet-off system 80
3.1.6. Tet-on system 80
3.1.7. ‘Leakiness’ in the tetracycline system 81
3.1.8. The use of insulating elements in transgenes 82
3.1.9. α-MHC driven rtTA expression in the heart 83
3.1.10. Transgene design rationale 84
3.1.11. Summary of experimental aims 85
3.2 Methods and Results 86
3.2.1. Acquisition of the CrT cDNA clone 86
3.2.2. pWTT1, a vector containing a tetracycline-response element and H19 insulator elements 86
3.2.3. Construction of pWTT1-CrT-myc, an H19 insulator-flanked transgene with a C-terminal c-myc epitope tag 87

3.2.4. Construction of pWTT1-CrT-HA, an H19 insulator-flanked transgene with a C-terminal haemagglutinin (HA) epitope tag 88
3.2.5. Construct validation- expression of pWTT1-CrT-myc and pWTT1-CrT-HA in 3T3-Tet-Off fibroblasts 92
3.2.5.1. Transfection optimisation 93
3.2.5.2. Stable line generation 93
3.2.6. Construct validation- immunocytochemistry 95
3.2.6.1. Autofluorescence in LV tissue 96
3.2.7. Construct validation- CrT mRNA expression 98
3.2.8. Construct validation- CrT activity *in vitro*. Cr uptake experiments 99
3.2.9. Generation of Creatine Transporter Responder (RCT) founder mice 101
3.2.10. Genotyping of RCT mice 102
3.2.11. Southern blot 102
3.2.12. α-MHC-rtTA (Opt rtTA) mice 103
3.2.12.1. Determination of zygosity of rtTA mice using qPCR 104
3.2.13. Breeding strategy 105
3.2.14. Induction of CrT-HA expression with dox-feeding 107
3.2.15. Opt rtTA mRNA is detectable in left ventricular tissue 108
3.2.16. *CrT* mRNA is elevated in some, but not all left ventricular ICT tissue 109
3.2.17. rtTA is undetectable in left ventricular tissue 110
3.2.18. CrT-HA is detectable in some, but not all left ventricular tissue 110
3.2.19. With one exception, myocardial creatine levels are not elevated in dox-fed ICT mice 111
3.2.20. Validation of the rtTA inducer line: Creation of a double-transgenic tet-on luciferase responder mouse line 113
3.2.21. Optimisation of the luciferase assay 114
3.2.22. Luciferase expression is driven by the rtTA inducer line 115
3.3. Discussion 117
3.3.1. *In vitro* validation of the constructs 118
3.3.2. Generation of transgenic mice 119
3.3.3. Choice of the Opt rtTA inducer line 120
3.3.4. Generation of a double transgenic luciferase reporter line 121
3.3.5. Explanations for the lack of CrT-HA expression in ICT mice 121
3.4. Summary and future directions 122
Chapter 4. Regulation of the Creatine Transporter via the IGF-1 pathway 124
4.1. Introduction 124
4.1.1. Regulation of the CrT 124
4.1.2. CrT regulation by substrate 124
4.1.3. The IGF-1 signalling pathway as a regulator of Cr transport 127
4.1.3.1. The regulatory role of insulin 127

4.1.3.2. Growth hormone 130
4.1.3.3. IGF-1 130
4.1.4. Regulation of CrT via PKA and PKC phosphorylation 131
4.1.5. Rapamycin and mTOR, and the influence of AMPK 131
4.1.6. Summary 133
4.2. Results 134
4.2.1. Kinetics of Cr uptake 134
4.2.2. Specificity of Cr uptake. 134
4.2.3. The effect of insulin on IGF-1R and creatine uptake 135
4.2.3.1. 3T3-CrT-HA cells 135
4.2.3.2. HL-1 cells 138
4.2.4. The effect of growth hormone on IGF-1R and creatine uptake 139
4.2.4.1. 3T3-CrT-HA cells 139
4.2.4.2. HL-1 cells 141
4.2.5. The effect of IGF-1 on creatine uptake 141
4.2.6. The effects of picropodophyllin (PPP) inhibition of the IGF-1 receptor (IGF-1R) on creatine uptake in HL-1 cells 143
4.2.7. The effect of PKA and PKC inhibition on creatine uptake following IGF-1R stimulation with insulin and GH 144
4.2.7.1. PKA inhibition with H89 following IGF-1R stimulation with insulin 145
4.2.7.2. PKC inhibition with BIM following IGF-1R stimulation with insulin 145
4.2.7.3. PKA inhibition following IGF-1R stimulation with GH 146
4.2.7.4. PKC inhibition following IGF-1R stimulation with GH 147
4.2.8. The effects of PKA and PKC inhibition on CrT without prior stimulation via IGF-1R 148
4.2.8.1. H89 149
4.2.8.2. Bisindolymaleimide 149
4.2.9. PKC stimulation with PMA and STX and phosphatase inhibition with a high concentration of the PKC inhibitor Gö 6976 151
4.2.10. Effects of compounds on cell viability- Trypan Blue exclusion tests 152
4.2.11. Rapamycin and the effect of the mTOR pathway on creatine uptake 153
4.2.12. Regulation of CrT mRNA levels in vitro 154
4.3. Discussion 156
4.3.1. The choice of cell types for *in vitro* CrT regulation assays 157
4.3.2. Insulin and its effect on Cr uptake 157
4.3.3. Growth hormone 159
4.3.4. IGF-1 160
4.3.5. Picropodophyllin (PPP) - mediated inhibition of IGF-1R 160
4.3.6. Regulation of Cr uptake via PKA and PKC 161
4.3.7. Effects of PKA and PKC inhibiton on the IGF-1 pathway 163

4.3.8. Rapamycin and mTOR....164
4.3.9. Conclusions....164
Chapter 5. Post-translational modification of the Creatine Transporter....166
5.1. Introduction....166
5.1.1. Post-translational modification and regulation of the CrT....166
5.1.2. *N*-linked glycosylation of the CrT....167
5.1.3. Phosphorylation of the CrT....169
5.2. Aims....173
5.3. Materials and Methods....174
5.3.1. Large scale immunoprecipitation....174
5.3.2. Silver staining....175
5.4. Results....175
5.4.1. The choice of cell type for characterisation of CrT post-translational modifications (PTMs)....175
5.4.2. Inhibition of *N*-linked glycosylation of the CrT....177
5.4.2.1. *In vitro* inhibition of *N*-linked glycosylation using tunicamycin....178
5.4.3. The effects of tunicamycin on Cr uptake....179
5.4.3.1. Tunicamycin and cell viability....180
5.4.4. Phosphorylation of the CrT....181
5.4.5. Investigating the presence of tyrosine phosphorylation in the CrT....183
5.4.6. Effects of PKA and PKC inhibition on the migration of the CrT....186
5.4.7. Effects of Cr treatment on the migration of the CrT....187
5.4.7.1. Incubation in the presence of Cr....187
5.4.7.2. Creatine withdrawal following exposure to Cr....188
5.4.8. Investigating the presence of phosphorylation in CrT following Cr incubation....189
5.4.9. Investigating the presence of phosphorylation in CrT following Cr incubation using the ProQ Diamond Phosphoprotein stain....190
5.4.10. Large-scale immunoprecipitation of the CrT, and subsequent LC-MS / MS analysis....191
5.5. Discussion....201
5.5.1. Identification of CrT on SDS-PAGE using anti-CrT and anti-HA antibodies....201
5.5.2. *N*-linked glycosylation and its effects on electrophoretic mobility and activity of the CrT....202
5.5.3.Phosphorylation of the CrT....204
5.5.4. PKA- and PKC-mediated phosphorylation of the CrT....204
5.5.5. Creatine and its effects on post-translational modification of the CrT....205
5.5.6. Attempts to identify phosphorylated CrT using phosphospecific antibodies....206
5.5.7. Immunoprecipitation and LC / MS-MS confirmation of CrT isoforms....207
5.5.8. Conclusions and future work....209
Chapter 6. Transcriptional regulation of the CrT: Work in progress and future directions....211
6.1. Introduction....211
6.1.1. Background and aims....211

6.1.2. Experimental strategy and planning 212
6.2. Methods and Results 213
6.2.1. Amplification of the CrT 5' UTR 213
6.2.2. siRNA knockdown of *Hey1* 215
6.2.2.1. Initial siRNA transfections using standard transfection protocol 216
6.2.2.2. Repeat siRNA knockdown of *Hey1* and *Cyclophilin B* using DharmaFECT optimised transfection protocol 217
6.2.2.3. Real-time RT-PCR results of *Hey1* and *cyclophilin B* knockdown 218
6.2.2.4. Creatine uptake following HEY1 knockdown 221
6.3. Discussion 222
6.4. Conclusions 224
Chapter 7. General discussion 226
References 232
Appendix I 253
Appendix II 260
Solutions and media 264

List of Figures

Figure 1-1. Major routes of Cr metabolism in the body. 22
Figure 1-2. Genomic map of the human CrT. The CrT is located on chromosome *Xq28*. 24
Figure 1-3. A CrT schematic. 29
Figure 1-4. The creatine kinase reaction. 34
Figure 1-5. Schematic of the CK / PCr system. 36
Figure 1-6. The correlations between total Cr concentration and (A) free ADP, (B) absolute values of [ΔGATP] of hydrolysis, and (C) PCr-total Cr ratio. 43
Figure 1-7. MR images and spectra comparing WT hearts to CrT-overexpressing hearts. 44
Figure 1-8 Proteomics comparison of LV tissue from a wild-type and CrT-OE heart. 46
Figure 3-1. The reverse tetracycline-controlled transcriptional activator (rtTA) system: “Tet-on”.. 82
Figure 3-2. Map of pWTT1, a cloning vector containing fragments from pWhere and pTRE-Tight. 87
Figure 3-3. Map of pWTT1-CrT-myc. 88
Figure 3-4. Map of pWTT1-CrT-HA. 90
Figure 3-5. Agarose gel electrophoresis of CrT-HA amplicon and linearised pWTT1 prior to ligation.. 91
Figure 3-6. 0.8% agarose gel showing DNA from 15 of the 30 transformants picked. 92
Figure 3-7. Stable transfection of 3T3-tet-off fibroblasts with pWTT1-CrT-L15 and 2 clones of pWTT1-CrT-HA. 94
Figure 3-8. Confocal microscope images showing expression of CrT-HA in stably transfected 3T3-Tet-Off fibroblasts. 95
Figure 3-9. Confocal microscope images showing CrT-HA expression in response to 7-day dox incubation. 96
Figure 3-10. Confocal microscope images showing a comparison of fluorescence in WT LV tissue samples in the presence and absence of anti-HA. 97
Figure 3-11. Total CrT expression in 3T3-CrT-HA cells compared to untransfected cells. 99
Figure 3-12. 14C-Creatine uptake in 3T3- CrT-HA cells, and untransfected cells, normalised to nmol Cr / mg protein / h. 100
Figure 3-13. 14C -Creatine uptake in 3T3-CrT-HA cells over a wide range of concentrations. 100
Figure 3-14. CrT-HA transgene. 101
Figure 3-15. Southern blot. 103
Figure 3-16: Breeding strategy for the creation of mice with doxycycline-induced control of CrT expression. 106
Figure 3-17. Representative gel showing PCR genotyping results of single and double transgenic animals. 107
Figure 3-18. Graph of the data represented in the table above. 109
Figure 3-19. Total *CrT* mRNA expression in LV of dox-fed double transgenic ICT mice. 110
Figure 3-20.Western blot analysis of HA, in LV tissue extracted from mice following 7-day dox feeding. 111
Figure 3-21. HPLC chromatograms. 112
Figure 3-22. Luminescence (arbitrary units) of HEK 293-T cells. 115

Figure 3-23. Luminescence of LV of double transgenic rtTA-LC1 mice 117
Figure 4-1. Regulation of the CrT via the IGF-1 pathway. 129
Figure 4-2. 14C-Creatine uptake in 3T3-CrT-HA cells and in HL1 cells. 135
Figure 4-3. Effect of insulin on creatine uptake in 3T3-CrT-HA cells. 137
Figure 4-4. Effect of insulin on creatine uptake in 3T3-CrT-HA cells 137
Figure 4-5. Effect of insulin on creatine uptake in HL-1 cells. 138
Figure 4-6. Effect of growth hormone on creatine uptake in 3T3-CrT-HA cells. 140
Figure 4-7. Effect of growth hormone on creatine uptake in 3T3-CrT-HA cells. 140
Figure 4-8. Effect of growth hormone on creatine uptake in HL-1 cells 141
Figure 4-9. Effect of IGF-1 on creatine uptake in 3T3-CrT-HA cells. 143
Figure 4-10. Effects of PPP on HL-1 cells incubated in the presence and absence of 1 nM insulin. 144
Figure 4-11. Effects of H89 on 3T3-CrT-HA cells (panel A) and HL-1 cells (panel B) incubated in the presence and absence of 1 nM insulin. 145
Figure 4-12. Effects of BIM on 3T3-CrT-HA cells (panel A) and HL-1 cells (panel B) incubated in the presence and absence of 1 nM insulin. 146
Figure 4-13. Effects of H89 on 3T3-CrT-HA cells (panel A) and HL-1 cells (panel B) incubated in the presence and absence of 1 nM GH. 147
Figure 4-14. Effects of BIM on 3T3-CrT-HA cells (panel A) and HL-1 cells (panel B) incubated in the presence and absence of 1 nM GH. 148
Figure 4-15. Effect of H89 on creatine uptake in 3T3-CrT-HA cells (panel A), and in HL-1 cells (panel B).. 149
Figure 4-16. Effect of BIM on creatine uptake in 3T3-CrT-HA cells (panel A), and in HL 1 cells (panel B). 150
Figure 4-17. Effect of PKC activators PMA and STX, and Gö 6976 at high concentration on creatine uptake in 3T3-CrT-HA cells. 152
Figure 4-18. Effects of H89 and BIM on 3T3-CrT-HA membrane integrity 153
Figure 4-19. Effect of rapamycin on creatine uptake in 3T3-CrT-HA cells. 154
Figure 4-20. mRNA expression levels of total CrT in 3T3-CrT-HA cells treated in insulin and growth hormone. 155
Figure 4-21. mRNA expression levels of total *CrT* in 3T3-CrT-HA cells treated in 5 nM rapamycin. 156
Figure 5-1 A CrT schematic showing predicted glycosylation and phosphorylation sites 173
Figure 5-2. Graph showing mRNA expression of endogenous CrT in samples. 176
Figure 5-3 Western blot analysis of CrT 176
Figure 5-4. Deglycosylation of CrT-HA with EndoH and PNGase. 178
Figure 5-5. *In vitro* deglycosylation of CrT-HA with tunicamycin. 179
Figure 5-7. Effects of tunicamycin on 3T3-CrT-HA 181
Figure 5-8. Dephosphorylation of CrT-HA with CIAP, and preservation of phosphorylation with sodium orthovanadate. 182
Figure 5-9. Western blots of 3T3-CrT-HA lysates treated with pervanadate for varying incubation times, demonstrating enhanced general tyrosine phosphorylation. 184
Figure 5-10. Western blots of the product of immunoprecipitation (anti-HA) of 3T3-CrT-HA lysates treated with pervanadate for varying durations. 186
Figure 5-11. Treatment of 3T3-CrT-HA cells with PKA inhibitor (H89) and PKC inhibitor (BIM 187

Figure 5-12. Treatment of 3T3-CrT-HA cells with creatine. 188

Figure 5-13. Treatment of 3T3-CrT-HA cells with creatine prior to Cr withdrawal. 189

Figure 5-14. Western blot of the product of immunoprecipitation (anti-HA) of 3T3-CrT-HA lysates treated with Cr at 250 μM and 5 mM for 4 h and 24 h. 190

Figure 5-15. Pro-Q Diamond phosphoprotein stain of IP product of cells incubated in 2 concentrations of Cr for different durations. 191

Figure 5-16. Detection of CrT-HA on an immunoblot following immunoprecipitation 193

Figure 5-17. Detection of CrT-HA protein band on SDS-PAGE, using silver staining 194

Figure 5-18. LC-MS/MS results showing analysis results of band 1 from figure 4-16 A. 195

Figure 5-19. LC-MS/MS results showing analysis results of band 2 from figure 4-16 A. 196

Figure 5-20. LC-MS/MS results showing analysis results of band 3 from figure 4-16 B. 197

Figure 5.21. LC-MS/MS results showing analysis results of band 2 from figure 4-16 B. 198

Figure 5.22. LC-MS/MS results showing analysis results of band 1 from figure 4-16 B. 199

Figure 6-1. The pGL3 luciferase reporter vector (Promega). 214

Figure 6.2. 1% agarose gel showing products of amplification of regions of the CrT 5' UTR, amplified using primers against transcripts 002 and 005 (Appendix II). 215

Figure 6-3. Results of Cr uptake assay following siRNa transfection of HL-1 cells using the standard transfection protocol. 217

Figure 6-4. Real-time PCR results showing efficiency of *cyclophilin B* knockdown 48 h post-transfection with 25 nM *cyclophilin B* siRNA. 219

Figure 6-5. Real-time PCR results showing efficiency of *Hey1* knockdown 48 h post-transfection with *Hey1* siRNA. 220

Figure 6-6. Real-time PCR results showing efficiency of CrT knockdown 48 h post-transfection with *Hey1* siRNA 221

Figure 6-7. Results of Cr uptake assay following *Hey1* siRNA transfection of HL-1 cells using the modified transfection protocol with DharmaFECT transfection reagent. 222

List of tables

Table 2-1. Genotyping primers for rtTA mice. 64
Table 2-2. Genotyping primers for RCT mice. 64
Table 2-3. Genotyping primers for luciferase mice. 64
Table 2-4. Primers and dual-labelled fluorogenic probes for rtTA allelic discrimination 65
Table 2-5. Primers used for RT-qPCR. 65
Table 2-6. Sequencing primers 71
Table 3-1. Oligonucleotides used to amplify rb CrT by PCR, and replace the already present c-myc tag with an HA tag. 89
Table 3-2. Summary of the three clones used for creating stable cell lines. 98
Table 3-3. Details of founder mice generated, and their assigned names. 102
Table 3-4. Ct values and calculation of relative rtTA gene copy number according to the ΔΔCt method 105
Table 3-5. Real-time RT-PCR results of amplification of *rtTA* mRNA from LV tissue.. 108
Table 3-6. Total Cr levels in LV of mice following 7 day dox feeding protocol. 112
Table 3-7. Summary of the numbers of double transgenic rtTA / CrT-HA mice (ICT) from each line that were put on a dox feeding protocol 113
Table 3-8. Luminescence (arbitrary units) of LV samples of double transgenic rtTA-LC1 mice after 7 days of dox administration. 116
Table 5-1. Summary of predicted PTM sites detected by LC-MS/MS (as depicted in figure 5-1). 200
Table 6-1. Detail of the volumes of reagents used to transfect HL-1 cells with siRNA. 218

Abbreviations

ADP	adenosine diphosphate
AGAT	arginine:glycine amidinotransferase
AK	adenylate kinase
Akt	protein kinase B
α-MHC	alpha-myosin heavy chain
AMP	adenosine monophosphate
AMPK	AMP-activated protein kinase
ANP	atrial natriuretic peptide
ANT	adenine nucleotide translocase/(transporter)
AP5A	p1, p5-di(adenosine-5') pentaphosphate, diadenosinepentaphosphate
α-SA	alpha skeletal muscle actin
ATP	adenosine triphosphate
BIM	bisindolylmaleimide
BLAST	basic local alignment search tool
β-GPA	beta-guanidinopropionic acid
β-MHC	beta-myosin heavy chain
BNP	brain natriuretic peptide
Bp	base pair
BSA	bovine serum albumin
cDNA	complementary DNA
CHF	chronic heart failure
CK	creatine kinase
CMV	cytomegalovirus
Cr	creatine
CrT	creatine transporter
CTCF	CCCTC binding factor
DIGE	difference gel electrophoresis
DNA	deoxyribonucleic acid
DMEM	Dulbecco's Modified Eagle's Medium
DMR	differentially methylated region
dNTP	deoxynucleotide triphosphate
Dox	doxycycline
DTT	dithiothreitol, Cleland's reagent
EAAT	glutamate transporter
EDTA	ethylenediamine tetraacetic acid

EF	ejection fraction
EGTA	ethylene glycol tetraacetic acid
EndoH	endoglycosidase H_f
FACS	fluorescence activated cell sorting
FBS	foetal bovine serum
FCS	foetal calf serum
GAA	guanidinoacetate
GAMT	guanidinoacetate N methyltransferase
GABA	gamma-aminobutyric acid
GAT-1	GABA transporter
GFP	green fluorescent protein
GH	growth hormone (somatotropin)
Gö6976	[12-(2-Cyanoethyl)-6,7,12,13-tetrahydro-13-methyl-5-oxo-5H-indolo(2,3-a)pyrrolo(3,4-c)-carbazole]
H89	(*N*-[2-(*p*-bromocinnamylamino)ethyl]-5-isoquinolinesulphonamide
HA	haemagglutinin
HBSS	Hank's Buffered Salt Solution
HEPES	4-(2-hydroxyethyl)-1-piperazineethanesulfonic acid
HF	heart failure
HPLC	High Performance Liquid Chromatography
ICR	imprinted control region
IGF-1	insulin-like growth factor 1
IGF-1R	insulin-like growth factor 1 receptor
IGF-2	insulin-like growth factor 2
IMM	inner mitochondrial membrane
IP	immunoprecipitation
KO	knockout
LC- MS/MS	liquid chromatography with tandem mass spectrometry
LV	left ventricle
LVH	left ventricular hypertrophy
MI	myocardial infarction
MMP	matrix metalloproteinase
MOPS	3-(N-morpholino)propanesulfonic acid
mRNA	messenger ribonucleic acid
MRS	magnetic resonance spectroscopy
mTOR	mammalian target of rapamycin
NADP	nicotinamide adenine dinucleotide phosphate
NCBI	National Center for Biotechnology Information
NMR	nuclear magnetic resonance
OE	overexpression

OMM	outer mitochondrial membrane
Opt rtTA	codon optimised (to eukaryotic bias) rtTA
ORF	open reading frame
PAGE	polyacrylamide gel electrophoresis
PBS	phosphate buffered saline
PCR	polymerase chain reaction
PCr	phosphocreatine
PDE3	phosphodiesterase 3
PDK1	3-phosphatinositide dependent protein kinase-1
PEV	position effect variegation
PGC-1α	PPARγ co-activator 1α
PI(3,5)P2	phosphatidylinositol (3,5)-biphosphate
PIKfyve	phosphoinositide kinase, FYVE finger containing
PKA	protein kinase A
PKC	protein kinase C
PI3K	phosphatidylinositol-3-phosphate-5-kinase
PIP3	phosphatidylinositol(3,4,5)-triphosphate
PMA	phorbol-12-myristate-13-acetate
PMSF	phenylmethylsulphonyl fluoride
PNGase F	N-Glycosidase F
PPARγ	peroxisome proliferator-activated receptor γ
PTM	post-translational modification
RMCE	recombinase-mediated cassette exchange
RIPA	radioimmunoprecipitation assay (protein extraction buffer)
RISC	RNA-induced silencing complex
RNAi	RNA interference
RT	room temperature
RT-PCR	reverse transcriptase- polymerase chain reaction
RT-qPCR	real-time (quantitative) reverse-transcriptase polymerase chain reaction
rtTA	reverse tetracycline transactivator
RV	right ventricle
SERT	serotonin transporter
SGK1	serum and glucocorticoid transporter 1
SGK3	serum and glucocorticoid transporter 3
shRNA	short-hairpin RNA
STX	sapintoxin
TAC	transverse aortic constriction
TAE	Tris/Acetate/EDTA
TBE	Tris/Borate/EDTA

Tet	tetracycline
tetO	tetracycline operon
tetR	tetracycline-repressor
TICK	tetracycline-inducible (mitochondrial) creatine kinase
TNB	5-thio-2-nitrobenzoic acid
TRE	tetracycline response element
tTA	tetracycline transactivator
UTR	untranslated region
VDAC	voltage dependent anion channel (also known as porin)
WT	wild-type

Chapter 1 Introduction

1.1. Creatine and the Creatine Transporter

1.1.1. Creatine and creatine metabolism

Creatine (Cr) is a naturally occurring guanidino compound, first described in 1832 by Michel Chevreul, who isolated it from skeletal muscle and named it after the Greek for flesh, *kreas.* In its phosphorylated form, it is known as phosphocreatine (PCr), a high energy phosphate whose involvement in muscle contraction was established in the 1960s [1]. Cr and PCr levels are highest in heart, skeletal muscle, spermatozoa and photoreceptor cells of the retina, and 94% of the total Cr in the body is found in muscle. Intermediate levels are found in the brain, intestine and endothelial cells, with only very low levels present in lung, spleen, kidney, blood cells and serum [2]. Following the discovery of PCr, and shortly afterwards, the creatine kinase (CK) reaction (the reversible reaction catalysing the formation of PCr from Cr), research focussed primarily on the biochemistry and pathology of the CK reaction itself, and its role in the metabolism of cells and tissues with high energy demands. In recent years, interest in Cr has been revived due to the recognition that Cr and the CK system are altered in a variety of diseases. The identification and cloning of many of the enzymes involved in Cr metabolism, in addition to the cloning and characterisation of the gene encoding the creatine transporter (CrT) have aided the understanding of Cr homeostasis in the cell. However, the regulation of the CrT is a complex field with a great deal still to be discovered.

1.1.2. Biosynthesis of creatine

Creatine is a non-essential nitrogenous organic acid, synthesised primarily in the kidney and

liver [3]. Typically, around 50% of the required Cr is obtained through an omnivorous diet, predominantly by consumption of meat, fish and other animal products. The remainder has to be synthesised. Two steps are involved in the *de novo* synthesis of Cr, and neither of the enzymes involved in these steps are expressed in the cardiomyocyte. The first step occurs in the kidney, and is catalysed by the enzyme $_{L}$-arginine:glycine amidinotransferase (AGAT), which transfers the amidino group of arginine to glycine, producing $_{L}$-ornithine and guanidinoacetic acid (GAA). The second step of synthesis takes place in the liver, and is catalysed by *S*-adenosyl-$_{L}$-methionine:*N*-guanidinoacetate methyltransferase (GAMT). Methylation of the amidino group of GAA yields Cr. Once formed, the Cr is carried in the blood from the site of synthesis to Cr-requiring tissues.

1.1.3. Degradation of creatine

The degradation of Cr is largely a spontaneous, non-enzymatic process. Studies performed *in vitro* showed that the reversible, non-enzymatic conversion of Cr to creatinine (Crn) (Cr→Crn) is both pH and temperature dependent, with the reaction favouring Cr at high pH and low temperature. However, *in vivo*, this reaction has been shown to be irreversible, with the reaction proceeding only in the direction of Cr degrading to Crn. Around 1.1% of the body's Cr degrades non-enzymatically into Crn. In addition, 2.6% of the body's PCr is converted into Crn, giving an overall conversion rate of the total Cr pool (Cr + PCr) of around 1.7% / day. This equates to around 2 g / day in a 70 kg man. Crn, a non-ionic molecule, is membrane permeant. Subsequently, it diffuses out of the tissues into the blood, and is for the most part excreted by the kidneys. This process is important, as the cyclization of Cr to Crn is the sole route for the removal of Cr from the cell. There is evidence to suggest that a small proportion of Crn is converted into other compounds, such as arginine and guanidinobutyrate [4]. The presence of Cr in the urine is rare, except in individuals supplementing their diets with Cr [5 6].

Figure 1-1 summarises the major routes of Cr metabolism in the body, with its synthesis from arginine and glycine, catalysed by AGAT and GAMT, through its uptake by the CrT on the plasma membrane into muscle cells, and its subsequent phosphorylation to yield PCr and contribute to the energy required for contraction of the cardiomyocyte.

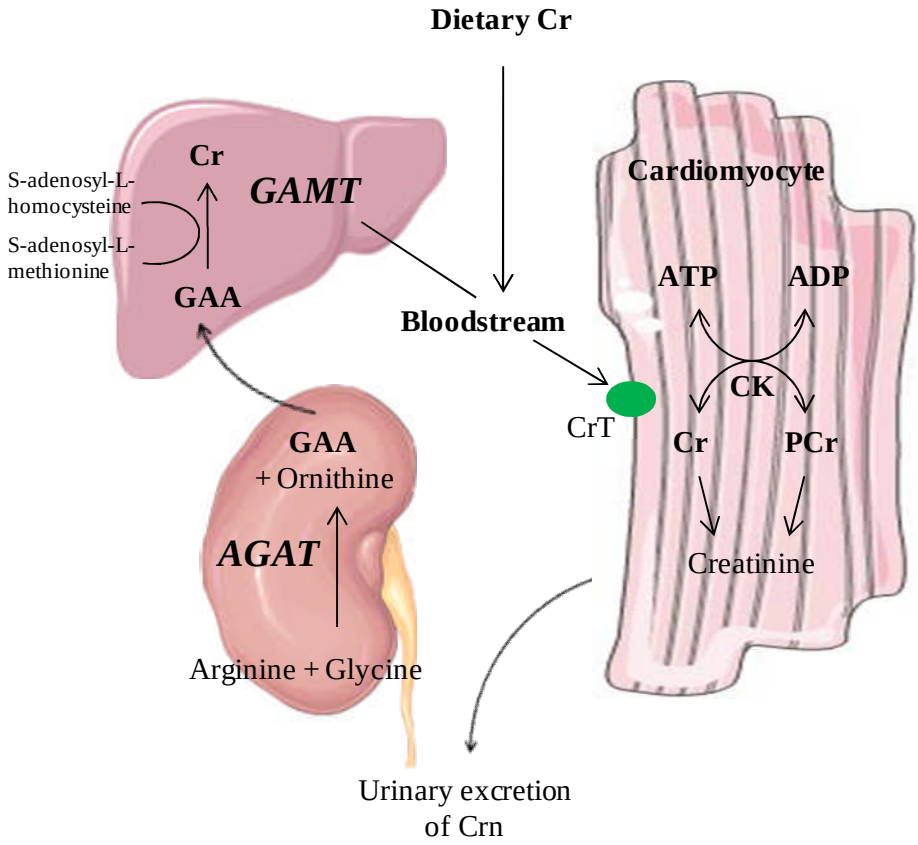


Figure 1-1. Major routes of Cr metabolism in the body. Up to 94% of Cr is found in muscle. Dietary Cr, or Cr produced by *de novo* synthesis is taken up from the blood by the plasma membrane-spanning CrT. The first step of Cr synthesis occurs in the kidney, where L-arginine:glycine amidinotransferase (AGAT) catalyses the formation of guanidinoacetic acid (GAA) from arginine and glycine. In the second step, S-adenosyl-L-methionine:N-guanidinoacetate methyltransferase (GAMT) catalyses the formation of Cr from GAA in the liver.

1.1.4. Cellular creatine uptake and the Creatine Transporter

Creatine uptake occurs against a steep concentration gradient from the blood into the tissues that require it [7]. This function is performed by the creatine transporter protein (CrT), a plasma membrane-bound transporter which facilitates the uptake of cellular Cr [8 9 10 11]. Two creatine transporter genes have been identified, denoted *CrT-1* and *CrT-2*, although it is uncertain

whether *CrT-2* is functional. This is discussed in greater detail below. This thesis deals primarily with CrT-1, a saturable Na^+ and Cl^- transporter protein, closely related to other members of the 'solute carriers family 6' (SLC6) family of proteins, which act as specific transporters for neurotransmitters, amino acids, and osmolytes [12]. The CrT-1 was denoted 'SLC6A8' by HUGO, the gene nomenclature committee. Other members of the SLC6 family include the γ-aminobutyric acid (GABA) transporter and the norepinephrine (NET) transporter.

1.1.5. The *CrT* gene

The human gene encoding CrT-1 is located on chromosome Xq28 [13] [14] [15]. *CrT-1* includes 2 polyA tails, with a coding region of 13 exons [16], and spans around 8.5 kb of genomic DNA. The first 8 exons encode transmembrane domains. *CrT-1* was shown to be linked to an X-linked mental retardation syndrome [17], following the discovery of mutations associated with severe speech and language delay, cerebral Cr deficiency and an increased urinary Cr / Crn ratio [18] [19]. An additional gene, *CrT-2* [20], has been identified in humans, and also encodes a creatine transporter, SLC6A10. Evidence suggests that transcripts from this gene are only produced in the testes, which also express mRNA transcripts from *CrT-1*. *CrT-2* is located on chromosome 16p11.1-16p11.2 [21] [22] [14]. The physiological significance of this gene remains unclear. Owing perhaps to different methodologies employed by the groups researching it, there is uncertainty regarding its predicted translation. One group stated CrT-2 is 50 amino acids larger than CrT-1 [14], whilst another group found it to incorporate a premature stop codon within exon 4, thus resulting in a non-functional or truncated protein [21]. It is known that there is 97% homology between the two transcripts, and there is consensus that the normal stop codon present in *CrT-1* is not present in *CrT-2*. No correlate of *CrT-2* has been identified in the mouse [23]. In addition to *CrT-1 and CrT-2,* a novel splice variant was discovered by Martinez-Muñoz *et al*, whilst

attempting to characterise *CrT-2*, and was denoted *Slc6a8c*. An open reading frame was found, and this predicted a truncated protein, comprising the last 5 transmembrane domains of the CrT-1 protein, SLC6A8. The authors suggested that this splice variant is conserved, as it was discovered in mouse as well as human [20]. The same group has recently established an LOVD (Leiden Open Variation Database) listing all variants of *Slc6a8*. In total, 109 *Slc6a8* variants are known and listed on the database, although only a small proportion of these are pathogenic, with many not leading to splicing errors [24]. In some cases, mutations encoding splice variants have been associated with X-linked mental retardation syndrome (XLMR), due to a Cr deficiency in the brain.

There is a small amount of inter-species variation in *CrT*, although cDNA sequences suggest a homology of 97% at the amino acid level between rat, rabbit, bovine and human CrT [10 25 26 27].

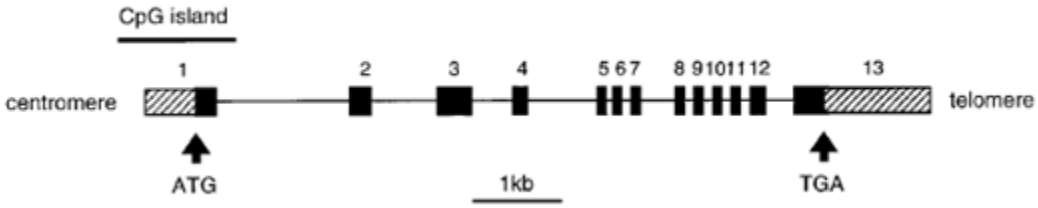


Figure 1-2. Genomic map of the human CrT. The CrT is located on chromosome *Xq28*. The solid areas represent exons, containing the open reading frame, and the shaded areas are the 5'- and 3'-untranslated regions. Taken from Sandoval *et al*, Genomics 1996 35(2), p383-385.

1.1.6. Expression of *CrT*

Several different sized *CrT* mRNA transcripts have been reported. One group demonstrated the presence of a 4.0 kb transcript in human lung, heart, brain, kidney, placenta, skeletal muscle, pancreas, spleen, thymus, testis, prostate, small intestine, ovary and colon. All of these tissues except lung, pancreas, spleen and ovaries, also expressed a 3.0 kb transcript [26]. The authors

concluded that the differences in transcript length were due to alternative polyadenylation in the non-coding region, suggesting that while there would be differences in the untranslated regions of the transcripts, they would encode the same protein. Other groups have found somewhat contradictory results, and it is uncertain whether this is due to methodological differences, or differences between the species researched. Guimbal and colleagues, as well as Schloss *et al* found larger mRNA transcripts, of 4.5-4.8 kb and 3.1-3.2 kb in both rat and rabbit [10] [28], suggesting the differences in sizes could be due to variation in the lengths of the non-coding regions of the gene. Another group identified a 4.3 kb transcript in rat brain, lung and kidney, and a smaller 3.0 kb transcript in kidney, lung and central nervous tissue [16]. They concluded that these 2 transcripts arose from alternative polyadenylation of a single transcript. The expression pattern of the transcripts was found to be essentially the same as that of creatine kinase (CK) [29], indicating a potential link between Cr uptake and CK activity.

1.1.7. The CrT, a saturable Na^+ and Cl^- -dependent membrane protein

As outlined previously, two genes, encoding creatine transporters have been identified- *CrT-1* and *CrT-2*. This thesis deals only with *CrT-1*, which from now on will be referred to simply as *CrT*, the gene encoding the functional and ubiquitously expressed CrT-1, SLC6A8.

The CrT performs an essential function, moving Cr against a high concentration gradient by means of a saturable sodium- and chloride-dependent co-transport, high affinity uptake process. This process has been studied in various tissues and cell types, including the heart [11] [1] [30] [31] [32]. Several studies have demonstrated the dependence of CrT on Na^+ [25] [10] [30], with a suggested stoichiometry of 1 or 2 Na^+ for 1 Cr [33] [30]. Na^+ cannot be replaced by other cations such as lithium or choline without a strong depression in the function of the CrT [10] [30] [27]. In a mouse

myoblast cell line, over 90% of Cr transport was found to be Na^+-dependent [11], demonstrating that Na^+ is key to the majority of cellular Cr uptake. The CrT makes use of the free energy of the [Na^+] gradient and the membrane potential maintained by the Na^+,K^+-ATPase [11]. Additionally, and in contrast to some other members of the SLC6 family, there is evidence to suggest the dependence of the CrT on Cl^- as well as Na^+ [9 10 34], with a stoichiometry of 2 Na^+ : 1Cl^- : 1 Cr molecule [9]. Furthermore, it has been suggested that the CrT expresses electrogenic transport activity, a process identified in another member of the SLC6 family, the GABA transporter (GAT-1) [9 11]. Cr transport is saturable, and a range of K_m values have been published, ranging from 15-100 µM in various cultured cell types [35]. K_m values for human and rabbit have been determined as 15-77 µM [9 7 26 27] and 35 µM [10] respectively. With estimates of human plasma Cr concentrations of 58 µM and rabbit concentrations of 149 µM [36], vastly lower than the mM concentrations seen in tissue, it is clear that the CrT works close to saturation, suggesting that the number of CrTs present in the plasma membrane may be key in the regulation of Cr accumulation.

Studies into the cellular localisation of the CrT have been hampered in part due to the limited availability of specific CrT antibodies, an issue which is discussed below. It appears that the CrT is not abundant in the plasma membrane, even in tissues containing high levels of Cr and PCr. In skeletal muscle, CrT has been shown to be predominantly associated with the sarcolemmal type I and type II fibres [37], whilst studies in the retina indicated a total of less than 0.03% total CrT membrane-protein content, despite the fact that the retina has a high requirement for Cr [38]. Research into *N*-linked glycosylation in the CrT indicated a role for glycosylation in the correct trafficking of CrT to the plasma membrane, suggesting that reduced CrT function in deglycosylated CrT mutants was due to both a reduction in CrT activity, and also due to altered localisation of the protein in the cell [39].

It is important to consider known issues regarding the specificity of anti-CrT antibodies available, and used widely, where studies involving the CrT are concerned. To date, no commercially available antibody tested by this laboratory has demonstrated specificity to the CrT, and another antibody, used extensively for various studies in the literature, was found to cross-react with PDH complexes, bringing into question much of the data that had been acquired through its use [40].

1.1.8. Putative structure of the CrT

To date, there is no crystal structure of the CrT. Its putative structure suggests 12 transmembrane-spanning domains (TMs), with the amino- and carboxy-terminal regions facing the cytoplasmic side of the membrane [10] [26]. Potential sites for both glycosylation and phosphorylation are found, with 2 putative glycosylation sites found on the extracellular loop between TM3 and TM4. Another glycosylation site is predicted in the very short loop between TM11 and TM12, although this may be inaccessible. Post-translational modifications of the CrT are discussed in detail in Chapter 5.

In 2005, the first structure for a member of the SLC6 family, the bacterial leucine transporter ($LeuT_{Aa}$), was determined at a high resolution of 1.65Å. [41]. The structure revealed the protein folds of the transporter, and also clearly showed the substrate binding site. As $LeuT_{Aa}$ is not Cl^--dependent, no information that could be related to the Cl^- binding site of CrT was gleaned. The structure of $LeuT_{Aa}$ reinforces the 'two gate' theory for these transporters, where exposure of the binding site to the outside of the cell enables the substrate to bind. Closure of the external gate then traps the substrate within the membrane. This is followed by the opening of an internal gate, which allows the release of the substrate into the cell. It is suggested that in $LeuT_{Aa}$, this

process requires major movements of transmembrane domains 1 and 6 (TM1 and TM6) relative to TM3 and TM8, with these domains together forming the substrate binding site [41]. Although homology between CrT and $LeuT_{Aa}$ is only 20-25%, the conservation of residues in SLC6 family members at key positions combined with the similarity of the topology between $LeuT_{Aa}$ and the putative CrT models suggest that it is a valuable structural model for the CrT. For example, work performed by Dodd and Christie suggesting a highly-conserved region in TM3 is involved in Cr binding in the CrT gained extra credibility following the publication of the $LeuT_{Aa}$ structural model, in which TM3 is strongly implicated in substrate binding [42 43], along with TMs 1, 6 and 8. This is discussed further below.

Only very few residues are better conserved between species in CrT than in other members of the SLC6 family [10]. One of these residues, Cys-144 (in TM3), which is not present in any of the other SLC6 transporters, was investigated by Dodd *et al* in order to establish its relevance to Cr binding. By means of site-directed mutagenesis, and chemical modification with methanethiosulfonates (MTS), they determined that it could indeed be close to a binding site or a permeation channel for Cr [42]. Further work was performed using the substituted cysteine availability method (SCAM) to replace 22 residues in TM3 of the CrT, one at a time, with cysteine [44]. Six of the resulting mutants were found to be inactive and MTS-sensitive, and these residues were aligned 3-4 amino acids apart along one face of the predicted α-helix of TM3. Three of the residues were additionally protected from MTSEA (an MTS) inactivation by Cr, and the authors suggested that these residues may be close to the Cr binding site. As TM3 of $LeuT_{Aa}$ is also involved in substrate binding, they concluded that these findings are in keeping with the $LeuT_{Aa}$ model, and therefore suggested that it is a suitable structural template for the mammalian CrT. A putative structure of the CrT is shown below, based on predictions following its cloning [26], combined with the information gleaned from the x-ray crystallography of the

$LeuT_{Aa}$ transporter, which has given insights into the substrate binding sites in members of the SLC6 family of transporters. Putative phosphorylation sites, identified using NetPhos [45], are also indicated. Again, these are discussed in greater detail in Chapter 5.

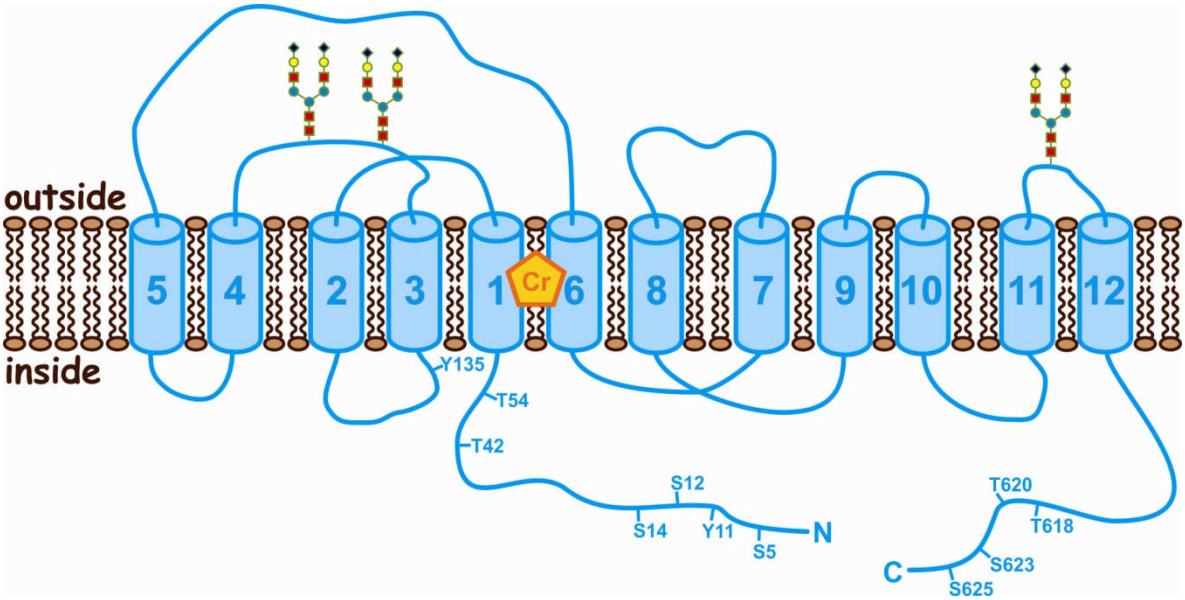


Figure 1-3. A CrT schematic. This representation of the secondary structure of the creatine transporter is based on the structure of the bacterial LeuTAa transporter (PDB code2A65), and showing putative phosphorylation sites. The probable sequences of intracellular CrT loops were informed by aligning the primary sequences of CrT and LeuTAa using MULTALIN [46] and evaluating this with respect to the known three-dimensional structure of LeuTAa. A total of 22 possible serine, threonine and tyrosine phosphorylation sites on the CrT were then predicted by NetPhos [45]. The subsets labelled on the figure are those which reside on the predicted intracellular loops. Putative glycosylation sites are also shown. The predicted binding site for Cr is also indicated, which is believed to incorporate TM3 and TM8 in addition to TM1 and TM6. Transmembrane domains are represented by blue cylinders. Schematic kindly provided by Dr. James Brown, created using CorelDraw 9.

1.1.9. CrT isoforms

Several different isoforms of the CrT have been identified, with many different molecular weight species being identified on SDS-polyacrylamide gel electrophoresis (SDS-PAGE). Bands of 50 kDa, 70 kDa, 80 kDa and 200 kDa have been observed, though the identification of these isoforms has been hindered by the unavailability of specific antibodies.

1.1.10. CrT regulation and expression during development

Recent studies have elucidated changes in the expression and function of the CrT during development. A study in the spiny mouse showed a limited capacity for endogenous Cr synthesis until approximately 34-37 days gestation, due to low expression of GAMT, and to a lesser degree, AGAT [47], suggesting that only shortly before birth does the spiny mouse attain the capacity to meet the postnatal requirement for endogenous creatine synthesis. The authors also determined that total Cr in the placenta and brain increased significantly during the second half of pregnancy. This increase coincided with a significant increase in the expression of *CrT* mRNA of 2-fold from mid-pregnancy to full-term. This could indicate a necessity for a maternal source of Cr, transferred across the placenta, during late pregnancy, when although the expression of *CrT* mRNA is increased, endogenous Cr synthesis is still low. If the developmental changes in the spiny mouse and the human are analogous, it is possible that premature birth could increase the likelihood of Cr deficiency in humans, due to the lack of *de novo* synthesis until full-term. The expression of *CrT* mRNA in the developing heart followed a different pattern, peaking at day 34 of gestation, but this was not accompanied by an increase in total Cr in the heart. Myocardial total Cr levels were stable from day 30 of gestation, but increased rapidly from birth to post-natal day 10. The authors suggested an increase in CrT activity as the explanation for this increase in Cr uptake, possibly by means of post-translational modifications (discussed later). It is noteworthy that the low expression of *CrT* mRNA, and low tissue Cr levels could point to a low requirement for Cr during early development, as irrespective of placental Cr levels, a lack of CrT on the plasma membrane would prevent Cr uptake into the cell, regardless of its source. It is also possible that during development, energy requirements are met to a greater degree by local glycolysis than mitochondrial oxidative phosphorylation.

Our group studied the changes in CrT function during maturation in the rat heart, and found that the abundance of *CrT* transcripts increases steadily from 2 days pre-birth until 80 days post-birth. These findings contrast with the findings of the study discussed above, where no change was found in spiny mouse heart from 34 days pre-birth to 10 days post-birth. A significant correlation was found between *CrT* mRNA and total Cr levels, as well as between *CrT* mRNA and Cr uptake, demonstrating a clear relationship between gene expression and CrT activity. This contrasted with the suggestion of Ireland *et al* that in the early stages post-birth in the spiny mouse, the increase in myocardial Cr levels is not due to an increase in gene expression. Ninety % of the total variance in Cr uptake capacity, and 70% of the variance in myocardial Cr content was attributable to changes in the expression of *CrT*. These results contrast with the literature on the mature heart, where CrT activity is regulated to a greater degree by substrate feedback mechanisms and post-translational modification [48].

1.1.11 CrT regulation by post-translational modification

Detailed discussion of the regulation of CrT by means of post-translational modifications, such as *N*-linked glycosylation and phosphorylation, can be found in Chapters 4 and 5.

1.2. The role of creatine in myocardial energetics and the phosphotransfer systems- synthesis of high-energy phosphates

1.2.1. Adenosine triphosphate

Adenosine triphosphate (ATP) has been described as the universal energy currency for most of the energy-requiring processes occurring in biological systems, including the brain, skeletal muscle and cardiac muscle. The heart has an absolute requirement for energy in the form of this high-energy phosphate, which is consumed by myosin ATPase, and is intrinsic to the excitation

and contraction of the cardiomyocytes. The concentration of ATP within the cardiomyocyte is maintained at ~10 mM, with ATP synthesis by oxidative phosphorylation in the mitochondria usually maintaining this, with some contribution from glycolysis. The production of ATP in the mitochondria is regulated through feedback from the products of ATP hydrolysis (outlined below), adenosine diphosphate (ADP) and inorganic phosphate (Pi). When ADP and Pi accumulate due to a mismatch between ATP utilisation and synthesis, mitochondrial ATP synthesis is stimulated.

1.2.2. Hydrolysis of ATP and $\Delta G_{\sim ATP}$

Free energy is liberated from ATP by hydrolysis, and it is this free energy change ($\Delta G_{\sim ATP}$) that provides the energy to drive all energetically-unfavourable ATP-utilising reactions, in particular providing the energy for contraction in the cardiomyocytes. This process is known as the 'ATPase' reaction, a unidirectional reaction with a stoichiometry of ≤ 1 proton for 1 ATP. In addition to the proton, ADP and inorganic phosphate are produced. The reaction is shown below.

$$\mathbf{ATP + H_20 \rightarrow ADP + Pi + H^+}$$

$\Delta G_{\sim ATP}$ is calculated from the constant value for ATP hydrolysis under standard conditions, represented as $\Delta G^{o}_{\sim ATP,}$ and is corrected for the actual concentrations of ATP, ADP and Pi in the cytosol. This is represented by the formula below.

$$\mathbf{\Delta G_{\sim ATP} = \Delta G^{o}_{\sim ATP} - RT\ ln\ [ATP]/[ADP][Pi]}$$

The maintenance of the free energy change of ATP hydrolysis in the myocardium is critical. If it decreases below a certain threshold, a steep reduction of contractile performance occurs, resulting in diastolic and then systolic dysfunction in the heart [49].

1.2.3. Creatine kinase and the creatine kinase reaction

Under conditions when the production of ATP by oxidative phosphorylation and glycolysis is inadequate, due to high ATP demand by the heart, other means of maintaining ATP availability, and thus a high phosphorylation potential are required. This means maintaining a high ratio of [ATP] to [ADP] and [Pi]. Two phosphoryltranferase enzymes catalyse reactions that fulfil these requirements in the heart; creatine kinase and adenylate kinase, and the role of CK will be dealt with in some detail. CK was first described in 1934, by Lohman. This enzyme reversibly transfers the high-energy γ-phosphate bond from ATP to the guanidine group of Cr, yielding ADP and phosphocreatine (PCr). The reaction in its simplified form is shown below:

$$\mathbf{Cr + ATP \rightleftharpoons PCr + ADP + H^{+}}$$

Four subunit isoforms of CK are expressed in vertebrates, in a tissue-specific manner. There are 2 cytosolic forms, M-CK (muscle) and B-CK (brain), in addition to 2 mitochondrial homodimers. *In vivo*, the cytosolic subunits combine, yielding 3 combinations of dimer, the MM-, MB-, and BB-CK isoforms. These have an approximate molecular weight of 80-86 kDa [50]. The predominant isoforms in the heart are M-CK, constituting 70% of the total CK activity, and the mitochondrial CK (Mt-CK), which constitutes 25% of CK activity [51 52].

Phosphocreatine is the major high-energy phosphate-containing compound in the heart, and is more abundant than ATP. In the healthy mammalian adult ventricular myocardium, the PCr / ATP ratio is around 2 : 1. This ratio is of key importance due to the involvement of PCr in the regeneration of ATP during times of high energy demand through the creatine kinase reaction, which is detailed below. PCr serves several other important purposes. The smaller size and lower polarity of PCr compared to ATP create an advantage for PCr in intracellular energy transport, as it has a greater intracellular diffusion ability than ATP [53], overcoming the diffusion limitations of adenine nucleotides [54]. Additionally, as Cr and PCr levels can accumulate to much greater levels than ATP in CK-containing cells, it allows a higher intracellular flux of high-

energy phosphates. CK is vital as it maintains a high phosphorylation potential, due to its capacity to regenerate ATP more rapidly than oxidative phosphorylation or glycolysis, also regenerating ATP faster than the rate at which it is consumed by ATPases [54]. Figure 1-4 overleaf outlines the CK reaction.

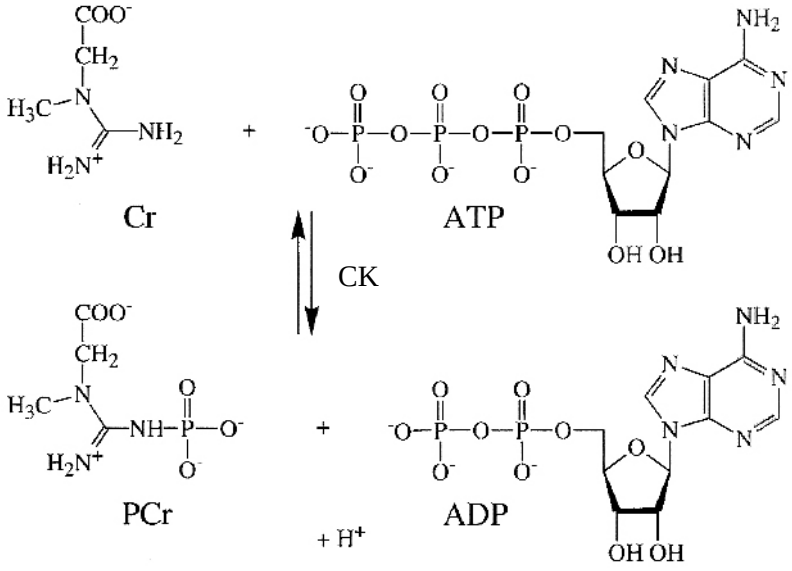


Figure 1-4. The creatine kinase reaction. The molecular structure of the compounds involved is shown. Note that PCr is much smaller and less charged than ATP, and therefore far more mobile in cells.

1.2.4. The phosphocreatine shuttle

The CK reaction has been shown to play several key roles. The first of these is as a temporal energy buffer, i.e. an energy reserve system. An example is that during the ATP supply-demand mismatch occurring in hypoxia and ischaemia in the heart. Here, the formation of ATP via the CK reaction slows the rate of ATP depletion. A second key role is that of a spatial energy buffer. This concept led to the proposal of the creatine phosphate shuttle [55]. Thirdly, the reaction fulfils a vital function by preventing a rise in intracellular ADP levels. Increased [ADP] causes a net loss of adenine nucleotides and the inactivation of cellular ATPases [56-57] [54]. Finally, the reaction acts as an energy transport system, and a proton buffer [54] [58].

The phosphocreatine shuttle was first proposed by Bessman [55] and has become widely accepted as a viable system for the transport of energy in muscle [59] [54]. Further evidence supporting the shuttle hypothesis came from the demonstration of the effect of Cr on the respiratory control of isolated mitochondria [60] [61]. Additionally it was proved that some of the CK isoenzymes are localised in subcellular compartments, functionally coupled to sites of energy production and utilisation [62] [54]. The observation that CK activity is present both in ATP-producing and ATP-utilising organelles suggests chemical energy is made and supplied within distinct cellular compartments *via* the CK reaction, and not by the simple diffusion of adenine nucleotides between organelles. The creatine phosphate shuttle essentially forms a link between sites of ATP synthesis and utilisation. The mitochondrial CK isoform, sMtCK, is complexed with the ATP-ADP translocase, and synthesises PCr from ATP produced in the mitochondria by oxidative phosphorylation, in a unidirectional manner. ATP is regenerated from the PCr at the other end of the shuttle by MM-CK, thus providing energy for muscle contraction. MM-CK is strongly bound to the contractile apparatus and is functionally coupled to Ca^{2+}-ATPase [63] [64]. A study into the deletion of the M-CK and sMtCK in mice showed that while they were not essential to baseline cardiac function, their deletion led to increased free ADP and decreased free energy from ATP hydrolysis. This caused decreased tolerance during high workloads and ischaemia [51], indicating the importance of the creatine phosphate shuttle in the heart under these conditions. Figure 1-5 outlines the CK / PCr system.

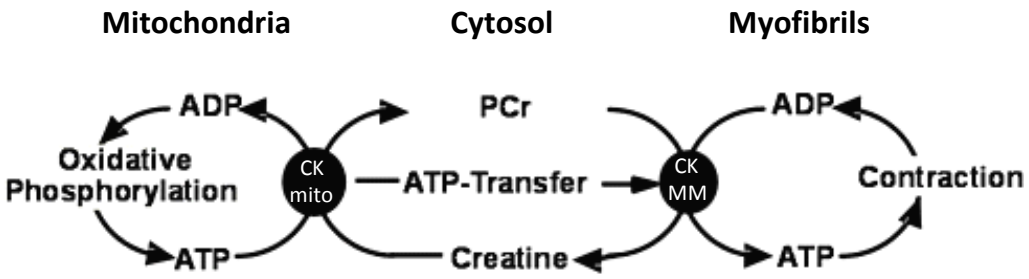


Figure 1-5. Schematic of the CK / PCr system. ATP synthesized by the mitochondria reacts with Cr in a reaction catalyzed by sMt-CK yielding PCr and ADP. PCr diffuses to the myofibrils where MM-CK catalyzes the reverse reaction to form ATP, providing energy for contraction in the myofibrils. Adapted from Holloway *et al*, Frontiers in Bioscience S3, p331-340.

1.2.5. Adenylate kinase

In addition to the CK system, another phosphoryltransfer system exists, and serves the same purpose in enabling communication between spatially separated intracellular ATP consumption and ATP production processes. This nucleotide phosphoryl exchange reaction is catalysed by the enzyme adenylate kinase (AK) [65], in the reaction shown below.

$$\mathbf{2ADP \rightleftharpoons ATP + AMP}$$

The discovery that the disruption of genes encoding mitochondrial and cytosolic CK isoforms did not lead to overt ventricular dysfunction led to the suggestion that there may be involvement of alternative phosphotransfer systems which are able to compensate for the loss of function in the CK system [66]. Whereas CK contributes to 89% of phosphotransfer in the intact myocardium, AK contributes just 10% [66]. As with CK, several isoforms of AK (AK1-AK7) have been identified [67] [68]. The main isoform in the heart is AK1. These isoforms are membrane-bound, both in the mitochondria and cytosol [69] [70]. In contrast to CK, which transfers 1 phosphoryl of ATP (the γ-phosphoryl), AK is able to transfer both the β- and γ-phosphoryls of ATP to utilisation sites [71]. This doubles the energetic potential of the ATP molecule [66]. Whilst useful in

cases of high [ADP], this process leads to a depletion of purines. There are many similarities between AK and CK, regarding their localisation, function and physiological importance.

1.3. Heart failure

Heart failure (HF) is a common, disabling and deadly medical condition [72]. It is a complex clinical syndrome, defined as the result of any structural or functional cardiac disorder that impairs the ability of the left ventricle to fill with or eject blood to such a degree that the heart is unable to meet the demands of the body [73]. Its main manifestations are dyspnoea, fatigue and fluid retention. In a large proportion of patients with HF in the Western world, causes are coronary artery disease, hypertension and dilated cardiomyopathy. HF caused by cardiomyopathy may have an underlying genetic cause in as many as 30% of patients [74]. Additionally, valvular heart disease is a common cause of HF, although it can be caused by almost any form of cardiac disease.

Heart failure causes a huge burden in morbidity and mortality worldwide, with an estimated 750,000 patients in the United Kingdom alone, according to the British Heart Foundation. The condition is primarily a disease of the elderly, increasing progressively with age [75]. Prevalence of HF rises sharply at ~75 years of age, to between 10 and 20%, and is increasing overall due to the phenomenon of the ageing population, combined with increased success in postponing coronary events in individuals at high risk, and increased survival rates of people suffering a first event [76 77]. The outlook for patients is poor, with mortality of 50% at 4 years. In the United States, more money is spent on the diagnosis and treatment of HF than any other diagnosis, with total costs for HF in 2005 of approximately $27.9 billion. European countries spend over 2% of

their total healthcare budgets on the management of HF. The incidence of HF in the developing world is also increasing, with predictions that by 2020, deaths from cardiovascular disease will exceed deaths from infectious and parasitic diseases for the first time [78].

The treatment of HF has been dominated primarily by pharmacological therapies, including the use of angiotensin-converting enzyme inhibitors, β-blockers, angiotensin receptor blockers, hydralazine and isosorbide dinitrate, digoxin and diuretics [79]. However, HF continues to be a huge problem, and the failure of once promising new therapies such as endothelin antagonists [80] to benefit HF patients, has led to a drive to identify new therapeutic strategies for HF. Several studies have identified reduced cardiac energy levels and flux as consistent features of HF, suggesting that cardiac energetics is a promising target for HF therapy [81] [82] [83]. In particular, insulin sensitisation holds promise as a potential route for metabolic intervention in the pathogenesis of HF [81]. Research into cardiac energetics and its influence on HF continue, and metabolic modulation may lead to the amelioration of the prognosis of the disease.

1.4. The role of energetics in heart failure

The concept that the failing heart is energy starved is consistent with the observation that energy-sparing treatments for heart failure reduce morbidity and mortality, whereas energy-consuming positive inotropic agents worsen the prognosis. Essentially, nourishing the failing heart properly can lead to recovery and an improvement in ability for work in the long term. The concept is supported by the findings of numerous studies into altered high-energy phosphate metabolism in animal and human hearts. [84] [85] [86]. The involvement of Cr in this "energy-starvation" hypothesis was first suggested in 1939, with the observation by Herrmann and

Decherd that the failing myocardium contains a significantly reduced Cr content. The depletion of PCr and free Cr levels in the heart has been described in a variety of animal models of heart failure, including aortic banding [87], and heredity models [88 89].

Creatine and the phosphocreatine shuttle play a key role in maintaining ATP levels, and it is established that the phosphocreatine shuttle acts as a buffer for ATP levels during times of high energy demand. Under such conditions, PCr levels decrease while ATP supplies are maintained owing to the buffering action of CK, although these also fall, albeit to a lesser degree, and in the later stages of heart failure. These changes lead to a decrease in the PCr / ATP ratio, which has been identified as a predictor of mortality in patients with dilated cardiomyopathy (DCM), with an established relationship between the PCr / ATP ratio and disease severity [90]. It has been shown that effective treatment of DCM, leading to clinical recompensation, can partially restore the PCr / ATP ratio [91]. The down-regulation of CrT function is a causal factor in the reduction of PCr and total Cr in heart failure. It has been stated that this is due to a reduction in CrT protein content [92 93], though these claims have to be interpreted with caution, due to the use of an unreliable anti-CrT antibody later found to cross-react with pyruvate dehydrogenase [40]. The question is whether this reduction of Cr uptake capacity in HF is adaptive or pathophysiological. A pathophysiological mechanism would be caused by a reduction of total Cr content. This would decrease the rate and extent of intracellular ATP transfer via the CK reaction, so reducing energy availability at the myofibrils. Conversely, an adaptive mechanism in response to decreasing PCr levels would reduce free Cr, thereby preventing a fall in the free energy change (ΔG) of ATP hydrolysis. This would maintain contractile function [92].

In addition to the loss of PCr and total Cr in the failing myocardium, there is an associated decrease in the total tissue purine content. The decline in total adenine nucleotides (TAN)

contributes to the 30-40% reduction in [ATP] sometimes observed in severe cases of HF in the human heart, as well as animal models [83]. A reduction of the TAN pool of ~30% has been classed as a 'tipping point' in the progression of myocardial dysfunction, beyond which a severely compromised energy state is reached [94 82].

1.5. Models of altered cardiac phosphotransfer

Cardiac biology has benefited greatly from the ability to generate genetically altered models in the mouse. These models have enabled insight into human heart failure in a way not possible with other experimental systems, allowing the manipulation of genes whose functions underlie mammalian cardiovascular function. The mouse is widely used, as despite its disadvantages, it has clear benefits for genetic studies. Short gestation and generally rapid breeding rates, combined with a well-characterised genome mean that the creation of murine genetic models has become a widespread method for the study of disease, including studies on deranged energetics of heart failure and on the role of Cr. Two conceptually different approaches exist for these studies in mouse models; the mutagenesis-driven, non-directed approach, and the disease-driven, directed approach [95]. The directed approach can itself be broken down into both gain-of-function, and loss-of-function approaches. Variations of both these approaches have been employed in the study of the CrT [96 97].

Loss-of-function models using targeted gene inactivation typically involve the creation of a 'knockout' (KO), where gene inactivation is driven by targeted homologous recombination. This approach has been used to create KO models of AGAT, GAMT [98] and CrT [96]. Additionally, The European Conditional Mouse Mutagenesis Program (EUCOMM) is currently working on the creation of a CrT knockout mouse model through the International Knockout Mouse Consortium

(IKMC). This could prove highly beneficial, as a previous CrT KO model had limitations (discussed later).

The gain-of-function model can be created by several different means, which are outlined in greater detail in Chapter 3. Random integration is one of these approaches, and has been widely used for 30 years [99]. This approach involves the injection of cDNA encoding the protein of interest into a one-cell stage embryo. Following random integration into the genome, the transgene is expressed, either ubiquitously, or in the tissue or organ of choice, depending on the choice of transgenic promoter. It was this approach that was used in our laboratory to create the cardiac-specific model of CrT overexpression [97]. The genetic models discussed below, targeting both the CrT as well as the synthesis pathway of Cr itself, have provided useful insights into the role of Cr and the CrT in myocardial energetics. Additionally, genetically-altered models affecting other aspects of cardiac metabolism, including those targeting CK, are briefly discussed.

1.5.1. Creatine transporter overexpression (CrT-OE) model

The potential of augmentation of Cr and PCr has relevance in the context of the energy-starved failing heart, where PCr and free Cr are reduced by 60-70%. CrT overexpressing mice were generated in our group using random integration transgenesis to create a mouse model that would be protected from cardiac stress through increased energy storage and transport potential [97]. In order to achieve increased Cr and PCr levels in the myocardium, a transgenic strategy was required, as oral supplementation of Cr leads to a down-regulation of the CrT, and myocardial [Cr] and [PCr] remain unchanged [31 100]. There are no known pharmacological activators of Cr uptake.

A rabbit CrT cDNA, downstream of the cardiac-specific *MLC2v* promoter, was used to drive transgenic expression of the CrT in this gain-of-function model. The strategy yielded two lines of CrT-overexpressing mice, both of which exhibited elevated Cr uptake, with up to a four-fold increase in one of the lines. The myocardial [Cr] varied between animals of the same line, which is noteworthy, as mice with higher levels of myocardial Cr (> 140 nmol / mg protein) were found to develop spontaneous left ventricular hypertrophy, dilatation and contractile dysfunction, the degree of which was proportionate to the concentration of Cr.

Further analysis of CrT-OE hearts showed that CK activity was unchanged, and [PCr] was increased, albeit to a lesser degree than [Cr]. [Pi] was unaltered, and there was a trend towards reduced levels of ATP. The resultant thermodynamic situation, created by the substantially elevated Cr levels was similar to that seen in hypertrophy and some models of heart failure [101] [102]. It was concluded that the deleterious effects of very high myocardial Cr were due to the inability of CK, in its role as a buffering system, to keep free ADP levels adequately low. Therefore, the free energy change of ATP hydrolysis (ΔG_{ATP}) was not maintained [82] [103]. This hypothesis was reinforced by the finding that there was a significant correlation between total Cr and free ADP, and between total Cr and ΔG_{ATP}. The following graphs show the relationship between the level of LV Cr and [ADP], ΔG_{ATP}, and the degree of phosphorylation in the total Cr pool.

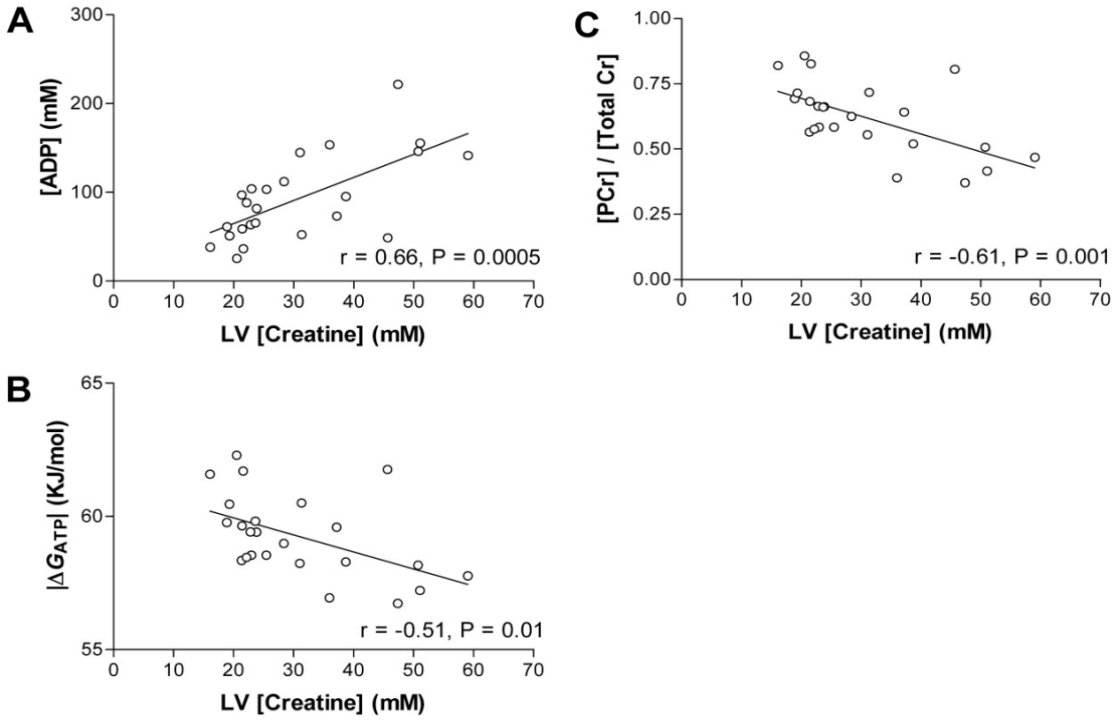


Figure 1-6. The correlations between total Cr concentration and (A) free ADP, (B) absolute values of [ΔGATP] of hydrolysis, and (C) PCr-total Cr ratio. Taken from Wallis *et al*, Circulation 2005 111:2477-2485.

The magnetic resonance (MR) images in the following figure clearly demonstrate the hypertrophy in CrT-OE mice with very high myocardial Cr, and the spectra demonstrate the increased levels of PCr in these hearts (although this is not increased proportionally to the elevation in total unphosphorylated Cr).

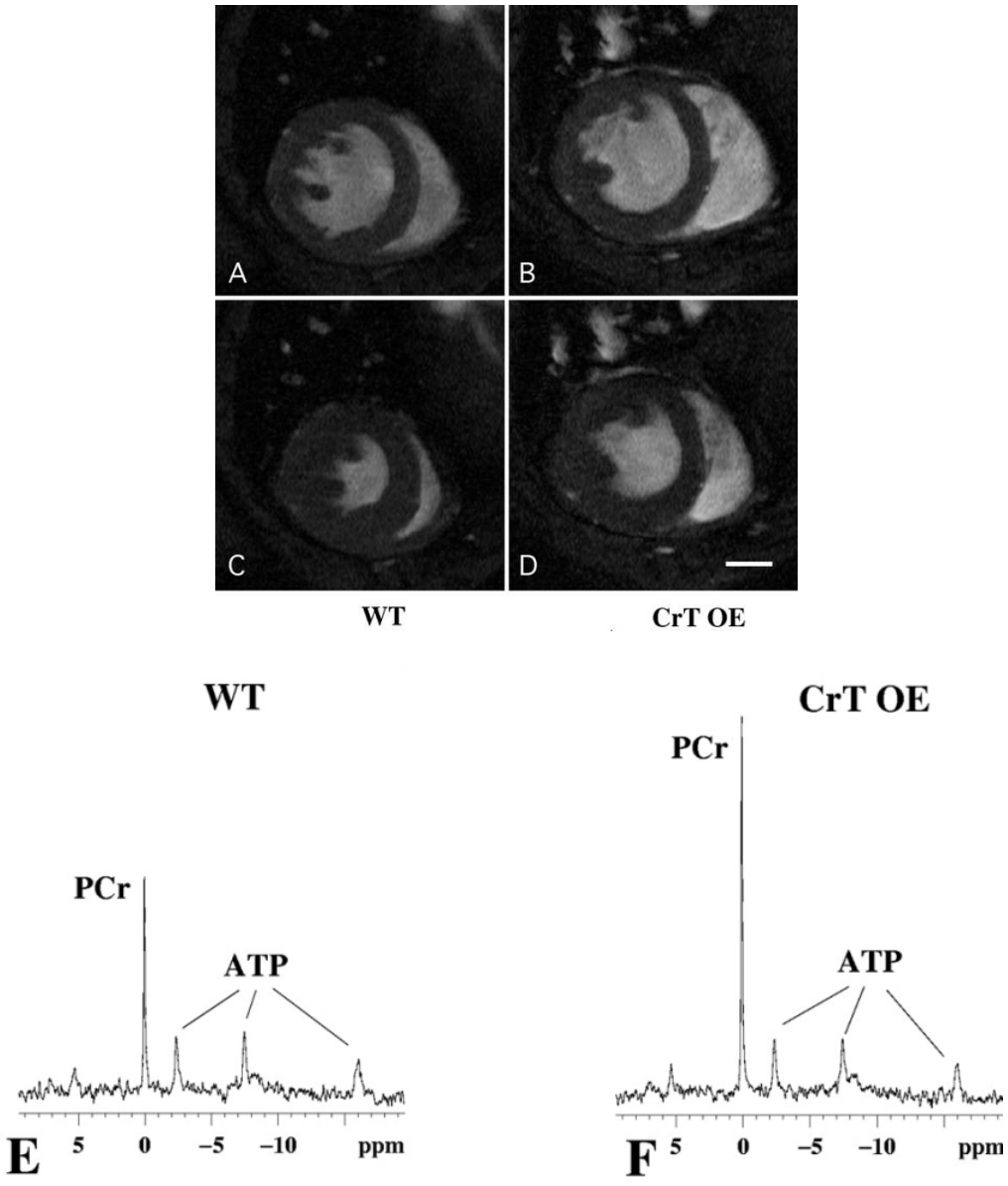


Figure 1-7. MR images and spectra comparing WT hearts to CrT-overexpressing hearts. Images are *in vivo* short-axis cine-MR from a WT mouse at end diastole (A), and end systole (C), and from a CrT-OE mouse at end diastole (B), and end systole (D). The bar represents 2 mm. Hypertrophy and reduced contractility is evident in the CrT-OE heart. Typical ^{31}P spectra from a perfused WT heart (E) and a perfused CrT-OE heart (F). Note the substantially increased PCr peak. Taken from Wallis *et al*, Circulation 2005 111:2477-2485.

A subsequent study in our group set out to establish more about the deleterious effects of very high [Cr] in these CrT-OE mice, by investigating the temporal relationship between elevated [Cr] and the onset of cardiac dysfunction, in addition to identifying potential contributory molecular mechanisms [104]. The study determined that myocardial [Cr] elevation is constant over

the first year of life, and that progressive LV dysfunction begins between 6-16 weeks of age. Whilst all CrT-OE mice had normal cardiac function in early life, the degree of elevation of [Cr] served as a predictor of the deterioration in cardiac function over 1 year. It was argued that an explanation for the observed normal cardiac function prior to 16 weeks of age could be that the phosphorylated fraction of Cr initially 'keeps up' with the increase in total Cr, thus maintaining normal ADP levels, but gradually loses the ability to keep the augmented Cr pool adequately phosphorylated. This hypothesis has not been possible to prove, due to technical issues regarding obtaining reliable spectra in 6 week-old perfused mouse hearts using ^{31}P-MRS. The study also made an interesting discovery regarding glycolytic capacity in the CrT-OE hearts. Screening for potential molecular changes that could lead to contractile dysfunction was performed using 2D difference in-gel electrophoresis (DIGE), and the most notable difference between CrT-OE and WT hearts was the down-regulation of α- and β-enolase. Enolase is a key enzyme in glycolysis, and reduction in its content has been reported in models of cardiomyopathy [105] and hypertrophy [106 107]. The extent of enolase down-regulation was found to be strongly correlated to Cr content, with higher Cr levels leading to greater decreases in enolase. This suggested a direct link between increased myocardial Cr levels and impaired glycolytic capacity in the CrT-OE model. Whilst the contribution of glycolysis to the cell's overall ATP content is generally believed to be small, there is evidence to suggest that it plays a greater role in the generation of myocardial ATP in the mouse than in other species, with glucose being favoured over fatty acids as the oxidative substrate of choice [108]. As such, glycolytically-derived ATP could be used preferentially for contraction in the mouse heart, meaning decreased glycolytic flux would be detrimental. Additional findings indicated that the protein content of the β-enolase repressor factor 1 (βERF-1), a negative regulator of β-enolase gene transcription, were elevated by 80% in CrT-OE hearts compared to WT, indicating the possibility of regulation of β-enolase at the transcriptional level. In conclusion, LV hypertrophy

and dysfunction in CrT-OE hearts is likely due to the reduced free energy change of ATP hydrolysis, combined with impaired glycolytic capacity.

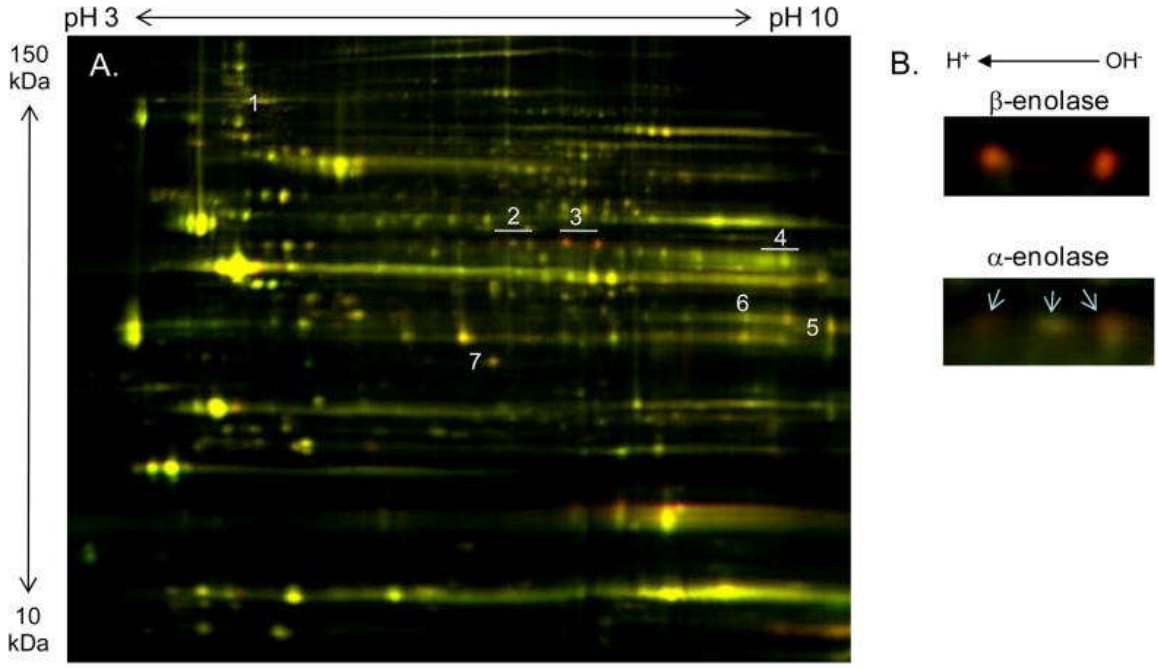


Figure 1-8 Proteomics comparison of LV tissue from a wild-type and CrT-OE heart. Panel A shows a representative 2D DIGE image comparing wild-type (labelled red, Cy3) and CrT-OE (labelled green, Cy5) myocardial protein profiles. Proteins are separated in the horizontal direction by isoelectric focusing point from pH ~3 to 10, and vertically by molecular weight from ~150 to 10kD. Panel B shows a magnification of the changes to β-enolase and α-enolase. In addition to a decrease in enolase content in CrT-OE hearts, protein elements of both β-enolase and α-enolase undergo acidic isoelectric shifts, which suggest that a post-translational modification may be acting on these proteins. Taken from Phillips *et al*, J Mol Cell Cardiol 2010; 48(4):582-590.

Most recently, research in our laboratory has established clearly that not only is *moderate* myocardial Cr elevation safe, but it is also beneficial in certain conditions (unpublished data). The second of the 2 lines of CrT-OE mice was chosen for a series of experiments, as it exhibits a lower level of elevation in [Cr] than the line previously investigated in 2005. On the basis of previous findings [97] [104], a 'cut-off' of 140 nmol / mg protein was chosen, as above this level, which is double the level seen in WT myocardium, dysfunction in the heart becomes apparent. It was demonstrated that this level of Cr elevation did not result in LV hypertrophy even in mice up to 18 months of age. Moderately elevated Cr was shown to reduce myocardial injury following ischaemia and reperfusion *in vivo*, with a 27% reduction in myocardial necrosis

compared to WT controls, and Cr levels inversely correlated with infarct size, suggesting dose-dependent protection. Additionally, this moderate elevation in Cr improved functional recovery following ischaemia / reperfusion injury *ex vivo*. The CrT-OE hearts showed a slower loss of function following the onset of ischaemia, and their return of function following reperfusion was more rapid and complete. However, in a model of HF (coronary artery ligation), CrT-OE mice showed no benefit over WT mice, with no difference between the groups in the degree of LV remodelling and dysfunction, and no difference in survival rates.

Wu *et al* used computer modelling to simulate cellular oxygen consumption and cardiac energy metabolism as a way to elucidate more about 'energy starvation' in HF [94], and their findings regarding elevated myocardial [Cr] are interesting. The model was adapted for the study of left-ventricular hypertrophy (LVH) by varying 3 biochemical 'pools', defined as the TAN pool, the total Cr pool, and the 'total exchangeable phosphate pool' (TEP). Interestingly, the authors concluded that while minor changes in these metabolite pools have no major impact on oxidative capacity, a 'tipping point' was defined, corresponding to the ~30% reduction in TAN pool described by Ingwall and Weiss [82]. Beyond this point, the myocardium becomes severely energetically compromised. It was also predicted that the total Cr pool attains a value associated with optimal ΔG ATP_{ase} during hypertrophic remodelling. Crucially therefore, due to the simulated relationships between the 3 pools, any increases or decreases to the total Cr pool alone would lead to a diminished energetic state. The authors suggest that the reduction of the total Cr pool seen in HF is adaptive and maintains equilibrium between the pools, thus preserving the energetic state of the heart. Although, as discussed, large increases in the Cr pool have been shown to be detrimental to cardiac function [97], our recent findings outlined above demonstrate that moderate Cr elevation is not detrimental to cardiac function.

In light of the findings outlined above, a transgenic mouse model with fine control over levels of *CrT* expression would be highly beneficial. The ability to control myocardial [Cr] in a dose-dependent manner, with the added benefit of temporal control, would overcome the limitations of the previous CrT-OE model.

1.5.2. CrT knockout model

A ubiquitous knockout model of CrT was recently created in order to mimic CrT deficiency in humans [96]. Although effects on the heart were not studied, these mice were found to have reduced Cr in brain and muscle, and exhibited learning and memory deficits resembling human CrT deficiency. However, HPLC analysis in our laboratory has indicated the presence of residual Cr in most tissues of these mice, suggesting that the model may not be a complete knockout. As mentioned previously, work by EUCOMM to create a CrT KO model is ongoing.

1.5.3. β-GPA models of chronic creatine depletion

Another approach to reduce intracellular [Cr] and gain insight into the functional significance of the CK / PCr system that has been used in several studies is oral feeding with the Cr analogue β-GPA. β-GPA is a competitive inhibitor of Cr uptake (discussed previously). This strategy has been shown to reduce myocardial PCr and Cr concentrations by about 80%, and reduce the CK reaction velocity by around 1 order of magnitude [109]. Typically, this severe Cr depletion has led to reduced contractile performance in *ex-vivo* hearts [110] [111] [112], with one notable exception [113]. Neubauer *et al* performed the first *in vivo* experiments on β-GPA-fed rats, in intact heart [109]. Contrary to the majority of results obtained from *ex-vivo* methods, they found that *in vivo* cardiac haemodynamics measurements, both at rest and during acute volume loading, showed no change after β-GPA feeding. They concluded that, in spite of the 90% reduction in CK reaction

velocity, normal haemodynamics are maintained *in vivo*, through cardiac and / or humoral compensatory mechanisms. However, it was found that chronic β-GPA feeding led to structural left ventricular dilatation.

There are clear disadvantages to the use of a competitive inhibitor such as β-GPA for a prolonged period, such as potential toxicity. It was previously identified that long β-GPA feeding durations, beginning at a young age, can lead to substantial cardiac hypertrophy [112].

1.5.4. Loss-of-function models targeting the synthesis of creatine

1.5.4.1. GAMT knockout

Mouse models have been created targeting the two enzymes (outlined previously) involved in the synthesis of Cr. The first of these is the guanidinoacetate-*N*-methyltransferase (GAMT) knockout, the study of which gives an insight into the effects of a substantially impaired CK / PCr system in the heart [98]. The ablation of this gene leads to reduced global Cr concentrations, with Cr only available through the diet, as *de novo* synthesis is not possible. The precursor of Cr, guanidinoacetate (GAA) was found to accumulate in the tissues of these mice. GAA can be phosphorylated, and although it has an efficiency 100-times lower than that of PCr, it enables the partial maintenance of high-energy phosphate stores. Our group demonstrated that these knockout mice do not develop significant LV hypertrophy, and exhibit normal cardiac function under 'baseline', unstressed conditions, indicating that ~1% of CK flux is adequate in these circumstances [114]. However, during periods of acute stress, an abnormal phenotype became apparent, with lowered resistance to ischaemia / reperfusion injury, and reduced contractile reserve with inotropic stimulation.

1.5.4.2. AGAT knockout

The arginine:glycine amidinotransferase (AGAT)-knockout mouse also lacks Cr due to the ablation of the first enzyme in the Cr synthesis pathway (AGAT). Unlike GAMT KO mice, these mice do not accumulate GAA. Interestingly, while AGAT hearts showed a complete loss of Cr and PCr, ATP levels were unaltered and Pi levels were increased. *Ex-vivo* function was found to be normal.

1.5.5. Other models targeting cardiac phosphotransfer

1.5.5.1. Creatine kinase-deficient mice

Mice with deletion of the muscle isoform (M-CK$^{-/-}$) [115] and sarcomeric mitochondrial (Mt-CK$^{-/-}$) [116] isoform of CK have been described, as well as a combined double-knockout (M/Mt-CK$^{-/-}$) [117]. M-CK$^{-/-}$ mice showed at most a mild cardiac phenotype [118], whereas studies on hypertrophy in Mt-CK$^{-/-}$ and M/Mt-CK$^{-/-}$ mice have produced conflicting results. While some studies failed to detect hypertrophy in either the single- or double-knockout mice [51 119 120 121 122], others reported the presence of cardiac hypertrophy at levels of 13-72% compared to WT in both strains [123 124 125 118]. Reasons for the inconsistency were thought to be due either to differences in the age and sex ratio, or due to the effect of genetic drift, as the knockout mice were on a mixed genetic background. Work performed by our group confirmed the influence of genetic background on these models, showing that Mt-CK$^{-/-}$ mice do not develop LV hypertrophy or dysfunction up to 1 year when on a pure C57BL/6 background [126]. These results contrasted with previous findings for the same model, but on a mixed 129Sv and C57BL/6 background, where LV mass was shown to be 35-72% higher than controls at 41 weeks of age [123]. The study showed increases in MM-CK activity and an increase in mitochondrial volume, and it is possible that these changes are adaptations that contribute to the lack of phenotype observed in this case which has been

reported in other studies. Studies of cardiac function in isolated perfused working heart models of Mt-CK$^{-/-}$ [119] and M/Mt-CK$^{-/-}$ [51] [125] have shown no functional change at baseline, during increased work, or during recovery, although M/Mt-CK$^{-/-}$ mice have been shown to have decreased myocardial perfusion and reduced maximal contraction velocity [123] [127], in addition to impaired recovery from ischaemia / reperfusion [122]. Mt-CK$^{-/-}$ and M/Mt-CK$^{-/-}$ mice have both been shown to be deficient in PCr [119] [51], although this is not the case in M-CK$^{-/-}$ mice. The stronger phenotype of Mt-CK$^{-/-}$ and M/Mt-CK$^{-/-}$ knockouts compared to M-CK$^{-/-}$ suggests that it is the Mt-CK isoform that is crucial for normal high energy-phosphate metabolism in the heart. A recent study by Dzeja *et al* aimed to establish more about the compensatory mechanisms involved in the M-CK$^{-/-}$ and M/Mt-CK$^{-/-}$ mice [128]. Hearts from M-CK$^{-/-}$ mice were shown to have increased glucose-6-phosphate (G-6-P) turnover, glucose utilisation and Pi compartmentation, with normal ATP γ-phosphoryl dynamics. They showed a lower PCr turnover. The changes observed in M/Mt-CK$^{-/-}$ mice indicated a redistribution of flux through AK, with increased dynamics of β-phosphoryls of ADP / ATP, G-6-P and γ- / β- phosphoryls of GTP. Additionally, they showed diminished PCr turnover and total phosphotransfer capacity. It was suggested that these rearrangements in phosphotransfer and substrate utilisation networks provide a compensatory mechanism for the genetically-induced CK deficiency.

1.6. Research aims and objectives

Deranged high-energy phosphate metabolism is associated with contractile dysfunction in the heart, in either a causal or consequential manner. A key factor in this deranged energy metabolism is the depletion of myocardial creatine. This thesis aims to create a temporal, inducible mouse model of myocardial creatine transporter overexpression, achieving increased levels of intracellular Cr within the cardiac tissue. This strategy will allow further investigation

into the effects of restoring Cr levels in acute, ischaemic conditions, as well as in chronic conditions of HF. Strategies targeted at modulating myocardial Cr levels through other means are also pursued, and these are outlined below.

This project aims at elucidating deranged energy metabolism by the following objectives:

(a) Increasing intracellular Cr levels and consequently CrT activity *in vivo*.

It is known that greatly elevated levels of myocardial Cr lead to spontaneous hypertrophy and HF [97]. In order to gain finer control over the level and onset of overexpression of the CrT, a new mouse model is created. The aims are to overcome potential developmental changes associated with prolonged supra-normal myocardial Cr levels, and also to enable the induction of CrT overexpression when required, that is following the depletion of Cr due to HF. It is hypothesised that such fine control over the CrT will be beneficial in HF, allowing improved cardiac function.

(b) Using an *in vitro* system of CrT overexpression to study regulation of CrT by known signalling pathways.

Based on previous suggestions that the CrT is regulated by kinases downstream of the IGF-1R, this study aims to examine the involvement of such signalling molecules in the regulation of CrT function. The identification of compounds and hormones involved in CrT regulation could lead to a greater understanding of the mechanisms involved in the down-regulation of CrT activity in HF, whilst potentially identifying novel ways of modulating Cr uptake.

(c) Investigating how post-translational modifications interfere with CrT activity.

Detection of PTMs present in the CrT, and their effects on its function, will be undertaken. There is still a great deal to be discovered regarding the structure and function of the CrT, in particular the role of putative glycosylation and phosphorylation sites. Further studies into its structure, using mass spectrometry on protein purified by immunoprecipitation from a cell line

over-expressing the CrT will allow the identification of PTMs, and also the confirmation of the presence of CrT species of various sizes, a challenging issue presented in previous studies.

(d) Studying the involvement of highly conserved consensus sites of the CrT 5'UTR on CrT activity.

A strategy involving RNA-interference to knock-down a transcription factor associated with the CrT and other members of the SLC6 family of transporters will be used as a preliminary step towards a greater understanding of the regulatory involvement of the CrT promoter region.

Chapter 2. General Materials and Methods

2.1. Introduction

This chapter outlines the general materials and methods used throughout the experiments undertaken in this thesis. Where appropriate, chapter-specific methods are outlined in the relevant results chapters.

2.1.1. Software

Microsoft Office 2007 was used for word-processing, spreadsheet analysis and figure preparation unless stated otherwise. GraphPad Prism version 5.0 was used for the preparation of all charts and graphs, and the associated statistical calculations. Endnote X4 was used for the compilation of the bibliography. Vector NTI 10.0 (Invitrogen, UK) and ApE v2.0 (A plasmid Editor, M. Wayne Davies) were used in the design and analysis of the constructs described in Chapter 3, and in some cases for primer design. All other primers were designed using NCBI Primer-BLAST. The online databases NCBI BLAST, Ensembl and UCSC Genome Browser were also used to access genomic information.

2.1.2. Chemical suppliers

Unless noted otherwise, chemicals were sourced from Sigma-Aldrich. The composition of key solutions is listed in Appendix II.

2.2. Cell culture, cell lines and transfections

2.2.1. Cell lines

2.2.1.1. NIH 3T3 Tet-Off

Stably-transfected NIH 3T3 fibroblasts (a murine embryonic fibroblast cell line) expressing the tetracycline transactivator (tTA) protein, were a gift from Dr. Nick Warwick, University of Oxford.

2.2.1.2. 3T3-CrT-HA

Stably-transfected NIH 3T3 Tet-Off fibroblasts, expressing the creatine transporter under the control of the TRE (tetracycline response element).

2.2.1.3. HEK293T

A highly transfectable derivative of the human embryonic kidney 293 cell line, incorporating the temperature-sensitive gene for SV40 T-antigen. These were acquired at low passage number from the American Type Culture Collection (ATCC).

2.2.1.4. HL-1 Cardiomyocytes

HL-1 cells were provided by Dr. W. C. Claycomb, Louisiana State University Health Science Center, New Orleans, LA, USA. They are derived from AT-1 cells (mouse cardiomyocyte tumour) and are able to maintain the differentiated cardiomyocytes phenotype and contractile activity *in vitro* through indefinite passages [129] [130].

2.2.2. General maintenance of cell lines

2.2.2.1. NIH 3T3 Tet-off, 3T3-CrT-HA and HEK293T cells

NIH 3T3 and CrT-HA Tet-Off cells were maintained in Dulbecco's modified Eagle's medium (DMEM) (Sigma), supplemented with 10 % FBS (Sigma), 100 µg/mL penicillin (Sigma), 100

µg/mL streptomycin (Sigma) and 2 mM l-glutamine (Sigma). Stably transfected NIH 3T3 Tet-Off fibroblasts were also supplemented with G418 (Geneticin, 200 µg/mL) (Roche) and 3T3-CrT-HA cells were supplemented additionally with puromycin, 2 µg/mL. All cultures were grown in a 5 % CO_2 humidified atmosphere at 37 ^{o}C.

Passaging of cells was performed using standard methods, with Trypsin-EDTA (Lonza, Switzerland). Media was removed from the culture vessel, which was then washed twice with sterile 1x PBS (Lonza, Switzerland). The cells were then incubated in Trypsin-EDTA for 5 min, and the flask agitated vigorously to ensure removal of the monolayer of cells from the flasks. The trypsin-EDTA was inactivated by the addition of an equal volume of complete medium, and the cells were pelleted by centrifugation for 5 min at 1000 x g. The resulting pellet was resuspended in an appropriate volume of medium.

Cells grown for use in uptake assays, or profiling of phosphorylation or glycosylation of the CrT were grown in phenol red-free media (PAA Labs) using charcoal-stripped FBS (Sigma, UK). When these cells were harvested, trypsin was inhibited using an equal volume of 0.25 mg/mL soybean trypsin inhibitor (Invitrogen).

2.2.2.2. HL-1 cardiomyocytes

HL-1 cells were grown in gelatine-fibronectin (Sigma) coated flasks containing Claycomb medium (JRH Biosciences, Sigma) supplemented with 10% FBS (Lot #027K8414, Sigma), 100 U/mL penicillin, 100 µg/mL streptomycin (Sigma), 2 mM L-Glutamine (Sigma) and 0.1 mM noradrenaline (stock made up in 30 mM ascorbic acid, Sigma). HL-1 cultures were fed with supplemented Claycomb medium every weekday, with the addition of excess media over the weekend.

HL-1 cells were also grown in a 5 % CO_2 humidified atmosphere at 37 ^{o}C. Passaging of HL-1 cells was performed using a different protocol, as recommended by Dr. Claycomb. Cells were detached by trypsinisation only after reaching full confluence. Trypsin was inhibited by addition of an equal volume of 0.25 mg/mL soybean trypsin inhibitor (Invitrogen) before adding wash medium (Claycomb medium supplemented with 5% FBS and penicillin/streptomycin only). Cells were then centrifuged at 500 g for 5 min before resuspension in an appropriate volume of Claycomb medium and seeded into gelatine-/fibronectin-coated flasks or plates.

2.2.3. Transient cell transfections

Plasmid DNA for transfection was purified from *E.coli* using an endotoxin-free Maxi Prep Kit (Qiagen). Transfections were carried out in 6-well tissue culture plates that had been seeded 24 hours earlier with 1 x 10^5 cells / well. Culture medium was changed with fresh serum-free medium 4 hours prior to transfection. Cells were transfected with 1 µg total DNA in 100 µL OptiMEM + Glutamax (Invitrogen) and 3 µL Genejuice transfection reagent (Merck Biosciences, UK) according to the manufacturer's instructions. The following day medium was changed to complete medium in the presence or absence of doxycycline (1 µg / mL). Transfection efficiency was routinely estimated by transfection with the control plasmid containing a GFP reporter.

2.2.4. Stable cell transfections

For the generation of stable cell lines, puromycin was added to the culture medium (2 µg/mL) 48 h following transfection. Colonies resistant to puromycin were isolated and pipetted into 12 well tissue culture plates containing 200 µL selection media for selection, growth and screening by western blotting. Where the transfected plasmid did not already contain an antibiotic

resistance cassette (e.g. pWTT1), stable lines were generated by co-transfection of the plasmid of interest at a 1:1 ratio with pPUR (Clontech) carrying a puromycin resistance cassette/gene. Doxycycline (1 µg/mL) was added to the culture medium of 3T3-Tet-Off cells when examining the response of the tetracycline inducible system.

2.2.5. RNA isolation from adherent cells *in vitro*

Total RNA was isolated from cells using the RNeasy Mini Kit (Qiagen). Cells in tissue culture plates were rinsed twice with PBS before direct lysis in 300 µL buffer RLT (lysis buffer). Cells grown in cell-culture flasks were rinsed twice with PBS, trypsinised and centrifuged at 300 g for five min before lysis in buffer RLT. The concentration of samples was quantified using a Nanodrop (Nanodrop Technologies, USA). Samples were then processed according to the manufacturer's instructions.

2.2.6. Storage of cells

Cells to be stored were trypsinised, mixed with an equal volume of serum-containing media and pelletted. The pellet was resuspended in 1 mL of 95% FBS and 5% DMSO and transferred to a cryovial. This was frozen in a beaker containing ethanol at -80^{o} C then transferred to a liquid nitrogen tank for long-term storage.

2.2.7. Seeding 6- and 24-well tissue culture plates for creatine uptake assays and transfections

Cells were trypsinised using standard methods and counted in trypan blue using a Neubauer Haemocytometer. 6-well plates were seeded with 2x10^{5} CrT-HA Tet-Off cells 24 h before the

uptake assay was performed and 24-well plates were seeded with $0.2x10^5$ cells. Where HL-1 cells were used, wells were seeded with double these numbers.

2.3 Radiolabelled-creatine uptake assays

Cells were seeded into 6- or 24- well tissue culture plates (Greiner Bio One, UK) and grown to 70 – 80% confluence in complete DMEM, supplemented with the relevant antibiotics. Media was aspirated from the wells and replaced with creatine-containing media (typically 250 µM), 'spiked' with a minimal amount of ^{14}C creatine. The plates were then incubated for 1 h at 37^oC in a CO_2 incubator. Following incubation, the radioactive medium was removed, and the wells washed 3 times in 2 mL (6- well plates) or 1 mL (24- well plates) PBS. Cells were then permeabilised in 0.5 mL (6- well plates) or 0.25 mL (24- well plates) PBS containing 0.5% Triton-X 100, scraped and aspirated. This step was repeated and the resulting lysate was incubated in 10 volumes of scintillation cocktail (Fluoransafe XE, BDH) in the dark at RT for 1 h. Samples were then analysed in a scintillation counter (Beckman LS 6500, Beckman, USA) against standards containing known quantities of 'spiked' media. The values were compared to those of the 'spiked' media and the uptake levels determined, expressed as nmol Cr / well / h.

Where the effects of small molecules on the activity of the CrT were being investigated, compounds were added to the media 1 h before the start of the uptake assay, and also included during the assay. Where the influence of hormones was being studied, cells were incubated in the presence of the compounds in question for 48 h prior to the start of the uptake assay. Cells were also incubated in phenol red-free media (PAA Labs) and charcoal-stripped FBS (Sigma), as outlined previously.

2.4 Immunofluorescence microscopy and immunocytochemistry

Cells were grown in the presence or absence of doxycycline to ~ 60% confluence on Lab-Tek cell chamber slides (Nunc). Medium was removed from the chambers, which were washed in PBS before fixation in 4% paraformaldehyde in PBS for 20 min at RT. Antigen retrieval was performed according to the method of Hanson *et al* (University of Florida) by submerging the coverslips in 100 mM tris pH 9.5, 5% urea at 95° C. Slides were rinsed in PBS and permeabilised in 0.5% Triton X-100 for 10 min at RT. Non-specific antibody binding was blocked by incubating the slides in 10% swine serum for 30 min at RT (this and all subsequent solutions prepared in 0.1% Triton X-100 in PBS). Slides were incubated for 2 h in the appropriate primary antibody before washing in PBS (3 times for 5 min): rat anti-HA (Roche, Germany), rabbit anti-CrT or anti Na^+ K^+-ATPase (Abcam, UK). Slides were then incubated with secondary antibodies for 1 h at RT and washed in PBS (3 times for 15 min). The fluorescent secondary antibodies were goat anti-rat-Texas red IgG (Vector Labs), goat anti-mouse Alexa-488 IgG (Invitrogen), and swine anti-rabbit TRITC (Dako). All incubation steps were performed in a humidified chamber. Slides were mounted in Vectashield Mounting Medium with DAPI (Vector Labs, USA). Immunofluorescence microscopy was performed on a Zeiss LSM510 META confocal imaging system containing blue diode (405 nm), argon (458, 477, 488, 504 nm), Helium-Neon (He-Ne) 543 nm and He-Ne 633 nm lasers.

2.5 Animal tissues

2.5.1. Mice

Mice were kept in specific pathogen-free conditions in individually ventilated cages (Techniplast) with a 12 h light-dark cycle and controlled temperature (20 ^{o}- 22 ^{o}C), and fed

standard chow and water *ad libitum* unless specified otherwise. Experiments were approved by the institutional ethical review committee and conform to the Guide for the Care and Use of Laboratory Animals published by the US National Institutes of Health (NIH Publication No. 85-23, revised 1996) as well as the UK Home Office Animals (Scientific Procedures) Act 1986.

2.5.2 Harvesting of cardiac tissue

Mice were sacrificed by cervical dislocation. Hearts were excised and exsanguinated in heparinised saline solution (0.9% NaCl, 0.5% heparin sulphate). The chambers of the hearts were separated, and snap-frozen in liquid nitrogen. Tissue was stored at -80 ^{o}C. Frozen samples were powdered on dry ice with a percussion homogeniser.

2.5.3.Nucleic acid extraction

2.5.3.1.Purification of genomic mouse DNA from ear biopsy

Ear biopsies were digested in 500 µL lysis buffer (100 mM EDTA, 50 mM Tris-HCl (pH 8.0), 1% SDS, 200 mM NaCl) supplemented with 3.3 µL Proteinase K (20 mg / mL). Samples were incubated overnight at 55 ^{o}C and vortexed briefly. DNA was further purified by isopropanol / ethanol precipitation. 600 µL isopropanol was added to each lysate, mixed thoroughly by inversion and centrifuged at 13,000 rpm for 10 min at RT in a bench-top microcentrifuge. The supernatant was discarded, and the pellet washed and re- centrifuged in 500 µL 70% ethanol for 5 min. Supernatants were discarded, and the DNA pellet was air-dried at RT for 30 min. 300 µL T0.1E was added, and the pellets were allowed to resuspend overnight at RT.

2.5.3.2.Purification of genomic mouse DNA from tail biopsy

Approx 0.5 cm-long tail biopsies were digested in 500 µL lysis buffer (5 mM EDTA, 100 mM Tris-HCl (pH 8.5), 0.5% Tween-20, 200 mM NaCl) supplemented with 1 mg/mL Proteinase K. Samples were incubated overnight at 55 ^{o}C, then centrifuged at 13,000 rpm for 2 min at RT. 500 µL isopropanol was added to each supernatant, mixed by inversion, and allowed to stand at RT for 30 min. Samples were then centrifuged at 13,000 rpm for 2 min at RT. The supernatant was discarded, and the DNA pellet was washed and re- centrifuged in 500 µL of 70% ethanol. Supernatants were discarded, and the pellet was allowed to air-dry at RT for 30 min. DNA was resuspended in 100 µL TE overnight, at RT.

2.5.3.3.RNA isolation from animal tissue

For isolation of RNA from tissue, 10 - 20 mg powdered frozen samples were added to 1 mL of Trizol reagent (Invitrogen) and disrupted by passing through a 20 gauge needle 5 - 10 times. The resulting homogenate was centrifuged at 12,000 *x g* for 10 min at 4 ^{o}C. The cleared homogenate was transferred to a fresh tube and 0.2 mL of chloroform was added. The solution was then agitated vigorously for 15 sec and incubated at RT for 2 - 3 min, before centrifugation at 12,000 *x g* for 15 min at 4 ^{o}C. The colourless upper aqueous phase was removed, and transferred to a fresh tube. RNA isolation from this aqueous phase continued utilising the RNeasy Mini Kit (Qiagen), according to the manufacturer's instructions. On-column DNase digestion with RNase-Free DNase (Qiagen) was routinely performed for all samples to eliminate potential genomic DNA contamination. Total RNA was eluted in 30 µL RNase-free water. RNA concentration and purity was determined using a Nanodrop ND-1000 Spectrophotometer (Nanodrop Technologies). RNA was deemed to be of a sufficient quality if its A_{260} : A_{280} ratio was in the range of 1.9 - 2.1. A representative number of RNA samples from each batch were run on a non-denaturing agarose gel to ensure RNA purity.

2.6. Polymerase chain Reaction (PCR)

2.6.1. Real-time quantitative PCR (qRT-PCR)

2.6.1.1. One-step qRT-PCR

cDNA synthesis and PCR amplification from 4 ng total RNA was performed in a single step using the Quantitect SYBR Green RT-PCR Kit (Qiagen). Quantitative RT-PCR reactions were carried out in triplicate in a Corbett Rotorgene 3000 (Qiagen). Reactions (10 µL) contained 2 µL template RNA, 5 µL 2 x Quantitect SYBR Green RT-PCR Master Mix, 0.5 µM forward and reverse primers, and 0.1 µL Quantitect RT mix. Primers are listed below. The cycling conditions comprised 30 min of reverse transcription at 50^{o} C, then 15 min polymerase activation at 95 ^{o}C followed by 40 cycles of 95^{o} C for 15 s, 55^{o} C for 20 s, 72^{o} C for 20 s. Finally, upon completion of cycling, PCR products were exposed to a hold at 60^{o} C for 15 s, then a temperature gradient (from 60^{o} C to 90^{o} C) for melting curve analysis and confirmation of a specific product.

2.6.1.2. Quantification of qRT-PCR results

For each sample, the cycling threshold (C_t) value (the selected threshold at which the fluorescence intensity of the reaction is in the log-linear phase of amplification) was fitted to a standard curve consisting of a 5 log serial dilution (in triplicate) of stock pooled RNA, to determine the starting amount of template. Rotor-Gene 6.1 software was used for sample analysis and quantification. The standard curve method was used for relative quantification, and results were normalised to the constitutive reference gene 36B4 (acidic ribosomal phosphoprotein P0, Primer Bank ID 6671569a1). [131 132].

2.6.2. Polymerase Chain Reaction (PCR) of genomic or plasmid DNA

PCR of plasmid or genomic DNA was performed using BioTaq DNA polymerase, Immolase (Bioline) or Phusion polymerase (Finnzymes, NEB). A typical 50 µL reaction included 50-100 ng genomic DNA, or 10 ng plasmid DNA, 200 µM of each dNTP (dATP, dCTP, dGTP and

dTTP), 0.5 µM of each primer, 5 µL of 10x reaction buffer, 1-2 mM $MgCl_2$ and 1 U Taq polymerase. DNA templates were initially denatured by heating the reaction to 96-98 ^{o}C for 2 min. The reaction mixture was then subjected to 30 thermo-cycles of: 94 ^{o}C for 1 min (denaturation), 67 ^{o}C for 1 min (annealing), 72 ^{o}C for 2 min (extension). This was followed by a final extension of 72 ^{o}C for 10 min. Final products were analysed by agarose gel electrophoresis. PCR primers are listed later, along with specific reaction mix and thermal cycler conditions.

2.6.2.1. PCR primers and probes

Name	**Sequence**
Opt rtTA-F	5'- CTG GGT TGC GTG TTG GAA GAT C -3'
Opt rtTA-R	5'- GTG GGA G\T CGA GCA GGC CCT CG -3'

Table 2-1. Genotyping primers for rtTA mice.

Name	**Sequence**
WTT1-F1	5'- CGT GTA CTA CAA GCC GCT GGT -3'
WTT1-R1	5'- GGT GGC AGG TAT TAG GGA TAA TGC -3'

Table 2-2. Genotyping primers for RCT mice.

N.B. ICT double transgenics were genotyped using a duplex reaction, combining the rtTA and WTT1 primers.

Name	**Sequence**
LC1-F	5'- TTA CAG ATG ATA TCG AGG -3'
LC1-R	5'- TAA CCC AGT AGA TCC AGA GG -3'

Table 2-3. Genotyping primers for luciferase mice.

Name	Sequence
(ApoB F) oIMR1544	5'- CAC GTG GGC TCC AGC ATT -3'
(ApoB R) oIMR1545	5'- TCA CCA GTC ATT TCT GCC TTT G -3'
rtTA-F1	5'- AGC TCC ACC TGG ACG GCG AG -3'
rtTA-R1	5'- ATC GAA ATC CGT TCC AGG GCG T -3'
(ApoB probe) oIMR200107	5'- JOE - CCA ATG GTC GGG CAC TGC TCA A-BHQ1 -3'
rtTA probe	5'- FAM-GCA TGG GCC ATG GCC ACG-TAM -3'

Table 2-4. Primers and dual-labelled fluorogenic probes for rtTA allelic discrimination

Gene	Reference	Sequence
36B4	[131]	(F) 5'- AGA TTC GGG ATA TGC TGT TGG C -3' (R) 5'- TCG GGT CCT AGA CCA GTG TTC -3'
CrT com2-F		5'- ACT GTG TGG AGA TCT TCC GC -3'
CrT com2-R		5'- CAG CAA GCT GGT CAC ATG TG- 3'
Opt rtTA-F3		5'- AAA TGT GAA AGT GGG TCC GC- 3'
Opt rtTA-R3		5'- AGA AAG GAC AGG CGT GGA GC- 3'
HEY 1-F		5'- TGC TGC ACA CTG CAG GAG GG- 3'
HEY 1-R		5'- AGA CCA GGC GAA CGC GAA GC- 3'
Cyclophilin B (mouse)-F		5'- AGC AAG TTC CAT CGT GTC ATC AAG G- 3'
Cyclophilin B (mouse)-R		5'- GCC ATG CTC ACC CAG CCA GG- 3'

Table 2-5. Primers used for RT-qPCR

2.7 Southern gel preparation

Transgene copy number was determined by Southern blot, using a ^{32}P-labelled probe [133]. Genomic DNA was isolated from 0.5 cm of a mouse tail and incubated for 16 hours at 37^{o} C

with an appropriate restriction endonuclease. Ten µg digested DNA was loaded to each lane of a 0.8% TAE agarose gel (without ethidium bromide) and separated overnight at 30 V. For construction of a standard curve, serial dilutions of known quantities of transgene plasmid DNA were added to wild-type samples. Gels were stained with 0.5 µg/mL ethidium bromide for 30 min before visualisation to evaluate success of restriction digestion. Gels were rinsed in dH_2O before and after depurination (0.25 M HCl for 30 min, with gentle rocking), denaturation (1.5 M NaCl, 0.5 M NaOH, for 20 min x 2) and neutralisation (1.5 M NaCl, 0.5 M Tris-HCl pH 7.0, for 20 min x 2). DNA was transferred overnight to a positively charged nylon membrane (Amersham Hybond N+, GE Healthcare, UK) in 20X SSC. DNA was immobilised by drying the membrane in an 80^{o}C oven for 30 min before UV cross-linking at 70,000 µJ/cm^2. Membranes were stored at RT, between sheets of 3MM for later hybridisation.

2.7.1. Southern hybridisation

The membrane was wet in 6X SSC before pre-hybridisation in modified Gilbert and Church buffer for 1 h at 68^{o}C. The selected oligonucleotide probe was ^{32}P-labelled using the Rediprime II random prime labelling system (GE Healthcare, UK) and purified using Sephadex G50 spin columns (mini Quick Spin Columns, Roche, Germany) to remove unincorporated ^{32}P. The labelled probe was added to the buffer and hybridised overnight at 68^{o}C. The following day the membrane was rinsed briefly in low stringency wash buffer before successive washes in low/medium/high stringency solutions (each 2 x 5 min), listed in Appendix II. Blot radioactivity levels were monitored at each stage with a Geiger counter to determine if further washing was needed.

Membranes were covered in plastic wrap and exposed to a phosphorscreen for 6 h. The phosphorscreen was scanned by a Packard Cyclone phosphorimager and images were analysed using Optiquant software (Perkin Elmer, USA). Membranes were also exposed to Hyperfilm ECL (GE Healthcare, UK) for 48 h at -80^{o}C before film development.

2.8 DNA Manipulation and Molecular Cloning

2.8.1 Plasmid DNA

Plasmids used are listed below:

pPUR	(Clontech)	Used for the selection of stable cell lines
pTRE-Tight	(Clontech)	TRE used in the cloning of pWTT1
pWHERE	(Invivogen)	Insulating elements used in the cloning of pWTT1
pWTT1	(a gift from Dr Dirk Isbrandt) and pWTT1-CrT-HA	Used for the cloning of pWTT1-L15

2.8.2 Small-scale preparation of plasmid DNA (Miniprep)

The Qiagen miniprep kit was used to prepare up to 15 µg high-copy plasmid DNA. Individual bacterial colonies were used to inoculate 3 mL of L-broth containing 100 µg/mL ampicillin and incubated overnight at 37^{o} C with vigorous shaking at 250 rpm. Plasmid DNA prepared by this method was used for subsequent sub-cloning and sequencing. The 3 mL overnight cultures were pelleted in 15 mL centrifuge tubes at 5400g for 10 min at 4^{o}C. The manufacturer's instructions for plasmid DNA preparation were then followed, before elution either in 30-50 µL water or 10 mM Tris-HCl, pH 8.5 (buffer EB in Qiagen miniprep kit).

2.8.3. Restriction endonuclease digestion

Enzymes were sourced from New England Biolabs (NEB) and Fermentas. Generally, 1 U of enzyme was added to 1 µg of purified DNA in a final volume of 20 µL of the appropriate buffer, followed by incubation at 37 ^{o}C for 1 h. For double digests, the manufacturer's instructions were followed for compatible enzyme/buffer combinations. Where buffers were incompatible and sequential digestion of DNA was necessary, the following protocol was followed: the initial digest was carried out as detailed above, then the digested DNA was purified using phenol:chloroform extraction, followed by an ethanol precipitation (detailed below). The DNA was then re-suspended, and the second digest allowed to proceed as normal. Reactions were routinely stopped by heat inactivation or the addition of DNA loading buffer before analysis by agarose gel electrophoresis.

2.8.4. DNA agarose gel electrophoresis

Agarose gels (0.8 – 2.0%) were made in 1 x TBE buffer containing 0.5 µg/mL ethidium bromide. Electrophoresis was performed in 1 x TBE buffer containing the same concentration of ethidium bromide. DNA samples contained a 1:6 ratio of DNA loading dye (NEB) and were routinely run alongside a 100 bp or 1 kb DNA ladder (NEB).

2.8.5. Purification of DNA from agarose gels

Low-melting point agarose (Flowgen, UK) was used. Gels were visualised briefly on an ultraviolet light box, and the desired fragments excised with a clean scalpel. DNA fragments were extracted using the QIAquick Gel Extraction Kit (Qiagen) according to the manufacturer's instructions, and eluted with 30-50 µL elution buffer (Buffer EB, 10 mM Tris-Cl, pH 8.5).

2.8.6. Phenol:chloroform extraction method and ethanol precipitation of DNA

The following method was used when purifying restriction fragments, plasmid or genomic DNA. A solution containing DNA for extraction was brought to a total volume of 100 µL with TE buffer and added to an equivalent volume of Phenol/Chloroform/Isoamyl alcohol (25:24:1, Sigma), vortexed and centrifuged at maximum speed for 5 min at RT. The top aqueous layer was transferred to a clean microfuge tube while the interphase and lower organic phase were discarded. Two-hundred and seventy µL ice-cold 100% ethanol and 9 µL 3M sodium acetate were added to the retained aqueous layer, vortexed thoroughly and kept at -20^{o}C for 30 min. The solution was then centrifuged at maximum speed for 15 min at 4 ^{o}C and the supernatant discarded. The resulting DNA pellet was washed with ice-cold 70% ethanol, vortexed thoroughly and centrifuged at maximum speed for 5 min. The ethanol was aspirated and the pellet was left to air-dry for 15 min at RT to remove residual ethanol. The final DNA pellet was re-suspended in T0.1E.

2.8.7. Linearising DNA vectors prior to ligation and cloning

Vectors were prepared for cloning typically by digesting 2 µg of plasmid DNA with the appropriate restriction enzyme, followed by agarose gel electrophoresis and extraction with the QIAquick kit. If required, the digested DNA was treated with shrimp alkaline phosphatase to prevent self-ligation of the digested backbone during cloning. 10 U shrimp alkaline phosphatase were added to the gel-extracted DNA (50 µL) in a total volume of 55 µL for 10 min at 37 ^{o}C, before heat inactivation at 65 ^{o}C for 15 min.

2.8.8. Ligation of DNA fragments

Simple ligations with sticky ends were carried out by incubating the DNA mixture (0.1 to 5 µg, in 1:1, 1:3 and 1:6 molar ratios of vector to insert DNA) with 1 x T4 DNA Ligase Reaction Buffer (NEB) and 200 U T4 DNA Ligase (NEB) in a 20 µL volume at 15^{o} C overnight.

2.8.9. Large-scale production of plasmid DNA (Maxiprep)

The Qiagen Maxiprep kit was routinely used to prepare up to 500 µg of high-copy plasmid DNA. The Qiagen endotoxin-free Maxiprep kit was used when purifying plasmid for introduction into mammalian cells. A starter culture of 3 mL L-broth containing the appropriate selective antibiotic was inoculated with a single bacterial colony and incubated for 8 h at 37^{o} C with shaking at ~ 300 rpm. Two-hundred and fifty mL L-broth (100 mL for high-copy number plasmids) were inoculated with 200 µL starter culture and incubated at 37^{o} C for 12 - 16 hours at ~300 rpm. Cells were harvested by centrifugation at 6000 g for 15 min at 4^{o} C. Following re-suspension of the bacterial pellet, DNA was purified according to the manufacturer's protocol. Endotoxin-free 50 mL polypropylene centrifuge tubes were used for DNA precipitation and washing, with centrifugation at 5000 g for 60 min. The purified plasmid DNA was re-suspended in 100 µL 10 mM Tris-HCl, pH 8.5. DNA concentration and purity were determined by measuring absorbance at 260 nm and 280 nm using a Nanodrop spectrophotometer (Thermo Scientific).

2.8.10. DNA Sequencing

Maxi- or mini-preps of DNA, and purified PCR products were sequenced by Source BioScience LifeSciences (Oxford, UK) who were provided with 1ng / µL per 100 bp product and primers at 3.2 pmol / µL according to their requirements. Results were analysed with the ContigExpress

and AlignX components of the Vector NTI software, and ApE (A Plasmid Editor).

Name	Sequence
CrT Seq 1	5'- CAC TCT CCT CCA TGC TGT -3'
CrT Seq 2	5'- CAT GAC ACT CTC CCA CCA CGA C -3'
CrT Seq 3	5'- AGA TGG ACT TCA TCA TGT C -3'
CrT Seq 4	5'- CAA CCT CAC ATG TGA CCA G -3'
CrT Seq 5	5'- CTG GTC ACA TGT GAG GTT G -3'
CrT Seq 6	5'- CTC AGG TGT GGA TCG ATG -3'
CrT Seq 7	5'- CAT CGA TCC ACA CCT GAG -3'
CrT Seq 8	5'- CCA GTT TGT AGG TGT GGA AG -3'
CrT Seq 9	5'- CCT TCC ACA CCT ACA AAC TG -3'
CrT Seq 13	5'- GTA GAA GAC GAT CAC CAT G -3'

Table 2-6. Sequencing primers

2.9. Protein expression studies

2.9.1. Protein extraction from cell lines and mouse tissue

Cell pellets or approximately 10 mg powdered tissue were sonicated for 30 seconds in lysis buffer containing 50 mM Tris pH 7.5, 150 mM NaCl, 2% SDS, 1 mM DTT, protease inhibitor cocktail (Roche, Germany) and PhosSTOP phosphatase inhibitors (Roche, Germany). Lysed samples were sonicated briefly on ice to disrupt nucleic acids, and centrifuged at 16,000 x *g* at 4^{o} C to remove cell debris.

2.9.1.1. Determination of protein concentration

Protein concentration was determined using the bicinchoninic acid assay (Pierce Thermo Scientific, UK), following a 20-fold dilution in order to eliminate any reducing effect of the DTT contained in the buffer on the assay results.

2.9.2. SDS polyacrylamide gel electrophoresis (SDS-PAGE)

Fifteen µg protein in 18 µL lysis buffer was mixed with 6 µL of 4x loading (Laemmli) buffer and boiled for five min at 95° C.

The Bio-Rad mini-protean electrophoresis cell system was used for SDS-PAGE. Samples were separated on pre-cast 12% Tris glycine SDS-page gels (Thermo-Pierce) at 200 V for 1 h in 1x Tris-HEPES running buffer (Thermo-Pierce). Protein was transferred to a Hybond-PVDF membrane (GE Healthcare, UK), previously permeabilised in 100% methanol for 2 min before equilibration in SDS transfer buffer for 5 min, in SDS transfer buffer at 300 mA for 90 min, at 4° C.

2.9.3. Immunoblotting

Membranes were blocked with 0.1% Tween-20 in PBS (PBS-T), containing 2% blocking reagent (ECL advance, GE Healthcare) for 1 h, followed by 2 h incubation at RT (or overnight at 4^{o} C) with primary antibodies (in blocking solution) and a 1 h incubation with appropriate peroxidase-conjugated secondary antibodies. Membranes were washed 6 x 5 min in PBS-T between primary and secondary incubations. Detection of immunoblot signals was performed

using the ECL advance chemiluminescence kit (GE Healthcare, UK) and the Fluorchem 8800 imager (Alpha Innotech, USA).

2.10. Biochemical measurements

2.10.1. HPLC determination of creatine levels

Mouse hearts were rapidly excised, the left ventricle separated and rapidly frozen in liquid nitrogen. The frozen tissue was powdered in a percussion homogenizer cooled on dry ice. An aliquot of 5-10 mg of powdered tissue was homogenized in 550 µl of 0.4N perchloric acid at 0 ^{o}C. 100µl was removed for subsequent protein quantification using the method of Lowry *et al* [134]. The homogenate was neutralised with 1M KOH before centrifugation of the supernatant for 5 min at 5500rpm, filtration of the supernatant through a 0.45µM filter and injection into the column (Supelco LC-18 reverse phase column, 25cm x 4.6mm, 5 µM pore size). The HPLC pump was a Jasco PU-2089 Plus, and the detector, a Jasco UV-2075 Plus UV detector (detection at 205nm).

Chapter 3. Cardiac-specific overexpression of the Creatine Transporter *in vivo*. Generation of an inducible murine model.

3.1. Introduction

The suggestion that the failing heart is energy-starved is an old one, with the observation of falling Cr levels in the failing myocardium first reported in 1939 by Herrman and Dechard, and numerous subsequent studies showing a reduction in PCr and free Cr levels (see General Introduction). If this depletion is causative in HF, then the restoration of normal levels of PCr and free Cr could be a valuable therapeutic tool. In order to restore Cr levels within the failing heart, a strategy to increase the number of plasma-membrane creatine transporters is one potential approach. Attempts to increase myocardial Cr levels through oral Cr supplementation lead to an increase in plasma Cr levels, but if this elevated plasma [Cr] is maintained, a down-regulation of the CrT occurs, resulting in unchanged net Cr uptake levels. A previous *in vivo* study in our group achieved transgenic overexpression of the CrT, driven by the *MLC2v* cardiac-specific promoter, but yielded surprising results. It was shown that substantial increases in creatine levels (2-4 fold) led to LV hypertrophy, dilatation and progressive dysfunction over one year. [97]. However, it has recently been shown that moderately elevated Cr levels, ranging from ~20%-100% above WT concentrations, showed normal ventricular function, normal inotropic reserve and normal mass, even at 18 months (unpublished data). Additionally, this moderately elevated [Cr] was shown to be protective against ischaemia / reperfusion injury; a reduction in loss of function with the onset of ischaemia was shown, along with a more rapid and complete return of function during reperfusion. The mice showed elevated [PCr], and crucially, an increase in the free energy change of ATP hydrolysis, suggesting an increased energy reserve to power intracellular ATPases. These findings highlighted the benefit of a moderate increase in

myocardial [Cr], and underlined the need to create a new model of overexpression. Previously, many CrT-OE mice have had to be excluded from studies, as their myocardial [Cr], which varied from animal to animal, did not fall within the 'therapeutic' range of 20% - 100% above WT levels.

This chapter describes a different approach towards overexpressing the CrT in order to overcome the limitations of the previous transgenic model in two ways. Firstly, the addition of a temporal element, using tetracycline induciblity as opposed to a traditional chronic overexpression model. Temporal overexpression of the CrT will allow finer control over the level of onset of overexpression of transgenic CrT, enabling the restoration of [Cr] and [PCr] only after they become depleted. This approach could also overcome the potentially confounding effects of neonatal overexpression. Secondly, the use of the tetracycline system should allow a degree of control over the *level* of overexpression, through doxycycline titration. This would be a considerable refinement of the previous CrT-OE model, allowing the use of far smaller numbers of animals due to an increased percentage of those that express the desired level of CrT. Ultimately, this would enable optimum tissue concentrations of Cr to be obtained. The design, generation and phenotyping of this cardiac-specific, temporal model for overexpression of the CrT using the tetracycline-inducible (Tet-On) system are outlined.

3.1.1. Limitations of existing models of Creatine Transporter overexpression

Transgene expression studies have enabled the overexpression of genes and characterisation of the phenotypes they drive. However, phenotypes that are caused by these genetic manipulations can be difficult to interpret if there are cell-non-autonomous or systemic effects, and issues such as embryonic lethality can render an overexpression strategy useless. Constitutive transgenic

models, with expression driven by a cardiac-specific promoter, can suffer from the effects of early embryonic transgene expression. For example, the commonly used *MLC2v* promoter mRNA has been detected as early as 8 days *post-coitum* [135]. Such phenomena may have contributed to the unexpected effects seen by Wallis *et al* [97] in their model of creatine transporter overexpression. Two transgenic lines were created by random integration, using a rabbit CrT with a c-terminal *c-myc* epitope tag, driven by the *MLC2v* promoter. As mentioned, while supranormal levels of myocardial creatine were observed in the transgenic mice, these levels varied considerably between animals. CrT-OE mice were shown to develop LV hypertrophy, dilatation, and systolic as well as diastolic dysfunction which led to congestive heart failure proportionate to the concentration of myocardial creatine. Importantly, mice showing a mild to moderate increase in creatine did not show substantial dysfunction, suggesting that future studies should be restricted to *in vivo* models with a phenotype of a mildly augmented creatine pool. It was postulated that, in mice expressing very high levels of CrT, this dysfunction could be due to the inability of the heart to keep the augmented creatine pool adequately phosphorylated, leading to increased free ADP levels and reduced free-energy change of ATP hydrolysis. A subsequent study on these transgenic lines showed that heart creatine levels in the CrT-OE mice remained constant throughout life and that LV dysfunction was not apparent until 16 weeks, but became more pronounced from then on [104]. As outlined in the General Introduction, this study also found that enolase levels were reduced in the CrT-OE hearts, suggesting impaired glycolytic capacity. The reduction in enolase was correlated with increasing myocardial [Cr]. This finding could explain the fact that cardiac dysfunction is not observed in these hearts until 16 weeks, despite supra-normal myocardial [Cr] from 6 weeks or earlier. It suggests that the thermodynamic hypothesis alone is not enough to explain the full phenotype.

A more suitable approach for CrT overexpression is the use of a temporal, binary system of expression. As discussed, this could circumvent the potentially deleterious effects of overexpression of the CrT during development and enable induction of the transgene to be restricted to restoring depleted myocardial Cr levels to normal. Additionally, it would enable finer control over levels of expression of the transgene, and resulting creatine levels, under baseline, acute and ischaemic conditions. There are 2 well characterised temporal systems, the Cre/*loxP* system and the tetracycline-inducible system (as used in the current project), and the pros and cons of each are discussed below.

3.1.2. The Cre/*lox*P system for conditional knockouts

The Cre/*lox*P system relies on site-specific DNA recombination to activate, silence or mutate the target gene. Typically, a gene of interest is targeted *in vitro*, in murine embryonic stem (ES) cells with a construct containing *lox*P sites, creating a 'floxed' gene. Targeted ES cells are then used to create a mouse strain, through the injection of ES cells with the desired genomic structure into blastocysts to give chimeric founders. These mice are then crossed with mice expressing *Cre* recombinase under the control of a cardiac-specific promoter, such as *α-MHC* or *MLC2v*, and the portion of the gene encompassed by the *lox*P sites is excised, resulting in site-specific modification of the target gene. Where overexpression of a transgene is required, an intervening stop sequence between a strong exogenous promoter and the coding region of the gene is floxed, and it is this that is excised by *Cre*, leading to transgene activation [136].

Inducibility can be achieved in this system with the use of α-MHC mER-Cre-mER mice, which express tamoxifen-inducible Cre, driven by the *α-MHC* promoter [136], enabling temporal control of expression in the adult heart. This system has been used successfully in cardiac models of

transgene overexpression [137], although tamoxifen-mediated mER-Cre-mER nuclear translocation can induce severe transient dilated cardiomyopathy in mice with or without *lox*P (floxed) transgenes. This is likely related to tamoxifen toxicity, as an analogue (raloxifene) does not lead to cardiomyopathy, but still initiates nuclear *Cre* translocation [138].

Many tissue-specific promoter-driven *Cre* mouse lines are available, making this system a versatile one. However, whilst conditional gene expression using the Cre/*lox*P system eliminates the developmental consequences of altered gene expression by allowing induction at a specific point in the organism's life cycle, it is irreversible. The desire for a tight, *reversible* system for CrT overexpression thus eliminated the Cre/*lox*P system as a basis for the generation of the inducible CrT-OE model.

3.1.3. The tetracycline-inducible system

The most commonly used binary transcription transactivation systems are the tetracycline-dependent regulatory systems, first described by Gossen and Bujard [139]. These involve the insertion of an expression construct via transgenesis, leading to the overexpression of a protein. Two transgenic strains are required; the responder line, carrying the transgene of interest under the control of the Tet operator, and the inducer line, carrying the tTA or rtTA line under the control of a tissue-specific promoter. Expression in double-transgenic animals can be temporal, and importantly, reversible controlled through the administration of tetracycline. The tetracycline analogue doxycycline (dox) is widely used instead of tetracycline, due to its low cost and efficiency at well below cytotoxic levels in the animal's diet [140 141].

3.1.4. Potential unwanted effects of the doxycycline and the tetracycline-inducible system in the heart

Tetracycline-inducible expression systems are generally regarded as advantageous over other inducible systems, as the required drug treatment is minimally intrusive on the general physiology of the transgenic animal [142]. Dox has documented effects on the heart, which become relevant in the context of a system targeting myocardial Cr overexpression. Dox is known to attenuate matrix metalloproteinase (MMP) expression in the heart, along with its activity in various tissues [143]. This is important, as the dynamic synthesis and breakdown of extracellular matrix proteins is a process that plays an important role in myocardial remodelling. Vinet and colleagues demonstrated the potentially negative effects of dox administration in a murine model of thoracic aorta constriction (TAC). Following TAC surgery, it was found that animals fed dox showed accelerated onset of cardiac hypertrophy and progression to congestive heart failure [144]. These findings demonstrate the need for suitable controls to be included in induction experiments, i.e. WT controls should also be administered dox.

Another potential cause of altered myocardial function in the Tet-systems is the tTA protein itself. This has been shown to alter myocardial function, although there have been inconsistencies regarding its reported effects on the heart. Some studies demonstrated that expression of tTA provided protection against ischaemia / reperfusion injury [145] [146]. Conversely, Sanbe *et al* discovered the spontaneous development of hypertrophy in 2 modified rtTA lines. The hypertrophy was so severe that all mice expressing this protein died within 2 months [147].

3.1.5. Tet-off system

In the original Tet-off system, the tetracycline-controlled transactivator (tTA) is unable to bind DNA when the inducer (dox) is present. Thus in the tTA system, the continuous administration of dox is required to suppress the transgene until expression is desired, at which point the dox is withdrawn from the diet. Depending on the tissue of interest and the rate of dox clearance, induction can take from 24 hours to 7 days [148].

3.1.6. Tet-on system

The modified 'reverse tTA' (rtTA) binds DNA only when the inducer is present. The rtTA system can respond to the addition of dox within 1 hour [149] enabling quick gene activation, although subsequent repression is dependent on the rate of clearance of dox from the tissue of interest.

The tet system effector is based on the repressor (*tetR*) of the Tn10 tet-resistance operon of *Escherichia coli*. This is fused to the VP16 transactivation domain of herpes simplex virus (HSV) that functions as a strong transcription activator, forming the tTA, or rtTA. In the rtTA, the *tetR* gene has been mutated so that it binds *tetO* sequences and activates transcription only in the presence of dox. Therefore, in the presence of the inducer, dox, rtTA dimers specifically bind to seven tandemly repeated 19-bp *tetO* sequences (the tetracycline response element- TRE), activating transcription from a minimal human cytomegalovirus promoter (hCMV) which is normally inactive [139]. This drives the expression of the gene of interest, the cDNA of which is cloned downstream of the *hCMV* minimal promoter.

3.1.7. 'Leakiness' in the tetracycline system

High basal activity, referred to as 'leakiness', is a problem reported in both types of the tet system, though it has been particularly problematic in the 'tet-on' system. Residual affinity of tTA for TRE in the 'tet-off' system, and the site of integration of the transgene in both 'tet-off' and 'tet-on' systems have been suggested as factors contributing to leakiness [150]. Additionally, in the 'tet-on' system, the expression of rtTA has been demonstrated in several instances to led to doxycycline-independent 'leaky' expression of the target gene [140] [151] [148] [152]. This is a result of the ability of rtTA to weakly bind to the TRE, even in the absence of doxycycline, and could be a problem in a system where rtTA is used to regulate the expression of a toxic protein, or a protein whose low level of expression would be enough to affect the function of endogenous proteins. The presence of chromosomal insulating elements has been shown to minimise leakiness [153]. Further developments to reduce leakiness in tet-systems are being made. One system involves the incorporation of AU-rich mRNA destabilising elements (AREs) into the 3' untranslated regions of tet-inducible constructs, thus reducing expression in the 'tet-on' system in the absence of dox by decreasing the stability of its mRNA [150]. Additional approaches include the targeted insertion of the both transactivator and responder genes into a specific locus, for example, *Rosa*26, known to be devoid of both silencing and enhancing elements [154], as well as the development of new TRE-reporters which, in addition to enhancing the stability of expression, also showed reduced basal leakiness [155]. The most recent development of a system involving the tet system combines optimised fluorescence-coupled shRNA technology with a Flp/FRT recombinase-mediated cassette exchange (RMCE) strategy, generating a system for the production of single-copy, tet-regulatable shRNA transgenic ES cells and mice [156]. The system provides a novel way to spatially, temporally and reversibly control endogenous gene expression in mice, via dox administration.

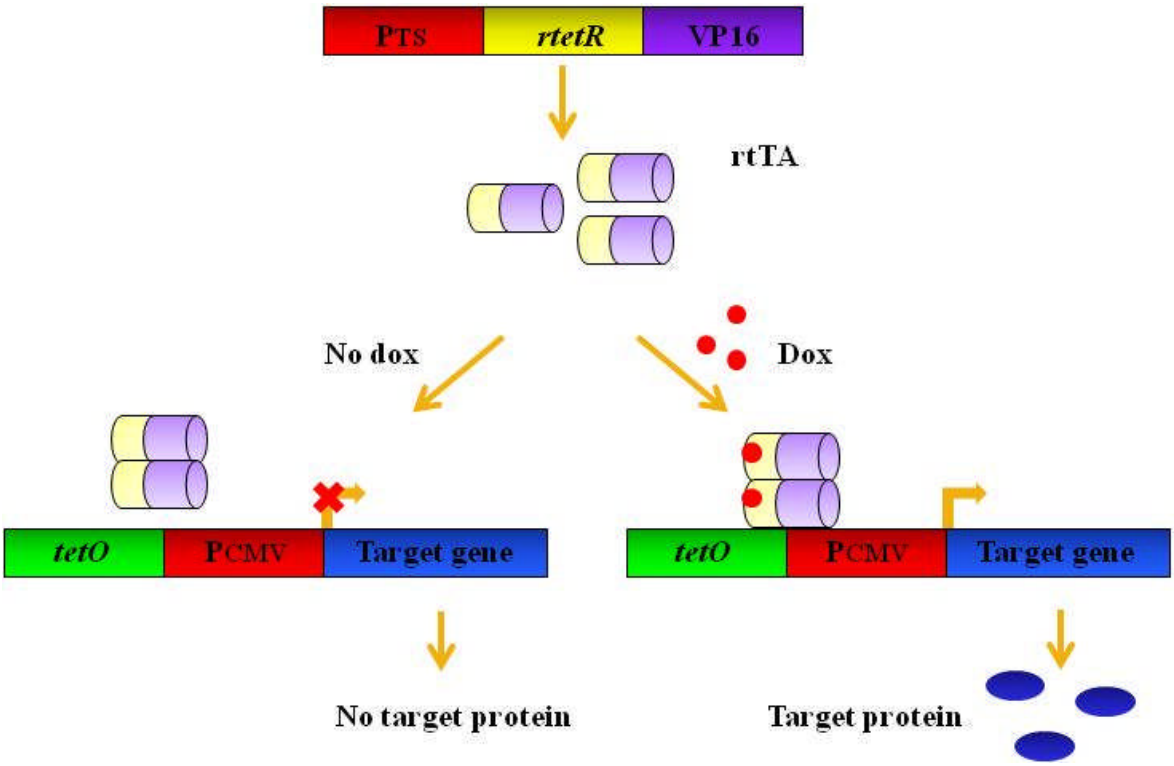


Figure 3-1. The reverse tetracycline-controlled transcriptional activator (rtTA) system: "Tet-on". A tissue-specific promoter (PTS) directs the expression of rtTA, a fusion protein of the reverse tetracycline repressor of *E.coli* (rtetR) and the transcription activation domain of viral protein 16 of herpes simplex virus (VP16). In the absence of dox, rtTA does not bind to the responsive elements of the tetracycline resistance operon of *E.coli* transposon TN10 (tetO). Contrastingly, in the presence of dox, rtTA binds to tetO, activating the minimal human cytomegalovirus promoter (PCMV), leading to transcription and expression of the downstream target gene. Adapted from Zhu et al, Cell & Developmental Biology 2002, 13, p121-128.

3.1.8. The use of insulating elements in transgenes

Variability of expression in transgenic mice, and particularly between different lines in tetracycline-regulated systems is a common phenomenon. It is known that transgenes are susceptible to positional effects due to their site of integration, and that integration of a gene proximal to heterochromatin sequences can lead to position effect variegation (PEV); that is, silencing of a proportion of the cells expected to express a gene, due to the gene's abnormal juxtaposition with heterochromatin [157] [158]. Insulators have been identified in a limited number of genes from various organisms [159], and are characterised by their ability to establish genomic barriers, protecting DNA sequences from neighbouring heterochromatin and distally located enhancers [160]. The presence of insulating elements in transgenic constructs seems to increase the

likelihood of expression when compared to unprotected constructs [161], in addition to reducing 'leakiness' in the tet-on system without affecting the level of transgene expression when induced with dox [153]. The plasmid used for cloning the CrT constructs was pWTT1, a plasmid comprising the tetracycline-response element from pTRE-Tight (Clontech) and the *H19* insulator elements of pWhere (Invivogen). pWhere also contains a differential methylated region (DMR) located between the mouse *Igf2* and *H19* genes which acts as a powerful insulator [162]. The enhancer blocking activity is dependent on four responsive elements to the vertebrate enhancer-blocking protein CTCF, which acts as an insulator and controls imprinting of *Igf2* [163]. While *H19* insulating elements have been reported to cause transgene expression to be 'shut off' when passed through the male germ line in a model of *Sox4* overexpression [164], possibly through imprinting effects, their potential benefits were considered to outweigh these risks, and they were included in the construct design for the CrT-OE.

3.1.9. α-MHC driven rtTA expression in the heart

Tetracycline-inducible systems have been used widely to regulate transgene expression in the heart [165 166 167 168 169]. The 5.5 kb α-myosin heavy chain (*α-MHC*) promoter has become the most commonly used promoter for spatiotemporal control of cardiac transgene expression [170 171]. Other promoters include the ventricular myosin light chain 2 (*MLC2v*) promoter [135] discussed previously, *mCK2*, an extended promoter / 5'-upstream enhancer sequence for muscle creatine kinase [172 173] and rat cardiac troponin T (*Tnnt2*) [174].

α-MHC is first expressed as early as 7.5 days post-coitus in the developing cardiac tube [175 176] and is constitutively expressed in the atria. This atrial expression continues throughout development, although at this stage, the β-MHC isoform predominates [175]. From 7 days after

birth, α-MHC expression increases and predominates consistently in the atria and ventricles throughout adulthood. The normally high activity of the α-MHC promoter is suppressed during the development of many of the experimental forms of cardiac hypertrophy. This suppression, combined with an isogenic switch to β-MHC, is a marker of LVH, and could in turn reduce transgene expression and hide a transgenic phenotype [177 178].

3.1.10. Transgene design rationale

cDNA from different species has been used commonly in other models of transgenesis. In this case, rabbit cDNA was used. The previous model of CrT-OE, created by Wallis *et al*, demonstrated effective transcription and translation into functional CrT using this cDNA. There is an expected 97% homology between rabbit, human bovine and rat *CrT* at the amino acid level, based on their respective cDNA sequences [35]. Whilst rabbit cDNA was chosen primarily due to the lack of availability of mouse CrT cDNA, the choice of rabbit cDNA was advantageous in that it enabled the design of primers able to differentiate between endogenous and transgenic *CrT* transcripts [48 97].

Initially, a construct with a c-myc C-terminal epitope tag was generated. Various commercial anti-CrT antibodies are available, though during our experiments, these proved unreliable and non-specific, cross-reacting with non-CrT polypeptides. Other antibodies used have demonstrated similar behaviour [40], reacting with E2 components of mitochondrial dehydrogenases. For this reason, the inclusion of an epitope tag in the CrT construct was considered essential in order to facilitate reliable protein detection, localisation and quantification. Early *in vitro* testing showed that anti-c-myc antibodies were unable to detect the epitope tag. Alongside the characterisation of the *CrT-myc* construct, efforts were made to detect *CrT-myc* in LV tissue from the previously described model of CrT-OE [97], by means of

immunohistochemistry on both paraffin-embedded sections and cryosections, neither of which proved successful. The inability to detect CrT would have been a significant disadvantage following establishment of the new model and thus necessitated the creation of a new construct utilising the haemagglutinin (HA) tag [179]. The HA epitope tag is widely used [180 181] and specific anti-HA antibodies are readily available. Additionally, the size of the HA tag (10 amino acids) is the same as the c-myc tag. It has been demonstrated that a c-myc C-terminal epitope tag does not inhibit CrT function [97], but it should be noted that the inclusion of an epitope tag could lead to unpredictable effects on protein function. Preserving the location and size of the tag with regard to the previous model seemed the best way to avoid deleterious effects on the function of the CrT. The choice of cloning vector (pWTT1) included *H19* insulating elements, chosen in order to protect the *CrT* from neighbouring heterochromatin and ensure a greater likelihood of transgene expression, as discussed previously.

3.1.11. Summary of experimental aims

The proposed benefits of restoring WT myocardial Cr levels in the failing myocardium were left partially unanswered by the previous model of CrT-OE. The experimental strategy described within this chapter aims to resolve these shortfalls through several critical means:

- The incorporation of a temporal element of gene control, enabling CrT to be overexpressed only when required, that is following the depletion of myocardial Cr due to the onset of HF.
- The ability to control the level of CrT-OE to ensure the desired concentration of myocardial Cr is achieved, thus avoiding the deleterious effects associated with myocardial [Cr] in excess of 200 % WT levels.

- The ability to detect and localise CrT within the myocardium, enabling insights into the functioning and processing of the protein.

It is hypothesised that the restoration of WT myocardial Cr levels following the onset of HF may 'rescue' the phenotype, and the proposed model aims to study this hypothesis.

3.2 Methods and Results

3.2.1. Acquisition of the CrT cDNA clone

A full-length cDNA clone of the *Oryctolagus cuniculus* creatine transporter gene (accession no. X67252) was obtained from Dr Julie Wallis (Dept. of Cardiovascular Medicine, University of Oxford) as part of the 'X10' construct, comprising the cardiac-specific *MLC2v* promoter upstream of the *CrT* cDNA, with a *c-myc* C-terminal epitope tag and an SV40 polyA tail derived from pBK-CMV (Agilent). This will be referred to as *CrT-myc.* This was contained within the pBluescript II vector (Stratagene).

3.2.2. pWTT1, a vector containing a tetracycline-response element and H19 insulator elements

The pWTT1 cloning vector (a gift from Dr Dirk Isbrandt) was used as the basis for the creation of a tet-inducible CrT-OE construct. The vector combines the *H19* insulating elements of pWhere (Invivogen) with the tetracycline inducible pTIGHT promoter of pTRE-TIGHT (Clontech).

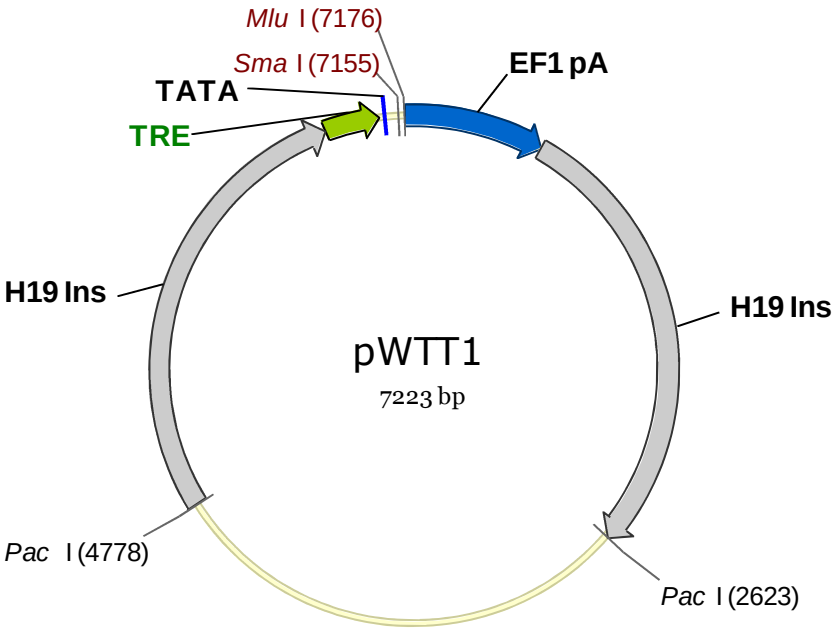


Figure 3-2. Map of pWTT1, a cloning vector containing fragments from pWhere and pTRE-Tight. The tetracycline-response element of pTRE-Tight was cloned into the MCS of pWhere, creating a vector with tetracycline response element (*TRE*) and MCS, flanked by *H19* insulators. TRE = tet response element, EF1 pA = EF1 polyadenylation signal, TATA = TATA box, H19 Ins = *H19* insulating element.

3.2.3. Construction of pWTT1-CrT-myc, an H19 insulator-flanked transgene with a C-terminal c-myc epitope tag

An initial construct was created, utilising *CrT* cDNA and a C-terminal *c-myc* epitope tag The pBluescript II backbone containing this construct was *Eco*RI restricted, and treated with Klenow to remove the 3' overhang. Following restriction with *Bss*HII, the resulting 2.6 kb fragment (*CrT-myc*) was gel extracted. This product, comprising *CrT* cDNA, the C-terminal *c-myc* epitope tag and an SV40 polyA signal, was subcloned into the *Sma*I – *Mlu*I restricted pWTT1 backbone.

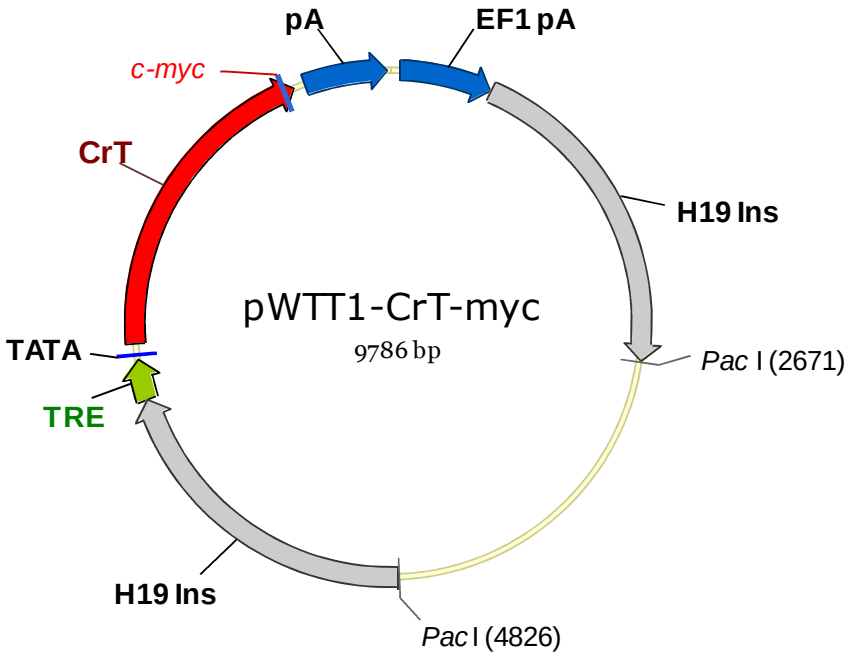


Figure 3-3. Map of pWTT1-CrT-myc. The transgene is flanked with *Pac*I restriction sites. The plasmid consists of H19 insulators, a tetracycline response element (*TRE*) downstream of a minimal CMV promoter, the *Oryctolagus cuniculus CrT* cDNA with a C-terminal *c-myc* epitope tag, and an *EF1* polyadenylation signal. TRE = tet response element, EF1 pA = *EF1* polyadenylation signal, TATA = TATA box, H19 Ins = *H19* insulating element, CrT = *CrT* cDNA

3.2.4. Construction of pWTT1-CrT-HA, an H19 insulator-flanked transgene with a C-terminal haemagglutinin (HA) epitope tag

Due to the inability to detect *CrT-myc* (described in detail later in this chapter), a strategy to replace *c-myc* with an *haemagglutinin* tag was devised. In order to replace the *c-myc* epitope tag in the previously described pWTT1-CrT-myc, a PCR-based approach was required, due to the lack of suitable restriction sites around the *c-myc* tag sequence. Another strategy was initially attempted, using a method termed 'oligo-fusion'. This aimed to utilise unique restriction sites *Blp*I (upstream of *c-myc*) and *Xba*I (downstream of *c-myc*), separated by 176 bp. Two shorter oligos with a region of homology were designed to 'bridge' this gap (necessary as the length is too great to be spanned by one oligo alone), incorporating the desired HA tag and necessary flanking sequences at the 5'- and 3'- ends. However, this strategy failed, due to an inability to successfully restrict the *Blp*I site. The PCR-based approach was then pursued, and involved designing primers flanking the *CrT* at the 5' end and *c-myc* at the 3' end. The 5' primer

incorporated an additional *Bam*HI site and the 3' primer, homologous with the final 20 bp of the *CrT* sequence, added the haemagglutinin (HA) tag sequence followed by a stop codon and additional *Hind*III restriction site. The primer sequences are outlined in the following table.

Name	**Sequence**
HA-*Bam*HI-X10	5'- GCG CGC GGA TCC CTT GAA TTC ACG CAG CCA CC -3'
HA-*Hind*III-X10	5'- GCG CGC AAG CTT TCA AAG AGC GTA ATC TGG AAC ATC GTA TGG GTA CAT GAC ACT CTC CAC CAC GA -3'

Table 3-1. Oligonucleotides used to amplify rb CrT by PCR, and replace the already present c-myc tag with an HA tag. Purple represents GC clamp, blue represents restriction site sequences (*Bam*HI in HA-*Bam*HI-X10 and *Hind*III in HA-*Hind*III-X10). Red represents stop codon, green represents HA tag sequence and black is 20 bp region of homology.

PCR was performed using Finnzymes Phusion high-fidelity hot-start DNA polymerase. PCR conditions are detailed in Appendix II. Following amplification and gel extraction of the product, cohesive ends were generated by a double restriction digestion reaction with *Bam*HI and *Hind*III.

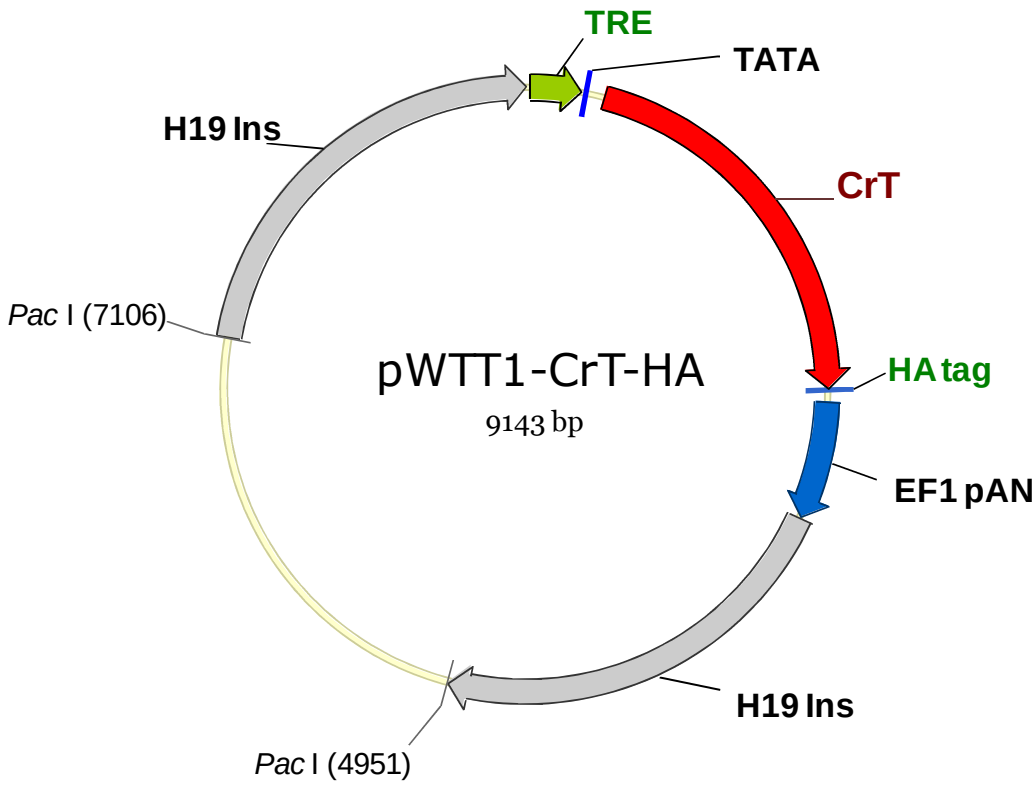


Figure 3-4. Map of pWTT1-CrT-HA. The transgene is flanked with *Pac*I restriction sites. The plasmid consists of H19 insulators, a tetracycline response element (TRE) downstream of a minimal CMV promoter, the *Oryctolagus cuniculus* CrT cDNA with a C-terminal haemagglutinin epitope tag, and an *EF1* polyadenylation signal. TRE = tet response element, EF1 pA = *EF1* polyadenylation signal, TATA = TATA box, H19 Ins = *H19* insulating element.

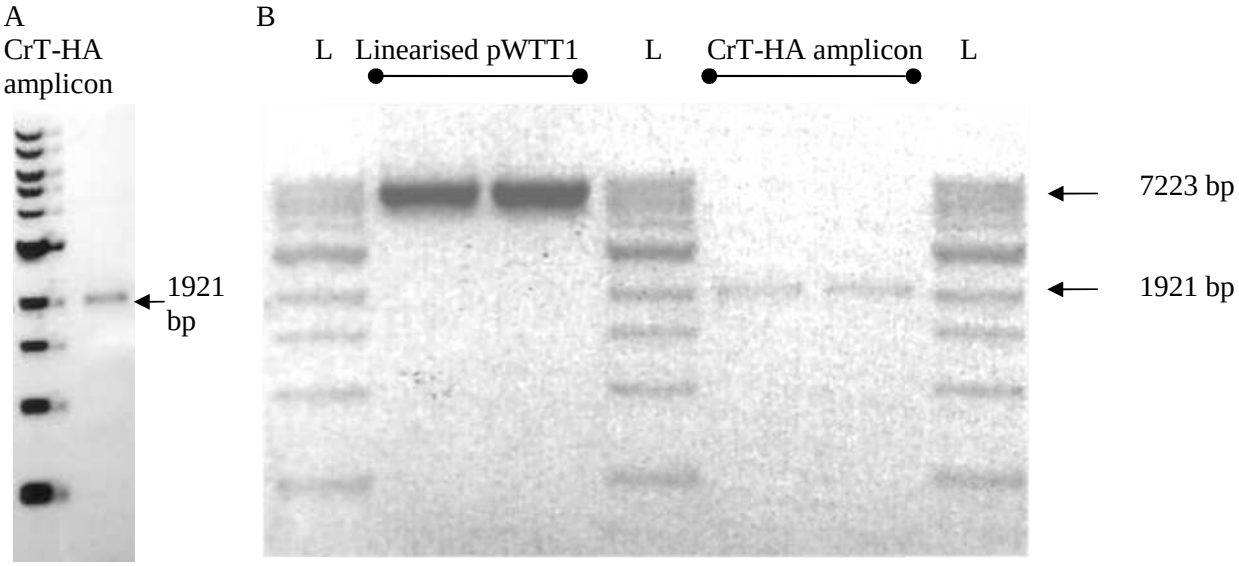


Figure 3-5. Agarose gel electrophoresis of CrT-HA amplicon and linearised pWTT1 prior to ligation. A shows the CrT-HA amplicon alone at 1921 bp, and B shows the linearised plasmid pWTT1 prior to ligation (7223 bp). L – 1 kb ladder (NEB).

The fragment was ligated with the *Bam*HI - *Hind*III restricted pWTT1 plasmid backbone to create pWTT1-CrT-HA. Ultracompetent *E.coli* were transformed with pWTT1-CrT-HA (Stratagene XL-10 Gold). Miniprep DNA was then prepared (described in General Materials and Methods) using the Qiagen Miniprep system, followed by diagnostic restriction digestion reactions and verification of the fragment size by agarose gel electrophoresis. Representative samples are shown in the following figure, 3-6.

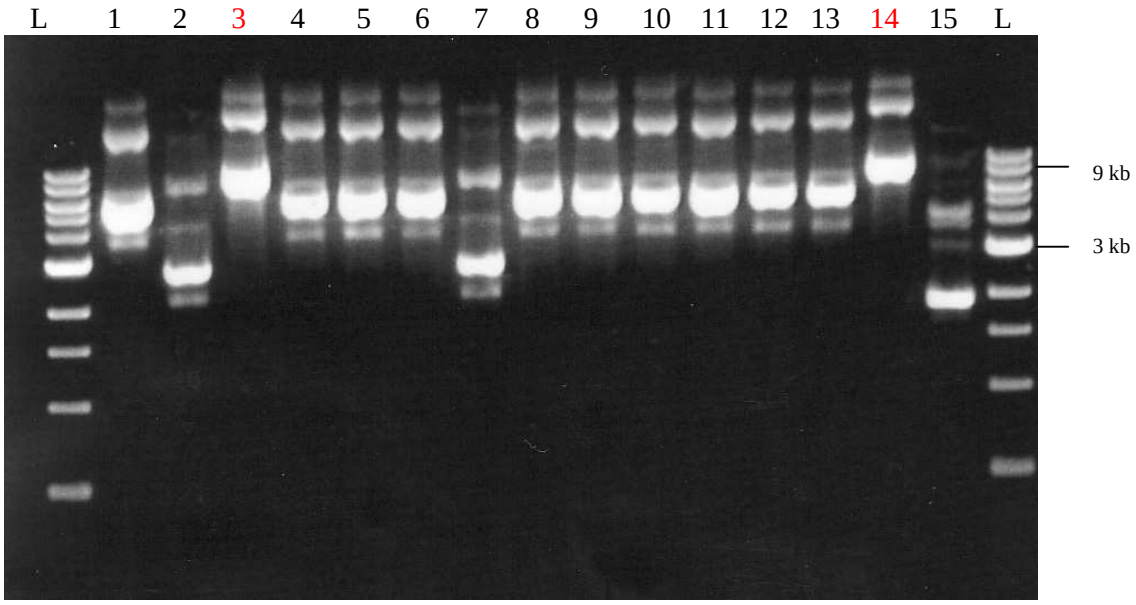


Figure 3-6. 0.8% agarose gel showing DNA from 15 of the 30 transformants picked. L- 1 kb ladder (NEB). Lanes 3 and 14 (red) represent two of the samples at the expected size of 9143 bp. These were selected for sequencing to confirm presence of the CrT-HA sequence. Sample 14 was subsequently used for the generation of the 3T3-CrT-HA stable cell line and the generation of founder mice.

Several clones were selected for further analysis by diagnostic restriction digestion reactions, and of these, two (LM14 and LM30) demonstrated the expected restriction patterns. Nucleotide sequencing confirmed that the expected CrT-HA amplicon in these clones was the correct sequence.

3.2.5. Construct validation- expression of pWTT1-CrT-myc and pWTT1-CrT-HA in 3T3-Tet-Off fibroblasts

pWTT1-CrT-myc and pWTT1-CrT-HA were transfected into 3T3-Tet-Off fibroblasts in order to assess transgene expression and response to dox treatment. Although these cells expressed the tet-off (tTA) protein, not the tet-on (rtTA) protein as would be used in the transgenic model, the system would demonstrate inducibility of the transgene *in vitro*.

3.2.5.1. Transfection optimisation

Repeated attempts to perform transient transfections with both constructs, using FuGENE (Roche, UK) and Genejuice (Merck, UK), proved unsuccessful. Flow cytometry experiments to compare the two transfection reagents demonstrated a 35% success rate with Genejuice when transfecting 3T3-Tet-Off cells with GFP, greater than that achieved with FuGENE, hence all further transfections were performed with Genejuice (flow cytometry data not shown). As further attempts to yield detectable CrT by transient transfections failed, presumably due to the large size of the construct, stable lines were established (see General Materials and Methods).

3.2.5.2. Stable line generation

3T3-CrT-HA cells were co-transfected with pPUR and either pWTT1-CrT-myc or pWTT1-CrT-HA (clone LM14), and stable lines were obtained (as detailed in General Materials and Methods). Twelve initial transfections were made with each of the pWTT1-CrT-myc, and each of 2 clones (14 and 30) of pWTT1-CrT-HA. To aid selection of the cell lines generated, western blots were performed to detect the presence of overexpressed protein, and representative samples are shown in the following figure. Of those lines, only 1 of clone LM14, and 1 of clone LM30 demonstrated CrT overexpression. Having demonstrated CrT overexpression, dox response was verified by 7 day, 1 µg / mL dox treatment (Melford, UK). As hoped, this suppressed CrT expression, as the cell system is a “tet-off” system. Of all the stable lines generated, line number 11 transfected with the pWTT1-CrT-HA clone number 14 (LM14) demonstrated the greatest overexpression of CrT, in addition to reliable dox-response. In this stable line, CrT-HA was detected with both the anti-HA antibody and the anti-CrT (epitope 14-27) antibody (a gift from Dr Theo Wallimann). From this point, these cells will be referred to as 3T3-CrT-HA.

High levels of overexpression with pWTT1-CrT-myc transfected cells were not achieved, nor did the low expression seen alter in response to dox treatment. Additionally, concurrent work to detect the presence of *CrT-myc* in tissue sections (both paraffin-embedded and cryosections) of the previously described model of CrT-OE were unsuccessful, demonstrating an inability to detect the *c-myc* tag either *in vitro* or *in vivo* (data not shown). For these reasons, combined with the known CrT antibody detection issues, no more work was performed in these cells, with all *in vitro* work focussing on the 3T3-CrT-HA cells from this point. An inability to detect transgenic CrT either in western blots or immunohistochemistry would have proved too great a disadvantage.

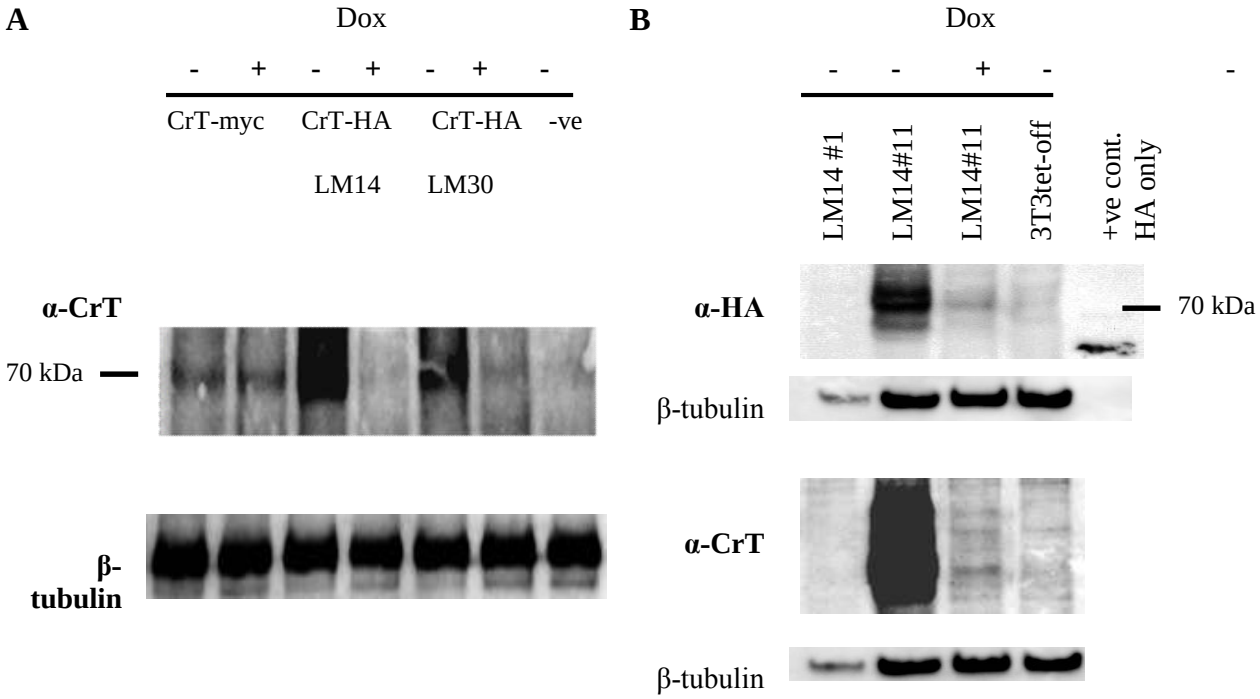


Figure 3-7. Stable transfection of 3T3-tet-off fibroblasts with pWTT1-CrT-L15 and 2 clones of pWTT1-CrT-HA (LM14 and LM30). Western blot analysis of CrT (a/b donated by Prof Wallimann vs rbCrT, epitopes 14-27) and HA. Cells were cultured in the presence or absence of dox for up to 7 days. (A) demonstrates minimal expression and no dox response with pWTT1-CrT-myc transfected cells, and pWTT1-CrT-HA clones LM14 and LM30 exhibiting high expression and dox response. Negative control is untransfected cell lysate. (B) demonstrates CrT-HA expression and dox response in stable cell line number 11, transfected with the pWTT1-CrT-HA clone LM14. This stable line was used for all further experiments, and is denoted 3T3-CrT-HA. LM14#1, a cell line that failed to overexpress CrT-HA, is included as a negative control. *E.coli* lysate expressing HA was used as a positive control. Membranes were stripped of the antibodies and re-probed with β-tubulin as a loading control. Molecular weights were determined using the Full Range molecular Weight Rainbow Marker (GE Healthcare, UK).

3.2.6. Construct validation- immunocytochemistry

Transgene expression was further validated by immunocytochemical analysis of the stably transfected 3T3-Tet-Off fibroblast line 3T3-CrT-HA (see General Materials and Methods). Cells were stained both with anti-HA and anti-CrT antibodies, both of which detected over-expressed protein. Whilst this expression was detected both in the cytoplasm and at the plasma membrane, plasma membrane expression appeared strongest.

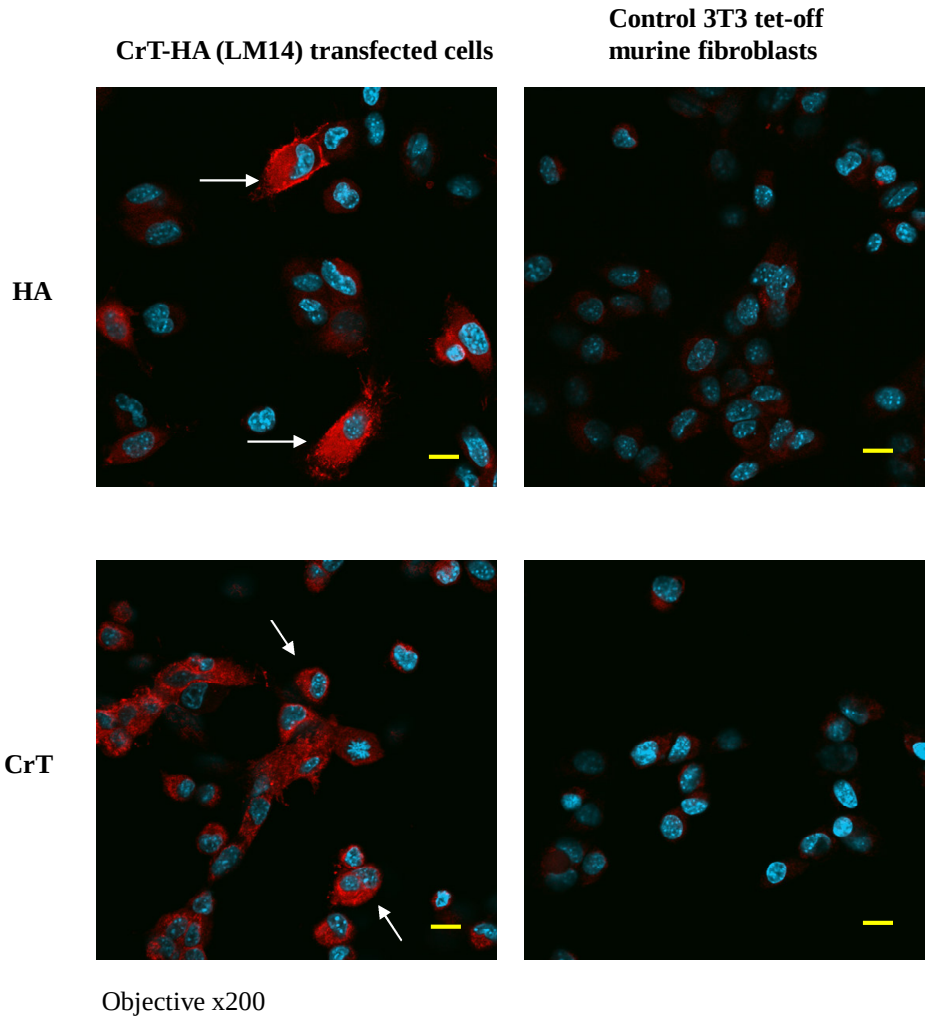


Figure 3-8. Confocal microscope images showing expression of CrT-HA in stably transfected 3T3-Tet-Off fibroblasts. CrT-HA expressing cells are shown in red, with nuclei staining blue (DAPI). Arrows denote representative overexpressing cells. A clear difference can be seen between CrT-HA expression (red) in 3T3-CrT-HA cells and control cells. The population of overexpressing cells is not homogeneous owing to the co-transfection and selection method employed in creating the stable cell line. Identical image capture settings were used for the acquisition of all images. Yellow scale bars = 20 µM.

Having established the presence of detectable CrT-HA in these cells, response to dox was confirmed by 7 d incubation of the cells in 1 µg / mL doxycycline (Melford, UK). CrT-HA

expression was greatly reduced in treated cells compared to control cells grown in the absence of dox. Minimal expression of CrT-HA was still detected after 7 days incubation with dox, suggesting a longer incubation could be required to totally eliminate the protein.

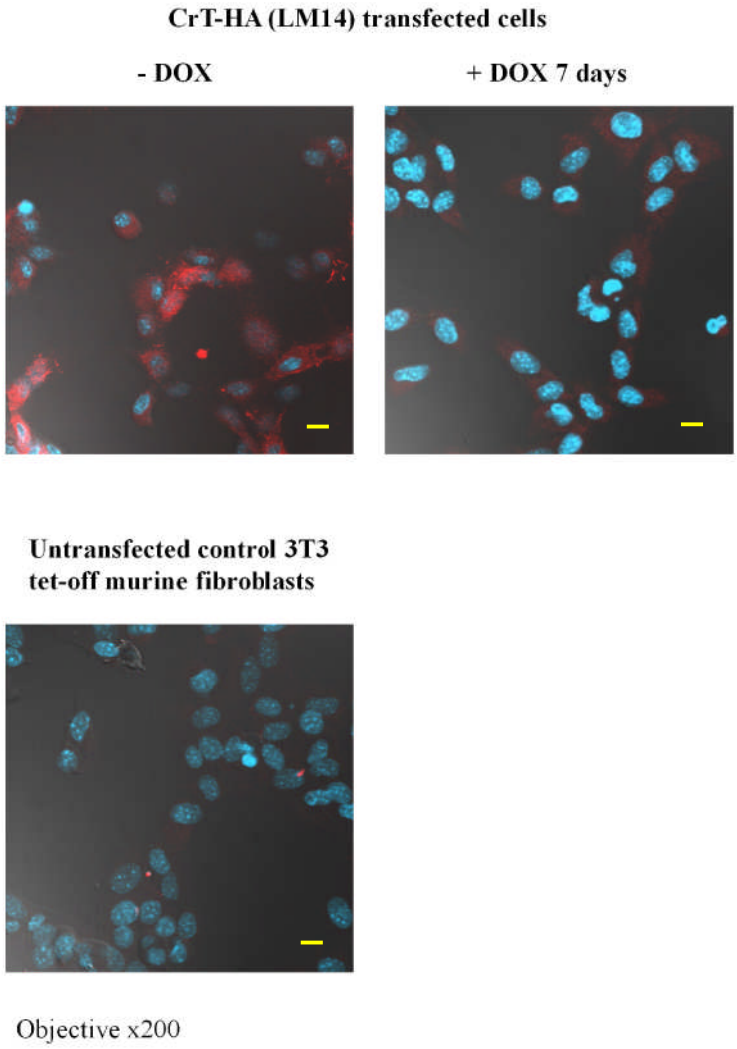
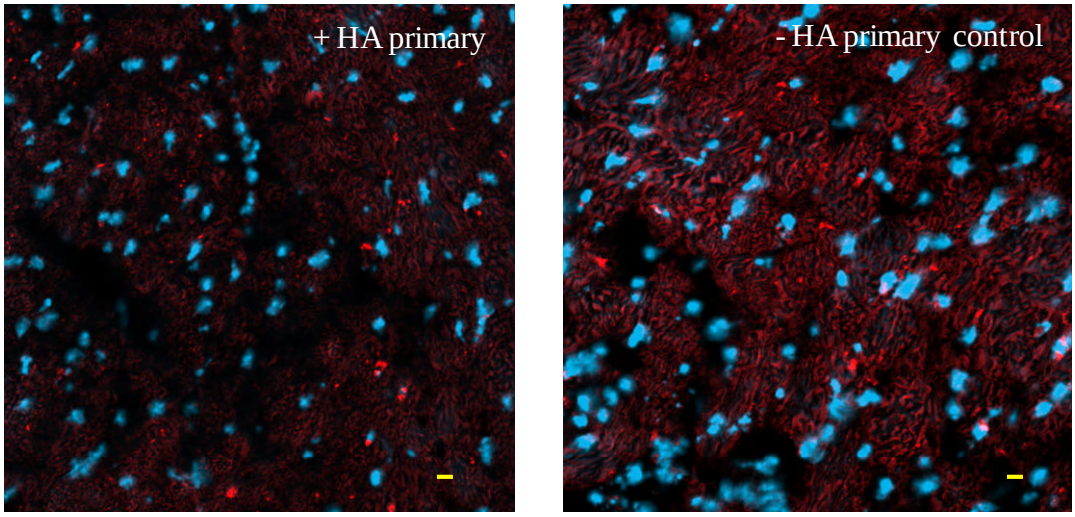


Figure 3-9. Confocal microscope images showing CrT-HA expression in response to 7-day dox incubation. CrT-HA positive cells are shown in red (anti-HA), and nuclei are stained blue (DAPI). A reduction in CrT staining is evident after 7- day dox incubation. Identical image capture settings were used for the acquisition of all images. Yellow scale bars = 20µM

3.2.6.1. Autofluorescence in LV tissue

Previous work on in our laboratory indicated that the anti-c-myc antibody used to probe the c-myc epitope tag can create difficulties in imaging, due to autofluorescence. To ensure that this would not be the case with anti-HA, cryosections of WT LV tissue were prepared and imaged

both in the presence and absence of anti-HA. Sections were initially incubated with anti-HA, with negative controls incubated in serum only. All sections were then stained with an appropriate secondary antibody (Alexa 546 anti-rat). Whilst a degree of general tissue autofluorescence was present, there was no difference between samples incubated with anti-HA and negative controls.



Objective x200

Figure 3-10. Confocal microscope images showing a comparison of fluorescence in WT LV tissue samples in the presence and absence of anti-HA. Following initial incubation in presence or absence of anti-HA, both samples were incubated in 2^{o} antibody, Alexa 456 anti-rat. Nuclei were stained blue (DAPI), and following confocal imaging it was clear that there was no difference in fluorescence between samples. Yellow scale bars = 20µM

Cell line name	Construct	CrT protein detected on Western?	Epitope tag detected on Western?	CrT detected with confocal?	Epitope tag detected with confocal?	Dox response detected?
L15	pWTT1-L15	-	-	n/a	n/a	-
LM14	pWTT1-CrT-HA	+	+	++	++	+
LM30	pWTT1-CrT-HA	+	+	+	+	+

Table 3-2. Summary of the three clones used for creating stable cell lines. LM14, a CrT-HA clone, was selected as the basis for further work.

3.2.7. Construct validation- CrT mRNA expression

3T3-CrT-HA cells were grown in the absence of Cr and dox, harvested and their mRNA extracted. Quantitative real-time RT-PCR was performed to determine total *CrT* expression levels, using *Com2* primers (see General Materials and Methods), specific to both endogenous (mouse) and transgenic (rabbit) *CrT*. Results were normalised to the reference gene, 36B4 (see General Materials and Methods). Results showed a 40-fold increase in total *CrT* expression when compared to untransfected control cells.

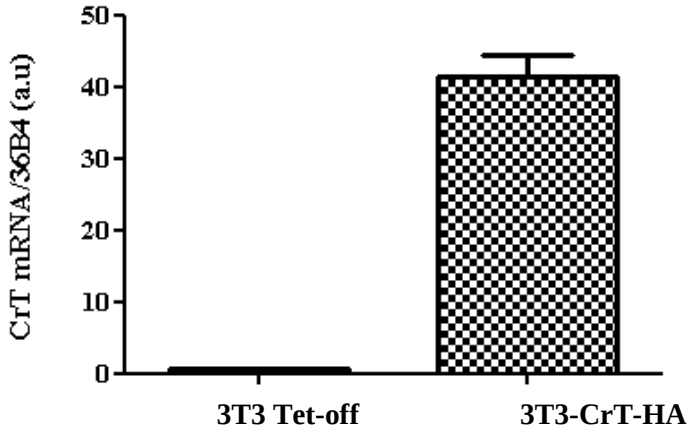


Figure 3-11. Total CrT expression in 3T3-CrT-HA cells compared to untransfected cells. *CrT* mRNA was quantified using *Com2* primers which are specific to both endogenous and transgenic *CrT*. Samples were tested in triplicate and normalised to 36B4. 3T3-CrT-HA cells showed ~ 40-fold greater CrT mRNA expression than control. Error bars represent SEM.

3.2.8. Construct validation- CrT activity *in vitro*. Cr uptake experiments

Having established the presence of transgenic *CrT* mRNA, and also verified the presence of a large amount of overexpressed CrT protein both by western blot and confocal microscopy, 3T3-CrT-HA cells, again incubated in the absence of dox (to induce expression of CrT-HA), were assayed for creatine uptake (see General Material and Methods) alongside untransfected control cells, in order to show that the overexpressed protein was functional. Cells grown in parallel to those to be used for the uptake assay were harvested simultaneously and protein levels were determined by the BCA assay. Cells overexpressing CrT exhibited a 10-fold increase in creatine uptake over the native uptake levels in untransfected cells (218 nmol creatine / mg protein / h vs. 21 nmol creatine / mg protein / h).

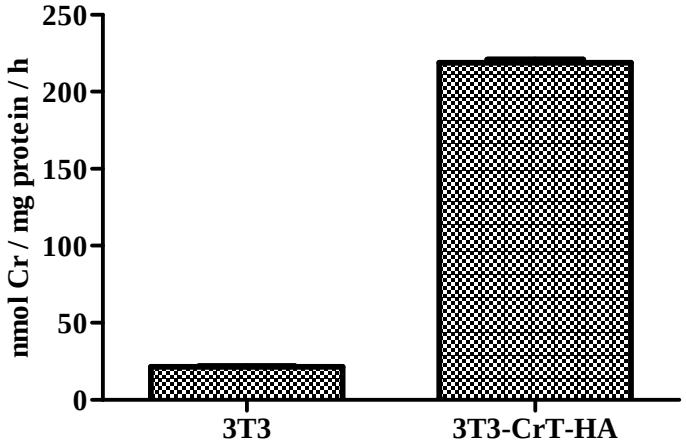


Figure 3-12. ^{14}C-Creatine uptake in 3T3- CrT-HA cells, and untransfected cells, normalised to nmol Cr / mg protein / h. All cells were grown in the absence of dox. Native uptake in 3T3-tet-off cells was low, with 10- fold greater uptake in 3T3-CrT-HA cells. Cells were incubated in the absence of dox, to induce transgene expression. *n=3*, error bars represent SEM.

Following confirmation of dramatically increased CrT activity in transfected vs. untransfected tet off cells, further Cr uptake experiments were performed in the presence of a range of Cr concentrations in dose-response experiments, in order to determine uptake kinetics. These demonstrated a K_m of around 45 µM, with V_{max} at 9.4 nmol Cr / well / h.

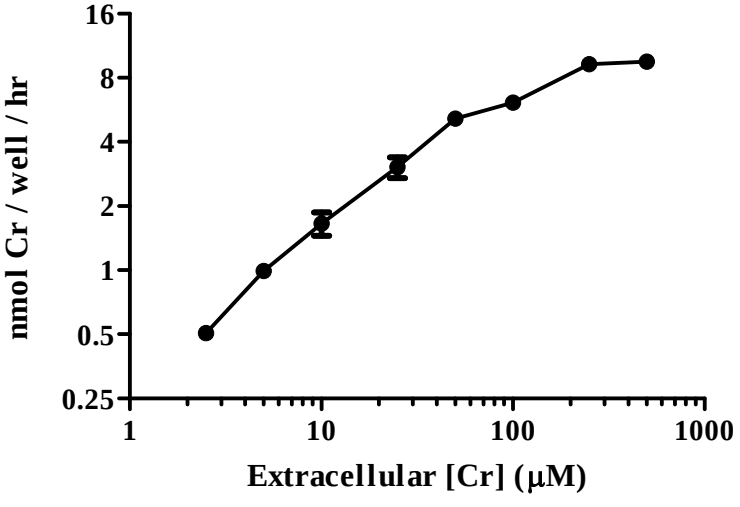
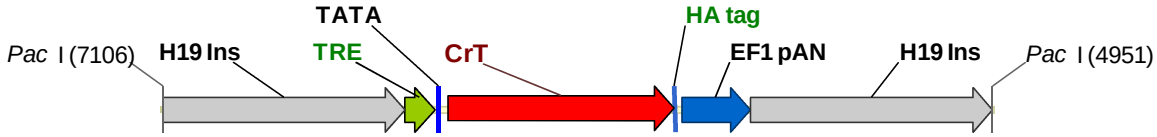


Figure 3-13. ^{14}C -Creatine uptake in 3T3-CrT-HA cells over a wide range of concentrations. The velocity of Cr uptake was expressed as nmol Cr / well / h. The velocity as a function of substrate concentration followed the Michaelis-Menten model. The Michaelis-Menten constant (K_m) was ~45 µM , with a V_{max} of 9.4 nmol /well / h. Cells were grown in the absence of dox. Duplicate results are shown; error bars represent SEM.

3.2.9. Generation of Creatine Transporter Responder (RCT) founder mice

Pronuclear microinjection and founder screening were performed by the Transgenic Core Facility (Wellcome Trust Centre for Human Genetics, University of Oxford). The pWTT1-CrT-HA transgene was linearised by *Pac*I digest, and the resulting linear fragment was microinjected into the male pronucleus of fertilised FVB/NCrl fertilised oocytes. These were cultivated overnight to the two-cell stage and then reimplanted into the oviduct of pseudopregnant CD1 foster mothers at 0.5 days post-coitum. Full details of this process are detailed in Appendix I.

In total, 10 transgenic founder lines were created, and 8 of these exhibited normal germline transmission. These 8 lines were used for further experiments.



Fragment of pWTT1-CrT-HA
6998 bp (molecule 9143 bp)

Figure 3-14. CrT-HA transgene. The 6988 bp *Pac*I - linearised transgene consists of the 0.3 kb tetracycline response element and minimal CMV promoter (TRE), *CrT* coding region, HA tag sequence and *EF1* polyadenylation site. The transgene is flanked by *H19* insulators and the direction of transcription is indicated by the arrows. TRE = tet response element, EF1 pA = EF1 polyadenylation signal, TATA = TATA box, H19 Ins = *H19* insulating element.

The following table shows details of the founder mice generated, indicating their assigned names, which are used throughout the text. Also indicated are the names of the subsequent double transgenic mice, the offspring of the founder lines bred with the rtTA inducer line. RCT 11 and RCT 12 did not exhibit normal germline transmission, and were excluded from further studies.

Founder ID No.	Assigned Name (responder line)	Date of Birth	Sex	Assigned name of double transgenic rtTA / CrT-HA	Successful germline transmission?
F0-3	RCT3	2.4.08	F	ICT 3	Yes
F0-16	RCT4	2.4.08	M	ICT 4	Yes
F0-722	RCT5	8.9.09	M	ICT 5	Yes
F0-758	RCT6	3.11.09	M	ICT 6	Yes
F0-760	RCT7	3.11.09	M	ICT 7	Yes
F0-765	RCT8	3.11.09	M	ICT 8	Yes
F0-769	RCT9	10.11.09	F	ICT 9	Yes
F0-771	RCT10	10.11.09	M	ICT 10	Yes
F0-773	RCT11	10.11.09	M	n/a	No
F0-774	RCT12	10.11.09	F	n/a	No

Table 3-3. Details of founder mice generated, and their assigned names. Of the 10 founder lines generated (RCT3-RCT12), 8 were selected for the breeding of double-transgenic rtTA / CrT-HA mice. RCT11 and RCT12 were excluded due to a lack of germline transmission.

3.2.10. Genotyping of RCT mice

The genotyping protocol was designed by the Transgenic Core Facility, employing primers WTT1-F1 and WTT1-R1, specific to the transgenic CrT. Conditions are listed in Appendix I.

3.2.11. Southern blot

A Southern blot strategy was optimized in order to determine transgene copy number and insertion number. Samples used were the founders' DNA along with several F1 DNA samples (extracted from tail). Digestion of the genomic DNA was performed with *EcoRV* prior to

separation on agarose gel. The Southern blot was probed with a ^{32}P-labelled BamHI-BglII probe, a fragment of pWTT1-CrT-HA. Detection threshold of one copy of the transgene was demonstrated, although the blot was uninterpretable, as no bands were detected in the samples themselves. The blot is shown in the figure below.

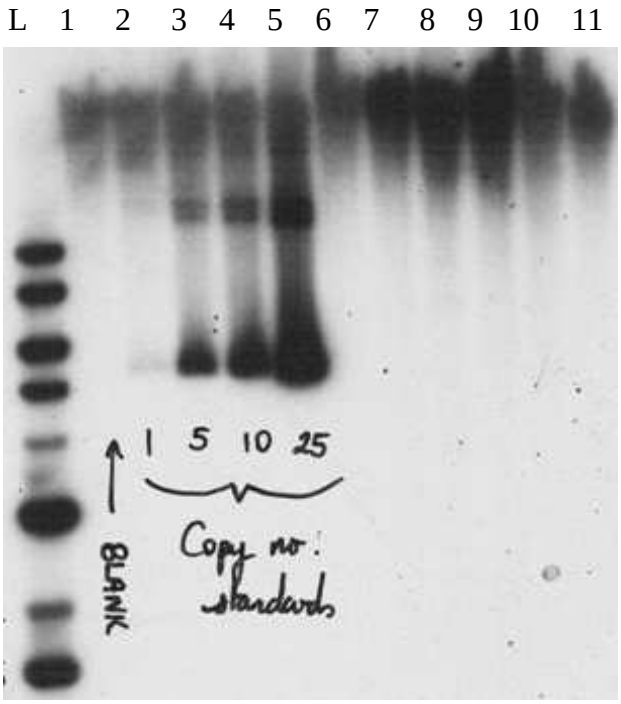


Figure 3-15. Southern blot. Blot shows WT tail DNA spiked with transgene as a copy number standard (lanes 1-5) , and founder animals (lanes 6-7) and F1 transgenic animals (lanes 8-11) confirmed by PCR genotyping, probed with a ^{32}P-labelled BamHI-BglII probe.

3.2.12. α-MHC-rtTA (Opt rtTA) mice

Mice expressing a codon-optimised variant of the rtTA protein, under the control of the α-MHC promoter, were obtained from the MMRRC. This line, Tg(Myh6-rtTA)8585Jam, originated in the MacDonald lab [182] and was on an FVB background. Mice were genotyped according to the protocol received from the MMRRC (see Appendix II). From this point on, these mice will be referred to simply as 'rtTA'.

3.2.12.1. Determination of zygosity of rtTA mice using qPCR

rtTA mice sourced from the MMRRC should have been homozygous, but after breeding it became apparent that they were heterozygous. The standard PCR genotyping protocol is unable to determine zygosity of the mice, so allelic discrimination by means of qPCR was necessary. The protocol was derived from Jackson Laboratories' protocol for the tTA allele and modified to suit the codon optimised rtTA line. Essentially, Ct values are used to calculate the relative Opt rtTA gene copy number according to the ΔΔCt method, through the difference between ΔCt compared to a known heterozygous control. The control is assigned a value of 1; concentrations between 1.8 - 2.2 are considered homozygous, and 0.8 - 1.2 heterozygous. The protocol is outlined in General Materials and Methods, along with primer sequences. The table below shows representative rtTA samples that were tested according to this method, including homozygous and heterozygous animals.

Replicate Name	Relative Conc.	Interpreted genotype	Calibrator
rtTA 7220	1.03	Heterozygote	
rtTA 7228	2.21	Homozygote	
rtTA 7672 (het)	1.00	Heterozygote	Yes
rtTA 7676 (WT)	0.03	WT	
rtTA 7669 (het)	1.16	Heterozygote	
rtTA7674 (WT)	0.01	WT	
rtTA 7675 (het)	1.02	Heterozygote	
rtTA 7222	1.93	Homozygote	
rtTA 7221	1.96	Homozygote	
rct 7435 -ve cont	0.00	WT	

Table 3-4. Ct values and calculation of relative rtTA gene copy number according to the ΔΔCt method (relies on the difference between ΔCt compared to a heterozygous control (indicated)). The control is assigned a value of 1; concentrations between 1.8-2.2 are considered homozygous, and 0.8-1.2 heterozygous. The calibrator sample is indicated.

3.2.13. Breeding strategy

rtTA mice were bred to homozygosity in order to ensure the maximum number possible of double-transgenic offspring. F_1 RCT mice (lines 3 – 12) were mated with rtTA mice to yield double transgenic pups. All 8 RCT founder lines selected were viable. Litter sizes were normal and offspring followed the expected Mendelian inheritance pattern of 50%. As discussed, RCT 11 and RCT 12 did not show normal Mendelian inheritance, with less than 10% of offspring carrying the transgene, and for this reason, were culled.

The number of founder animals generated led to a high number of mice to be bred, and subsequently genotyped and potentially characterised. A total of 10 founder RCT lines, 8 ICT lines and the Opt rtTA line led to 19 transgenic lines to maintain throughout this study. The

strategy pursued led to a considerable length of time from the creation of viable founder lines to the testing of the subsequent double transgenic ICT mice; the minimum possible time being around 30 weeks.

Both rtTA and RCT mice were on an FVB background. This is due to (a) the fact that the Opt rtTA mice are supplied from the MMRRC on this background, and (b) pronuclear microinjection has a significantly higher success rate in pronuclei of fertilised FVB oocytes than in C57BL/6 oocytes. The following schematic diagram shows the breeding strategy for each of the 8 RCT lines used in the breeding of the double transgenic ICT mice. Fifty % of the offspring of these crosses were expected to express both the desired genes. Double transgenic (ICT) mice were not used subsequently for breeding- all ICT mice were bred from an RCT x Opt rtTA cross.

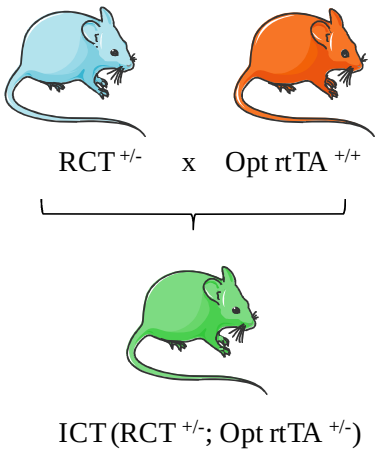


Figure 3-16: Breeding strategy for the creation of mice with doxycycline-induced control of CrT expression. The diagram shows the breeding strategy performed following the generation of RCT mice, through pronuclear microinjection of the CrT-HA construct. This strategy was followed for each of the lines tested. The strategy led to a total of 19 transgenic lines being bred through the course of the study.

Genotyping protocols were optimised for both RCT and rtTA lines, and it was found that these reactions worked well in a multiplex PCR. All subsequent genotyping on ICT double transgenic mice was performed using this method. The figure below shows an example gel, demonstrating

the 372 bp PCR product amplified from RCT mice, and the 264 bp band amplified from rtTA mice. PCR conditons are shown in General Materials and Methods.

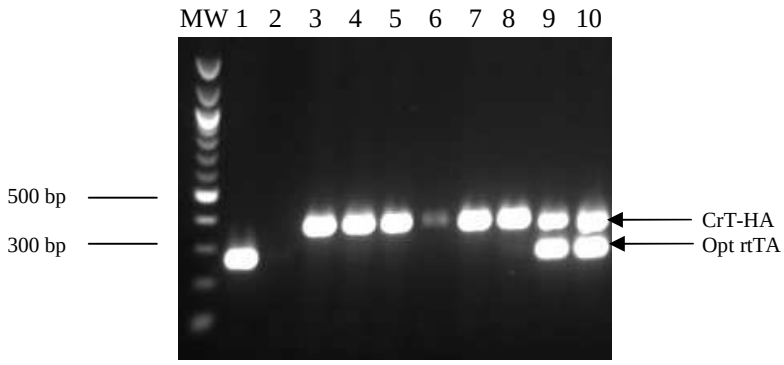


Figure 3-17. Representative gel showing PCR genotyping results of single and double transgenic animals. The CrT-HA product is the higher 372 bp band and the rtTA product is 264 bp. Lanes 1-8 are either negative, or single transgenics. Lanes 9 and 10 show double-transgenic samples. The molecular weight ladder (denoted 'MW') is NEB 100 bp.

3.2.14. Induction of CrT-HA expression with dox-feeding

To induce gene expression in the rtTA / CrT-HA double transgenic (ICT) mice, dox was administered via the drinking water. Dox was provided at a concentration of 0.2 mg / mL, with the addition of 1% sucrose to enhance palatability. All dox-feeding procedures included the following controls: a) rtTA only dox-fed, b) RCT only dox-fed, c) WT dox-fed, and d) double transgenic (ICT) administered 1% sucrose without dox. Water bottles were protected in aluminium foil, to protect dox from the light, and changed every 48 h. Dox was administered for 7 days prior to culling the mice.

Body weights of the mice were monitored throughout the 7 day period of dox administration, to ensure neither the dox or the sucrose were affecting body weight (either due to palatability, toxicity or calorific value due to the presence of dox and sucrose). Additionally, water consumption was monitored. No changes were found in any of these parameters when compared

to control mice with normal drinking water (data not shown). At the point of culling, heart, liver, and lung were harvested and snap-frozen in liquid nitrogen for analysis. Hearts were separated into LV, RV, LA and RA. LV tissue was used in all analyses.

3.2.15. Opt rtTA mRNA is detectable in left ventricular tissue

Expression of rtTA mRNA was detected in Opt rtTA mice and also in ICT (double transgenic) mice, using quantitative real-time PCR (see General Materials and Methods) following 7 days doxycycline administration via the drinking water. Results of the quantitative real-time PCR, performed on double-transgenic ICT3 and ICT4 mice and normalised to the reference gene 36B4 are shown in table 3-5. Whilst variable, expression was detected in all LV tissue from animals expressing rtTA.

Sample name	rtTA genotype	CrT-HA genotype	Expression Opt rtTA / 36B4 (arbitrary units)
rtTA 7493	-	-	0.041877459
rtTA 8243	+	+	1.133781136
rtTA 8246	+	+	1.216810465
rtTA 8246v	+	+	0.894364351
rtTA 8247	+	+	0.755014327
rtTA 8250	+	+	1.031166518
rtTA 8252	+	+	0.973769731
rtTA 8253	+	-	1.25652388

Table 3-5. Real-time RT-PCR results of amplification of *rtTA* mRNA from LV tissue. All samples with the exception of the WT control (7493) show expression of *rtTA* mRNA. Results are normalised to the reference gene 36B4.

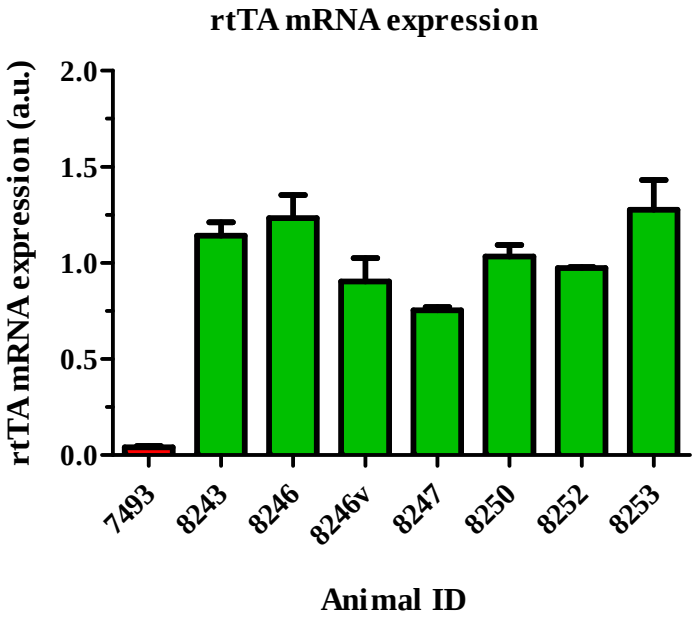


Figure 3-18. Graph of the data represented in the table above. WT control is indicated in red. All other animals are double-transgenic ICT expressing rtTA, with the exception of 8253, an rtTA animal. Error bars represent SEM.

3.2.16. *CrT* mRNA is elevated in some, but not all left ventricular ICT tissue

Total *CrT* mRNA was measured in the same samples, and while there was a certain degree of variation between samples, dox-fed double transgenic mice did not demonstrate greatly increased expression of *CrT* mRNA, with some samples expressing less than WT. The exception was 8250, an ICT4 dox-fed animal that demonstrated a significant increase in *CrT* mRNA expression compared to WT.

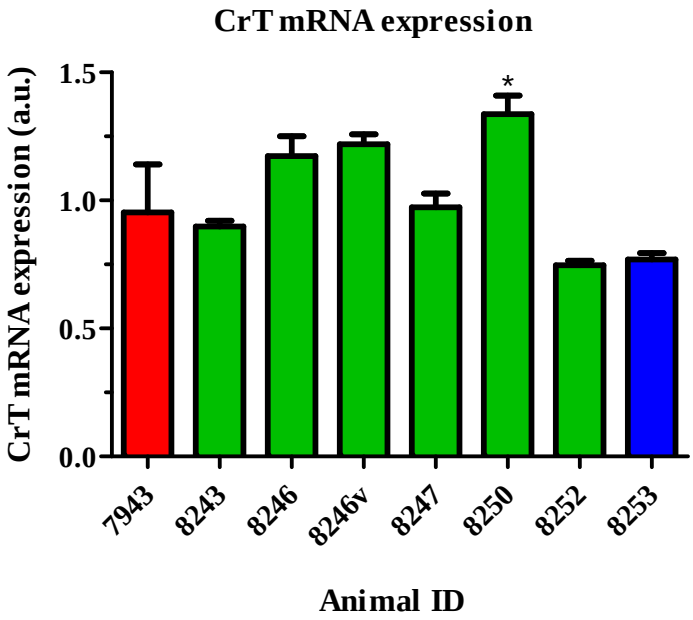


Figure 3-19. Total *CrT* mRNA expression in LV of dox-fed double transgenic ICT mice. 7943 (in red) is WT control, and 8253 is single transgenic rtTA (blue).8243, 8246, 8246v, 8247, 8250 and 8252 are double-transgenics. Error bars represent SEM. There was a significant increase in total CrT expression in animal 8250 (ICT4) vs. control. Values are mean ± SEM. * p< 0.05 (One-way ANOVA with Dunnett's multiple comparison test)

3.2.17. rtTA is undetectable in left ventricular tissue

Western blots were performed in order to determine the presence of rtTA protein in mice expressing *rtTA* mRNA. An rtTA-specific antibody was used (anti-TetR, Mobitec, Germany). However, it was not possible to verify α-MHC driven rtTA expression in left ventricular tissue, despite several attempts for optimisation. Positive control samples also failed to yield any bands, and as such, despite known rtTA mRNA expression, it was not possible to prove either the presence or absence of rtTA protein.

3.2.18. CrT-HA is detectable in some, but not all left ventricular tissue

Detection of the CrT-HA protein by western blot demonstrated the presence of CrT-HA in one sample only- ICT4 8250, the same animal shown to have statistically-significant elevated *CrT* mRNA. The band appeared at the expected size of ~70 kDa. No bands were observed in either

the dox-fed WT control (7943), or the double transgenic ICT4 8248 not administered dox. However, CrT-HA was not detected in either of the other 2 dox-fed double transgenic animals tested, ICT3 8243 or ICT4 8252, which appeared the same as control samples. The blot was probed with anti-HA (Roche), as described in General Materials and Methods.

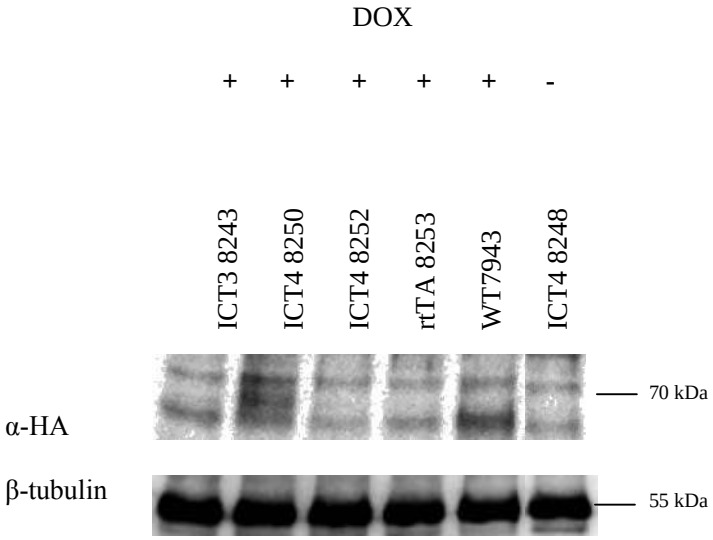


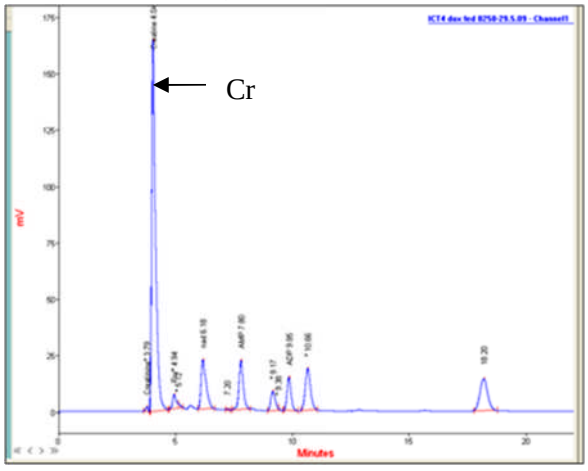
Figure 3-20.Western blot analysis of HA, in LV tissue extracted from mice following 7-day dox feeding. The 3 ICT4 animals are double transgenic, ICT4 8248 is the double transgenic –dox control and rtTA 8253 and WT7943 are negative. ICT4 8250 demonstrated a band at the expected size for CrT-HA, 70 kDa, although this was not observed in either of the other 2 dox-fed, double transgenic mice.

3.2.19. With one exception, myocardial creatine levels are not elevated in dox-fed ICT mice

HPLC was performed on LV tissue lysates of all double transgenic ICT mice that were dox fed in order to quantify myocardial Cr levels. The method used is detailed in General Materials and Methods. To date, all 8 viable ICT lines have been tested using this method. With the exception of one animal, ICT4 8250, which exhibited a 2.3-fold elevation in LV Cr levels, no Cr values above those of the wild-type have been detected. The HPLC results from this mouse are shown on the following page, and compared to a WT chromatogram. The magnitude of the Cr peak (indicated by the arrow) in the CrT overexpressing animal is clearly much greater than that of the WT sample, when compared to the unaltered peaks alongside. Confirmation of the high

value is shown in the table below, where the result is normalised to mg protein and compared to other representative samples run on HPLC. WT LV [Cr] is typically 60-80 nmol / mg protein, and the results show that all samples with the exception of 8250 had WT [Cr]. In total, 46 mice were dox-fed and LV [Cr] was determined in all of these animals by HPLC. Data for the majority of animals tested which demonstrated unaltered LV [Cr] are not shown.

ICT 4 8250, with elevated creatine



WT sample

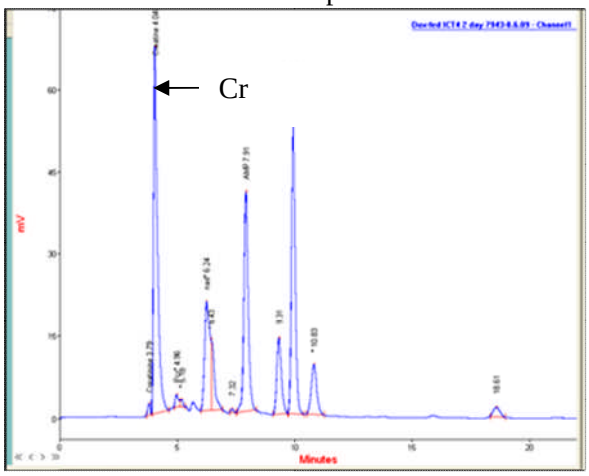


Figure 3-21. HPLC chromatograms. These showing the difference between the creatine peak (as indicated by the arrows) in sample ICT4 8250 compared to non-transgenic WT sample- note size of creatine peak relative to other peaks in trace. WT chromatogram is representative of all the other dox-fed animals tested.

Animal ID	**rtTA genotype**	**CrT-HA genotype**	**Dox fed?**	**nmol total creatine/ mg protein**
ICT3 8243	+	+	+	68.9423049
ICT4 8250	+	+	+	160.2799267
ICT4 8252	+	+	+	62.12711268
rtTA 8253	+	-	+	62.50408457
WT 7943	-	-	+	60.75663462
ICT4 8248	+	+	-	64.79286204

Table 3-6. Total Cr levels in LV of mice following 7 day dox feeding protocol. Animal 8250 (shown in red) shows ~2.3 x WT [Cr], although all other double transgenic mice tested following dox administration show WT levels of Cr.

The following table summarises the number of double transgenic rtTA / CrT-HA mice that were put on a dox feeding protocol, with details of their origin. One line only was found to overexpress CrT-HA, and of the 13 mice tested from this line, ICT4, only 1 animal demonstrated supra-normal myocardial [Cr]. A total of 33 other mice, including some from all of the other lines, were also dox-fed, though none demonstrated elevated myocardial Cr.

Founder ID No.	Assigned name of double transgenic rtTA / CrT-HA	Number of double-transgenic mice dox-fed	Number of dox-fed mice overexpressing CrT-HA
F0-3	ICT 3	10	0
F0-16	ICT 4	13	1
F0-722	ICT 5	6	0
F0-758	ICT 6	4	0
F0-760	ICT 7	3	0
F0-765	ICT 8	4	0
F0-769	ICT 9	3	0
F0-771	ICT 10	3	0
F0-773	n/a	No	n/a
F0-774	n/a	No	n/a

Table 3-7. Summary of the numbers of double transgenic rtTA / CrT-HA mice (ICT) from each line that were put on a dox feeding protocol. One animal only, ICT4 8250, demonstrated elevated LV [Cr]. Numbers of controls included in the dox feeding protocols are not included.

3.2.20. Validation of the rtTA inducer line: Creation of a double-transgenic tet-on luciferase responder mouse line

In order to determine the cause of lack of expression of CrT-HA in the 10 lines tested, the function of the rtTA inducer line was verified. Mice containing the luciferase gene, downstream

of a tet-inducible promoter were obtained [183] (a gift from Dr. P. Pollard, Wellcome Trust Centre, University of Oxford). These mice were bred with the rtTA inducer line used in the generation of the ICT lines, to determine whether the cause of the lack of CrT-HA transgene expression lay with this inducer line, or with the RCT founder lines. Double transgenic mice, denoted 'rtTA-LC1', (indicating the presence of the rtTA and LC1 genes) were bred, and the presence of LC1 and rtTA was confirmed by genotyping. The mice were administered doxycycline at a concentration of 0.2 mg / mL for 7 days, with 1% sucrose, and culled. Organs were excised for detection of luciferase expression.

3.2.21. Optimisation of the luciferase assay

HEK 293-T cells were grown to ~70% confluence, and transfected with the luciferase reporter vector, pGL3 control (Promega UK, Southampton, UK), using FuGENE transfection reagent (Roche), with plasmid : FuGENE ratios of 2:6 and 2:8 (for transfection protocol, see General Materials and Methods). Additional transfections with eGFP (Clontech) were performed as validation of transfection efficiency (results not shown). Forty-eight hours post-transfection, the cells were harvested and lysed in lysis buffer CCLB (Cell Culture Lysis Buffer, Promega). GFP-transfected cells were analysed for expression on a fluorescence microscope. Transfection efficiency was shown to be low at 10% (data not shown).

A luminescence assay was performed using the Promega Luciferase Assay System, and results measured on a Labsystems Luminoskan Ascent luminometer. Both transfection ratios used were successful, though plasmid : FuGENE at a ratio of 2 : 6 yielded far higher expression of luciferase than a ratio of 2 : 8. No luminescence was detected in the untransfected control sample. Results are shown in the following figure.

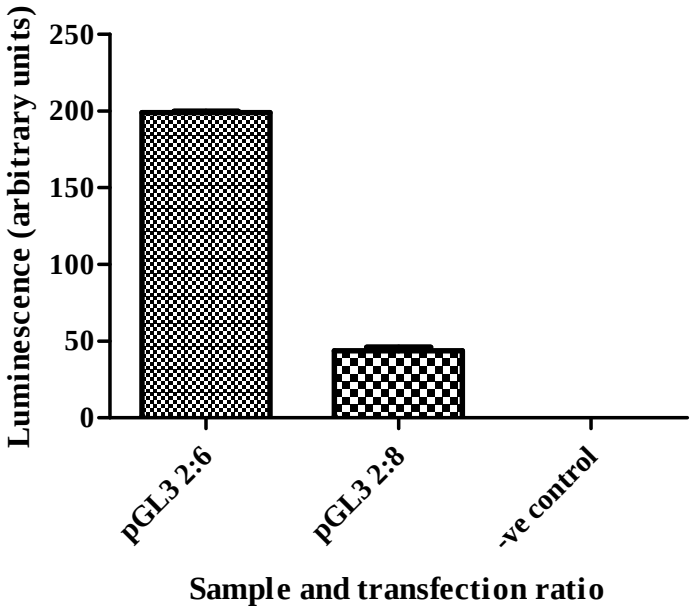


Figure 3-22. Luminescence (arbitrary units) of HEK 293-T cells. These are transfected with 2 different ratios of transfection reagent : plasmid, compared to untransfected control cells. *n=2* per sample, error bars represent SEM.

3.2.22. Luciferase expression is driven by the rtTA inducer line

LV tissue harvested from the dox-fed double-transgenic rtTA-LC1 mice was crushed, and the extraction protocol described by Manthorpe *et al* [184] was followed. The values obtained indicated clear evidence of expression of luciferase in all double-transgenic dox-fed LV samples, although there was a variation in luminescence levels. LV from single transgenic ($rtTA^-/LC1^+$) animals, and LV from double-transgenic animals not administered dox (both used as negative controls) showed no luminescence. The table below shows the results of the luciferase assay, detailing genotypes and dox feeding status.

Sample ID	LC1	rtTA	Sex	Dox fed?	Luminescence
1627	+	-	m	Yes	0.0096
					0.0079
1628	+	+	m	Yes	293.7
					266.1
1629	+	+	m	Yes	45.76
					42.14
1632	+	+	f	Yes	13.16
					12.8
1633	+	-	f	Yes	0.0084
					0.0107
1634	+	+	f	Yes	8.066
					8.033
1639	+	+	m	No	0.0684
					0.0577

Table 3-8. Luminescence (arbitrary units) of LV samples of double transgenic rtTA-LC1 mice after 7 days of dox administration. Double transgenic dox-fed animals all showed clear LC1 expression in LV. None of the negative controls showed luminescence.

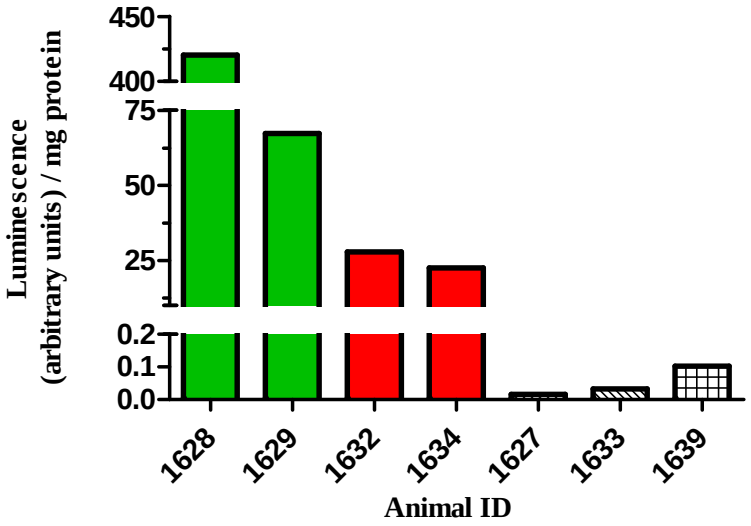


Figure 3-23. Luminescence of LV of double transgenic rtTA-LC1 mice after 7 days of dox administration, normalised to protein. Green bars represent double transgenic dox-fed males, red bars represent double transgenic dox-fed females. Hatched bars represent negative controls.

3.3. Discussion

Owing to the limitations of a previous model of creatine transporter overexpression, namely varied levels of overexpression and early foetal and embryonic transgene expression, a strategy for temporal CrT overexpression was pursued. The aim was to produce a model whose transgene overexpression was tightly controlled, both in terms of onset and levels of overexpression.

A CrT construct, incorporating a C-terminal epitope tag and flanked by *H19* insulating elements was cloned. A stable cell line overexpressing the transgene was created, and an array of *in vitro* validations was performed. CrT-HA protein was detected in these cells by western blot, and localised using confocal microscopy. Functionality of the transgenic protein was confirmed with

^{14}C-creatine uptake assays and transfected cells were shown to exhibit a 10- fold increase over control Cr uptake levels. Additionally, dox inducibility of this construct was validated.

A total of 10 transgenic founder lines were created by random integration. The 8 lines exhibiting normal germline transmission were crossed with the Tg(Myh6-rtTA)8585Jam (rtTA) inducer line to yield double-transgenic offspring. CrT-HA transgene expression was tested with real-time RT PCR, western blot and biochemical analysis of LV creatine levels. Despite the presence of *Opt rtTA* mRNA in the LVs of all double transgenic animals, LV creatine was found to be elevated in just one animal of all those tested. At least 5 double-transgenic mice from each of the 8 lines were dox-fed and tested- in total, 46 mice. To exclude the possibility that the lack of dox-induced CrT-HA expression was due to a non-functional rtTA, breeding was set up between the rtTA line and a luciferase (LC1) reporter line [183]. Dox-feeding the offspring of this cross identified the responder lines as the cause of lack of CrT overexpression.

3.3.1. *In vitro* validation of the constructs

Initial cloning with a construct utilising a c-myc epitope tag was abandoned, due to an inability to detect it either *in vitro* or in tissue sections. Use of the pWTT1-CrT-HA construct was pursued, and in order to validate the constructs prior to the generation of transgenic mice, a series of experiments were performed to demonstrate mRNA- and protein-expression of the CrT-HA protein. Additional experiments confirmed functionality of CrT-HA. Dox-inducibility tests were performed in NIH murine 3T3 fibroblasts already stably-expressing the tTA protein. Although different to the rtTA 'Tet-On' approach used in the creation of the transgenic lines, this cell system demonstrated that the TRE in the construct was functional. An interesting result was the apparent localisation of CrT-HA protein in the 3T3-CrT-HA cells, elucidated by confocal microscopy. CrT-HA was expressed throughout the cytoplasm as well as the in cell

membrane, where its presence was expected. A possible explanation for this could be the level of overexpression. The large amount of overexpressed protein could overwhelm the cell's ability to successfully process all the protein, resulting in a lower percentage of glycosylated and / or phosphorylated protein than under normal conditions. Glycosylation is known to be involved with the trafficking of CrT to the plasma membrane, with glycosylation-deficient mutants present in the membrane at lower levels than fully mature CrT [39].

It is noteworthy that the transient transfection of 3T3 tet-off fibroblasts with pWTT1-CrT-HA was not possible. It could be due to the large size of the construct (9.1 kb). The generation of stable cell lines also proved difficult, with a low success rate of 1 in 12. If this can be related to the success of the founder lines in expressing CrT-HA, then perhaps it is unsurprising that only one exhibited any degree of overexpression.

3.3.2. Generation of transgenic mice

The pWTT1-CrT-HA construct was microinjected in to the male pronuclei of fertilized oocytes, yielding transgenic founder mice. Initial attempts at microinjection gave a very low success rate, and due to this the decision was made to perform all microinjections on an FVB background. However, the ultimate goal was to backcross to C57BL/6, as the previous model of CrT-OE was generated on a C57BL/6 background, and it has been shown that genetic background can have a significant impact on phenotype [126]. Additionally, FVB oocytes are considered a more successful basis for microinjection than C57BL/6 oocytes, due to their large pronuclei and the clarity of the cytoplasm and nuclear structure. It is known that C57BL/6 eggs have a lower survival rate following microinjection when compared to other strains and that in general, there are strain-dependent differences in the efficiency of transgenic mouse production. Strain-specific effects and the effect of mixed background on both knockout models of cardiac

energetics [126] and tetracycline-inducible models of transgene expression have been demonstrated. For example, a model of Charcot-Marie-Tooth disease type 1A created on a mixed genetic background showed variable levels of expression of *LacZ* or *pmp22* expression between mice, whereas backcrossing the transgene on to CBA/Ca background gave higher and more uniform levels of expression compared to the C57BL/6J background [185]. Tet-inducible systems have, however, been shown to work successfully on both FVB and C57BL/6 backgrounds [167 186 187].

3.3.3. Choice of the Opt rtTA inducer line

The codon-optimised α-MHC line (FVB/N-Tg(Myh6-rtTA)8585Jam/Mmmh), originated by Valencik *et al* and supplied by the MMRRC, was used. This line comprises a codon-optimised version of the reverse tetracycline transactivator cloned behind the Robbins 5.5 kb α-myosin heavy chain promoter. In another rtTA mouse line [141], Valencik *et al* found that despite an abundance of rtTA mRNA, they were unable to detect rtTA protein. They suggested that the reason for this was due to the severe prokaryotic codon usage bias exhibited by the rtTA coding sequence originally used by Gossen and Bujard [141]. Transresponder protein (TR) was also undetectable in response to dox administration. When they substituted rtTA for its 'codon-optimised' form (termed Opt-rtTA), the expression of similar levels of mRNA were found to lead to a large increase in TR protein expression, with the authors claiming an increase in the tetracycline-inducible transgene system from 20- fold to 832- fold in the heart [182]. This inducer line has been used successfully to drive dox-induced expression in the heart in several mouse models, including PGC-1α [188] and Myc [189]. Therefore this inducer line was chosen for this project.

In spite of Valencik and colleagues' successful detection of the rtTA protein using the VP16 specific antibody 2GV4, it has not proved possible to detect the protein using commercially available antibodies in our laboratory. Other studies have demonstrated that the tTA protein is not readily detectable, hypothesising that expressed levels are below the threshold of detection. However, Opt rtTA mRNA was detected in all animals tested, and later tests of the inducer line confirmed that the rtTA is functional in this line.

3.3.4. Generation of a double transgenic luciferase reporter line

Owing to the failure of the majority of ICT mice to express the CrT-HA transgene and demonstrate elevated myocardial creatine, a strategy to ascertain which element of the system was at fault was required. The absence of detectable rtTA protein in the LVs of rtTA mice necessitated validation of the inducer line. rtTA mice were bred with a luciferase reporter line, with the *LC1* gene under the control of the TRE. Resulting double-transgenic offspring were dox-fed, and subsequently tested for luciferase expression. All dox-fed double transgenic animals expressed LC1 in the LV, providing clear evidence that the rtTA inducer line works, and also that the concentration of dox chosen (0.2 mg / mL) was sufficient to induce gene expression. Background levels of LC1 only were found in double-transgenic mice that had not been dox-fed, indicating tight regulation of expression and minimal leakiness, despite the potential for leaky expression using the rtTA system outlined in the introduction to this chapter.

3.3.5. Explanations for the lack of CrT-HA expression in ICT mice

Evidence proving the efficacy of the inducer line in driving expression in tet-responder LC1 mice indicates that in this case, failure to induce expression of CrT-HA is due to the RCT responder lines. It is likely that this was owing to positional effects of transgene insertion, due to

the strategy of random integration employed in the generation of the founder animals. Previous experiments showed that the construct was functional in transfected cell lines, driving expression of CrT-HA and responding to doxycycline. There is considerable evidence demonstrating the effects of positional effects and variegated expression in the tetracycline system [167 170 190]. However, this does not clarify the result obtained from the single animal of all those tested that showed considerably elevated myocardial Cr. Another possible cause is the use of the *H19* insulating elements. Despite their documented advantages, they have been shown to prevent transgene expression on at least one occasion, and perhaps this could explain the stochastic occasional expression observed [164]. It is widely documented that numerous founder lines are often required to achieve successful expression of transgenes using the tetracycline binary systems, with Sanbe *et al* stating that, on average, between 5-20 founders are needed [147]. Whilst the generation of more founders could perhaps yield a functional CrT-OE line, it seems likely that a different approach would be beneficial.

3.4. Summary and future directions

Rabbit CrT cDNA, with a C-terminal haemagglutinin epitope tag, was cloned downstream of a tetracycline-responsive promoter, and flanked by H19 insulating elements in the vector pWTT1. Validation of the construct was enabled by the creation of stable cell lines overexpressing the pWTT1-CrT-HA construct. Expression was determined at the mRNA level and the protein level *in vitro*, and functionality of the overexpressed protein was also determined *in vitro* by means of Cr uptake assays. The HA fusion protein was readily detectable on western blot, and dox-inducibility was demonstrated. None of the founder lines tested showed gene expression when crossed with an inducer line, with the sole exception of RCT4. Testing revealed the inducer line to be functional, indicating that the lack of CrT overexpression was due to the founder lines.

These findings demonstrate shortfalls in the generation of transgenic mice using random integration. The possibility that a functional founder line could eventually be created using this method cannot be ruled out, although it seems that an alternative strategy for founder generation, such as one using targeted integration, would be preferable. This would increase the likelihood of generating a functional founder, whilst minimising the need to create multiple founder lines, by virtue of gene integration into a specific locus, such as *Rosa 26*, which has been prevalidated as being a suitable docking site for inducible Tg expression [154]. Additionally, the use of transgene insulating elements in this instance has to be questioned, and their exclusion from future constructs could be beneficial.

Chapter 4. Regulation of the Creatine Transporter via the IGF-1 pathway

4.1. Introduction

4.1.1. Regulation of the CrT

The regulation of *CrT* transcription and CrT activity, either through the involvement of external regulatory pathways, or by post-translational modification, is complex and not fully elucidated. The experiments within this chapter were designed to discover more about regulation through phosphorylation, by identifying candidate regulators in known signalling pathways with molecules which have previously been determined to have an effect on the CrT, and also candidate molecules. The main pathway selected for investigation is the IGF-1 pathway. Insulin and IGF-1 were previously shown to enhance Cr uptake, but the mechanism and signalling pathway were not investigated [11]. PKA- and PKC- mediated phosphorylation are investigated- evidence of possible involvement in the regulation of the CrT from the literature merits further investigation, particularly in relation to the IGF-1R pathway. mTOR (mammalian target of rapamycin), a kinase believed to be downstream of IGF-1R, was also chosen for investigation. Conflicting reports of the influence of these kinases on CrT activity exist in the literature, although many of the studies performed previously were in artificial *in vitro* systems, such as *Xenopus* oocytes, which bear little relevance to the heart.

4.1.2. CrT regulation by substrate

As long ago as 1987, a link between extracellular Cr concentration and creatine transport in human muscle cells was established [100]. Whilst oral supplementation of Cr is known to markedly

increase plasma Cr levels, by as much as 10 – 20 fold [191], any increase it has on intracellular levels is much smaller. This suggests more complex regulation than extracellular Cr alone. At least two papers have suggested that *intracellular* Cr plays a role in CrT regulation [100 25]. In these cases, the authors found that incubating cells in high extracellular Cr over time led to a marked reduction in Cr transport, and attributed this effect to a two- to three- fold loss in maximal CrT activity, while affinity of the CrT for Cr remained unchanged [25 100]. These results suggest that high extracellular Cr leads to an initial increase in intracellular creatine levels, which then feed-back, limiting Cr transport [31]. It is also accepted that there is a relationship between Cr influx into, and efflux from the cell; thus, Cr homeostasis in the cell is maintained by these processes, with the CrT regulating influx and maintaining intracellular Cr levels. Boehm *et al* established that feeding a 3% creatine diet to rats for a 6 week period led to a ~30% decrease in the content of the plasma-membrane CrT, similar to the decrease that was found in CrT activity. Plasma membrane CrT content on the heart vesicles that Boehm *et al*. were studying could vary, in a manner consistent with Cr uptake, while the total CrT protein content of the tissue remained the same. Therefore, they concluded that in this case the regulation of creatine transport was due to a decrease in the number of *active* CrT units on the plasma membrane, as opposed to other forms of regulation [31]. This conclusion is supported by the findings of Guerrero-Ontiveros and Wallimann, who also demonstrated a down-regulation of the CrT in response to prolonged Cr-feeding in rat skeletal muscle [29]. Both of these studies are now known to be flawed, owing to the use of an unreliable anti-CrT antibody, known to cross-react with PDH. This raises a degree of uncertainty about their findings relating to CrT protein levels. Odoom *et al* found that incubation of myoblasts in cyclohexamide (an inhibitor of protein synthesis) enhanced Cr uptake 2.4-fold. This could suggest the synthesis of a protein in response to high intracellular Cr which inhibits further Cr uptake, either by inhibiting CrT activity, or by functionally removing the transporter from the plasma membrane, a phenomenon also described

by Loike *et al* [100]. It has also been suggested that chronic regulation may involve the sodium concentration across the cell membrane, and also factors which directly stimulate or inhibit the CrT [191].

Yet more evidence linking intracellular Cr content to the rate of Cr uptake comes from studies performed using competitive inhibitors of Cr. The most effective of these inhibitors is 3-guanidinopropionate, or β-guanidinopropionic acid (β-GPA), a guanidinocarboxylic acid. [192]. This compound actively competes with Cr at its uptake site on the CrT. After 6 weeks of β-GPA feeding, Boehm and colleagues established a fivefold increase in the plasma-membrane CrT content in rat cardiomyocytes, and whilst Cr uptake levels were increased, this was only twofold at most, leading the authors to suggest that in those conditions, the CrT is subject to kinetic inhibition, or that some of the over-expressed protein might be dysfunctional. They were unable to draw definite conclusions, although they clearly demonstrated the link between up-regulation of CrT expression in the event of Cr depletion [31]. Once again, this study used an unreliable antibody, and perhaps a more plausible explanation for the five-fold increase in plasma-membrane CrT they observed is the known cross-reactivity of the antibody used against CrT in the study with PDH [40].

Further evidence regarding the regulation of CrT by Cr was shown by ten Hove *et al*, in a study investigating the regulation of CrT in both CrT overexpressing mice, and GAMT KO mice, (lacking the ability to synthesise Cr, and fed with a Cr-free diet). In the overexpressing mice, *CrT* mRNA levels were shown to correlate with Cr uptake, and the GAMT KO mice showed a 7-fold increase in Cr uptake when Cr was added to their diet, accompanied by a small increase in *CrT* mRNA [48]. This is discussed in more detail in Chapter 6. These findings suggest that the CrT is active over a very large dynamic range, and that the chronic absence of Cr, such as in

GAMT KO mice, is an extremely strong stimulus for an increase in CrT activity. The findings in the GAMT KO mice also indicate that transcriptional regulation of the CrT may be less important than regulation through other means, such as post-translational modification.

4.1.3. The IGF-1 signalling pathway as a regulator of Cr transport

4.1.3.1. The regulatory role of insulin

It has long been recognised that insulin can enhance creatine uptake, with insulin reportedly increasing the transfer of Cr from the circulation into skeletal muscle [193] [194]. Steenge *et al* determined that insulin can enhance muscle creatine accumulation in humans when present at physiologically high or supraphysiological concentrations, and concluded that this was likely the result of an insulin-mediated increase in muscle creatine transport rather than creatine delivery [195]. A detailed study by Odoom *et al* [11] studied the effects of various hormones, including insulin, on Cr uptake in G8 mouse myoblasts. It was expected that stimulation of the CrT would occur following insulin treatment, as insulin was previously reported to stimulate the Na^+, K^+ - ATPase [196] [197] [11]. This stimulation is a proposed cause of enhanced Cr accumulation. The insulin-driven activation of the Na^+, K^+ - ATPase leads to an increased Na^+ gradient across the cell membrane, which probably increases the electrochemical gradient used to drive the CrT. This in turn results in increased creatine uptake [198]. However, Odoom *et al* found that insulin at physiological concentrations (0.2 - 0.8 nM) had no effect on creatine accumulation in the cells, whereas at 3.0 nM it led to a highly significant increase of 230%. These results were unexpected, as stimulation of the Na^+, K^+ - ATPase had previously been shown to occur at physiological insulin concentrations [199]. The finding that stimulation of Cr uptake occurred in the presence of the higher than physiological concentration of 3 nM insulin suggested the

possibility of the involvement of an signalling network leading to the up-regulation of the CrT, in addition to the effects of the Na^+, K^+ - ATPase.

Existing evidence suggests that insulin regulates the CrT, by phosphorylation through a different signalling pathway. Current literature points to the involvement of the IGF-1 receptor (IGF-1R) on the CrT, via several intermediate kinases. Both the insulin receptor and IGF-1R have been shown to have tyrosine kinase activity [200], and it has long been suspected that there is a role for tyrosine phosphorylation in the regulation of creatine content in skeletal muscle [11]. Insulin and IGF-1 have been shown to exert an effect on the phosphatidylinositol-3-kinase (PI3-kinase) pathway, involving the 3-phosphoinositide (PIP-3)-dependent kinase (PDK1) [201], which may stimulate the CrT through PKC. Additionally, PDK1 triggers the activation of the serum and glucocorticoid transporter 1 (SGK1). SGK1 has, in turn, been shown to stimulate the CrT [202], and is expressed in heart, as well as skeletal muscle, brain and kidney [203]. In *Xenopus* oocytes expressing CrT, Shojaiefard *et al* demonstrated that creatine induced a current, taken as an indicator of CrT activity via Na^+ co-transport, which was significantly enhanced by coexpression of wild-type SGK1. This effect was mimicked by SGK3. They concluded that SGK1 and SGK3 increase CrT activity by increasing the maximal transport rate of the CrT. However, CrT does not contain a putative SGK consensus motif, which suggested that there is another mechanism linking SGK1 with CrT. Phosphatidylinositol-3-phosphate-5-kinase PIKfyve (PIP5K3) has previously been shown to regulate the related glucose transporter GLUT4 [204], and Strutz-Seebohm *et al* demonstrated a link between the activation and phosphorylation of PIKfyve and enhanced trafficking of CrT to the plasma membrane, via the intermediary $PI(3,5)P_2$ [205]. Thus another pathway leading to enhanced Cr uptake is defined.

The literature is inconsistent regarding the influence of insulin on the CrT. Indeed several studies have shown that insulin does not enhance Cr uptake in skeletal muscle. Brault and Terjung demonstrated that in anaesthetised rats, insulin had no effect on ^{14}C-Cr uptake in soleus, red gastrocnemius or white gastocnemius muscle fibres in the presence of 0.1 µU – 1 mU insulin [206]. They concluded that insulin does not have any effect on the creatine transport process. Willott *et al* also found that insulin did not influence creatine uptake in isolated rat soleus muscle, suggesting that Cr uptake is dependent on sodium and intracellular Cr levels. [207].

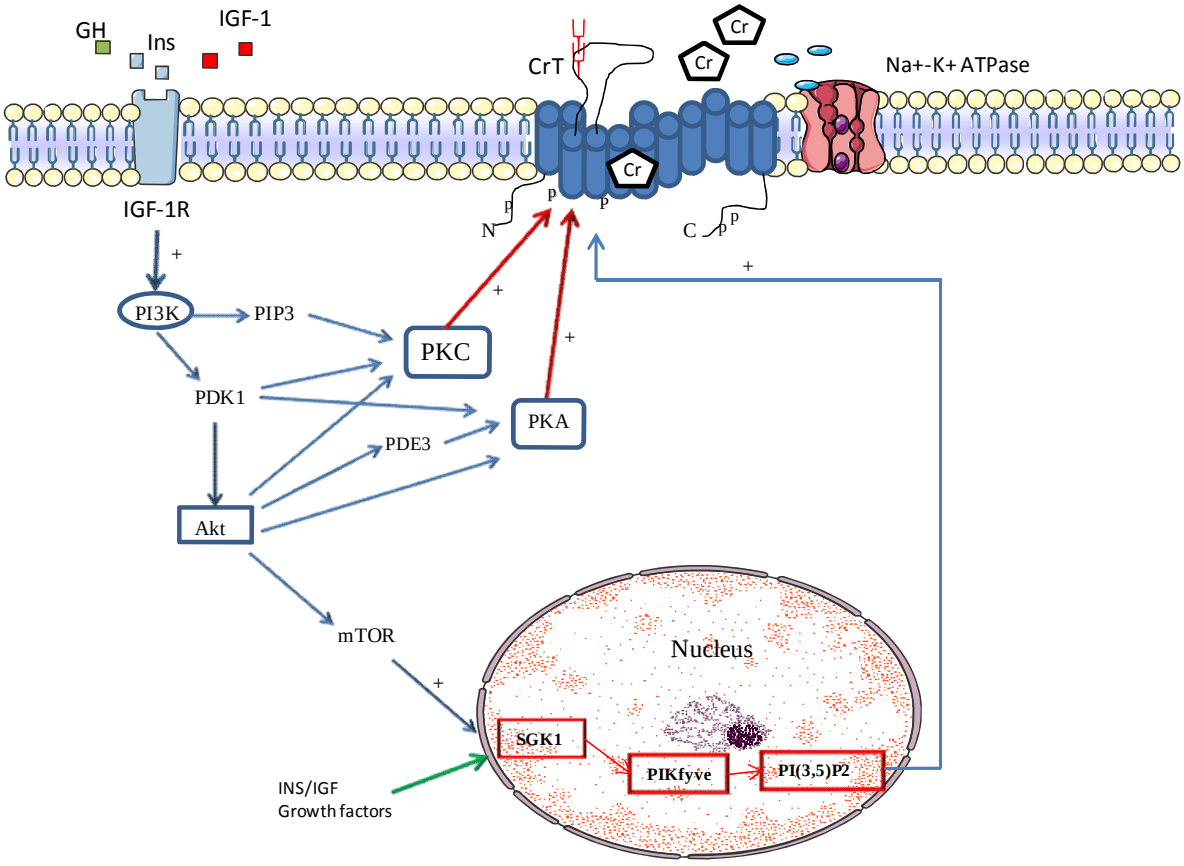


Figure 4-1. Regulation of the CrT via the IGF-1 pathway. This figure demonstrates the key components targeted in the experiments contained within this chapter, related directly or indirectly to the IGF-1 signalling pathway. Hormones (GH, insulin and IGF-1) act on the IGF-1R to induce signalling via PI3K, upregulating the CrT on the plasma membrane, thus leading to increased Cr uptake. Other kinases involved include PKA and PKC. Insulin, GH and IGF-1 may also act on the nuclear kinase, SGK1, which is also potentially mediated by mTOR, leading to modulation of mRNA activity via mRNA transcription. Key: p = phosphorylation site, PI3K = phosphatidylinositol-3-phosphate-5-kinase, PIP3 = phosphatidylinositol(3,4,5)-trisphosphate; PDK1 = 3-phosphoinositide dependent protein kinase-1; Akt = protein kinase B; PDE3 = phosphodiesterase 3; PIKfyve = phosphoinositide kinase, FYVE finger containing; PI(3,5)P2 = phosphatidylinositol (3,5)-bisphosphate; (+) = induction / activation. Available glycosylation sites are indicated by Y.

4.1.3.2. Growth hormone

GH is involved in the IGF-1R signalling pathway discussed previously, stimulating the release of IGF-1, which in turn activates the IGF-1 pathway through IGF-1R. Little evidence of its influence on the CrT exists in the literature. However, GH has been shown to attenuate LV remodelling early after MI [208]. More recently, a study in rats found that, post-MI, 4-week GH supplementation did not offset the decline in cardiac structure and function, although increasing levels of growth hormone-stimulating hormone with an agonist did attenuate the degree of functional decline and remodelling [209]. A study by Omerović *et al* showed that GH led to increased expression of *CrT* during post-infarct remodelling in rats [210]. This may have been due to signalling via SGK1 [202], leading to enhanced mRNA transcription, through the pathway indicated in figure 5.1. The findings led the authors to suggest that this increase in myocardial [Cr] may be an explanation for the beneficial effects of GH on myocardial energy metabolism and preservation of cardiac function that have been observed in the settings of post infarct remodelling and CHF. In conclusion, two potential pathways exist through which GH may act on the CrT. Therefore, GH was selected for further investigation as a mediator of Cr uptake.

4.1.3.3. IGF-1

IGF-1 was previously shown to up-regulate Cr uptake in myoblasts, although to a lesser degree than insulin [11]. More recent studies have demonstrated a positive effect as a result of IGF-1 supplementation post-MI. A rat model showed acute administration of IGF-1 improved cardiac contractility, with an increase in force of between 22% and 24% [211]. As with GH, IGF-1 levels have been observed to be significantly lower in HF when compared to control [212 213]. Although the role of IGF-1 in HF is still not clearly understood, the potential that this effect may be associated with up-regulation of the CrT through direct stimulation of IGF-1R warrants investigation.

4.1.4. Regulation of CrT via PKA and PKC phosphorylation

Both PKA- and PKC-mediated phosphorylation have been implicated in the regulation of the CrT, with the identification of putative phosphorylation sites on the protein [26 214]. In addition to the potential direct effects of PKA- and PKC-mediated phosphorylation on the regulation of the CrT, it is likely that these kinases are both downstream of the IGF-1R, and could therefore be involved with the regulation of the CrT through the IGF-1 signalling pathway. PMA-induced activation of PKC has previously been shown to have an effect on the CrT, leading to its down regulation in *Xenopus* oocytes [9]. Owing to the artificial system used in these studies on PKA- and PKC- mediated regulation of the CrT, further investigations in more relevant cells, such as 3T3-CrT-HAs and HL-1s are highly relevant. Though still artificial systems, the HL-1 milieu in particular is directly relevant to the cardiac phenotype.

4.1.5. Rapamycin and mTOR, and the influence of AMPK

Mammalian target of rapamycin (mTOR) is a serine / threonine kinase involved in stimulating cellular nutrient uptake. It forms two known multiprotein complexes, which are downstream targets for activation by the serine / threonine protein kinase Akt. One of these complexes is mTOR complex 2 (mTORC2), which exerts cardiac protective actions via further Akt phosphorylation and activation [215 216].

Shojaiefard *et al* found that in *Xenopus* oocytes, Cr induced a current that was significantly enhanced by the co-expression of mTOR alongside CrT, enhancing maximal current without significantly altering affinity. Following pre-incubation with rapamycin (a selective inhibitor of mTOR), the creatine-induced current was reduced and stimulation of its inducible kinase, ^{K119N}SGK1, was abrogated [217]. The authors discovered that while co-expression of CrT and

SGK1 also led to enhanced creatine currents, co-expression of CrT, mTOR and SGK1 did not enhance the effect more than mTOR or SGK1 alone. It was therefore suggested that these two kinases may act through overlapping mechanisms, or that mTOR is upstream of SGK1 and exerts its influence on the CrT via SGK1. The authors concluded that, in this system, the CrT is stimulated by mTOR. Another study investigating SGK1 found no difference in its levels in GAMT KO mice versus WT, despite their 7-fold increase in CrT activity [48].

5'-adenosine monophosphate-activated protein kinase (AMPK) has been characterized as an upstream inhibitor of mTOR, via its activation of tuberin (TSC2) [218]. AMPK is a key regulator of energy homeostasis, and acts by switching off energy-consuming processes in favour of those that generate energy [219]. Thus it is relevant in conditions of energy imbalance, such as heart failure, where Cr transport is reduced. Hui *et al* investigated the role of AMPK in the regulation of CrT in kidney epithelial cells, and also studied the role that mTOR plays within this system. They found that AMPK regulates CrT plasma membrane expression in kidney proximal tubule cells and oocytes, suggesting that mTOR is indeed involved. The AMPK activator ZMP inhibited Cr currents when injected into oocytes expressing CrT and mTOR to a similar level seen following pre-incubation with rapamycin. Injecting rapamycin-pretreated oocytes with ZMP had no additive inhibitory effect, hence the conclusion that the ZMP-dependent inhibition was occurring through the mTOR pathway.

Another study found contrasting results. In experiments performed by Darrabie *et al* on rat neonatal cardiomyocytes and HL-1 cells, AMPK activation with 5-aminoimidazole-4-carboxamide-1-β-$_D$-ribonucleoside (AICAR) increased Cr transport. Additionally, the authors found that inhibiting mTOR with rapamycin had no significant effect on Cr transport [219]. These

results suggest that the regulation of Cr transport by AMPK, involving mTOR, varies by cell type.

On the basis of the candidate compounds and pathways outlined above having an involvement on regulation of the CrT, several were selected to investigate further using two different cell systems; the stable CrT-overexpressing fibroblast line 3T3-CrT-HA (the generation of which is outlined in Chapter 3), and the highly relevant HL-1 immortalised murine cardiomyocyte line. Previous studies conducted into CrT regulation have been performed mainly in oocytes overexpressing cDNA, that may not have the appropriate regulatory machinery, and therefore the results obtained may not be relevant to the cardiac milieu.

4.1.6. Summary

In this study, hormones selected for investigation included insulin, growth hormone, and IGF-1, all IGF-1R agonists, in addition to the pharmacological inhibitors and activators of kinases described next. Picropodophyllin (PPP) was used as a selective inhibitor of the IGF-1R. H89 was chosen as an inhibitor of PKA and bisindolylmaleimide (BIM) as a PKC inhibitor. H89 (*N*-[2-(*p*-Bromocinnamylamino)ethyl]-5-isoquinolinesulphonamide) is a potent and selective inhibitor of PKA [220], and BIM (bisindolylmaleimide 1) is a potent inhibitor of PKCα, a less potent inhibitor of PKCβ and a very weak inhibitor of PKCζ (IC_{50}= 5.8 μM) [221]. Phorbol 12-myristate 13-acetate (PMA) was used as a PKC stimulator [222]. Additional stimulators of PKC used are sapintoxin D (STX), a preferential activator of PKCα at concentrations up to 100 nM (at concentrations of 1 μM it activates other isoforms as well) [223], and Gö 6976, an inhibitor of PKC at nM concentrations, which exhibits general phosphatase inhibition at concentrations of

1 μM [224] [225]. Rapamycin was selected to investigate the effects of the mammalian target of rapamycin (mTOR) on CrT regulation.

4.2. Results

Following the creation of an *in vitro* system of CrT overexpression, a series of experiments to study potential regulation by key candidate molecules on the IGF-1R pathway were performed. Initially, regulation of CrT by activity and function was investigated, using the 3T3-CrT-HA cell line overexpressing the rbCrT (Chapter 3) and the immortalised cardiac-derived HL-1 cell line.

4.2.1. Kinetics of Cr uptake

^{14}C- Creatine uptake experiments showed that V_{max} was around 250 μM extracellular creatine, with a K_m of around 125 μM. Subsequently, all uptake experiments were performed with an extracellular creatine concentration of 250 μM. As reported previously (Chapter 3), cells expressing CrT-HA exhibited a 10 fold increase in creatine uptake over the native uptake levels in untransfected 3T3 cells (218 nmol creatine / mg protein / h vs. 21 nmol creatine / mg protein / h).

4.2.2. Specificity of Cr uptake.

Creatine uptake experiments were performed to investigate the effects of competitive inhibition. β-guanidinopropionic acid (β-GPA), a creatine analogue and competitive inhibitor of Cr uptake, was used in order to determine the level of inhibition of creatine uptake over a range of concentrations. An increase in β-GPA concentration led to reduced creatine uptake, demonstrating that Cr uptake occurs specifically via the CrT, and therefore, that any effects on

Cr uptake observed in these systems following the intervention in signalling pathways are due to their influence on the CrT. The reduction in Cr uptake following β-GPA treatment was more pronounced in 3T3-CrT-HA cells than HL-1 cells, owing to the greatly increased expression of the CrT in the 3T3-CrT-HA cells. Creatine uptake in 3T3-CrT-HA cells is around 20 times greater than that in HL-1 cells.

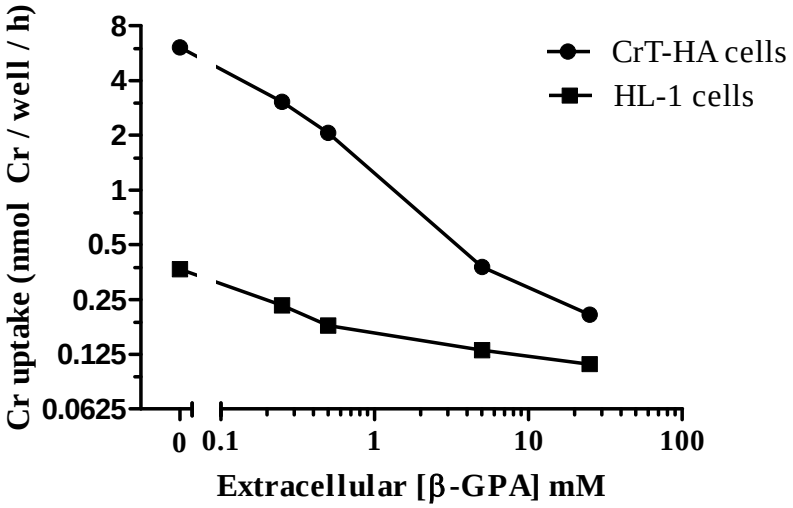


Figure 4-2. 14C-Creatine uptake in 3T3-CrT-HA cells and in HL1 cells. All samples were incubated in 250μM extracellular creatine, in addition to the creatine analogue β-GPA at varying concentrations. Uptake was measured over 1 h. Samples were run in duplicate, plots show average values ± SEM.

4.2.3. The effect of insulin on IGF-1R and creatine uptake

4.2.3.1. 3T3-CrT-HA cells

Uptake experiments were performed in 3T3-CrT-HA cells which had been pre-incubated in insulin at various concentrations for 48 h. This incubation period was chosen based on the results of a previous study, conducted in myoblasts by Odoom *et al*, that found an incubation of this period enhanced Cr uptake. Uptake was measured over 1 h, in the presence of 250 μM extracellular creatine spiked with ^{14}C-creatine. Cells were grown in phenol red-free media supplemented with charcoal-stripped FBS and antibiotics (see General Materials and Methods),

from 4 hours after plating, and the uptake assays themselves were also performed under these conditions.

Uptake experiments demonstrated an increase in Cr uptake in 3T3-CrT-HA cells pre-incubated in all concentrations of insulin, with the greatest enhancement of uptake (301%) at a concentration of 1 nM. Concentrations of 3 nM and 10 nM insulin led to a 278% and 225% increase in Cr uptake respectively. The increases at 1 nM and 3 nM were shown to be significant. These results are shown in figure 5.3. Insulin uptake assays were repeated in order to confirm the effect initially observed. A wider range of insulin concentrations was used, although otherwise, experimental conditions were identical to those described above. While the increase of ~300% initially observed in the presence of 1 nM insulin was not repeated, a statistically significant increase in Cr uptake was seen at concentrations from 0.1 nM to 100 nM. The maximum increase observed was ~ 150%. The results shown in figure 5.4 are the combination of 2 independent assays, normalised to % control and presented together.

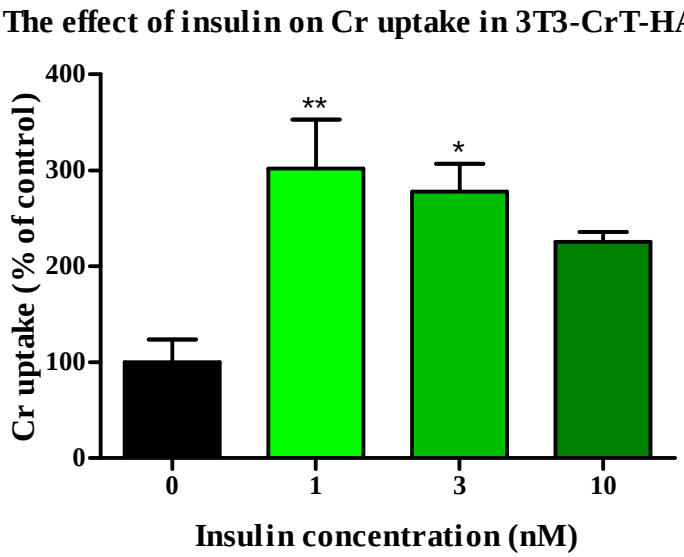


Figure 4-3. Effect of insulin on creatine uptake in 3T3-CrT-HA cells. *n=3* for all groups. Cells were pre-incubated for 48 h in insulin at various concentrations, and Cr uptake was measured over 1 h. Values are mean ± SEM. ** p< 0.01, * p< 0.05, compared to Cr only control group (One-way ANOVA with Dunnett's multiple comparison test).

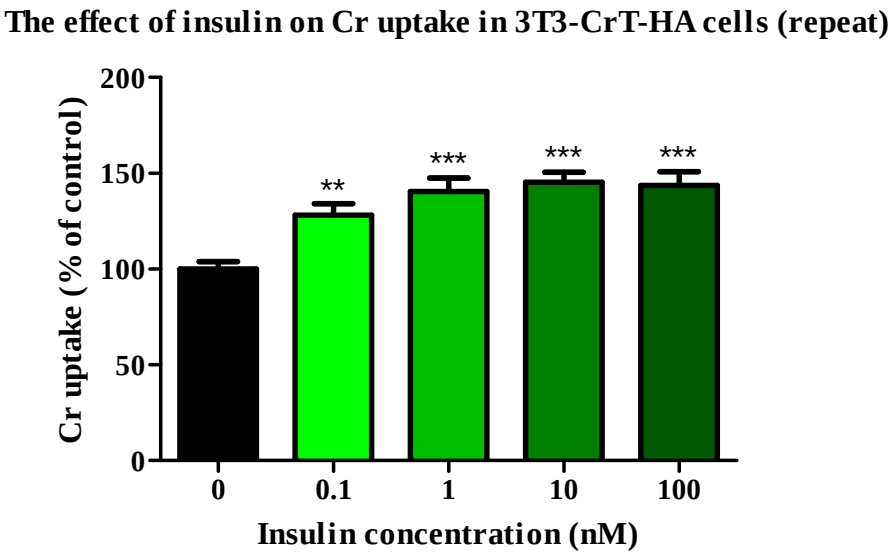


Figure 4-4. Effect of insulin on creatine uptake in 3T3-CrT-HA cells. *n=12* for control, *n=6* for all other groups. Cells were pre-incubated for 48 h in insulin at various concentrations, and Cr uptake was measured over 1 h (One-way ANOVA with Dunnett's multiple comparison test). Values are mean ± SEM. ***p< 0.001, ** p< 0.01, compared to Cr only control group (One-way ANOVA with Dunnett's multiple comparisosn test).

4.2.3.2. HL-1 cells

Additional Cr uptake assays were performed to determine the effect of insulin in HL-1 cells. Pre-incubation was 48 h, as with the 3T3-CrT-HA cells. Cell culture conditions were as described for HL-1 cells in General Materials and Methods. Unlike with the 3T3-CrT-HA cells, phenol red-free medium, and charcoal-stripped FBS were not used, owing to an inability to sustain healthy HL-1 cells in such medium. Insulin pre-treatment did not lead to a significant increase in Cr uptake. However, a trend towards increased uptake was observed at insulin concentrations of 1 nM and 3 nM. It is noteworthy that in subsequent experiments investigating the effects of PKC inhibition following IGF-1R stimulation, a significant increase in Cr uptake was observed in HL-1 cells, in insulin concentrations of 1 nM.

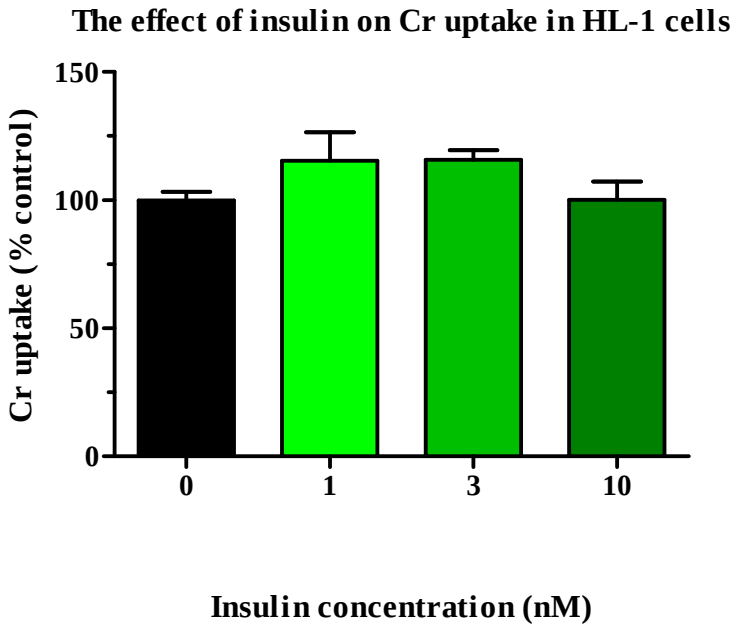


Figure 4-5. Effect of insulin on creatine uptake in HL-1 cells. *n=6* for control, *n=3* for all other groups. Cells were pre-incubated for 48 h in insulin at various concentrations, and Cr uptake was measured over 1 h. Values are mean ± SEM. No significant difference was observed in Cr uptake between control and treated samples (One-way ANOVA with Dunnett's multiple comparison test).

4.2.4. The effect of growth hormone on IGF-1R and creatine uptake

4.2.4.1. 3T3-CrT-HA cells

The effects of growth hormone on the activity of the CrT were studied. Uptake assays were performed on 3T3-CrT-HA cells over 1 h, following a 48 h pre-incubation in GH. Incubations for shorter periods failed to have an effect on Cr uptake (data not shown), and 48 h was selected as GH is believed to influence the CrT via the IGF-1R, as does insulin. Cells were grown in phenol red-free media supplemented with charcoal-stripped FBS, as well as antibiotics at the usual concentrations (see General Materials and Methods). Creatine uptake was elevated at all concentrations of GH used, with 240%, 186% and 154% increases at 10 ng/mL, 25 ng/mL and 100 ng/mL respectively. The increases at 10 ng/mL and 25 ng/mL were shown to be significant.

GH uptake assays were repeated in order to confirm the effect initially observed. A wider range of GH concentrations was used, although otherwise, experimental conditions were identical to those described above. Three independent uptake assays were performed, and the results combined following normalisation to % control. These results are shown in the figure below. The large increase in Cr uptake observed in the early experiments was not repeated, although a statistically significant increase was observed at GH concentrations of 10 and 100 ng / mL, with both of these concentrations leading to around 125% uptake compared to control.

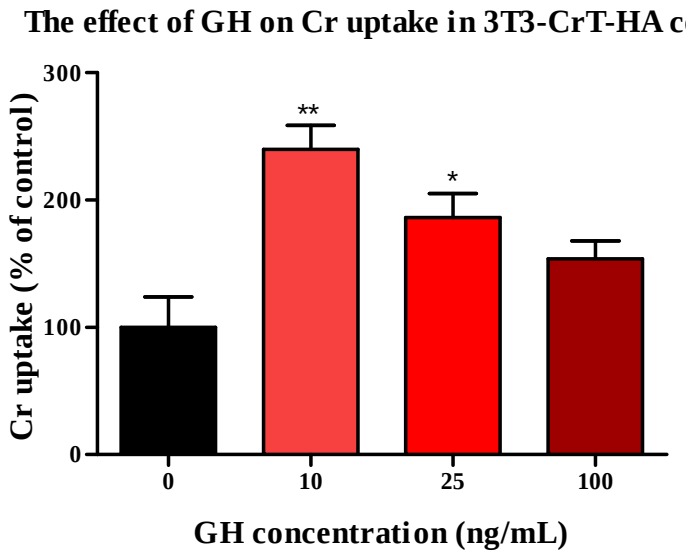


Figure 4-6. Effect of growth hormone on creatine uptake in 3T3-CrT-HA cells. *n=3* per group. Cells were pre-incubated for 48 h in GH at various concentrations, and Cr uptake was measured over 1 h. Values are mean ± SEM. ** p< 0.01, * p< 0.05, compared to Cr only control group (One-way ANOVA with Dunnett's multiple comparison test).

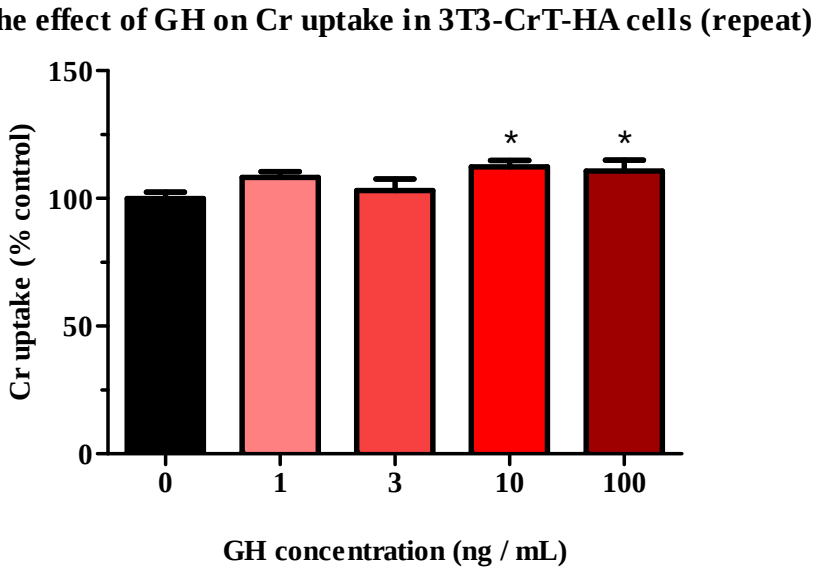


Figure 4-7. Effect of growth hormone on creatine uptake in 3T3-CrT-HA cells. *n*=18 for control, n=*9* for all other groups. Cells were pre-incubated for 48 h in GH at various concentrations, and Cr uptake was measured over 1 h. Values are mean ± SEM. * p< 0.05, compared to Cr only control group (One-way ANOVA with Dunnett's multiple comparison test).

4.2.4.2. HL-1 cells

Additional Cr uptake assays were performed to determine the effect of GH in HL-1 cells. Pre-incubation was 48 h, as with the 3T3-CrT-HA cells. Cell culture conditions were as described for HL-1 cells in General Materials and Methods. Again, unlike with the 3T3-CrT-HA cells, phenol red-free medium and charcoal-stripped FBS were not used, owing to an inability to sustain healthy HL-1 cells in such medium. GH pre-treatment did not lead to an increase in Cr uptake. As in the case of the previously reported Cr uptake experiments in HL-1 cells, subsequent experiments investigating the effects of PKC inhibition following IGF-1R stimulation did show an increase in Cr uptake following GH treatment at 10 ng / mL.

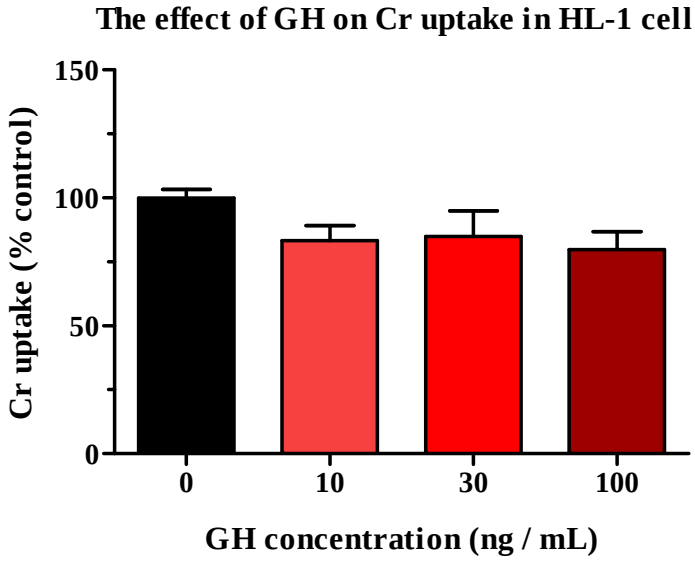


Figure 4-8. Effect of growth hormone on creatine uptake in HL-1 cells. *n=6* for control, n=*3* for all other groups. Cells were pre-incubated for 48 h in GH at various concentrations, and Cr uptake was measured over 1 h.Values are mean ± SEM. No significant effect was observed between control and samples incubated in GH (One-way ANOVA with Dunnett's multiple comparison test).

4.2.5. The effect of IGF-1 on creatine uptake

The final hormone selected for stimulation of the IGF-1R pathway, in order to determine the downstream effects on the CrT, was IGF-1. All assays were performed in phenol red-free media, supplemented with charcoal-stripped FBS, to eliminate effects of other hormones, as for the

previous insulin and GH Cr uptake experiments. Initially, 3T3-CrT-HA cells were incubated only briefly in the presence of IGF-1, as evidence in the literature suggests that the IGF-1R is stimulated rapidly in its presence. Trial incubations of 5, 15 and 30 minutes were performed, and Cr uptake measured over a period of 1 h. These conditions did not lead to an increase in Cr uptake (data not shown).

Subsequent experiments involved pre-incubations in the presence of IGF-1 for longer durations prior to the commencement of Cr uptake assays. Two additional incubation times were performed, 2 h and 24 h. A small increase in Cr uptake was observed in the 2 h pre-incubated cells at all concentrations of IGF-1 used (3, 10, 30 and 100 ng / mL), and following 24 h pre-incubation, Cr uptake increased in cells incubated at concentrations of 3, and 10 ng / mL. The increase was not statistically-significant when compared to control samples, although the small increase in uptake seen is similar to that observed in the most recent Cr uptake experiments performed in the presence of insulin and GH (figures 5.4 and 5.6). It is possible that repetition of these experiments, leading to increased sample replicates, would lead to statistical significance.

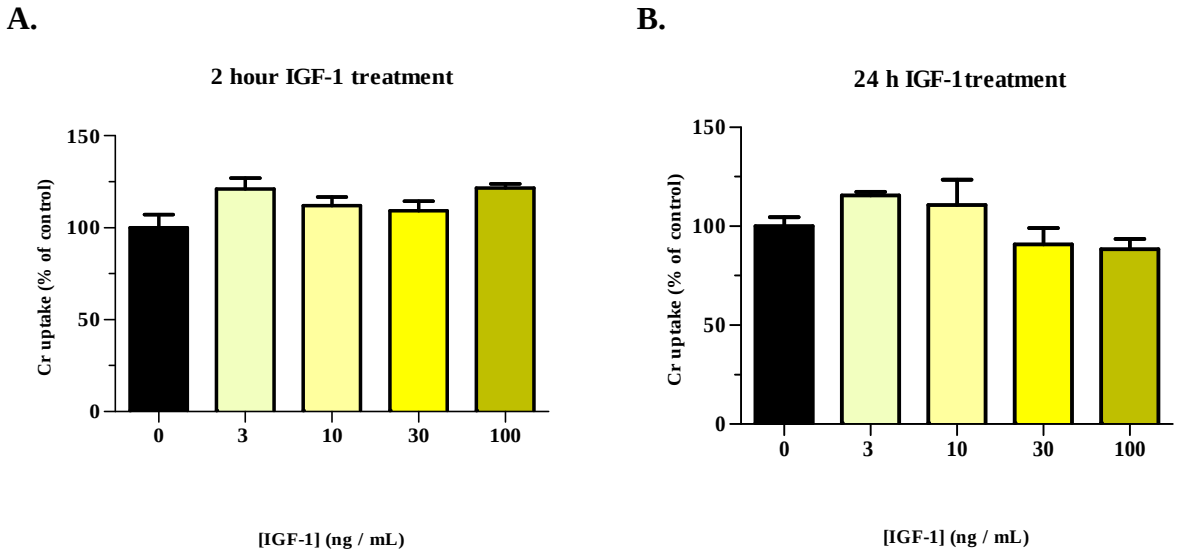


Figure 4-9. Effect of IGF-1 on creatine uptake in 3T3-CrT-HA cells. *n=6* for control, n=*3* for all other groups. Cells were pre-incubated for 2 h (panel A), and 24 h (panel B) in IGF-1 at various concentrations, and Cr uptake was measured over 1 h.Values are mean ± SEM. No significant difference was observed between control and treated samples in either 2 h or 24 h incubations (One-way ANOVA with Dunnett's multiple comparison test).

4.2.6. The effects of picropodophyllin (PPP) inhibition of the IGF-1 receptor (IGF-1R) on creatine uptake in HL-1 cells

In order to determine whether IGF-1R is involved in CrT regulation, PPP, a specific inhibitor of IGF-1R, was used. The IGF-1R was activated by pre-incubation with insulin (1 nM) for 48 h prior to the uptake assay and the addition of PPP. There were differences between those samples pre-treated with insulin and controls. PPP treatment alone caused a significant reduction in creatine uptake at all concentrations, suggesting a degree of constitutive IGF-1R activity at baseline. Compared to control, the insulin-treated sample showed a small increase in Cr uptake. The effect of PPP was reduced in insulin-treated cells, though it prevented the enhanced Cr uptake seen with insulin alone.

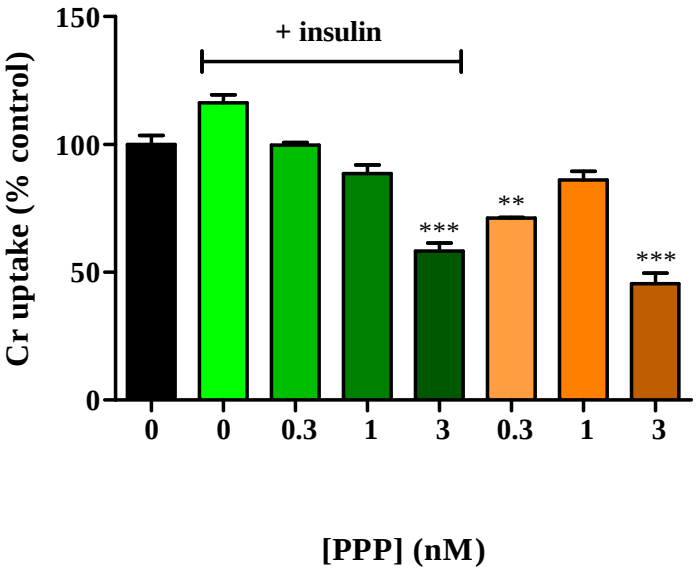


Figure 4-10. Effects of PPP on HL-1 cells incubated in the presence and absence of 1 nM insulin. Where relevant, cells were pre-incubated in insulin for 48 h. Cr uptake was measured over 1 h. Stars (*) representing significance in the graph are compared to control in the absence of insulin, with insulin pre-treatment preventing a significant decrease in Cr uptake at all concentrations except 3 nM. *n=3* for all groups. Values are mean ± SEM. One-way ANOVA with Bonferroni's multiple comparisons test. ** p< 0.01, *** p< 0.001

4.2.7. The effect of PKA and PKC inhibition on creatine uptake following IGF-1R stimulation with insulin and GH

PKA and PKC are believed to be involved in the regulation of the CrT, through the IGF-1 signalling pathway, downstream of the IGF-1R (figure 5.1). In order to test this hypothesis, cells were incubated in the presence of either 1 nM insulin, or 10 ng / mL GH, concentrations that had previously been shown to stimulate the IGF-1R pathway. Following 48 h stimulation with these hormones, either the PKA inhibitor H89, or the PKC inhibitor BIM were added to the cells at various concentrations. Creatine uptake was then measured over a period of 1 h. As described previously, extracellular [Cr] in the assays was 250 μM, and was 'spiked' with radiolabelled Cr. 3T3-CrT-HA cells were grown in phenol red-free complete medium supplemented with charcoal-stripped FBS. HL-1 cells were grown in complete Claycomb medium (see General Materials and Methods).

4.2.7.1. PKA inhibition with H89 following IGF-1R stimulation with insulin

In both 3T3-CrT-HA cells and HL-1 cells, insulin led to an increase in Cr uptake. The addition of H89 blocked this enhanced Cr uptake, with the exception of 1 concentration, 0.3 μM, in 3T3-CrT-HA cells, indicating that PKA inhibition prevents the enhanced uptake seen following insulin stimulation of the IGF-1R. This effect was observed in both cell lines.

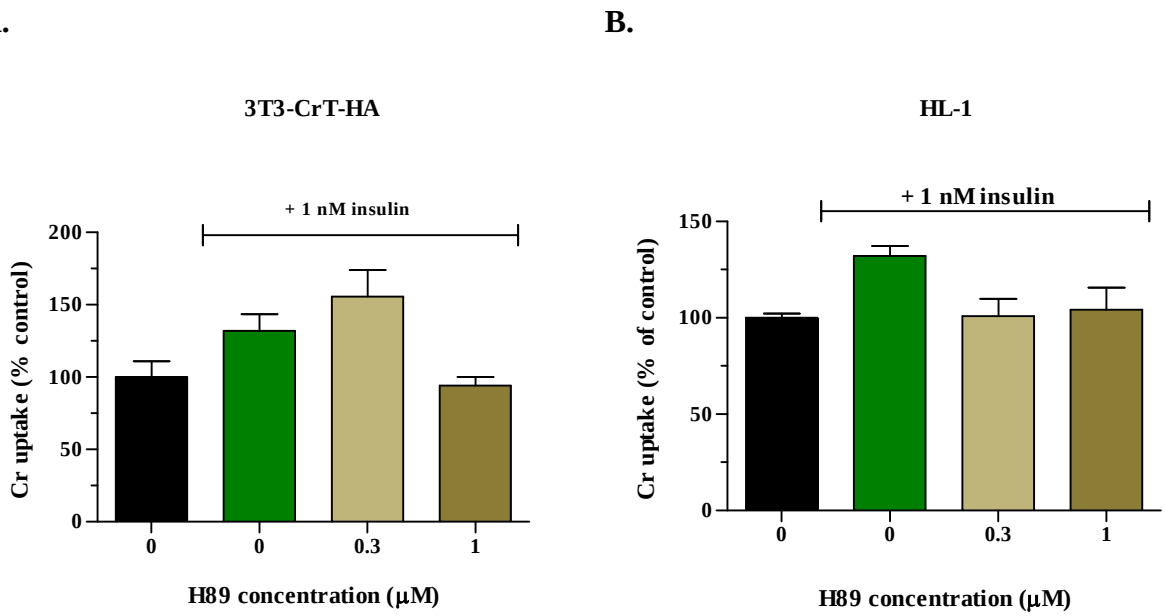


Figure 4-11. Effects of H89 on 3T3-CrT-HA cells (panel A) and HL-1 cells (panel B) incubated in the presence and absence of 1 nM insulin. Cells were incubated in 1 nM insulin for 48 h prior to the addition of H89, then Cr uptake was measured over a 1 h period. In 3T3-CrT-HA cells, no significant difference was observed between the insulin-treated control and any of the insulin + H89 samples (One-way ANOVA with Bonferroni's multiple comparison test). With the exception of 0.3 μM H89 in 3T3-CrT-HA cells, H89 prevented the insulin-associated increase in Cr uptake the cells. All concentrations of H89 prevented this increase in HL-1 cells. *n=3* for all groups. Values are mean ± SEM.

4.2.7.2. PKC inhibition with BIM following IGF-1R stimulation with insulin

A significant increase was observed in Cr uptake in both 3T3-CrT-HA cells and HL-1 cells treated with 1 nM insulin compared to control. In both cell lines, this increase was totally prevented by the addition of BIM to the cells at all concentrations tested, with a statistically significant decrease in all BIM-treated samples when compared to insulin-treated controls.

These results demonstrate complete inhibition of the enhanced Cr uptake associated with IGF-1R stimulation by insulin in the presence of PKC inhibition with BIM.

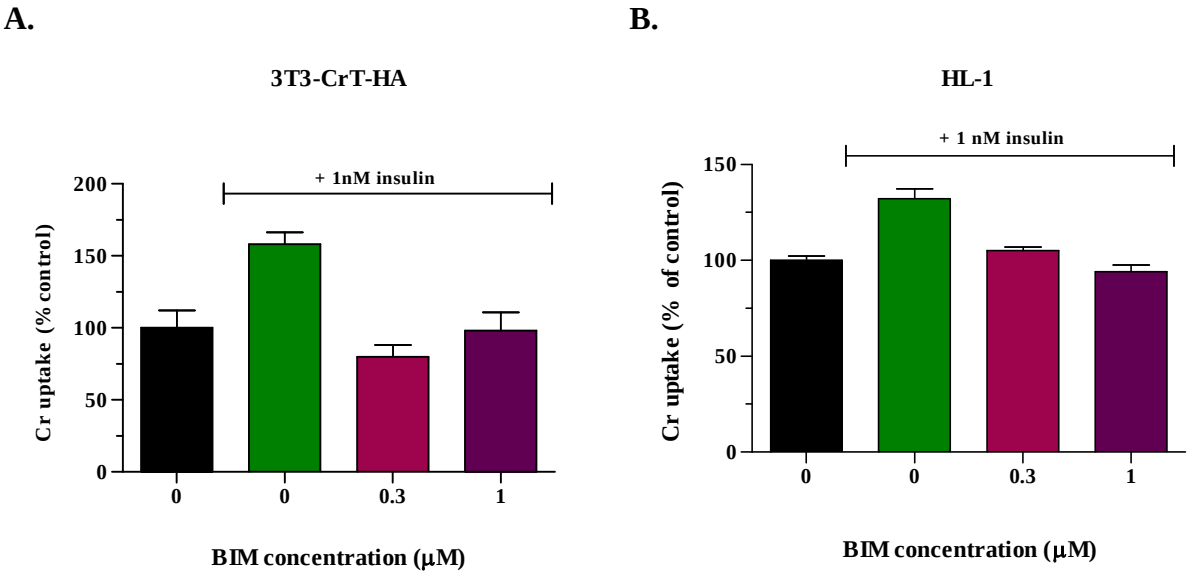


Figure 4-12. Effects of BIM on 3T3-CrT-HA cells (panel A) and HL-1 cells (panel B) incubated in the presence and absence of 1 nM insulin. Cells were incubated in 1 nM insulin for 48 h prior to the addition of BIM, then Cr uptake was measured over a 1 h period. In 3T3-CrT-HA cells, there was a significant difference between the control and insulin-treated sample. Additionally, a significant decrease in Cr uptake was observed between insulin-treated control and all concentrations of BIM in the presence of insulin (One-way ANOVA with Bonferroni's multiple comparison test). Statistical significance was mirrored exactly in the HL-1 cells. n=3 for all groups. Values are mean ± SEM.

4.2.7.3. PKA inhibition following IGF-1R stimulation with GH

Inhibition of PKA with H89 following 48 h treatment of both cell lines with GH led to similar effects to those observed following treatment with insulin and H89. The results in HL-1 cells are clearer due to a greater response to GH. Whilst significance was not demonstrated, it can be seen that, particularly in HL-1 cells, the enhanced Cr uptake associated with GH treatment was prevented in the presence of the PKA inhibitor.

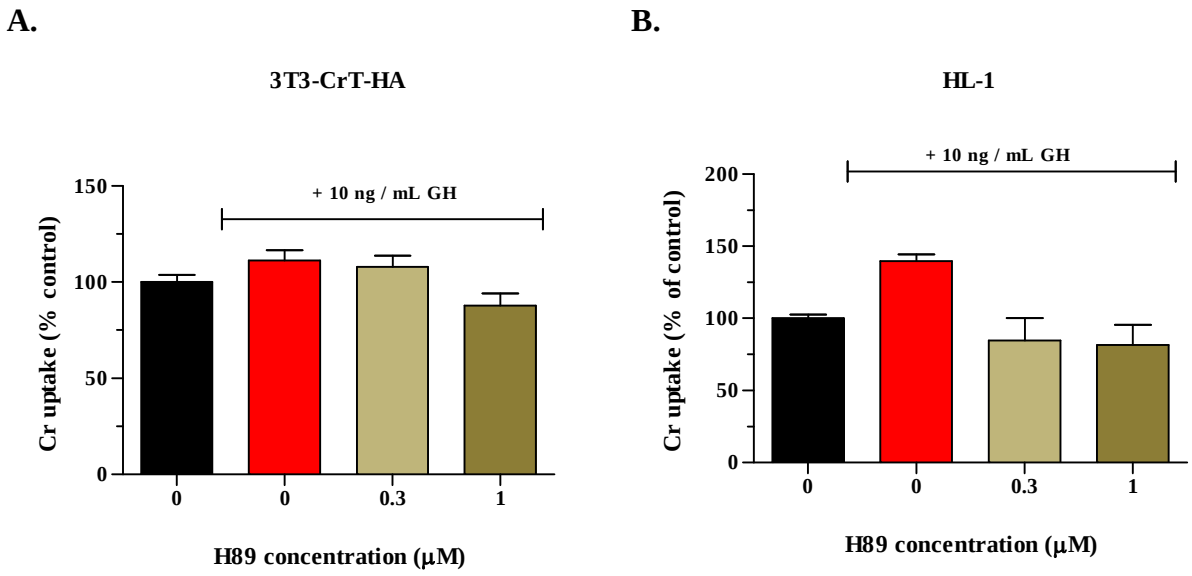


Figure 4-13. Effects of H89 on 3T3-CrT-HA cells (panel A) and HL-1 cells (panel B) incubated in the presence and absence of 1 nM GH. Cells were incubated in 1 nM GH for 48 h prior to the addition of H89, then Cr uptake was measured over a 1 h period. No significant differences were observed between samples in either cell type, although the results in HL-1 cells clearly show that the increased Cr uptake associated with GH incubation was ablated (One-way ANOVA with Bonferroni's multiple comparison test). n=3 for all groups. Values are mean ± SEM.

4.2.7.4. PKC inhibition following IGF-1R stimulation with GH

Treatment with GH led to enhanced Cr uptake in both cell types, and at higher concentrations of BIM, this effect was ablated. However, this was not the case in either cell line treated with a concentration of 0.3 μM BIM in the presence of GH. Once again, this shows that inhibiting PKC, certainly with higher concentrations of BIM, blocks the stimulatory effect of IGF-1R stimulation on the CrT.

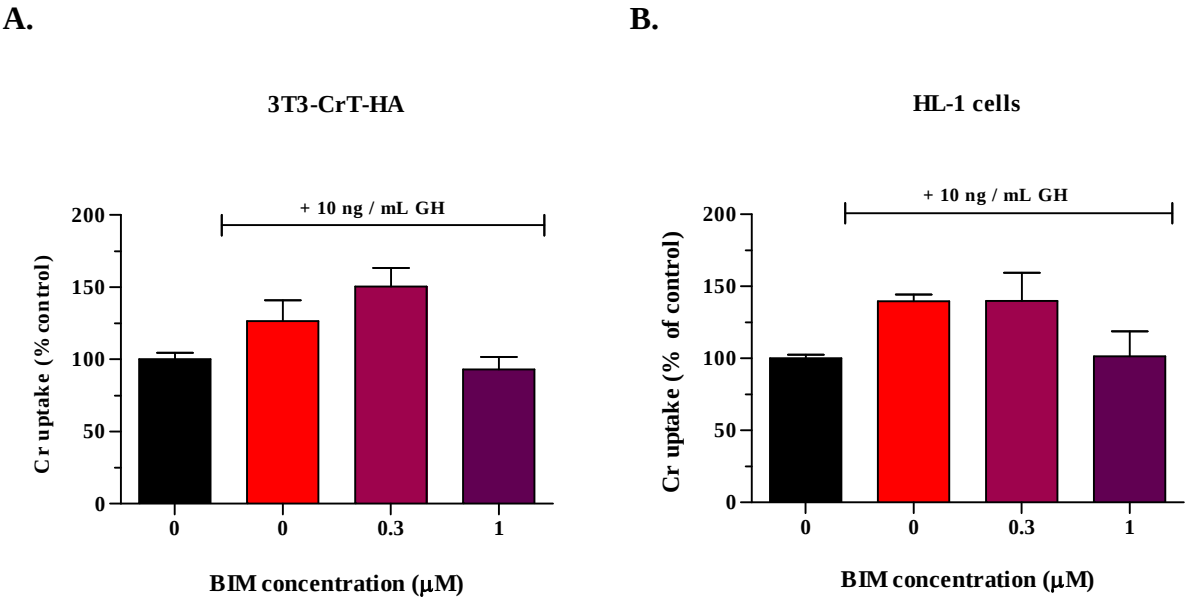


Figure 4-14. Effects of BIM on 3T3-CrT-HA cells (panel A) and HL-1 cells (panel B) incubated in the presence and absence of 1 nM GH. Cells were incubated in 1 nM GH for 48 h prior to the addition of BIM, then Cr uptake was measured over a 1 h period. In 3T3-CrT-HA cells, there was no significant difference between any of the samples. (One-way ANOVA with Bonferroni's multiple comparison test). However, the enhanced Cr uptake following GH treatment was ablated with 1 μM BIM treatment in both cell lines. *n=3* for all groups. Values are mean ± SEM.

4.2.8. The effects of PKA and PKC inhibition on CrT without prior stimulation via IGF-1R

In order to verify that the effects of PKA and PKC inhibition post IGF-1R stimulation were not due to independent PKA- or PKC-mediated effects, 3T3-CrT-HA cells and HL-1 cells were incubated in the presence of the PKA inhibitor H89 or the PKC inhibitor BIM alone. Incubations were in 250 μM extracellular creatine spiked with ^{14}C-creatine, in supplemented DMEM (see General Materials and Methods). All uptake assays were performed after a 1 h pre-incubation in the inhibitors. Trypan blue cell viability tests were performed alongside the uptake assays in order to determine that the cell membranes were intact following the treatments, and the results are shown later.

4.2.8.1. H89

Incubation in increasing concentrations of H89 led to a trend towards a small reduction in Cr uptake in 3T3-CrT-HA and HL-1 cells with no significant difference compared to control.

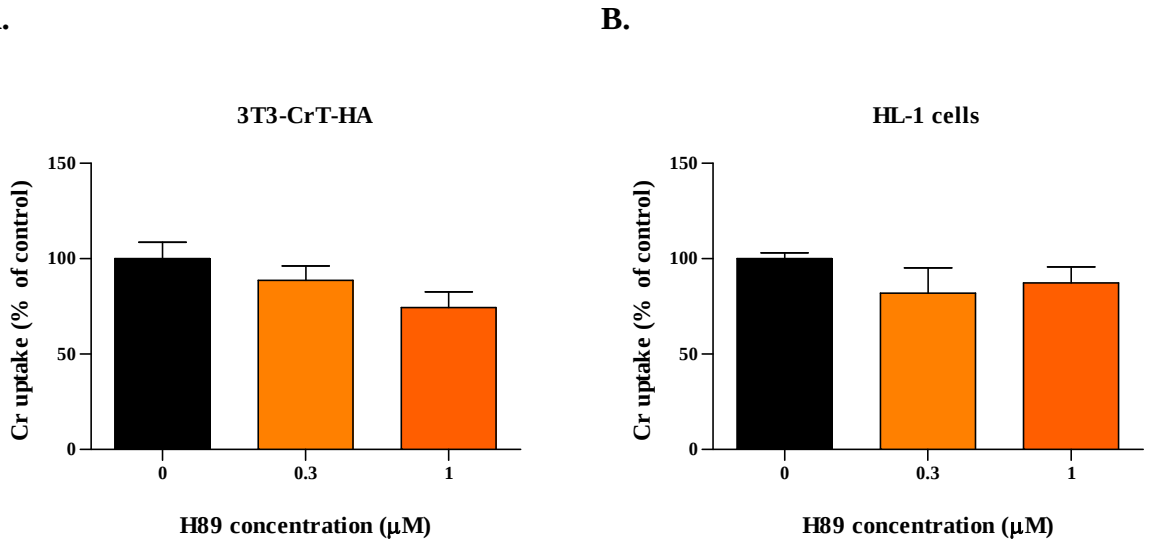


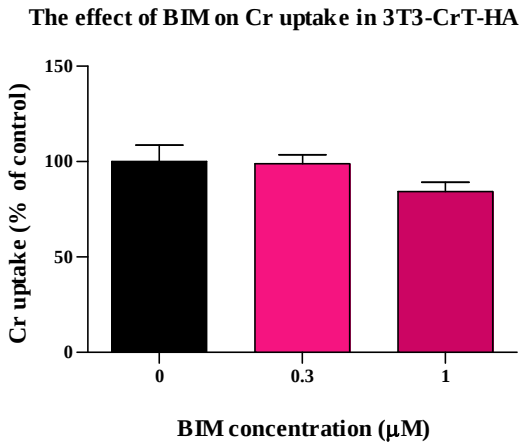
Figure 4-15. Effect of H89 on creatine uptake in 3T3-CrT-HA cells (panel A), and in HL-1 cells (panel B). n=3 per group. Values are mean ± SEM. No significant difference was observed in any of the treated samples when compared to control (One-way ANOVA with Dunnett's multiple comparison test).

4.2.8.2. Bisindolymaleimide

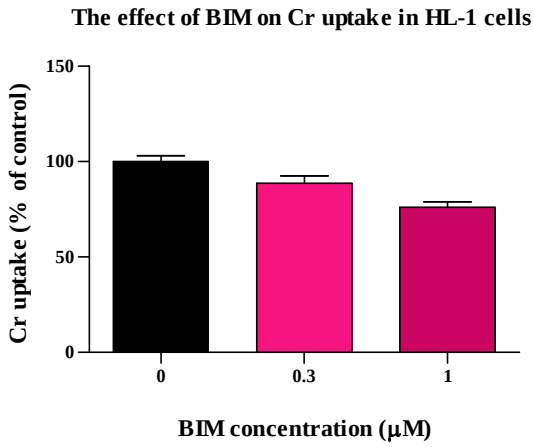
In both 3T3-CrT-HA and HL-1 cells there was a minor trend towards a decrease in creatine uptake with increasing BIM concentration. This decrease was not significant.

A separate experiment (shown in panel C of the figure below) measuring Cr uptake over a period of 1 h in 3T3-CrT-HA cells, in the presence of BIM with no pre-incubation period, and one additional very high concentration, showed the opposite effect. A statistically-significant increase in Cr uptake was observed at this high concentration, with a non-significant increase at concentrations of 1 μM.

A.



B.



C.

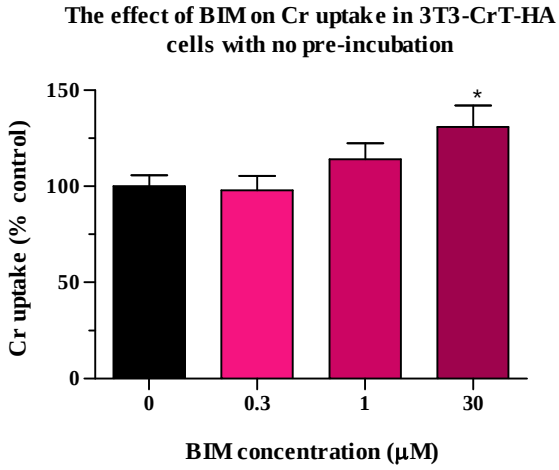


Figure 4-16. Effect of BIM on creatine uptake in 3T3-CrT-HA cells (panel A), and in HL 1 cells (panel B). n=3 for all groups. Values are mean ± SEM. A significant decrease in Cr uptake was observed in both cell types treated with 30 μM BIM. *** p< 0.001 compared to Cr only control group (Dunnett's multiple comparison test). Panel C shows the effect of BIM on Cr uptake with no pre-incubation. *N=6* per group (the combination of 2 independent experiments). Values are mean ± SEM. These conditions conversely led to an increase in Cr uptake, statistically significant at 30 μM. *p<0.05 compared to Cr only control group (One-way ANOVA with Dunnett's multiple comparison test)

4.2.9. PKC stimulation with PMA and STX and phosphatase inhibition with a high concentration of the PKC inhibitor Gö 6976

Having established that neither PKA or PKC have high constitutive activity in the context of Cr uptake, PKC was stimulated by PMA and STX, to determine its effects on Cr uptake. PMA, a general stimulator of PKC isoforms, is also reported to have a stimulatory effect on Akt (PKB). STX preferentially activates the α-isoform of PKC. Treatments were also performed with Gö 6976. At 3 nM, this *inhibits* PKC-α, but at the micromolar concentration used is reported to inhibit phosphatases. PMA activation of the PKC pathway has previously been shown to take place rapidly, within 30 min of exposure to PMA (unpublished data), and this experiment was performed with no pre-incubation, for a total duration of 30 min. Radiolabelled Cr, along with the usual 250 μM Cr, was added to the 3T3-CrT-HA cells at the same time as either PMA, STX or Gö 6976. The cells were incubated in standard medium. PKC activation with both PMA and STX led to a statistically-significant increase in Cr uptake. A high concentration of Gö 6976 also led to statistically-significant increased Cr uptake, likely due to its general effect of phosphatase inhibition.

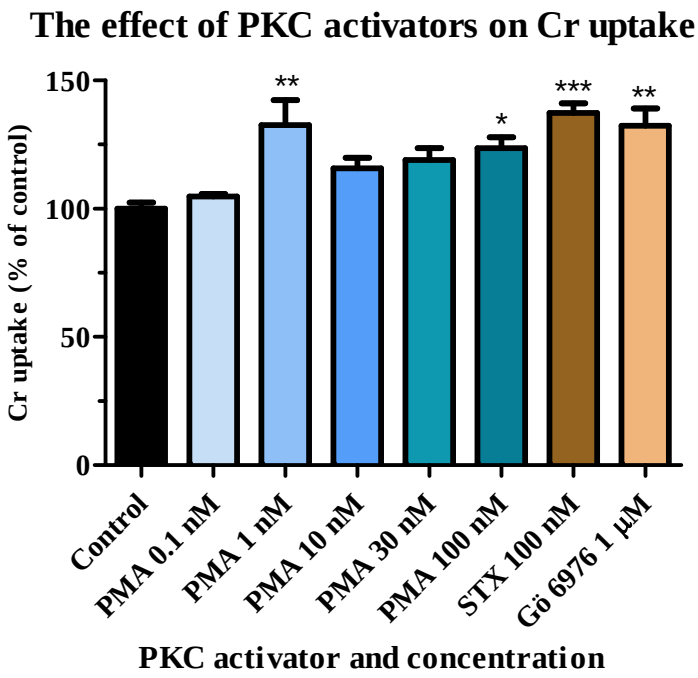


Figure 4-17. Effect of PKC activators PMA and STX, and Gö 6976 at high concentration on creatine uptake in 3T3-CrT-HA cells. *n=3* per group. Values are mean ± SEM. All compounds led to significant increase in Cr uptake after a 30 min incubation period. * p< 0.05, ** p< 0.01, *** p< 0.001 compared to Cr only control group (One-way ANOVA with Dunnett's multiple comparison test).

4.2.10. Effects of compounds on cell viability- Trypan Blue exclusion tests

Trypan blue exclusion tests were performed on cells incubated in H89 and BIM, to verify that their plasma membranes were still intact following treatment, and demonstrate that any inhibitory effect on Cr uptake was specific, not due to a decrease in cell membrane integrity. Were cell membrane integrity compromised, this could impact on the results obtained through radiolabelled-Cr uptake assays. However, no difference was seen in membrane integrity levels between any of the samples compared to control, even in the presence of extremely high concentrations of H89 and BIM. The 10% DMSO positive control did cause a significant increase in dead cell number, demonstrating the validity of the method. It can therefore be concluded that H89 and BIM decrease Cr uptake without affecting cell membrane integrity, thus providing confidence in the Cr uptake assay findings.

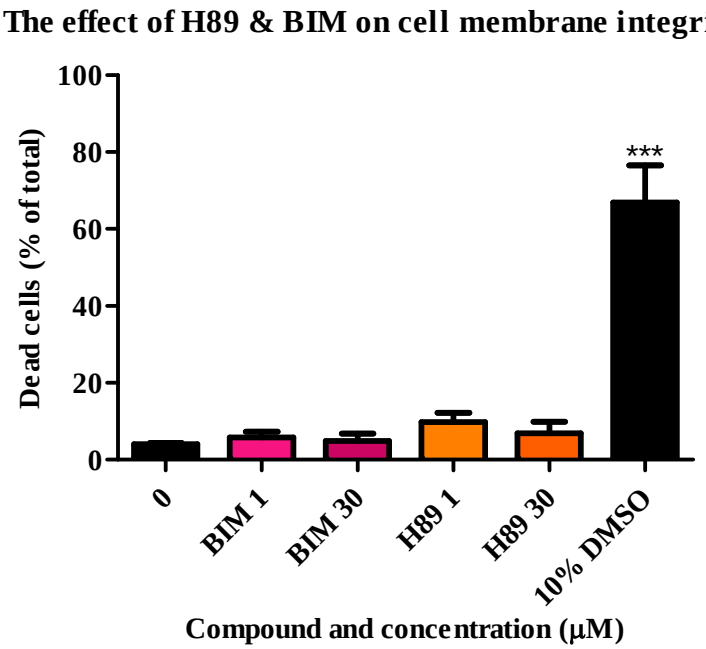


Figure 4-18. Effects of H89 and BIM on 3T3-CrT-HA membrane integrity. Cells were incubated in the presence and absence of tunicamycin for 2 h. *n=4* for control, *n=2* for treated cells. Values are mean ± SEM. No significant difference was observed between any of the treated samples compared to untreated control, with the exception of the 10% DMSO positive control. *** $p < 0.001$ compared to Cr only control group (One-way ANOVA with Dunnett's multiple comparison test).

4.2.11. Rapamycin and the effect of the mTOR pathway on creatine uptake

3T3-CrT-HA cells were pre-treated with rapamycin, an inhibitor of mTOR (mammalian target of rapamycin), to determine the effects of mTOR inhibition on creatine uptake. Figure 4.1 shows the proposed position of mTOR in the regulatory pathway. These experiments aimed to determine whether the effect of enhanced IGF-1R signalling on Cr uptake is due to the activation of mTOR (via SGK1), as well as PKA and PKC, already shown to be important in the IGF-1R signalling cascade. A pre-treatment with insulin was not used in this case- the potential direct effect on SGK1 which could lead to enhanced Cr uptake could make the results difficult to interpret. Cells were pre-treated with rapamycin at 3 concentrations for 24 h prior to the uptake assay. A minor, though statistically-significant reduction ($p < 0.05$) was observed in the samples incubated in 5 nM rapamycin. This was not reproduced at a higher concentration. This

effect, albeit minimal, suggests that in these cells, rapamycin at 5 nM does indeed downregulate the CrT, potentially via mTOR.

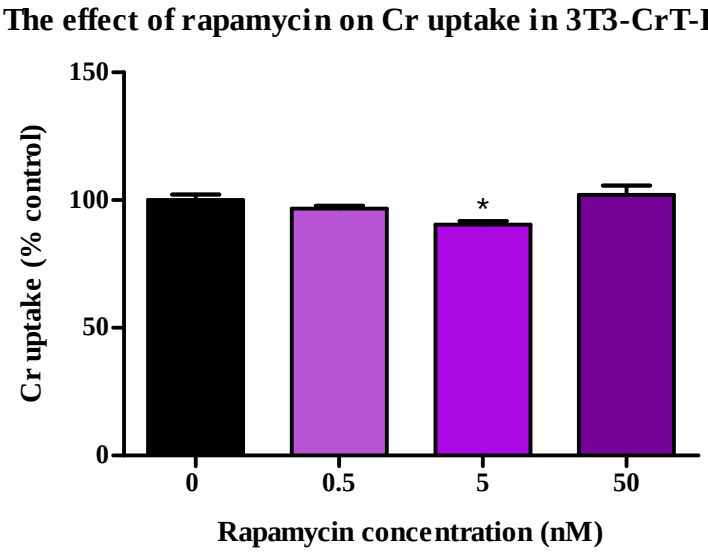


Figure 4-19. Effect of rapamycin on creatine uptake in 3T3-CrT-HA cells. n=6 for control group, n=3 for all other groups. Values are mean ± SEM. * $p < 0.05$, compared to Cr only control group (One-way ANOVA with Dunnett's multiple comparison test).

4.2.12. Regulation of CrT mRNA levels in vitro

Total (transgenic plus endogenous) *CrT* mRNA was measured in cells incubated in the presence of insulin and growth hormone using real-time quantitative RT-PCR (see General Materials and Methods section), in order to determine whether observed effects on creatine uptake were due to the influence of the IGF-1 pathway via a change in the activation of protein kinases, and not altered mRNA transcription. A primer pair specific to both *Oryctolagus cuniculus* and *Mus musculus* CrT was used (Com2, listed in General Materials and Methods).

Little variation in mRNA expression is seen between different insulin and growth hormone concentrations, with no statistically-significant differences between any of the groups compared to control.

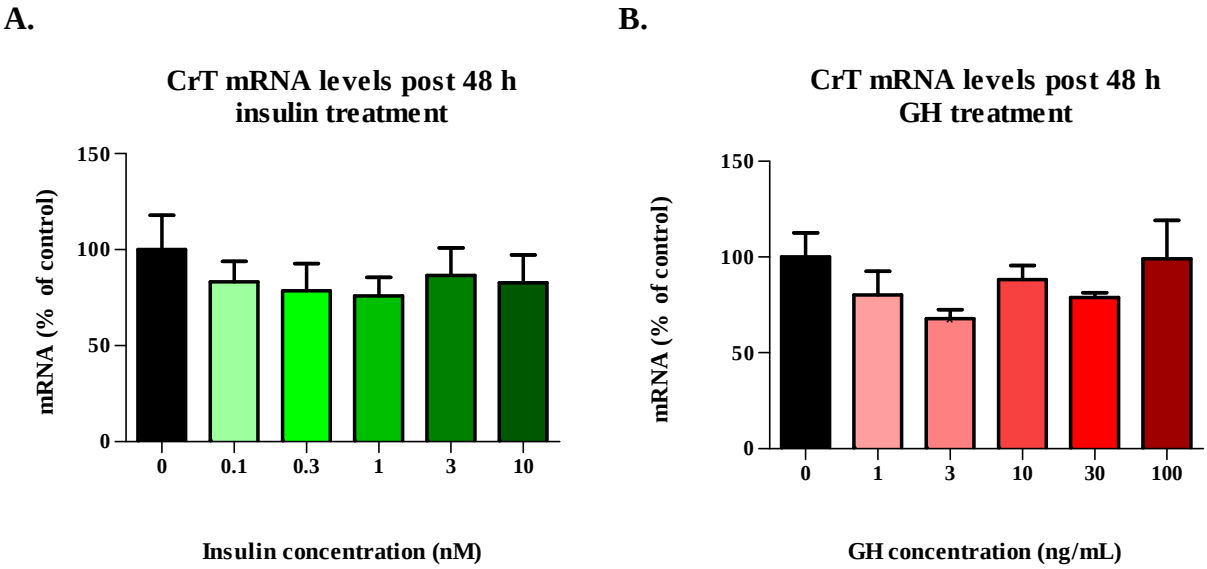


Figure 4-20. mRNA expression levels of total CrT in 3T3-CrT-HA cells treated in insulin and growth hormone. Expression was normalised to 36B4 and expressed as a percentage of WT. *n*=3 for all samples. Values are mean ± SEM. No significant differences were observed between any of the groups compared to control (One-way ANOVA with Dunnett's multiple comparison test).

The effect of rapamycin on mRNA transcription was also investigated, as a proposed mode of action of mTOR is via transcriptional regulation. Figure 5-21 shows the effect of 24 h rapamycin exposure at 5 nM on CrT mRNA transcription. There was an decrease in *CrT* mRNA expression that could explain the reduced Cr uptake at 5 nM, suggesting that mTOR regulates CrT via transcriptional regulation. These data are provided courtesy of Dr Sevasti Zervou.

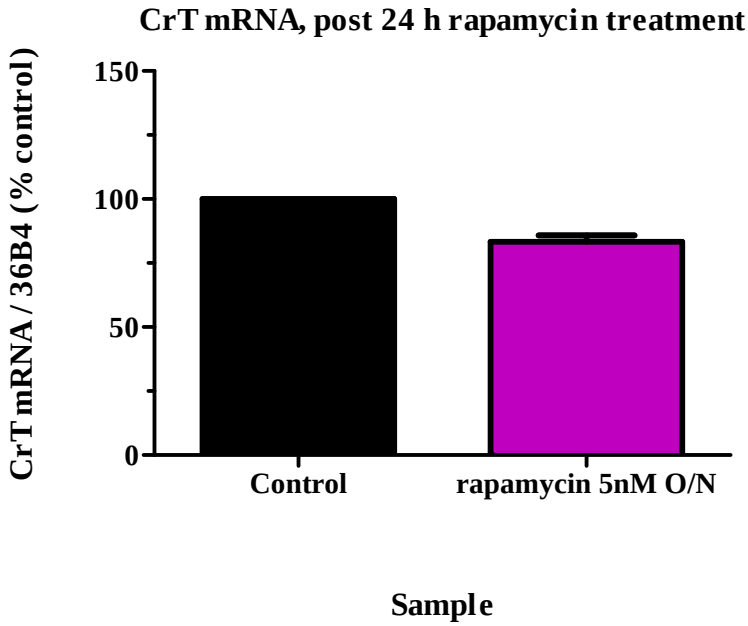


Figure 4-21. mRNA expression levels of total *CrT* in 3T3-CrT-HA cells treated in 5 nM rapamycin. Expression was normalised to 36B4 and expressed as a percentage of WT. *n*=3 for all samples. Values are mean ± SEM.

4.3. Discussion

Deranged energy metabolism, including reduced levels of free Cr and PCr are features of the failing myocardium. Regulating CrT activity would be a potential way of restoring energy homeostasis. Chapter 3 dealt with a transgenic approach to restoring Cr levels in the failing heart by the overexpression of CrT *in vivo*, and the approach chosen in this chapter set out to achieve the same goal, through a different strategy. This involved the use of an *in vitro* system with elevated CrT expression that can prove useful when exploring signalling pathways and dissecting CrT regulatory mechanisms. The aim was to use pharmacological inhibitors and stimulators acting against known members of a pathway previously suggested to be a regulator of CrT. The identification and manipulation of pathways affecting CrT regulation could yield potential therapeutic benefits, through the restoration of depleted energy reserves.

4.3.1. The choice of cell types for *in vitro* CrT regulation assays

The stable CrT-overexpressing cell line (3T3-CrT-HA) was used frequently for technical reasons, including their high levels of Cr uptake, which enabled easier and more accurate experimental read-outs to be obtained, particularly in the case of ^{14}C-Cr uptake assays. They also provided a 'cleaner' system than HL-1 cells, which require noradrenaline supplementation in their growth medium. Noradrenaline has previously been shown to enhance Cr uptake [11]. 3T3-CrT-HA cells are hardy and fast-growing. These characteristics facilitated reliable experiments, minimising complications with cell culture. Generally, these cells were used in the first instance in order to set up the assay in question, and where possible, the experiment was later repeated using the HL-1 cell line. HL-1 cells retain a cardiomyocyte-like phenotype, including 'beating' in culture, and are therefore relevant in the cardiac milieu. Additionally, reproducibility between the two cell lines provides greater confidence in the results obtained.

4.3.2. Insulin and its effect on Cr uptake

In this study, initial experiments showed that 48 h pre-incubation with insulin led to a statistically-significant increase in Cr uptake in 3T3-CrT-HA cells at extracellular concentrations of 1 nM and 3 nM, with 1 nM causing the greatest increase compared to untreated cells, mimicking the results observed by Odoom *et al* in myoblasts [11]. mRNA expression was unchanged in these insulin-incubated cells. Shorter pre-incubation periods in insulin, of 2 h and 24 h were tried, and these failed to change Cr uptake (data not shown), suggesting that there is no acute response to insulin. Subsequent repeats of the experiments performed with a 48 h pre-incubation failed to reproduce the initial large effect seen in response to insulin, although a smaller, statistically-significant response was observed. It is possible that this reduced response is due to the high passage number of the cells by this time, as a high passage number could affect signal transduction pathways. However, the level of CrT-HA

expression was tested in 3T3-CrT-HA cells at high (~60) passage and was unchanged from values obtained initially when validating the cell line (as described in Chapter 3), demonstrating that CrT activity had not altered under basal conditions.

Due to their greater relevance to the heart, the response of HL-1 cells to insulin stimulation was also tested, in order to determine whether the effect on the CrT was the same as observed in 3T3-CrT-HA cells in a system more relevant to the cardiac milieu. Insulin at a concentration of 1 nM also led to statistically-significant enhanced Cr uptake, though at lower levels than those seen in 3T3-CrT-HA fibroblasts.

It is important to consider the relevance of insulin in the setting of HF. It is recognized that insulin resistance is a feature of chronic HF [226] [227], with increased circulating insulin levels a feature of chronic HF, and to an even greater degree in acute decompensated HF [228]. Additionally, the increased sympathetic nervous stimulation in HF leads to increased adrenergic stimulation. Noradrenaline, shown to enhance Cr uptake in myoblasts [11], is also associated with an effect on glucose homeostasis, through increasing insulin resistance, though some studies have failed to establish a link between HF and elevated plasma noradrenaline levels [229]. PI-3-kinase, downstream of the insulin receptor, is also affected by this increased insulin resistance. Its decreased stimulation as a result of reduced sensitivity to insulin, could be one factor leading to the decrease in myocardial [Cr] in HF.

It is clear that insulin affects Cr uptake in both of these cell lines, though at different levels. This could be due to variations in the signalling pathways between the cell types, and the effect could also be exaggerated by the overall lower Cr uptake levels exhibited by the HL-1 cell line, which

expresses far lower levels of CrT than the 3T3-CrT-HA cells, creating more 'background' when performing ^{14}C-Cr uptake assays. However, the positive effect of insulin on Cr uptake demonstrates regulatory effects via a signalling pathway that is of relevance in cardiac cells, likely to be the IGF-1R pathway, which could contribute towards the restoration of depleted Cr in the diseased myocardium. The observation that increased Cr uptake occurs in two different cell lines confirms insulin as a long-term modulator of Cr concentration. As discussed, no acute affect of insulin was seen. However, the positive results obtained following the longer 48 h pre-incubation period closely mimic effects seen by various groups on research in other muscle types and cell systems, such as myoblasts [11], and skeletal muscle [195].

4.3.3. Growth hormone

Cells incubated for 48 h in the presence of growth hormone (GH) exhibited greatly increased creatine uptake compared to control cells, whilst expression of CrT mRNA remained unchanged across the range of GH treatments. This effect was less in HL-1 cells and not statistically-significant, though this was in part due to high levels of variation between sample replicates. As with insulin, subsequent repeats of these assays in 3T3-CrT-HA cells failed to reproduce such a large effect on Cr uptake. As in the case of the insulin treatments, these experiments were performed with cells at a much higher passage number than in the initial experiments, and it is possible that, as GH is potentially acting via the same signalling pathway as insulin, this was the cause of the reduced effect. GH is known to mediate IGF-1 release *in vivo*, via an endocrine response, though this is not relevant in the *in vitro* setting. Overall, these results suggest a role for GH in the up-regulation of Cr uptake, both in murine fibroblasts overexpressing CrT, and importantly, also in immortalized cardiac cells. The results suggest that, as with insulin, growth hormone is a long-term mediator of Cr uptake, possibly via the IGF-1 pathway.

4.3.4. IGF-1

The final approach used to test the influence of IGF-1R stimulation on the CrT was treatment with IGF-1. IGF-1 treatment has been shown to protect isolated cardiomyocytes from hypoxia / reoxygenation injury [230], and this could be linked to enhanced Cr uptake via the IGF-1 pathway. Additionally, the locally acting IGF-1 isoform (mIGF-1) was shown to protect neonatal cardiomyocytes and HL-1 cells from oxidative and hypertrophic stresses after 24 h incubation [231]. Initially, short duration treatments were attempted, as evidence suggests that IGF-1 acts extremely quickly on the IGF-1R. No effect was seen following incubation periods of up to 30 min, so longer incubations of 2 h and 24 h were performed. Although a small increase in Cr uptake was observed following both durations of treatment, particularly at 3 ng / mL and 10 ng / mL, these increases were not significant. Ideally, repeats of these experiments need to be performed, in order to confirm whether this trend is consistent. It has previously been shown in myoblasts that IGF-1 enhances Cr uptake less than insulin [11], and this is a possible explanation for the lack of a significant increase in uptake.

4.3.5. Picropodophyllin (PPP) - mediated inhibition of IGF-1R

PPP is a potent inhibitor of the IGF-1R, inhibiting its phosphorylation [232] [233], and was used to reinforce evidence for the involvement of the IGF-1R pathway in the regulation of the CrT. 3T3-CrT-HA cells were pre-treated with insulin for 48 h in order to stimulate the IGF-1R, prior to the addition of PPP at the start of the uptake assay. In control cells incubated in the absence of insulin, PPP significantly inhibited Cr uptake at all concentrations used. In cells pre-treated with insulin, all concentrations of PPP used prevented the increased Cr uptake associated with insulin treatment. This demonstrates a key link between the IGF-1R and enhanced Cr uptake- inhibition of the IGF-1R prevents the increased Cr uptake mediated by insulin. The reduction of Cr uptake

in cells not pre-treated with insulin suggests either a degree of constitutive activity of the IGF-1R, or an off-target effect of PPP. PPP is also known to reduce phosphorylation of Akt, indirectly downstream of IGF-1R [234], and it is possible that this could affect mTOR phosphorylation, also implicated in CrT regulation.

4.3.6. Regulation of Cr uptake via PKA and PKC

PKA inhibition in unstimulated cells with 2 h treatments of H89 gave a trend towards decreased uptake. This effect was mirrored in HL-1 cells, although none of these effects were statistically-significant. These results suggest the possibility of a very low degree of constitutive PKA activity. If PKA phosphorylation played a significant role under basal conditions, inhibition of Cr uptake would be expected at lower concentrations, as H89 has an IC_{50} of around 50 nM [220]. Previous studies using compounds known to directly activate PKA demonstrated no effect on Cr transport in transfected cells [9 26], although this is in contrast to the findings within this thesis, described later.

BIM treatment gave consistent results in both cell lines, and a downward trend in Cr uptake was seen at concentrations of 300 nM and 1 μM, though this was not significant. If the trend is genuine, this suggests possible involvement of PKCα at the lower concentration, and potentially PKCβ at the higher concentration. This downregulation, if genuine, may occur via translocation of the CrT to the cytoplasm. Wang *et al* suggested that while PKC-mediated phosphorylation of the CrT most likely does not play a major role in regulation of the CrT, its involvement in the regulation of Cr uptake could not be ruled out, as evidence indicates that stimulation of GABA transport (by the closely related GABA transporter) by a tyrosine phosphatase inhibitor can be

blocked by PKC activation [235] [236], in contradiction to the findings regarding the CrT in this thesis.

An interesting observation was made when quantifying Cr uptake in cells treated with BIM for the duration of the uptake assay, but no pre-incubation period. Under these conditions, BIM *increased* the Cr uptake in control cells, suggesting that a longer incubation is required for uptake inhibition. These results mimic those mentioned previously regarding the related GABA transporter [235] [236]. It is interesting that the effect of BIM should be so dependent on incubation time. This raises the possibility that a separate pathway is affected by BIM, which leads to a brief initial increase in Cr uptake, before the influence on PKC causes the decrease observed over longer periods. Ultimately, inhibition of PKC with a different compound (for example, low concentrations of Gö 6976 or rottlerin) would be a useful test, in order to confirm whether these observations are indeed PKC-mediated, or simply off-target effects of BIM. If this brief period of enhanced Cr uptake is indeed an off-target effect, a possible explanation could be due to the documented effect of BIM on the kinase glycogen synthase kinase 3 (GSK-3). This kinase is known to be inhibited by BIM [237]. The phosphorylation state of GSK-3 is regulated by Cr [238], thus demonstrating a connection, and perhaps indicating a negative feedback mechanism whereby the inhibition of GSK-3 affects the regulation of the CrT. The observation of an increase in Cr uptake (although over a brief period) is more in keeping with previous literature and could go some way to explaining it- Dai *et al* found that *Xenopus* oocytes expressing CrT exhibited decreased Cr uptake when treated with the protein kinase C activator phorbol 12-myristate 13-acetate (PMA), and suggested that activation of PKC has an inhibitory effect on Cr uptake [9].

Confirmation of the regulatory effect of PKC on the CrT was provided by the reverse experiments- PKC activation. Activators used were PMA and STX. Both of these compounds led to statistically-significant increases in Cr uptake. This is an important finding, as previous reports in the literature (mentioned above) have found that PKC activation via PMA led to a *decrease* in Cr transport [9 26]. It is important to note, however, that owing to the C1 domain it shares with PKC [239] (a binding site for phorbol esters, such as PMA), Akt (PKB) may also be targeted by PMA treatment. PMA has been reported to inhibit Akt signalling [240], and this potential 'off-target' effect could influence Cr uptake. As discussed previously, the results within this thesis were obtained using more relevant cell systems than these previous studies used, providing a more accurate insight into the role of PKC in CrT regulation in a cardiac cell phenotype than previous studies.

4.3.7. Effects of PKA and PKC inhibiton on the IGF-1 pathway

The effects of inhibiting PKA (with H89) and PKC (with BIM) were tested following stimulation of IGF-1R with both insulin and GH. Essentially, the increased Cr uptake observed in the presence of both insulin and GH was ablated by the addition of either H89 or BIM. This supports the hypothesis that the IGF-1 pathway acts via a mechanism dependent on both PKA and PKC. The fact that the effect of PKA and PKC inhibition is far greater under these stimulated conditions than at baseline suggests that they are both downstream of the IGF-1R. In context with the effects of PKA and PKC inhibition observed in the absence of any activation, via IGF-1R or otherwise (described previously), these results demonstrate that PKA and PKC are both activated via the IGF-1R pathway, and form an essential part of the regulation of the CrT.

4.3.8. Rapamycin and mTOR

The results shown in this thesis display a very low decrease in Cr transport in 3T3-CrT-HA cells treated with 5 nM rapamycin. This effect is not seen at higher or lower concentrations. However, treatment with 5 nM rapamycin was found to lead to an up-regulation of *CrT* mRNA expression, suggesting that the minor effect observed on Cr uptake could be due to enhanced *CrT* transcription levels associated with the inhibition of mTOR. It is possible that this effect occurs via SGK1 (outlined in the introduction). Inhibition of mTOR in the absence of stimulation with insulin excludes the possibility of an off-target effect via direct action of insulin on SGK1, thus suggesting that the effect seen is due to the direct effect of rapamycin on mTOR itself. Although the increase observed in Cr uptake is not a large one, there is evidence in the literature to suggest that mTOR positively regulates Cr transport [217]. Conversely, a recent study by Darrabie *et al* found that rapamycin did not affect Cr uptake in rat neonatal cardiomyocytes [219]. This was in spite of an increase of *CrT* mRNA levels seen following prolonged incubation with rapamycin.

4.3.9. Conclusions

Of the compounds and hormones tested via IGF-1R, several exhibited a regulatory effect on the CrT. Insulin and growth hormone both led to an increase in Cr uptake in both cell types tested, suggesting the involvement of IGF-1R as a mediator of Cr transport. These results are backed up by the finding that the IGF-1R inhibitor, PPP, effectively blocks any increase in Cr uptake mediated by either insulin or GH. Downstream of IGF-1R, via intermediate kinases including PI3K, are PKA and PKC. Although these kinases were found not to exert a strong effect on the CrT under unstimulated conditions, following IGF-1R stimulation they played a significant role, and both PKA and PKC inhibition served to reverse IGF-1R mediated increases in Cr uptake. Whilst reinforcing the evidence of the regulatory role of IGF-1R over the CrT, this also indicates

that both PKA and PKC are essential components of this regulatory pathway. Importantly, these data, acquired from two appropriate *in vitro* systems, are in contrast to previous findings that concluded that a) PKA does not play a role in CrT regulation, and b) that PKC activation *inhibits* Cr uptake. In addition to these findings, a (minor) regulatory role has also been described for mTOR through preliminary studies. Unlike the IGF-1R- mediated regulation detailed, this effect appears to be mediated, at least in part, by an up regulation of *CrT* mRNA transcription.

Chapter 5. Post-translational modification of the Creatine Transporter

5.1. Introduction

5.1.1. Post-translational modification and regulation of the CrT

Little is known about the regulation of CrT activity and expression, and indeed how such regulation is involved in the decrease seen in CrT function in heart failure. Previous studies have highlighted the potential importance of CrT regulation via post-translational modification, as differences in CrT activity have not been fully explained by altered transcription alone [48]. The previous chapter investigated the role of signalling pathways on CrT activity. These pathways rely on post-translational modifications (PTMs), and as such, this chapter attempts to identify such modifications in the CrT that could be involved in its regulation.

A previous study in our laboratory which examined the correlation between *CrT* mRNA and CrT protein expression gave a clear indication of the potential involvement of post-translational modifications in the regulation of the CrT [48]. Two mouse models of genetically-altered myocardial Cr concentration were investigated; a model of CrT overexpression (CrT-OE) exhibiting supra-normal myocardial Cr levels, and also the guanidinoacetate-*N*-methyl transferase knock out ($GAMT^{-/-}$) model, a mouse model unable to synthesise Cr, therefore totally reliant on dietary Cr intake (both discussed previously). Both of these models demonstrated Cr uptake altered beyond the level of variation observed in *CrT* transcription. CrT-OE mice with elevated myocardial Cr levels showed no change in endogenous *CrT* mRNA, whereas in $GAMT^{-/-}$ mice, despite a 7-fold increase in Cr uptake capacity, *CrT* mRNA levels

were increased by only 1.4-fold. WT mice have also been investigated, and despite showing a decrease in CrT activity when fed Cr, they showed no decrease in *CrT* mRNA expression. Lack of substrate is known to be a powerful signal for the upregulation of CrT activity in myocardium as well as skeletal muscle and myoblasts [31 100]. It was concluded that, due to the relatively low levels of up-regulation observed in *CrT* mRNA, the variation in Cr uptake observed was likely more greatly influenced by post-translational means than by transcriptional regulation. Some research has been conducted into post-transcriptional modifications in the CrT, namely *N*-linked glycosylation and to a lesser degree phosphorylation. This chapter looks into these events and attempts to provide novel information on their relevance to the regulation of Cr uptake.

5.1.2. *N*-linked glycosylation of the CrT

N-linked (asparagine-linked) glycosylation involves the addition of saccharides to the amide nitrogen of asparagine side-chains in proteins. The CrT has been shown to be a glycoprotein [241 39]. Several studies on other members of the SLC6 family of transporters have shown that multiple protein species with different electrophoretic mobility exist, in each case encoded by a single cDNA. This is the case for GAT-1 (GABA transporter) [242], human NET (norepinephrine transporter) [243], 5-HTT (serotonin transporter) [244] and human DAT (dopamine transporter) [245]. West *et al* established that the CrT runs as a 70-80 kDa component on SDS-PAGE, but following treatment with *N*-glycosidase F (PNGase F, used to remove high-mannose N-glycans from glycoproteins), this band migrated at a rate equivalent to the reduced size of 50 kDa [241]. Therefore, they concluded that the CrT is a glycoprotein.

Straumann and colleagues performed a series of elegant experiments in order to determine more about the effects of *N*-linked glycosylation on the CrT [39]. Using a system of HEK-293 cells

overexpressing rat CrT with an N-terminal HA tag, they showed that native CrT migrated on LDS-PAGE in the form of two distinct bands, one a diffuse band of 75-91 kDa, and another of 58 kDa. They concluded that the 58 kDa species represented the active form of CrT, located at the plasma membrane. These data corresponded to those obtained in different studies using the same antibody [34 246 247 31]. The anti-CrT antibody used in these studies has been shown to cross-react with pyruvate dehydrogenase (PDH) complexes, bringing previous results into question [40], although in this case the results were then verified with an anti-HA antibody against the N-terminal HA tag in their over-expressing cell line, and matched the results obtained with their anti-CrT antibody against the 58 kDa species. However, an additional band was detected with the anti-HA antibody alone, the diffuse 75-91 kDa band. The authors suggested that this finding may be either an LDS-resistant homodimeric form of CrT, or an artefact caused by aggregate formation due to high levels of CrT overexpression.

The authors treated cell lysate from their CrT overexpressing cell line with 2 enzymes to investigate this *N*-linked glycosylation; EndoH (endoglycosidase H_f) which removes unprocessed *N*-glycans, and PNGase F, which removes all *N*-glycans *in vitro*. Treatment with EndoH yielded a third CrT species, with an apparent mass of 48 kDa, and PNGase F treatment yielded a fourth CrT band, with an apparent mass of 43 kDa. It was postulated that the shift in migration pattern resulting from treatment with EndoH and PNGase F was respectively due to the removal of one or both of the canonical glycosylation sites predicted within the extracellular loop between transmembrane domains II and III at positions Asn^{192} and Asn^{197}. The occurrence of these predicted sites is conserved throughout the neurotransmitter transporter family [39]. It was concluded that the monomeric non-glycosylated form of CrT has an electrophoretic mobility of 43 kDa, the partially glycosylated form (observed following EndoH treatment) has a mobility of 48 kDa, and the fully glycosylated form (after PNGase F treatment) migrates at an apparent 58

kDa. Interestingly, the apparent mass of these deglycosylated forms of the CrT on SDS-PAGE are considerably different to the mass predicted by the transporter's amino acid sequence (~ 72 kDa). The effects observed following these treatments led the authors to suggest the involvement of 2 of the 3 predicted glycosylation sites on the CrT, located on extracellular loop 2, between transmembrane domains 3 and 4. The third putative glycosylation site, on the short extracellular loop between transmembrane domains 11 and 12, was not believed to be affected by these treatments. The enzymatic deglycosylation results were supported by *in vitro* treatment of cells with tunicamycin, a pharmacological inhibitor of *N*-linked glycosylation. Treatment led to a change in CrT migration comparable to that seen after PNGase F treatment. Additionally, mutagenesis of the 2 glycosylation sites also led to similar results to those seen following incubation with EndoH and PNGaseF. Inhibition of glycosylation, either tunicamycin-induced or in the glycosylation mutants created by the group, did not affect the function of the CrT, although it was suggested that glycosylation of the CrT is related to its localisation within the cell, as although deglycosylated CrT was active, the only form of CrT found at the plasma membrane was the fully mature, glycosylated form. A study on the closely related serotonin transporter (5-HTT) also found that glycosylation had no effect on transporter activity [244]. In contrast, a study on the dopamine transporter (DAT), another member of the SLC6 family, showed that deglycosylation led to reduced dopamine uptake capacity, and reduced catalytic activity in the DAT at the cell surface.

5.1.3. Phosphorylation of the CrT

Little is known about the presence or effects of phosphorylation on the regulation of the CrT, though several consensus PKA- and PKC-dependent protein phosphorylation sites have been identified in the sequence of mammalian CrT [26 9]. Additionally, consensus amino acid sequence motifs for protein kinases flanking Tyr^{11} and Ser^{625} residues have been identified [248]. Early

studies showed that the activation of PKC-dependent phosphorylation with the PKC activator PMA (phorbol 12-myristate 13-acetate) almost completely ablated Cr uptake in *Xenopus* oocytes expressing the human CrT, whereas PKA activation had no effect on Cr uptake [9]. This suggested that, despite the presence of consensus PKA-dependent phosphorylation sites on the CrT, PKA phosphorylation is not involved in the regulation of Cr uptake, while PKC-mediated phosphorylation does play a role. It should be noted that in oocytes, PKC-mediated down-regulation of function may be secondary to PKC-induced depolarisation of the oocyte's resting membrane potential. Therefore, the results of studies conducted in such models which exhibit down-regulation of CrT in response to PKC activation should be treated with caution [249]. This is particularly noteworthy given the findings of the previous chapter, which clearly demonstrated that, in the systems tested, PKC activation leads to up-regulation of the CrT.

Zhao and colleagues investigated the effect of starvation on myocellular Cr levels in gastrocnemius muscle in rats [248]. An increase in myocellular Cr was explained by a decrease in serine phosphorylation of the CrT, detected using a phosphospecific antibody on the product of an immunoprecipitation performed with an anti-Cr antibody. The observation that neither CrT protein levels or mRNA expression had changed led to the conclusion that reduced serine phosphorylation was the cause of increased Cr transport. No change was seen in tyrosine phosphorylation. The authors therefore concluded that serine phosphorylation, possibly mediated by PKC, has a regulatory effect on CrT activity, either affecting Cr uptake rate, or the transporter's ability to bind Cr. However, it should be noted that these assays were all reliant on an unspecified anti-CrT antibody. It has been reported that anti-CrT antibodies can be non-specific (discussed previously in the General Introduction) and in our hands, no commercially available anti-CrT antibodies have specifically bound epitopes of the CrT. It was not verified that the resulting product was indeed rich in CrT, and therefore subsequent blots on this IP

product with rabbit antiphosphoserine or mouse antiphosphotyrosine antibodies could have been non-specific to the CrT. For these reasons, these results should also be treated with caution.

Tyrosine phosphorylation is known to play a role in the regulation of other members of the SLC6 family [250]. For example, in GAT1, expressed both endogenously in hippocampal neurons, and heterologously in Chinese hamster ovary cells, inhibitors of tyrosine phosphatases increased GABA uptake due to redistribution of GAT1 to the cell surface [236]. Additionally, tyrosine phosphorylation of the CrT was shown to have a regulatory effect in skeletal muscle of rats during sepsis. Sepsis led to an increase in free myocellular Cr, and this was accompanied by an increase in the tyrosine phosphorylation of the CrT [235]. As with the study described above on the effects of starvation on the CrT, this study used an unverified anti-CrT antibody, a point to be taken into account when considering the findings.

In summary, several studies have investigated the role of post-translational modifications in CrT regulation. *N*-linked glycosylation has been shown to be heavily involved in CrT maturation, although consensus regarding the effects it has on the electrophoretic mobility and function of the CrT is lacking. The two most recent studies questioning the role of *N*-glycosylation in the CrT [241] [39] (outlined previously) differed in their conclusions, with deglycosylation of the CrT yielding different sized species. Glycosylation was also implicated in CrT trafficking, but not in regulating CrT activity. The presence of phosphorylation on the CrT, as well as any potential regulatory effects it may have, are less clearly defined. The existence of putative phosphorylation sites, outlined above, has been demonstrated in several publications. Whilst some studies have investigated the roles of particular types of phosphorylation on the CrT, it is an area that needs further investigation. Results obtained in the study of serine and tyrosine phosphorylation of the CrT could be unreliable, as the protein obtained was potentially

precipitated with a non-specific anti-CrT antibody. As discussed, in the experience of our laboratory there are no anti-CrT antibodies available, commercially or otherwise, able to reliably and specifically bind CrT extracted from LV tissue. Additionally, another antibody raised against the CrT was shown to cross react with PDH [40]. The anti-CrT (epitope 14-27) antibody used in this thesis (a gift from Dr Theo Wallimann) has been shown to specifically bind CrT in cell extracts, and is the only antibody tested to do so. Therefore, this is the anti-CrT antibody that has been used throughout this thesis.

As a basis for investigation of the CrT, a prediction of serine, threonine and tyrosine sites was made using NetPhos [45]. These sites, in addition to the identified glycosylation sites, are depicted in figure 5-1.

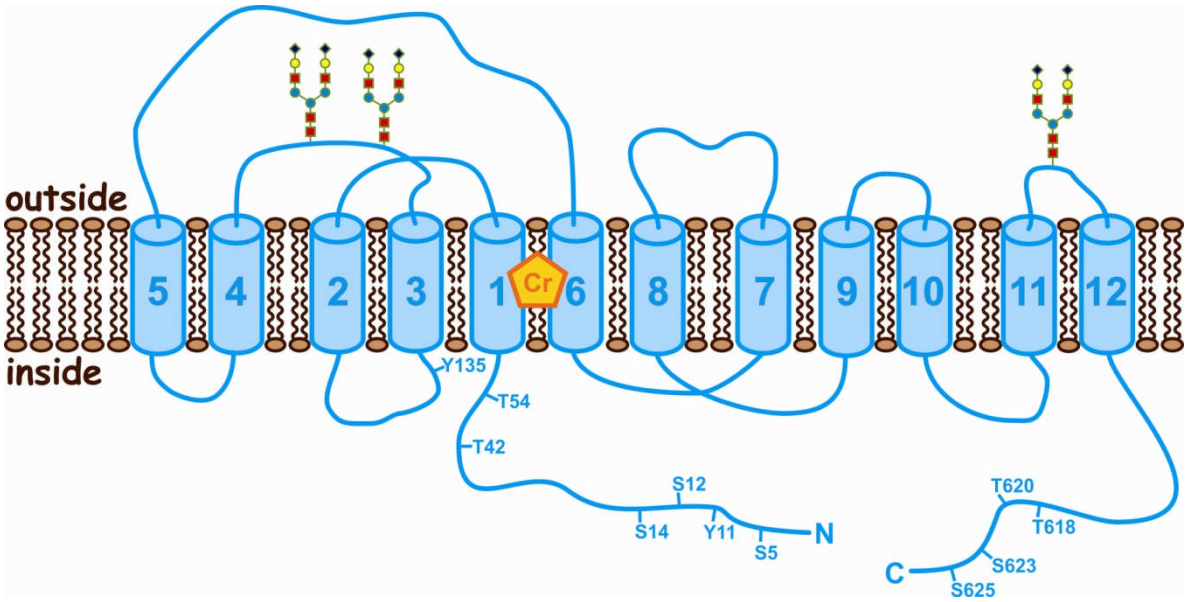


Figure 5-1 A CrT schematic showing predicted glycosylation and phosphorylation sites (as shown in Chapter 1). A schematic representation of the secondary structure of the creatine transporter, based on the structure of the bacterial LeuTAa transporter (PDB code2A65), and showing putative phosphorylation sites. The probable sequences of intracellular CrT loops were informed by aligning the primary sequences of CrT and LeuTAa using MULTALIN [46] and evaluating this with respect to the known three-dimensional structure of LeuTAa. A total of 22 possible serine, threonine and tyrosine phosphorylation sites on the CrT were then predicted by NetPhos [45]. The subsets labelled on the figure are those which reside on the predicted intracellular loops. Putative glycosylation sites are also shown. S = serine, T = threonine, Y = tyrosine. The predicted binding site for Cr is also indicated, which is believed to incorporate TM3 and TM8 in addition to TM1 and TM6. Transmembrane domains are represented by blue cylinders. Schematic kindly provided by Dr. James Brown, created using CorelDraw 9.

5.2. Aims

As outlined previously, there are discrepancies regarding the effect of glycosylation on the CrT, involving potential changes in electrophoretic mobility relating to glycosylation status. This work seeks to resolve the uncertainty regarding this issue. This section also aims to establish the existence of predicted phosphorylation sites, using several methods, including phosphospecific antibodies and mass spectrometry, ultimately determining their effect on CrT function. These techniques could also enable the elucidation of the effects of substrate exposure on the phosphorylation status of the CrT,

and are feasible owing to the creation of the 3T3-CrT-HA cell line, which overexpresses CrT-HA. CrT-HA is isolated by optimised immunoprecipitation protocols against HA, overcoming previous difficulties caused by unreliable antibodies.

5.3. Materials and Methods

Below are details of methods specific to techniques used in this chapter alone. They are in addition to the methods listed in the General Materials and Methods section.

5.3.1. Large scale immunoprecipitation

Ten 75 cm^2 flasks of 3T3-CrT-HA cells were grown to confluence, trypsinised and harvested, then washed 2x in ice-cold PBS. An equivalent amount of NIH 3T3 Tet-Off cells were also grown as a negative control. The cell pellets were lysed in 2% SDS lysis buffer (detailed previously) containing Complete Protease Inhibitor Cocktail (Roche) and PhosSTOP phosphatase inhibitors (Roche), then sonicated on ice. The resulting lysate was diluted with NET buffer (50 mM Tris-HCl pH 7.5, 5 mM EDTA, 150 mM NaCl, 0.5% NP40) to reduce the total SDS content to 0.1%, then incubated with 50 µL protein A agarose (Sigma) on a rotator for 1 h. Following centrifugation, the lysate was incubated with 50 µL α-HA agarose (Sigma) on a rotator at 4^o C overnight. The beads were washed 3x in ice-cold NET buffer, then incubated in 400 µL ice-cold elution buffer (100 mM glycine, pH 2.5) on a rotator at 4^o C for 20 min. Six hundred µL methanol and 150 µL chloroform were added to 200 µL of the eluate, the mixture vortexed and 450 µL Milli-Q water added. Following centrifugation at 16,000 g, the upper aqueous phase was removed, 450 µL methanol added and the resulting mixture vortexed and centrifuged at 16,000 g for 2 min. The supernatant was removed, the pellet air-dried and then

reconstituted in 40 µL 1x Laemmli buffer, followed by boiling for 3 min prior to loading onto an SDS mini protein gel.

5.3.2. Silver staining

Following SDS-PAGE, the gel was fixed for 1 h in fixing solution (40% EtOH, 10% acetic acid), then washed in 30% ethanol, twice for 20 min and Milli-Q water for 20 min. The gel was then washed in 0.02% $Na_2S_2O_3$ for 1 min and Milli-Q water, twice for 20 seconds before incubation in ice-cold 0.1% $AgNO_3$ solution for 20 min at 4^o C. After four washes in Milli-Q water, the gel was developed in 3% Na_2CO_3, 0.05% formalin solution until bands were visible, then washed in Milli-Q water and fixed in 5% acetic acid for 5 min before washing and storing at 4^o C in 1% acetic acid. The bands were excised from the gel and submitted to the Proteomics Core Facility (CCMP, Henry Wellcome Building for Genomic Medicine, University of Oxford) for trypsin digestion and subsequent LC / MS-MS analysis.

5.4. Results

5.4.1. The choice of cell type for characterisation of CrT post-translational modifications (PTMs)

CrT was undetectable in HL-1 cells using an antibody against amino acids 14-27 of the CrT (gifted by Theo Wallimann). This is unsurprising given that the same antibody failed to detect CrT in left ventricular tissue and standard, untransfected 3T3 cells, which all show similar levels of *CrT* mRNA expression. As 3T3-CrT-HA cells show 10 times greater Cr uptake than untransfected 3T3 cells, with CrT being detectable by both anti-CrT 14-27 and anti-HA, they were chosen as the most suitable *in vitro* system for isolating CrT and studying PTMs. Figures

4-2 and 4-3 compare the mRNA expression of 3T3-CrT-HA cells to HL-1 and untransfected 3T3, and also the ability to detect CrT protein, using the anti-CrT 14-27 antibody, on lysates of these cells.

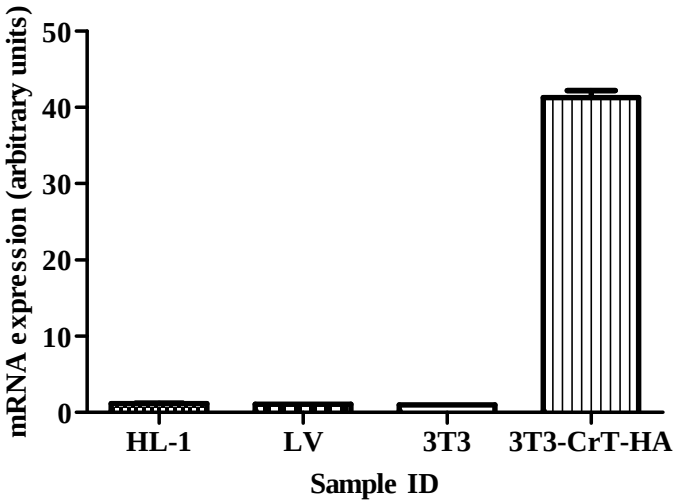


Figure 5-2. Graph showing mRNA expression of endogenous CrT in samples. These samples are from HL-1 cells, mouse LV tissue, untransfected murine fibroblasts (3T3) and stably-transfected 3T3 (3T3-CrT-HA). All samples were run in triplicate. Error bars represent SEM. Expression of CrT mRNA in all samples is similar with the exception of the transfected cells, which show around 40x higher expression.

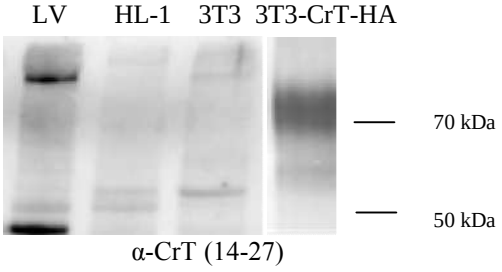


Figure 5-3 Western blot analysis of CrT using α-CrT (epitope 14-27) (1:10,000) antibody, in mouse LV tissue, HL-1 and 3T3, and 3T3-CrT-HA lysates. CrT was not detected in any of the lysates with the exception of the cells overexpressing CrT, 3T3-CrT-HA. This suggests low expression levels in the untransfected cells, although they are known to express CrT. Bands in the LV, HL-1 and 3T3 lanes are non-specific. The bands in the 3T3-CrT-HA lane are CrT, and display the usual migration pattern seen, with a major diffuse band between 70-80 kDa, and a less intense band at 58 kDa. Molecular weights were determined by comparison with a molecular weight standard (Precision Plus Protein ™ Standard, Biorad, UK)

5.4.2. Inhibition of *N*-linked glycosylation of the CrT

To investigate the presence of *N*-linked glycosylation in CrT *in vitro*, 3T3-CrT-HA protein lysates were treated with inhibitors of glycosylation. Either EndoH or PNGase F was added to the protein samples prior to SDS-PAGE and western blotting. The protein blots were probed with anti-HA and anti-CrT antibodies. Band patterns resulting from both anti-HA and anti-CrT probing were the same, and appeared as an obvious diffuse band of 70-80 kDa in the untreated inhibitor-free control sample, and as a fainter band at around 58 kDa. Barely visible, but present in all samples, were 2 additional bands, with apparent molecular weights of 150 kDa and 200 kDa.

Following treatment with EndoH, there was a reduction in the intensity of the 70 kDa band, and a substantial reduction in the intensity of the band at 58 kDa. A smaller band, migrating at 48 kDa, became visible. When treated with PNGase F, the 70 kDa diffuse band was totally ablated, and a smaller band with an apparent size of 43 kDa was observed. The intensity of the 58 kDa band was reduced significantly, as observed following EndoH treatment. As all bands were detected by both antibodies, it can be concluded that these corresponded to CrT-HA.

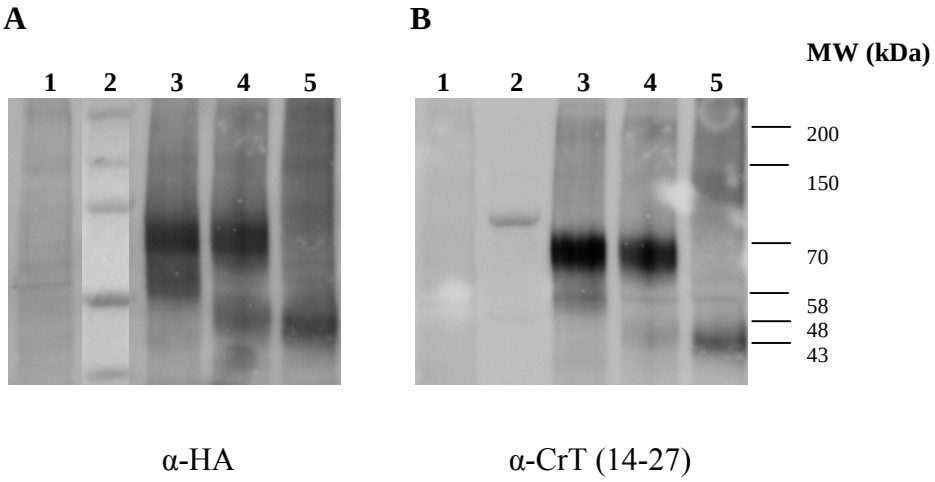


Figure 5-4. Deglycosylation of CrT-HA with EndoH and PNGase. Western blot analysis of 3T3-CrT-HA lysates in the untreated form, and also following treatment with inhibitors of *N*-linked glycosylation EndoH and PNGase. (A) Membrane probed with anti-HA, (B) is the same membrane probed with anti-CrT (14-27) after stripping off the anti-HA antibody. Untransfected NIH 3T3 cells served as –ve control. In both membranes, 1= negative control, 2= MW ladder, 3= untreated control lysate, 4= Endo H-treated lysate and 5= PNGase-treated lysate. Treatment with inhibitors revealed the presence of different sized CrT species, indicating that the CrT is a glycoprotein. Following probing with anti-HA (1:200,000) (Roche, UK), the membrane was stripped and re-probed with anti-CrT (14-27) (1:10,000). Blots with both antibodies yielded the same results. Molecular weights were determined by using a molecular weight standard (Precision Plus Protein ™ Standard, Biorad, UK)

5.4.2.1. *In vitro* inhibition of *N*-linked glycosylation using tunicamycin

To determine whether *N*-linked glycosylation of CrT is involved in CrT function, 3T3-CrT-HA cells were treated *in vitro* with two concentrations of tunicamycin, a strong inhibitor of *N*-linked glycosylation that blocks the synthesis of all *N*-glycans. This approach had an advantage over the one described above, as cells could be assessed for Cr uptake following tunicamycin treatment (described in the subsequent paragraph). Concentrations of 2.5 μM and 5 μM tunicamycin were chosen. Previous research has shown that cells remain viable following incubation in concentrations of 5 μM tunicamycin [39], despite the fact that the compound is a known inhibitor of the cell cycle [251]. Typically, concentrations used for *in vitro* inhibition of *N*-linked glycosylation have ranged from 0.05 - 5 μg / mL [252 253]. In order to determine the extent of *N*-linked glycosylation inhibition at lower concentrations, a titration was performed (data not shown), and it was found that a minimum concentration of 2.5 μM was required. Tunicamycin

incubations were carried out over 2 h, on untreated cells and also cells pre-incubated for 48 h in 500 µM Cr. Following protein extraction, samples were separated on 4-20 % SDS gradient gels prior to western blotting and probing of the blots with anti-HA. Results were broadly similar to those observed following the treatment of lysates with PNGase F; the diffuse 70 kDa was almost totally ablated along with the 58 kDa band, and a smaller band of 43 kDa was visible. No differences were observed between the two concentrations of tunicamycin treatment, and pre-treatment of cells with Cr did not have an effect.

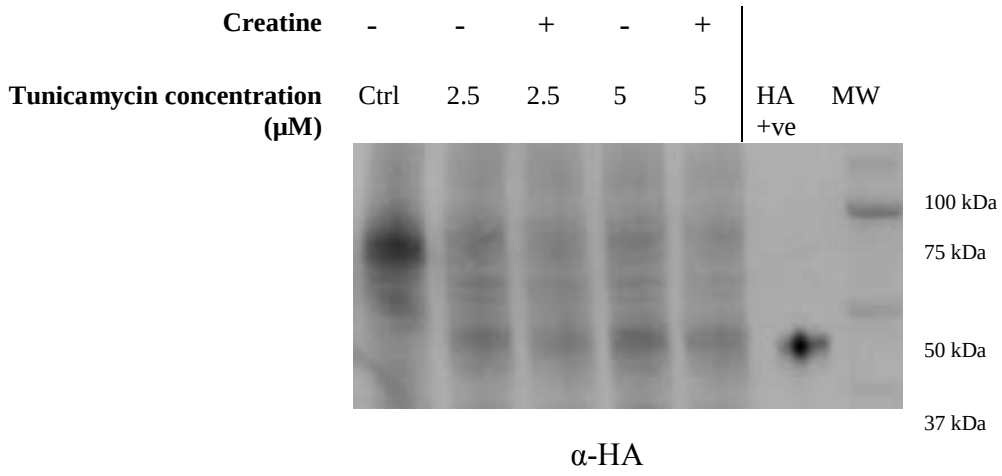


Figure 5-5. *In vitro* deglycosylation of CrT-HA with tunicamycin. Western blot analysis of 3T3-CrT-HA lysate in untreated form, and also following 2 h incubation in the presence of the inhibitor of *N*-linked glycosylation tunicamycin at varying concentrations, in the presence and absence of 500 µM Cr. The presence of Cr had no effect. The 43 kDa band appearing post-tunicamycin treatment is the same size as that observed following PNGase treatment, indicating complete deglycosylation. The membrane was probed with the anti-HA antibody (1:200,000) (Roche, UK). An HA positive control is shown (HA +ve). Molecular weights were determined by using a molecular weight standard, indicated 'MW' in the figure (Precision Plus Protein ™ Standard, Biorad, UK)

5.4.3. The effects of tunicamycin on Cr uptake

To determine the effect of inhibition of *N*-linked glycosylation on Cr uptake, 3T3-CrT-HA cells were pre-treated with tunicamycin for 2 h prior to performing a Cr uptake assay (see General Materials and Methods). At concentrations of 0.5 µg / mL tunicamycin and above, there was a

trend towards decreased Cr uptake, which became significant at 2.5 µg / mL and 5.0 µg / mL, with a reduction of ~20% compared to untreated control.

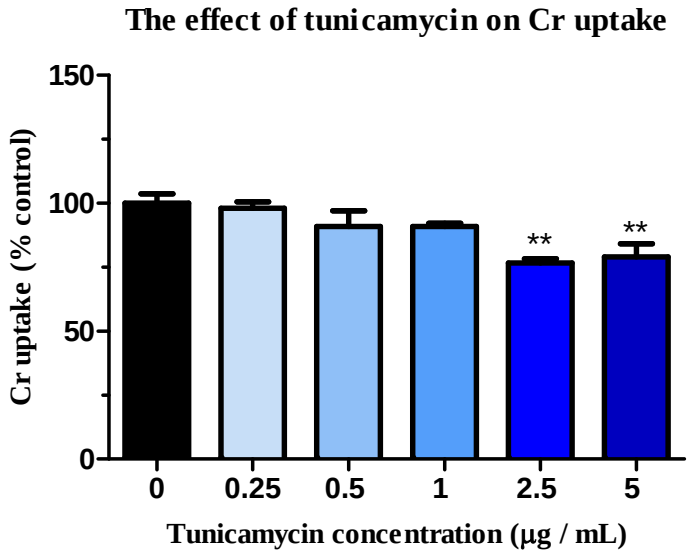


Figure 5-6. . Effect of tunicamycin on creatine uptake in 3T3-CrT-HA cells. Following 2 h incubation in various tunicamycin concentrations, decrease in Cr uptake was statistically significant only at 2.5 and 5 µg / mL tunicamycin. *n=6* for control, *n=3* for all other groups. Values are mean ± SEM. ** $p < 0.01$ compared to Cr only control group (One-way ANOVA and Dunnett's multiple comparison test).

5.4.3.1. Tunicamycin and cell viability

A trypan blue exclusion test was performed on cells incubated in tunicamycin under the same conditions as those in the uptake experiment, with the 2 highest concentrations of tunicamycin used, to determine the extent of membrane integrity post-treatment. There was no significant difference between treated cells and controls. Ten % DMSO, known to be toxic, was used as a positive control.

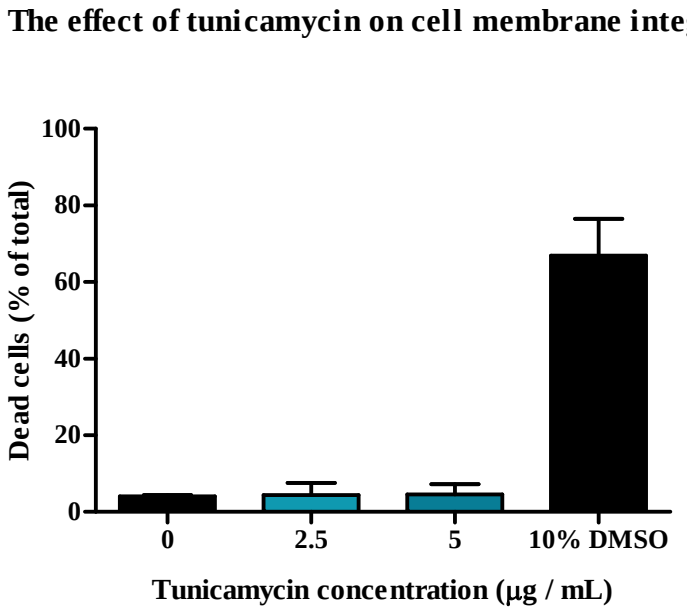


Figure 5-7. Effects of tunicamycin on 3T3-CrT-HA. Cells were incubated in the presence and absence of tunicamycin for 2 h. *n=4* for control, *n=2* for treated cells. Values are mean ± SEM. There was no significant difference in % dead cells between the tunicamycin-treated cells and the control group (One-way ANOVA and Dunnett's multiple comparison test).

5.4.4. Phosphorylation of the CrT

To elucidate more about the general phosphorylation status of the CrT, 3T3-CrT-HA cells were lysed under normal conditions (General Materials and Methods) with the addition of PhosSTOP® phosphatase inhibitors (Roche, UK). All lysates used for the investigation of phosphorylation were prepared in this way unless stated otherwise. Two treatments were then performed, with the intention of (a) preserving any phosphorylation present in the CrT, and (b) dephosphorylating the protein totally, to enable a comparison to be made between the two. For preservation of phosphorylation, cells were incubated in the presence of 1 µM sodium orthovanadate, an inhibitor of protein tyrosine phosphatases, for 1 h before harvesting. In order to dephosphorylate the CrT, a digest with calf intestinal (alkaline) phosphatase (CIAP) (a phosphatase that catalyses the removal of phosphate groups) was performed prior to SDS-PAGE separation on a 4-20 % gradient, and blotting of the protein. Blots were probed with anti-HA. Cells were starved of Cr for 24 h prior to harvesting, using charcoal-stripped FBS as a substitute

to normal FBS in complete media, as previous findings have indicated that CrT activity is upregulated in the absence of substrate [31]. The aim was to establish whether this upregulation is associated with altered levels of phosphorylation.

Both the sodium orthovanadate- and CIAP-treated samples were run alongside an untreated control. Dephosphorylation of the CrT with CIAP treatment caused a substantial shift in its migration pattern. The prominent 70 kDa band was greatly reduced in intensity, and replaced with a band at around 62 kDa. A band was still present at 58 kDa, as in the control sample, though it was less intense than in the untreated control. Treatment of cells with sodium orthovanadate did not alter the migration pattern of either of the CrT bands.

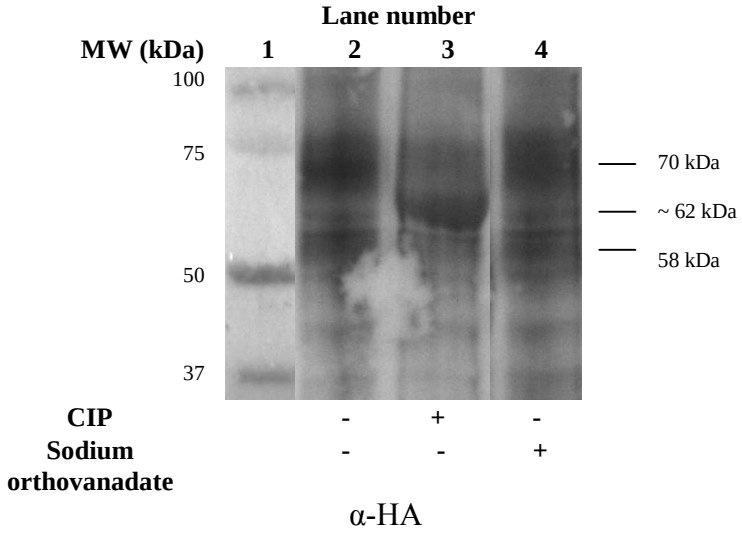


Figure 5-8. Dephosphorylation of CrT-HA with CIAP, and preservation of phosphorylation with sodium orthovanadate. Western blot analysis of 3T3-CrT-HA lysate in untreated form (lane 2), and also following 2 h incubation in the presence of 1 µM sodium orthovanadate (lane 4), alongside lysate digested with CIAP (lane 3). Sodium orthovanadate had no effect on the migration of CrT, whereas CIAP treatment caused a shift in CrT mobility from 70 kDa to around 62 kDa. Membrane was probed with α-HA (1:200,000) (Roche, UK). Lane 1 is the molecular weight standard (Precision Plus Protein ™ Standard, Biorad, UK).

5.4.5. Investigating the presence of tyrosine phosphorylation in the CrT

Having established the presence of phosphorylation in the CrT in the absence of Cr, work was undertaken to identify the type of phosphorylation present, by probing blots of 3T3-CrT-HA cell lysates with different phosphospecific antibodies. Initially, 4A4 (anti phosphoserine) and 4G10 (anti phosphotyrosine) antibodies (Millipore, Billerica, MA, USA) were tested. Several attempts to optimise the antibodies revealed that it was not possible to detect an adequate signal with either. New antibodies were acquired (a kind gift from Dr. Stephan Feller, Weatherall Institute of Molecular Medicine, University of Oxford). These were 4G10 and PY99, both monoclonal anti phosphotyrosine antibodies raised in-house. To provide a suitable positive control, 3T3-CrT-HA cells were treated with pervanadate prior to harvesting. Pervanadate, formed by the combination of vanadate and H_2O_2, is a strong inhibitor of protein-tyrosine phosphatases (PTPases), and therefore alters the equilibrium between phosphorylation and dephosphorylation. It is a greater inhibitor of tyrosine phosphatases than H_2O_2 alone [254 255 256]. Cells were treated with freshly-prepared 50 μM pervanadate for 5, 15 and 30 min, with H_2O and H_2O_2 controls, incubated for 30 min, prepared alongside. Following treatment, the cells were immediately washed 2x in ice-cold PBS and stored at -80^{o}C until protein extraction. The lysis buffer for these cells differed from that used routinely; radioimmunoprecipitation buffer (RIPA) was used (Appendix II), with the addition of 2x Complete protease inhibitors (Roche), and 5x of both PII and PIII phosphatase inhibitors (Sigma). Vanadate (1 mM) and molybdate (1 mM) were also included. Titrations with anti-4G10 once again proved unsuccessful, failing to identify any bands. However, a western blot with anti-PY99 yielded clear results, highlighting the increased general tyrosine phosphorylation present in those samples treated with pervanadate (shown in figure 4-9). A longer treatment duration with pervanadate also led to higher levels of tyrosine phosphorylation. Following the identification of general tyrosine phosphorylation, the membrane was stripped and re-probed with anti-HA antibody (Roche), in order to verify the

presence of CrT. CrT bands of the expected sizes were present. Due to the degree of non-specific protein phosphorylation present in the lysates, it was not possible to determine whether tyrosine-phosphorylated CrT was present on the blot.

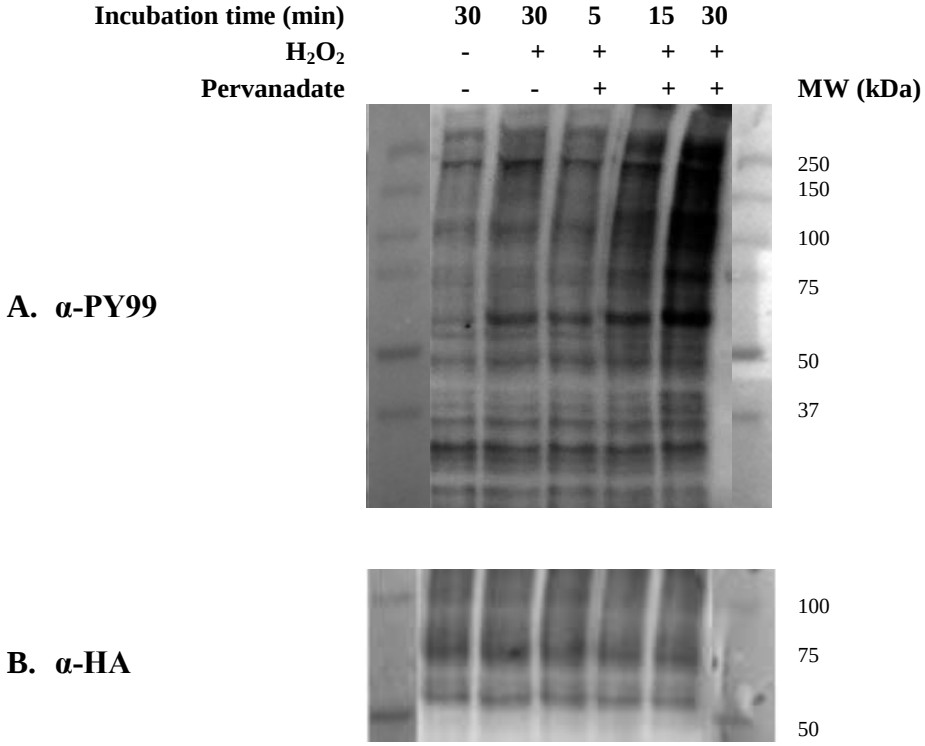


Figure 5-9. Western blots of 3T3-CrT-HA lysates treated with pervanadate for varying incubation times, demonstrating enhanced general tyrosine phosphorylation. Growing cells were treated with 50 μM pervanadate for 5, 15 and 30 min. **A**. Control cells were treated with H_2O and H_2O_2 for 30 min. Lysates were run on 4-20% SDS-PAGE then transferred to nitrocellulose and probed with anti-PY99 (1:5000), and then the secondary antibody, anti-mouse HRP (1:100,000) (Promega). Enhanced general tyrosine phosphorylation was demonstrated in the presence of vanadate, increasing with longer incubation periods. **B.** The membrane was stripped and re-probed with α-HA, to demonstrate the presence of CrT, visible at 70-80 kDa, and 58 kDa. Molecular weights were determined by using a molecular weight standard (Precision Plus Protein™ Standard, Biorad, UK).

Owing to the non-specific nature of the method described above, anti-HA immunoprecipitation was performed on the pervanadate-treated cell lysates, in order to purify the CrT-HA protein. The immunoprecipitation was performed using 50 μL anti-HA agarose (Sigma), with 300 μg of starting protein. The immunoprecipitation was performed according to the manufacturer's protocol, with an overnight incubation, followed by elution of the protein from the agarose beads in 2x SDS sample loading buffer. This aggressive method of elution explains the presence

of heavy bands in the following western blot images at 50 kDa and 25 kDa, the result of the elution of the IgG heavy- and light-chain components of the anti-HA antibody. The immunoprecipitation product was run on SDS-PAGE (4-20 % gradient), transferred to nitrocellulose, and probed with anti-PY99, as outlined previously. No evidence of tyrosine-phosphorylated bands in the expected size range (70-80 kDa, or 58 kDa) was present. Subsequent stripping and re-probing of the membrane with anti-HA (Roche) confirmed the presence of CrT-HA protein on the membrane. These results suggest a lack of tyrosine phosphorylation on the CrT, even following pervanadate stimulation.

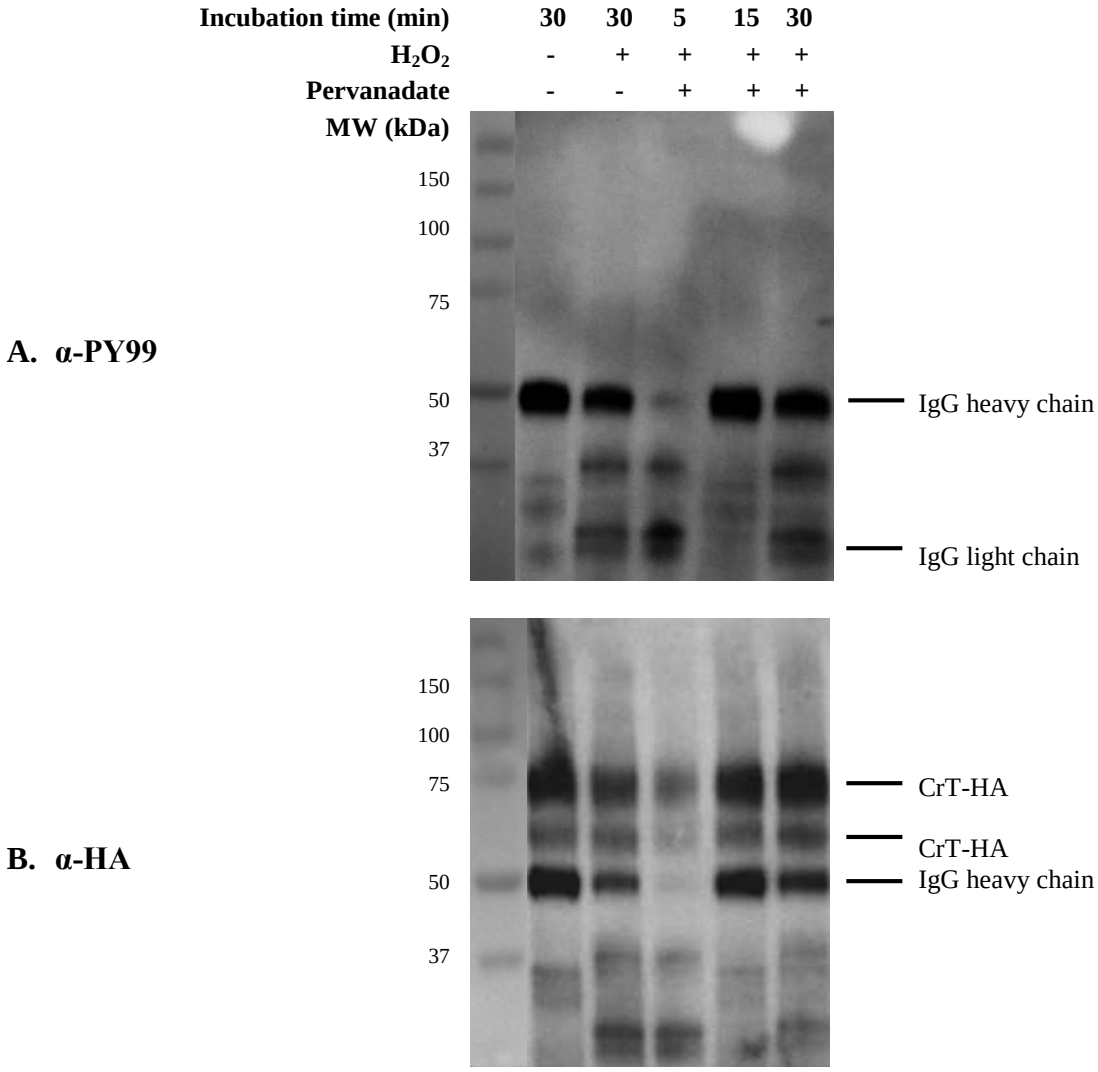


Figure 5-10. Western blots of the product of immunoprecipitation (anti-HA) of 3T3-CrT-HA lysates treated with pervanadate for varying durations. In blot A, probing with anti-PY99 (1:5000), followed by the secondary antibody, anti-mouse HRP (1:100,000) (Promega) revealed no tyrosine-phosphorylated protein at the expected size of CrT-HA (70-80 kDa, and 58 kDa). In blot B, stripping and re-probing the membrane with α-HA demonstrated the presence of CrT, suggesting that the CrT-HA does not exhibit tyrosine phosphorylation, even following pervanadate stimulation. Bands at 50 kDa and 25 kDa, are the result of the elution of the IgG heavy- and light-chain components of the anti-HA antibody. Molecular weights were determined by using a molecular weight standard (Precision Plus Protein™ Standard, Biorad, UK).

5.4.6. Effects of PKA and PKC inhibition on the migration of the CrT

3T3-CrT-HA cells were incubated in the presence of various concentrations of H89 and BIM for 2 h to establish whether either PKA or PKC were constitutively active, and if so, whether this could be detected by an altered CrT migration pattern. Cells were lysed in 2% SDS lysis buffer (see General Materials and Methods), with the addition of PhosSTOP® phosphatase inhibitors

(Roche, UK), and run on 12 % SDS-PAGE. No difference was observed in the migration of CrT extracted from cells pre-treated in H89. None of the concentrations of BIM caused an alteration in the migration of the 70 kDa band of CrT. Migration of the 58 kDa band also appeared unaffected.

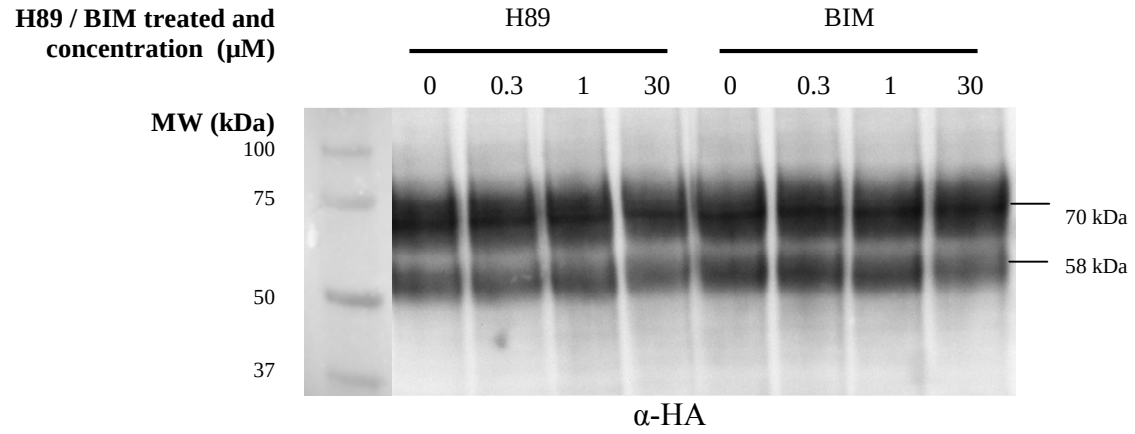


Figure 5-11. Treatment of 3T3-CrT-HA cells with PKA inhibitor (H89) and PKC inhibitor (BIM). Cells were incubated in the presence of 0.3, 1 and 30 µM H89 and BIM prior to western blot analysis of the lysate, alongside the lysate of untreated cells. No difference was observed in either the H89-treated samples, or the BIM-treated samples. Membrane was probed with anti-HA (1:200,000) (Roche, UK). Molecular weights were determined by using a molecular weight standard (Precision Plus Protein ™ Standard, Biorad, UK)

5.4.7. Effects of Cr treatment on the migration of the CrT

5.4.7.1. Incubation in the presence of Cr

As CrT activity is strongly regulated by [Cr], the effects of prolonged incubation on the migration of CrT-HA in the presence of Cr were investigated. It was hoped that this may provide information on the involvement of PTMs following exposure to substrate. 3T3-CrT-HA cells were incubated in the absence of Cr, and also in two concentrations of Cr (25 µM and 500 µM) for 48 h prior to cell harvesting and protein extraction. Cells were lysed in 2% SDS lysis buffer (see General Materials and Methods), with the addition of PhosSTOP® phosphatase inhibitors, prior to 12 % SDS-PAGE. There was no difference between the migration of CrT

compared to control in either 2 h or 36 h treated cells, whether incubated at 25 µM or 500 µM Cr. A repeat of this experiment, including an additional group of cells incubated in 5 mM Cr, confirmed that there was no effect on the migration of the CrT (data not shown).

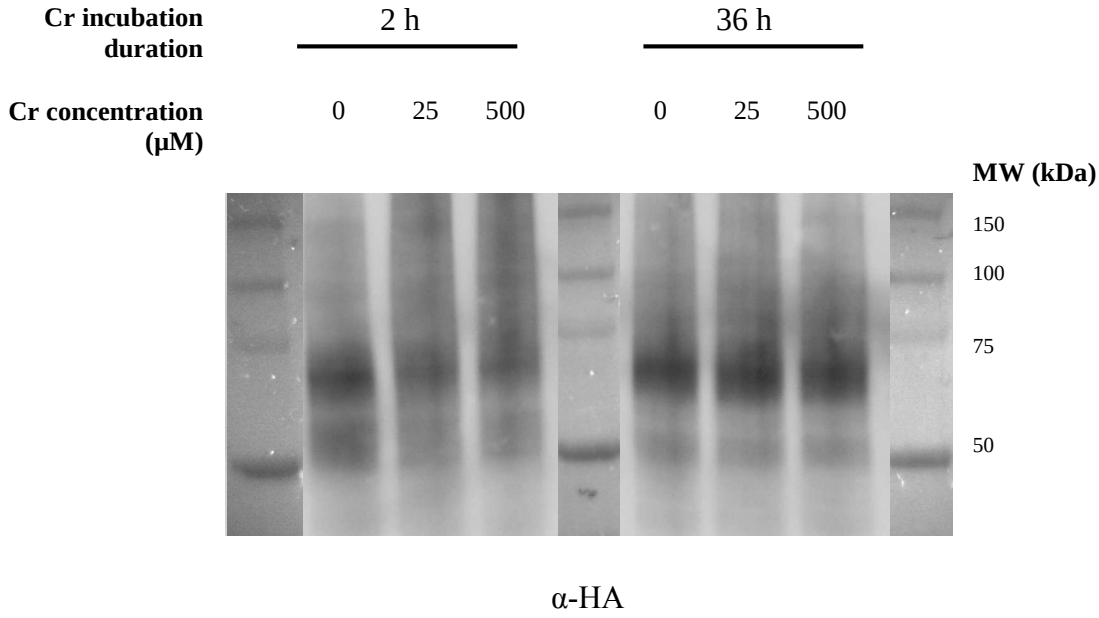


Figure 5-12. Treatment of 3T3-CrT-HA cells with creatine. Cells were incubated in the presence of two concentrations of creatine for 2 h and 36 h prior to western blot analysis of the lysate alongside the lysate of untreated cells. None of the Cr-treated cells demonstrated altered electrophoretic mobility when compared to the control sample from Cr-starved cells. Membrane was probed with anti-HA (1:200,000) (Roche, UK). Molecular weights were determined by using a molecular weight standard (Precision Plus Protein™ Standard, Biorad, UK).

5.4.7.2. Creatine withdrawal following exposure to Cr

To determine whether the reverse conditions of Cr withdrawal following prolonged exposure to Cr have an effect on the migration of the CrT, 3T3-CrT-HA cells were incubated in the presence of 500 µM Cr for 24 h, then the medium was substituted for Cr-free medium (containing charcoal-stripped FBS). The cells were starved of Cr continued for a further 36 h. Cells were then lysed in 2% SDS lysis buffer (see General Materials and Methods), with the addition of PhosSTOP® phosphatase inhibitors. No difference was observed between the migration of CrT

from cells treated with 500 µM Cr or those starved of Cr, when compared to untreated control cells.

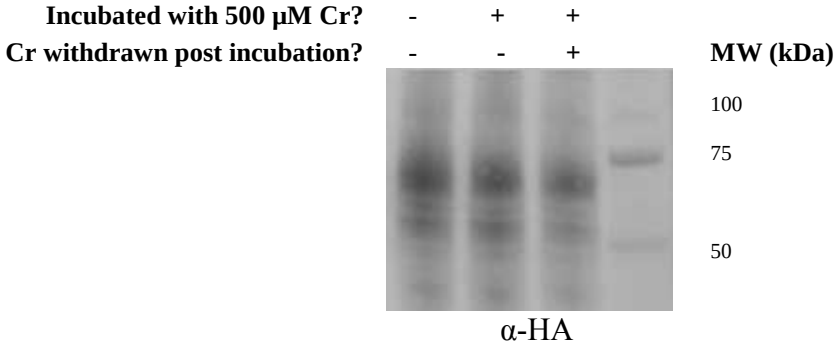


Figure 5-13. Treatment of 3T3-CrT-HA cells with creatine prior to Cr withdrawal. Cells were incubated in the presence of creatine for 24 h prior to Cr withdrawal, alongside cells incubated in Cr for the full incubation period. Western blot analysis of the cell lysate alongside the lysate of untreated cells showed no alteration in the migration pattern between of the Cr-treated, Cr-withdrawn and control lysates. Membrane was probed with anti-HA antibody (1:200,000) (Roche, UK). Molecular weights were determined by using a molecular weight standard (Precision Plus Protein™ Standard, Biorad, UK).

5.4.8. Investigating the presence of phosphorylation in CrT following Cr incubation

It was previously shown that tyrosine phosphorylation of the CrT was undetectable by western blot on the lysate of cells incubated in the absence of Cr. The effect of incubating cells in the presence of Cr on tyrosine phosphorylation of the CrT was investigated. Western blots were performed on the products of immunoprecipitation to enable the use of anti-phosphospecific antibodies. An anti-HA immunoprecipitation was performed on the lysates of cells incubated in both 250 µM and a saturating concentration of 5 mM Cr for 4 h and 24 h. These cells were lysed in RIPA buffer (as described previously), with the addition of 2x Complete protease inhibitors (Roche), and 5x of both PII and PIII phosphatase inhibitors (Sigma, UK). Vanadate (1 mM) and molybdate (1 mM) were also included. The immunoprecipitation was performed according to the manufacturer's instructions (Sigma), and the resulting product was eluted with 2x SDS sample loading buffer. The products were run on 4-20 % SDS-PAGE, and transferred to nitrocellulose, prior to probing with anti-PY99, to determine the presence of tyrosine

phosphorylation. The figure below clearly demonstrates the absence of any bands in the expected size range for CrT-HA, indicating a lack of detectable tyrosine phosphorylation of the CrT following exposure to Cr.

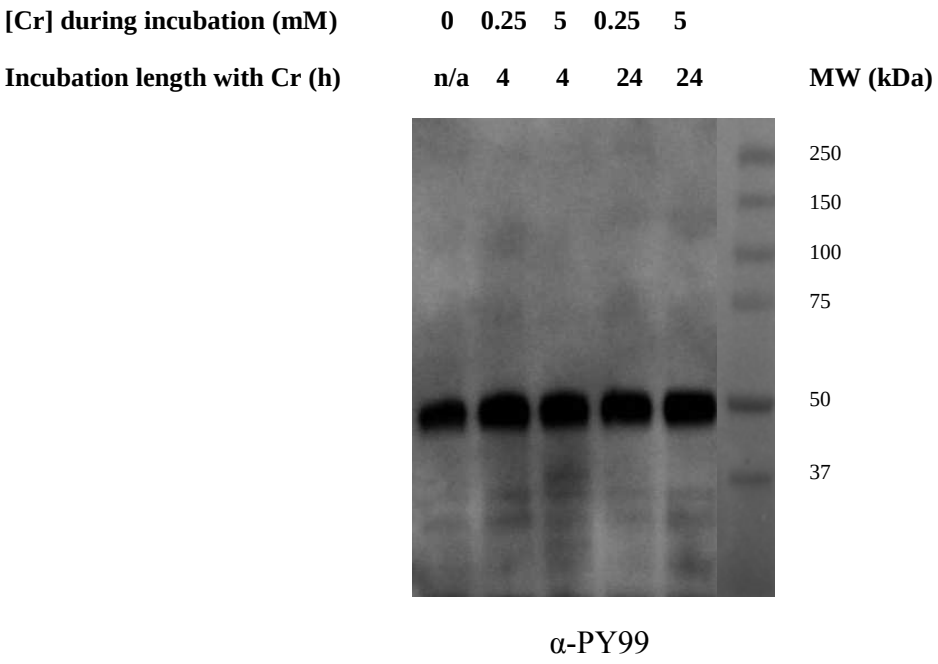


Figure 5-14. Western blot of the product of immunoprecipitation (anti-HA) of 3T3-CrT-HA lysates treated with Cr at 250 μM and 5 mM for 4 h and 24 h. Probing with anti-PY99 (1:5000), followed by the secondary antibody, α-mouse HRP (1:100,000) (Promega) revealed no tyrosine-phosphorylated protein at the expected size of CrT-HA (70-80 kDa, and 58 kDa), suggesting that the CrT-HA does not exhibit tyrosine phosphorylation, even following exposure to Cr. Bands at 50 kDa, and 25 kDa, are the result of the elution of the IgG heavy- and light-chain components of the α HA antibody. Molecular weights were determined by using a molecular weight standard (Precision Plus Protein™ Standard, Biorad, UK).

5.4.9. Investigating the presence of phosphorylation in CrT following Cr incubation using the ProQ Diamond Phosphoprotein stain

Western blots were performed on the products of immunoprecipitation to enable a phosphoprotein stain. An anti HA immunoprecipitation was performed on the lysates of cells incubated in both 250 μM and a saturating concentration of 5 mM Cr for 4 h and 24 h. These cells were lysed in RIPA buffer (as described previously), with the addition of 2x Complete protease inhibitors (Roche), and 5x of both PII and PIII phosphatase inhibitors (Sigma, UK). Vanadate (1 mM) and molybdate (1 mM) were also included. The immunoprecipitation was

performed according to the manufacturer's instructions (Sigma), and the resulting product was eluted with 2x SDS sample loading buffer. The products were run on 4-20 % SDS-PAGE, and the gel was stained with the Pro-Q Diamond phosphoprotein staining reagent (Invitrogen, UK) according to the manufacturer's instructions. A band corresponding to the major diffuse CrT species was identified in all samples at around 80 kDa, although this appeared strongest in the lysate of cells which had not been treated with Cr during growth. The band appeared weakest in those samples treated with Cr for 24 h.

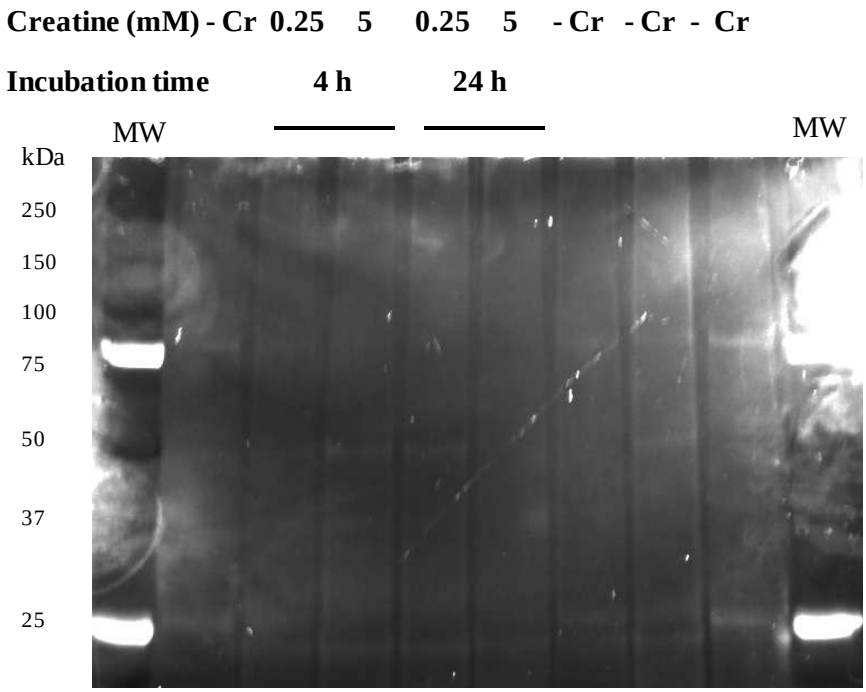


Figure 5-15. Pro-Q Diamond phosphoprotein stain of IP product of cells incubated in 2 concentrations of Cr for different durations. A band at around 80 kDa corresponds to the diffuse major CrT species routinely observed following western blot. Intensity of the band appeared to decrease with increasing [Cr] and incubation length.

5.4.10. Large-scale immunoprecipitation of the CrT, and subsequent LC-MS / MS analysis

In total, five large-scale immunoprecipitations were performed, with each sample consisting of the contents of 5 – 10x 175 cm^2 tissue culture flasks of cells. Such large numbers of cells were required in order to efficiently isolate adequate amounts of protein (by immunoprecipitation) for the purposes of LC-MS / MS detection of CrT-HA (particularly the presence of PTMs), owing

to the relatively low proportion of the over-expressed protein compared to total cell protein levels. LC-MS / MS was chosen as a suitable method for this analysis, as it is an extremely sensitive technique, able to detect small amounts of protein. The cells used for these assays were prepared both in the presence and absence of Cr, in order to determine any effect that the presence of substrate would have on PTMs identified on the CrT. The method proved extremely challenging to optimise, and numerous attempts were made to isolate and purify large amounts of CrT-HA. Only the most successful results are detailed below.

CrT-HA was purified from 3T3-CrT-HA cells by immunoprecipitation according to the protocol outlined at the beginning of this chapter. Additionally, an IP on untransfected 3T3 cells was performed to provide a negative control. Following elution of the IP product, the anti-HA-conjugated agarose beads were boiled in SDS loading buffer in order to elute any remaining bound protein. A small fraction of the IP product was taken (5% of total) and separated on SDS-PAGE prior to probing with anti-HA. The IP eluate yielded 3 immunoreactive species. The expected band was observed at 70-80 kDa, and additional bands were seen at around 150 kDa, and 200 kDa. The blot shows that there was a detectable amount of the 70-80 kDa CrT-HA species still bound to the beads post-elution, indicating some loss of protein during the elution step. The 58 kDa band was also visible. No bands appeared in the negative control lane.

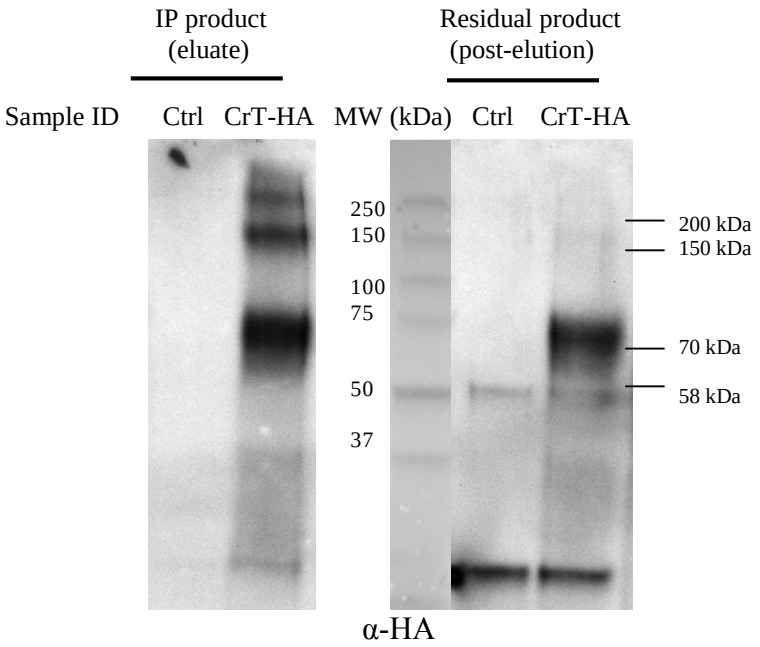


Figure 5-16. Detection of CrT-HA on an immunoblot following immunoprecipitation. 3T3-CrT-HA cell lysate was immunoprecipitated with anti-HA agarose beads (Sigma, UK). Negative control samples were untransfected 3T3 fibroblasts. A small fraction of the IP product was probed with anti-HA (Roche, UK) to confirm the presence of CrT-HA prior to submission of samples for MS analysis. 3 bands, of 70-80 kDa, 150 kDa, and 200 kDa were observed. Post-elution, the agarose beads were boiled in SDS loading buffer to establish elution efficiency. A reduced amount of the predominant 70-80 kDa band was observed, indicating elution had not been completely efficient. Molecular weights were determined by using a molecular weight standard (Precision Plus Protein ™ Standard, Biorad, UK)

Half of the IP eluate was loaded on an SDS-PAGE gel, and following separation proteins were visualised by silver staining (see Materials and Methods at the beginning of this chapter). Two representative silver-stained gels are shown in figure 4-16. Protein bands at the sizes indicated by the red arrows in the figure below were excised and analysed by LC-MS / MS and were subsequently found to contain CrT. Both gels show problems encountered concerning the IP and silver stain, primarily the presence of high levels of non-specific protein in addition to CrT. This led to difficulty in determining which of the bands was CrT. In gel A, the band yielding the greatest level of CrT was number 3, at around 70 kDa. Gel B was overloaded with protein, leading to 'negative' bands which show as white bands on a dark background.

CrT was identified by subsequent LC-MS / MS analysis in bands corresponding to 43 kDa, 48 kDa, 58 kDa, 70 kDa and ~150 kDa. No CrT was identified in the larger band of 200 kDa. Figures 4-17 to 4-21 show summaries of LC-MS / MS results for each of the band sizes in which CrT-HA was positively identified, in size order from 150 kDa down to 43 kDa. Despite positive identification of these 5 species, no PTMs were identified in any of the samples. It is likely that this was due to inadequate sequence coverage of the CrT-HA detected by LC-MS / MS.

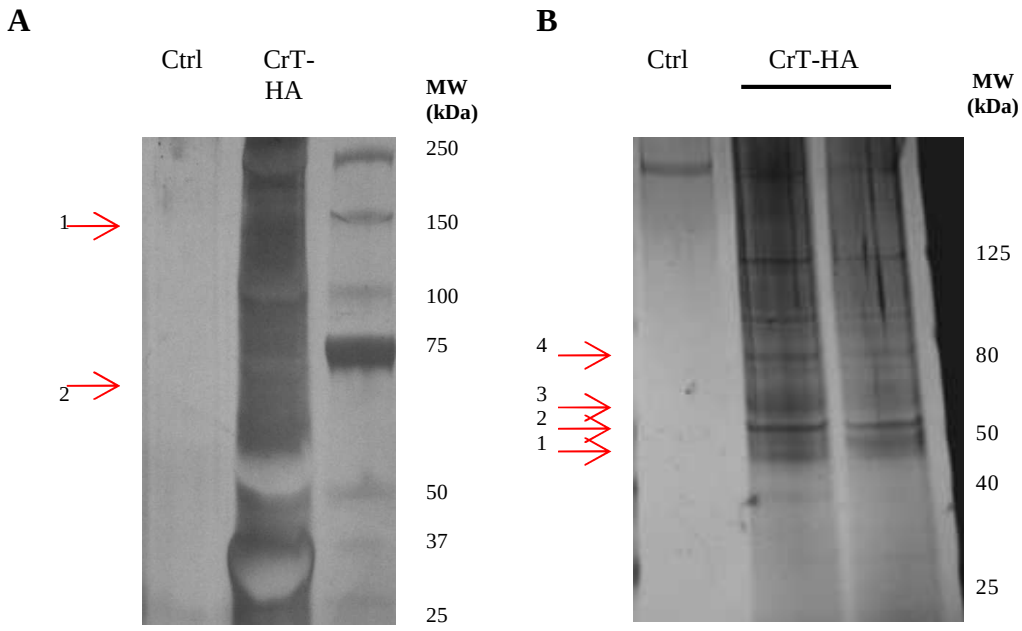


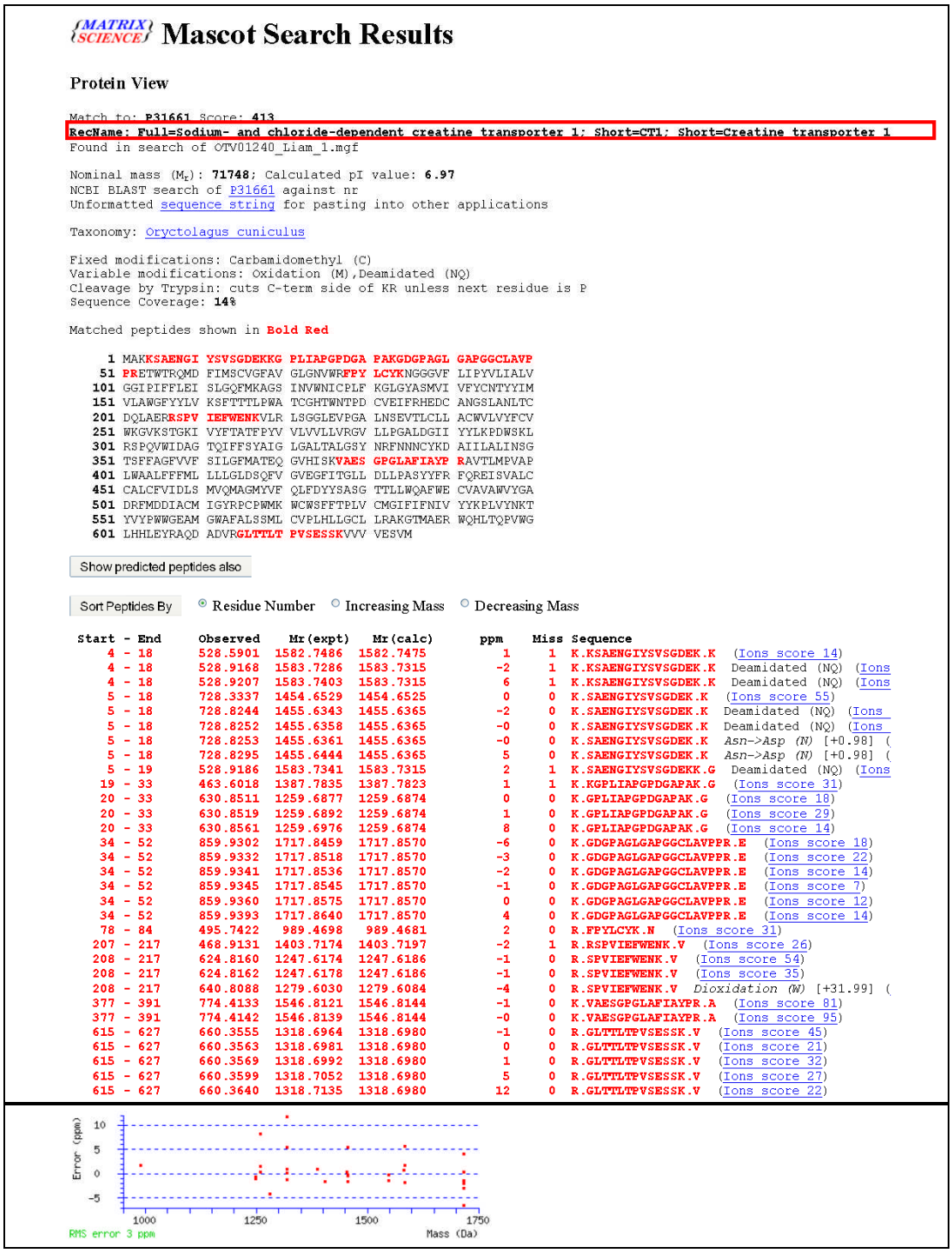
Figure 5-17. Detection of CrT-HA protein band on SDS-PAGE, using silver staining. 3T3-CrT-HA cell lysate was immunoprecipitated with α-HA agarose beads (Sigma, UK). A and B are silver-stained gels run at separate times, with the product of 2 different IPs. Over-staining is evident in gel A. Negative control samples on both gels were untransfected 3T3 fibroblasts. Following silver staining, the arrowed bands were excised from the gels and passed to the Proteomics facility for extraction, followed by LC-MS/MS identification and analysis of CrT. All arrowed bands contained CrT, confirming the presence of CrT-HA at 43, 48, 58, 70-80 and 150 kDa. Molecular weights were determined by using a molecular weight standard (Gel A- Full Range Molecular Weight Rainbow Marker, GE Healthcare, UK, Gel B- Precision Plus Protein ™ Standard, Biorad, UK).



Figure 5-18. LC-MS/MS results showing analysis results of band 1 from figure 4-16 A. This demonstrates positive identification of CrT-HA at 150 kDa, with a sequence coverage of 15%.



Figure 5-19. LC-MS/MS results showing analysis results of band 2 from figure 4-16 A. This demonstrates positive identification of CrT-HA 70-80 kDa species, with a sequence coverage of 12%.



MATRIX SCIENCE **Mascot Search Results**

Protein View

Match to: **P31661** Score: **413**
RecName: Full=Sodium- and chloride-dependent creatine transporter 1; Short=CT1; Short=Creatine transporter 1
Found in search of OTV01240_Liam_1.mgf

Nominal mass (M_r): **71748**; Calculated pI value: **6.97**
NCBI BLAST search of P31661 against nr
Unformatted sequence string for pasting into other applications

Taxonomy: Oryctolagus cuniculus

Fixed modifications: Carbamidomethyl (C)
Variable modifications: Oxidation (M),Deamidated (NQ)
Cleavage by Trypsin: cuts C-term side of KR unless next residue is P
Sequence Coverage: **14%**

Matched peptides shown in **Bold Red**

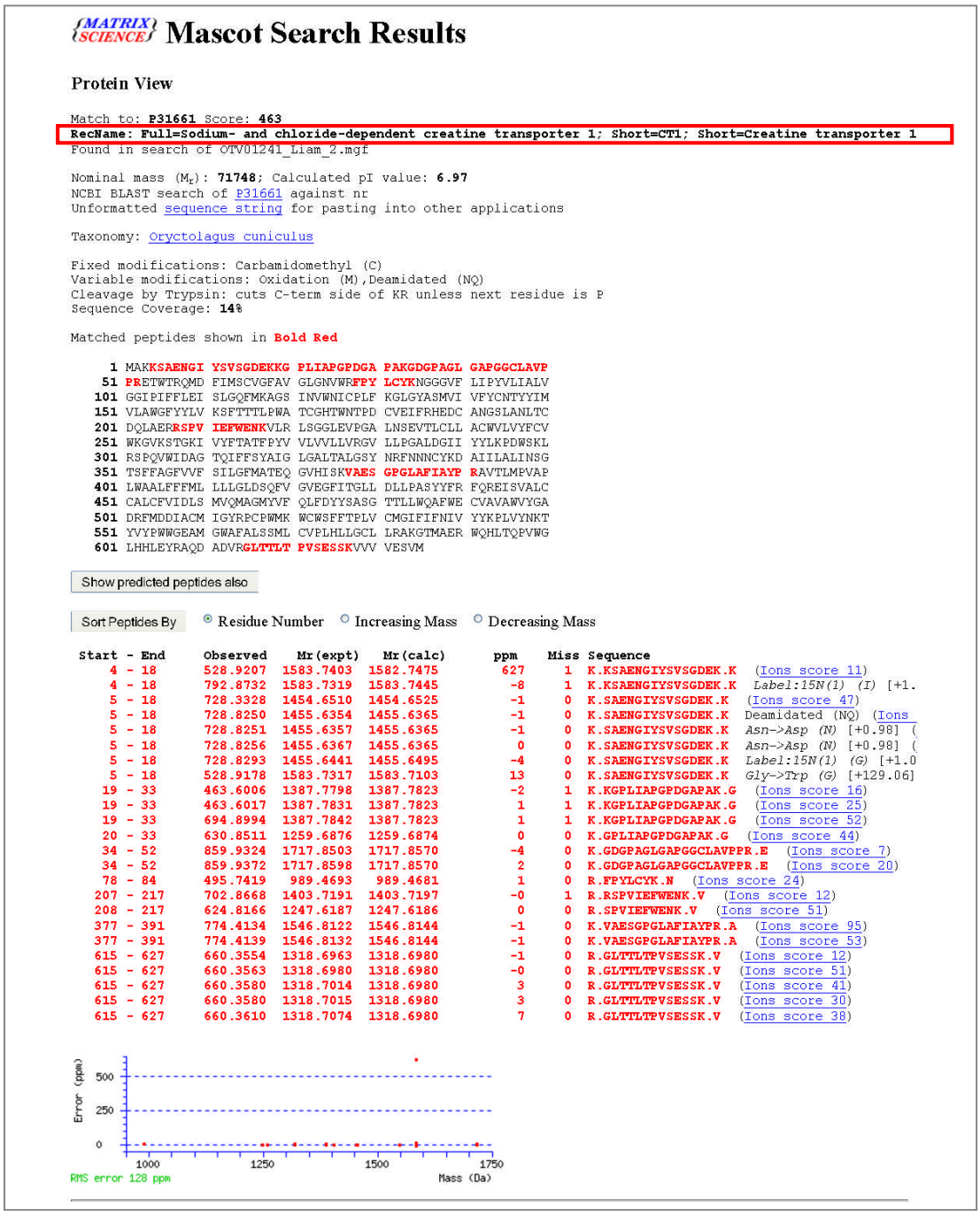
```
    1 MAKKSAENGI YSVSGDEKKG PLIAPGPDGA PAKGDGPAGL GAPGGCLAVP
   51 PRETWTRQMD FIMSCVGFAV GLGNVWRFPY LCYKNGGGVF LIPYVLIALV
  101 GGIPIFFLEI SLGQFMKAGS INVWNICPLF KGLGYASMVI VFYCNTYYIM
  151 VLAWGFYYLV KSFTTTLPWA TCGHTWNTPD CVEIFRHEDC ANGSLANLTC
  201 DQLAERRSPV IEFWENKVLR LSGGLEVPGA LNSEVTLCLL ACWVLVYFCV
  251 WKGVKSTGKI VYFTATFPYV VLVVLLVRGV LLPGALDGII YYLKPDWSKL
  301 RSPQVWIDAG TQIFFSYAIG LGALTALGSY NRFNNNCYKD AIILALINSG
  351 TSFFAGFVVF SILGFMATEQ GVHISKVAES GPGLAFIAYP RAVTLMPVAP
  401 LWAALFFFML LLLGLDSQFV GVEGFITGLL DLLPASYYFR FQREISVALC
  451 CALCFVIDLS MVQMAGMYVF QLFDYYSASG TTLLWQAFWE CVAVAWVYGA
  501 DRFMDDIACM IGYRPCPWMK WCWSFFTPLV CMGIFIFNIV YYKPLVYNKT
  551 YVYPWWGEAM GWAFALSSML CVPLHLLGCL LRAKGTMAER WQHLTQPVWG
  601 LHHLEYRAQD ADVRGLTTLT PVSESSKVVV VESVM
```

Show predicted peptides also

Sort Peptides By ◉ Residue Number ○ Increasing Mass ○ Decreasing Mass

Start - End	Observed	Mr(expt)	Mr(calc)	ppm	Miss	Sequence
4 - 18	528.5901	1582.7486	1582.7475	1	1	K.KSAENGIYSVSGDEK.K (Ions score 14)
4 - 18	528.9168	1583.7286	1583.7315	-2	1	K.KSAENGIYSVSGDEK.K Deamidated (NQ) (Ions
4 - 18	528.9207	1583.7403	1583.7315	6	1	K.KSAENGIYSVSGDEK.K Deamidated (NQ) (Ions
5 - 18	728.3337	1454.6529	1454.6525	0	0	K.SAENGIYSVSGDEK.K (Ions score 55)
5 - 18	728.8244	1455.6343	1455.6365	-2	0	K.SAENGIYSVSGDEK.K Deamidated (NQ) (Ions
5 - 18	728.8252	1455.6358	1455.6365	-0	0	K.SAENGIYSVSGDEK.K Deamidated (NQ) (Ions
5 - 18	728.8253	1455.6361	1455.6365	-0	0	K.SAENGIYSVSGDEK.K *Asn->Asp (N)* [+0.98] (
5 - 18	728.8295	1455.6444	1455.6365	5	0	K.SAENGIYSVSGDEK.K *Asn->Asp (N)* [+0.98] (
5 - 19	528.9186	1583.7341	1583.7315	2	1	K.SAENGIYSVSGDEKK.G Deamidated (NQ) (Ions
19 - 33	463.6018	1387.7835	1387.7823	1	1	K.KGPLIAPGPDGAPAK.G (Ions score 31)
20 - 33	630.8511	1259.6877	1259.6874	0	0	K.GPLIAPGPDGAPAK.G (Ions score 18)
20 - 33	630.8519	1259.6892	1259.6874	1	0	K.GPLIAPGPDGAPAK.G (Ions score 29)
20 - 33	630.8561	1259.6976	1259.6874	8	0	K.GPLIAPGPDGAPAK.G (Ions score 14)
34 - 52	859.9302	1717.8459	1717.8570	-6	0	K.GDGPAGLGAPGGCLAVPPR.E (Ions score 18)
34 - 52	859.9332	1717.8518	1717.8570	-3	0	K.GDGPAGLGAPGGCLAVPPR.E (Ions score 22)
34 - 52	859.9341	1717.8536	1717.8570	-2	0	K.GDGPAGLGAPGGCLAVPPR.E (Ions score 14)
34 - 52	859.9345	1717.8545	1717.8570	-1	0	K.GDGPAGLGAPGGCLAVPPR.E (Ions score 7)
34 - 52	859.9360	1717.8575	1717.8570	0	0	K.GDGPAGLGAPGGCLAVPPR.E (Ions score 12)
34 - 52	859.9393	1717.8640	1717.8570	4	0	K.GDGPAGLGAPGGCLAVPPR.E (Ions score 14)
78 - 84	495.7422	989.4698	989.4681	2	0	R.FPYLCYK.N (Ions score 31)
207 - 217	468.9131	1403.7174	1403.7197	-2	1	R.RSPVIEFWENK.V (Ions score 26)
208 - 217	624.8160	1247.6174	1247.6186	-1	0	R.SPVIEFWENK.V (Ions score 54)
208 - 217	624.8162	1247.6178	1247.6186	-1	0	R.SPVIEFWENK.V (Ions score 35)
208 - 217	640.8088	1279.6030	1279.6084	-4	0	R.SPVIEFWENK.V *Dioxidation (W)* [+31.99] (
377 - 391	774.4133	1546.8121	1546.8144	-1	0	K.VAESGPGLAFIAYPR.A (Ions score 81)
377 - 391	774.4142	1546.8139	1546.8144	-0	0	K.VAESGPGLAFIAYPR.A (Ions score 95)
615 - 627	660.3555	1318.6964	1318.6980	-1	0	R.GLTTLTPVSESSK.V (Ions score 45)
615 - 627	660.3563	1318.6981	1318.6980	0	0	R.GLTTLTPVSESSK.V (Ions score 21)
615 - 627	660.3569	1318.6992	1318.6980	1	0	R.GLTTLTPVSESSK.V (Ions score 32)
615 - 627	660.3599	1318.7052	1318.6980	5	0	R.GLTTLTPVSESSK.V (Ions score 27)
615 - 627	660.3640	1318.7135	1318.6980	12	0	R.GLTTLTPVSESSK.V (Ions score 22)

Figure 5-20. LC-MS/MS results showing analysis results of band 3 from figure 4-16 B. This demonstrates positive identification of CrT-HA species at 58 kDa, with a sequence coverage of 14%.



MATRIX SCIENCE **Mascot Search Results**

Protein View

Match to: **P31661** Score: **463**
RecName: Full=Sodium- and chloride-dependent creatine transporter 1; Short=CT1; Short=Creatine transporter 1
Found in search of OTV01241_Liam_2.mgf

Nominal mass (M_r): **71748**; Calculated pI value: **6.97**
NCBI BLAST search of P31661 against nr
Unformatted sequence string for pasting into other applications

Taxonomy: Oryctolagus cuniculus

Fixed modifications: Carbamidomethyl (C)
Variable modifications: Oxidation (M),Deamidated (NQ)
Cleavage by Trypsin: cuts C-term side of KR unless next residue is P
Sequence Coverage: **14%**

Matched peptides shown in **Bold Red**

```
    1 MAKKSAENGI YSVSGDEKKG PLIAPGPDGA PAKGDGPAGL GAPGGCLAVP
   51 PRETWTRQMD FIMSCVGFAV GLGNVWRFPY LCYKNGGGVF LIPYVLIALV
  101 GGIPIFFLEI SLGQFMKAGS INVWNICPLF KGLGYASMVI VFYCNTYYIM
  151 VLAWGFYYLV KSFTTTLPWA TCGHTWNTPD CVEIFRHEDC ANGSLANLTC
  201 DQLAERRSPV IEFWENKVLR LSGGLEVPGA LNSEVTLCLL ACWVLVYFCV
  251 WKGVKSTGKI VYFTATFPYV VLVVLLVRGV LLPGALDGII YYLKPDWSKL
  301 RSPQVWIDAG TQIFFSYAIG LGALTALGSY NRFNNNCYKD AIILALINSG
  351 TSFFAGFVVF SILGFMATEQ GVHISKVAES GPGLAFIAYP RAVTLMPVAP
  401 LWAALFFFML LLLGLDSQFV GVEGFITGLL DLLPASYYFR FQREISVALC
  451 CALCFVIDLS MVQMAGMYVF QLFDYYSASG TTLLWQAFWE CVAVAWVYGA
  501 DRFMDDIACM IGYRPCPWMK WCWSFFTPLV CMGIFIFNIV YYKPLVYNKT
  551 YVYPWWGEAM GWAFALSSML CVPLHLLGCL LRAKGTMAER WQHLTQPVWG
  601 LHHLEYRAQD ADVRGLTTLT PVSESSKVVV VESVM
```

Show predicted peptides also

Sort Peptides By ◉ Residue Number ○ Increasing Mass ○ Decreasing Mass

Start - End	Observed	Mr(expt)	Mr(calc)	ppm	Miss	Sequence
4 - 18	528.9207	1583.7403	1582.7475	627	1	K.KSAENGIYSVSGDEK.K (Ions score 11)
4 - 18	792.8732	1583.7319	1583.7445	-8	1	K.KSAENGIYSVSGDEK.K *Label:15N(1) (I)* [+1.
5 - 18	728.3328	1454.6510	1454.6525	-1	0	K.SAENGIYSVSGDEK.K (Ions score 47)
5 - 18	728.8250	1455.6354	1455.6365	-1	0	K.SAENGIYSVSGDEK.K Deamidated (NQ) (Ions
5 - 18	728.8251	1455.6357	1455.6365	-1	0	K.SAENGIYSVSGDEK.K *Asn->Asp (N)* [+0.98] (
5 - 18	728.8256	1455.6367	1455.6365	0	0	K.SAENGIYSVSGDEK.K *Asn->Asp (N)* [+0.98] (
5 - 18	728.8293	1455.6441	1455.6495	-4	0	K.SAENGIYSVSGDEK.K *Label:15N(1) (G)* [+1.0
5 - 18	528.9178	1583.7317	1583.7103	13	0	K.SAENGIYSVSGDEK.K *Gly->Trp (G)* [+129.06]
19 - 33	463.6006	1387.7798	1387.7823	-2	1	K.KGPLIAPGPDGAPAK.G (Ions score 16)
19 - 33	463.6017	1387.7831	1387.7823	1	1	K.KGPLIAPGPDGAPAK.G (Ions score 25)
19 - 33	694.8994	1387.7842	1387.7823	1	1	K.KGPLIAPGPDGAPAK.G (Ions score 52)
20 - 33	630.8511	1259.6876	1259.6874	0	0	K.GPLIAPGPDGAPAK.G (Ions score 44)
34 - 52	859.9324	1717.8503	1717.8570	-4	0	K.GDGPAGLGAPGGCLAVPPR.E (Ions score 7)
34 - 52	859.9372	1717.8598	1717.8570	2	0	K.GDGPAGLGAPGGCLAVPPR.E (Ions score 20)
78 - 84	495.7419	989.4693	989.4681	1	0	R.FPYLCYK.N (Ions score 24)
207 - 217	702.8668	1403.7191	1403.7197	-0	1	R.RSPVIEFWENK.V (Ions score 12)
208 - 217	624.8166	1247.6187	1247.6186	0	0	R.SPVIEFWENK.V (Ions score 51)
377 - 391	774.4134	1546.8122	1546.8144	-1	0	K.VAESGPGLAFIAYPR.A (Ions score 95)
377 - 391	774.4139	1546.8132	1546.8144	-1	0	K.VAESGPGLAFIAYPR.A (Ions score 53)
615 - 627	660.3554	1318.6963	1318.6980	-1	0	R.GLTTLTPVSESSK.V (Ions score 12)
615 - 627	660.3563	1318.6980	1318.6980	-0	0	R.GLTTLTPVSESSK.V (Ions score 51)
615 - 627	660.3580	1318.7014	1318.6980	3	0	R.GLTTLTPVSESSK.V (Ions score 41)
615 - 627	660.3580	1318.7015	1318.6980	3	0	R.GLTTLTPVSESSK.V (Ions score 30)
615 - 627	660.3610	1318.7074	1318.6980	7	0	R.GLTTLTPVSESSK.V (Ions score 38)

Figure 5.21. LC-MS/MS results showing analysis results of band 2 from figure 4-16 B. This demonstrates positive identification of the 48 kDa species of CrT-HA, with a sequence coverage of 14%.



Mascot Search Results

Protein View

Match to: **P31661** Score: **496**
RecName: Full=Sodium- and chloride-dependent creatine transporter 1; Short=CT1; Short=Creatine transporter 1
Found in search of OTV01242_Liam_3.mgf

Nominal mass (M_r): **71748**; Calculated pI value: **6.97**
NCBI BLAST search of P31661 against nr
Unformatted sequence string for pasting into other applications

Taxonomy: Oryctolagus cuniculus

Fixed modifications: Carbamidomethyl (C)
Variable modifications: Oxidation (M),Deamidated (NQ)
Cleavage by Trypsin: cuts C-term side of KR unless next residue is P
Sequence Coverage: **16%**

Matched peptides shown in **Bold Red**

```
    1 MAKKSAENGI YSVSGDEKKG PLIAPGPDGA PAKGDGPAGL GAPGGCLAVP
   51 PRETWTRQMD FIMSCVGFAV GLGNVWRFPY LCYKNGGGVF LIPYVLIALV
  101 GGIPIFFLEI SLGQFMKAGS INVWNICPLF KGLGYASMVI VFYCNTYYIM
  151 VLAWGFYYLV KSFTTTLPWA TCGHTWNTPD CVEIFRHEDC ANGSLANLTC
  201 DQLAERRSPV IEFWENKVLR LSGGLEVPGA LNSEVTLCLL ACWVLVYFCV
  251 WKGVKSTGKI VYFTATFPYV VLVVLLVRGV LLPGALDGII YYLKPDWSKL
  301 RSPQVWIDAG TQIFFSYAIG LGALTALGSY NRFNNNCYKD AIILALINSG
  351 TSFFAGFVVF SILGFMATEQ GVHISKVAES GPGLAFIAYP RAVTLMPVAP
  401 LWAALFFFML LLLGLDSQFV GVEGFITGLL DLLPASYYFR FQREISVALC
  451 CALCFVIDLS MVQMAGMYVF QLFDYYSASG TTLLWQAFWE CVAVAWVYGA
  501 DRFMDDIACM IGYRPCPWMK WCWSFFTPLV CMGIFIFNIV YYKPLVYNKT
  551 YVYPWWGEAM GWAFALSSML CVPLHLLGCL LRAKGTMAER WQHLTQPVWG
  601 LHHLEYRAQD ADVRGLTTLT PVSESSKVVV VESVM
```

Show predicted peptides also

Sort Peptides By ◉ Residue Number ○ Increasing Mass ○ Decreasing Mass

Start - End	Observed	Mr(expt)	Mr(calc)	ppm	Miss	Sequence
4 - 18	528.5899	1582.7479	1582.7475	0	1	K.KSAENGIYSVSGDEK.K (Ions score 24)
4 - 18	792.8727	1583.7309	1583.7315	-0	1	K.KSAENGIYSVSGDEK.K *Asn->Asp (N)* [+0.98]
4 - 18	792.8769	1583.7392	1583.7315	5	1	K.KSAENGIYSVSGDEK.K *Asn->Asp (N)* [+0.98]
5 - 18	728.3351	1454.6556	1454.6525	2	0	K.SAENGIYSVSGDEK.K (Ions score 53)
5 - 18	728.8241	1455.6336	1455.6365	-2	0	K.SAENGIYSVSGDEK.K Deamidated (NQ) (Ions
5 - 18	728.8250	1455.6354	1455.6365	-1	0	K.SAENGIYSVSGDEK.K *Asn->Asp (N)* [+0.98] (
5 - 18	728.8255	1455.6364	1455.6365	-0	0	K.SAENGIYSVSGDEK.K *Asn->Asp (N)* [+0.98] (
5 - 18	728.8292	1455.6439	1455.6365	5	0	K.SAENGIYSVSGDEK.K *Asn->Asp (N)* [+0.98] (
5 - 18	528.9190	1583.7352	1583.7103	16	0	K.SAENGIYSVSGDEK.K *Gly->Trp (G)* [+129.06]
5 - 19	528.9191	1583.7356	1583.7315	3	1	K.SAENGIYSVSGDEKK.G Deamidated (NQ) (Ions
19 - 33	463.6011	1387.7816	1387.7823	-1	1	K.KGPLIAPGPDGAPAK.G (Ions score 33)
19 - 33	463.6016	1387.7829	1387.7823	0	1	K.KGPLIAPGPDGAPAK.G (Ions score 21)
19 - 33	694.8993	1387.7840	1387.7823	1	1	K.KGPLIAPGPDGAPAK.G (Ions score 29)
20 - 33	630.8508	1259.6870	1259.6874	-0	0	K.GPLIAPGPDGAPAK.G (Ions score 26)
20 - 33	630.8513	1259.6880	1259.6874	0	0	K.GPLIAPGPDGAPAK.G (Ions score 31)
24 - 33	440.7297	879.4449	879.4450	-0	0	I.APGPDGAPAK.G (Ions score 35)
34 - 52	859.9344	1717.8543	1717.8570	-2	0	K.GDGPAGLGAPGGCLAVPPR.E (Ions score 34)
34 - 52	859.9346	1717.8546	1717.8570	-1	0	K.GDGPAGLGAPGGCLAVPPR.E (Ions score 30)
34 - 52	859.9368	1717.8590	1717.8570	1	0	K.GDGPAGLGAPGGCLAVPPR.E (Ions score 28)
34 - 52	859.9377	1717.8609	1717.8570	2	0	K.GDGPAGLGAPGGCLAVPPR.E (Ions score 50)
34 - 52	859.9395	1717.8645	1717.8570	4	0	K.GDGPAGLGAPGGCLAVPPR.E (Ions score 21)
78 - 84	495.7403	989.4660	989.4681	-2	0	R.FPYLCYK.N (Ions score 23)
78 - 84	495.7436	989.4727	989.4681	5	0	R.FPYLCYK.N (Ions score 8)
207 - 217	468.9138	1403.7196	1403.7197	-0	1	R.RSPVIEFWENK.V Deamidated (NQ); *Amidated*
208 - 217	624.8148	1247.6150	1247.6186	-3	0	R.SPVIEFWENK.V Deamidated (NQ); *Amidated*
208 - 217	624.8167	1247.6189	1247.6186	0	0	R.SPVIEFWENK.V Deamidated (NQ); *Amidated*
333 - 339	480.2043	958.3940	958.3967	-3	0	R.FNNNCYK.D (Ions score 11)
377 - 391	774.4141	1546.8136	1546.8144	-1	0	K.VAESGPGLAFIAYPR.A (Ions score 95)
615 - 627	660.3558	1318.6971	1318.6980	-1	0	R.GLTTLTPVSESSK.V (Ions score 50)
615 - 627	660.3559	1318.6972	1318.6980	-1	0	R.GLTTLTPVSESSK.V (Ions score 18)
615 - 627	660.3607	1318.7069	1318.6980	7	0	R.GLTTLTPVSESSK.V (Ions score 21)
615 - 627	660.3642	1318.7138	1318.6980	12	0	R.GLTTLTPVSESSK.V (Ions score 20)

Figure 5.22. LC-MS/MS results showing analysis results of band 1 from figure 4-16 B. This demonstrates positive identification of the 43 kDa species of CrT-HA, with a sequence coverage of 16%.

The following table summarises the findings of all LC-MS/MS analyses performed, and indicates the predicted PTM sites that were detected, showing that in no instances was there evidence of amino acid changes. It is possible that changes ocured in those predicted sites that were not detected in the analyses.

Predicted PTM site	Sequence covered by LC-MS/MS?	Amino acid change?
S 5	Yes	No
Y 11	Yes	No
S 12	Yes	No
S 14	Yes	No
T 42	Yes	No
T 54	Yes	No
Y 135	No	n/a
N 192	No	n/a
N 197	No	n/a
T 618	Yes	No
T 620	Yes	No
S 623	Yes	No
S 625	Yes	No

Table 5-1. Summary of predicted PTM sites detected by LC-MS/MS (as depicted in figure 5-1). The table shows those predicted sites covered by LC/MS-MS, and whether the amino acid detected differs from that predicted.

5.5. Discussion

5.5.1. Identification of CrT on SDS-PAGE using anti-CrT and anti-HA antibodies

Little is known about the regulation of the CrT by post-translational means, particularly phosphorylation, as previous studies have been hampered by potentially unreliable anti-CrT antibodies. Additionally, conflicting reports exist in the literature with regard to the different sized forms of the CrT. The work contained in this chapter aimed to resolve some of these issues, and the most suitable cell system available for these investigations was the CrT-overexpressing 3T3-CrT-HA line. Although murine CrT extracted from HL-1 cells would theoretically have been a preferable basis for analysis, owing to the cells' cardiomyocyte-like milieu, the inability to detect native HL-1 CrT by western blot prevented this. Previous studies have also reported that, owing to the relatively low expression of native CrT in the cell membrane, isolation of an adequate amount of the protein to facilitate structural studies is highly challenging. A study on the related GABA transporter, isolated from rat brain membranes, required 500 mg of membrane protein, plus numerous purification steps in order to yield just 43 μg of the transporter protein [257]. It is known that 3T3-CrT-HA cells express far higher levels of protein than the untransfected cells. Concerns due to the influence of the C-terminal HA tag present in the 3T3-CrT-HA line were minimal, owing to (a) the small size of the epitope tag (10 amino acids), (b) the fact that the cell line has been validated and is known to transport Cr very effectively, and (c) the existence of a similar system used successfully in the literature [39]. For these reasons, it is extremely unlikely that it causes a quantifiable shift in the mobility of the protein on SDS-PAGE. It also has obvious benefits, overcoming the potential of non-specificity. This is crucial, as one of the anti-CrT antibodies used by several groups to identify the CrT in recent years was demonstrated to be unreliable, cross-reacting with PDH in addition to CrT [40]. The anti-CrT antibody used throughout this thesis (a kind gift from Dr. Theo Wallimann, ETH Zurich) differs from the previous anti-CrT antibody, and is believed to be specific to CrT,

although typically led to greater levels of background than the anti-HA antibody. For these reasons, anti-HA was used predominantly in these experiments, and in some cases to verify results obtained with the anti-CrT antibody.

Both antibodies bound two major bands in 3T3-CrT-HA cell lysate. A major, diffuse band appeared at around 70-80 kDa, with a less intense band also appearing at around 58 kDa. This was in concordance with previous findings in our laboratory. Additionally, extremely faint bands were identified at 150 kDa and 200 kDa. Whilst a CrT species of around 200 kDa has been reported previously [241] [39], there is no evidence of previous identification of a species with an electrophoretic mobility of 150 kDa on SDS-PAGE.

5.5.2. *N*-linked glycosylation and its effects on electrophoretic mobility and activity of the CrT

N-linked glycosylation has previously been suggested to be a major route of CrT regulation [39].Treatment of cell lysates with the endoglycosidase, EndoH, and the amidase PNGase F, clearly demonstrated that the CrT is a glycoprotein. EndoH treatment led to a marked decrease in the apparent size of the 58 kDa band, causing it to migrate at 48 kDa, indicating the loss of one glycan. The larger diffuse band appeared less affected, although its mobility was increased to a small degree, possibly indicating deglycosylation in this band also. Its intensity was also reduced. Treatment with PNGase gave striking results indicating further deglycosylation-potentially the removal of both glycans on the extracellular loop between TM3 and TM4. These results were consistent with those shown by Straumann *et al* in glycosylation-deficient mutants [39]. The exceptions are the two bands observed at 150 kDa and 200 kDa. These were still visible, unchanged in size but very faint. It is possible that these isoforms were also deglycosylated, but

owing to their size, poor resolution on the SDS-PAGE gel masked the altered electrophoretic mobility. This could be revisited by running the gel out much further, or using a lower concentration of acrylamide. *In vitro* treatment with tunicamycin yielded results very similar to those seen following PNGase treatment. The results demonstrate a significant effect on the migration of CrT on SDS-PAGE, suggesting the removal of both glycans on the extracellular loop between TM3 and TM4.

The appearance of the untreated 70-80 kDa band is concordant with the findings of West *et al* [241]. However, they reported that PNGase F treatment led to a species with an apparent mobility of 50 kDa. This was not what was found in the results reported in this thesis, with deglycosylation leading to species with the same migratory characteristics as those reported by Straumann and colleagues. This suggests that the CrT is glycosylated in two positions, and that one of these positions is insusceptible to treatment with EndoH, indicating that it is an unprocessed *N*-glycan. The shift in mobility of the deglycosylated CrT is far greater than would be expected as an effect of the decreased mass of the protein alone. This phenomenon has been observed in other members of the SLC6 family, with the deglycosylation of the SERT (serotonin transporter) and NET (norepinephrine transporter) showing apparent reductions in mass of ~20 and ~30 kDa respectively following deglycosylation [244 258]. It is possible that this increased mobility could be due to an increased binding of SDS to the hydrophobic CrT [241].

Tunicamycin treatment of 3T3-CrT-HA cells reduced Cr uptake at the higher concentrations used (2.5 µg / mL and 5 µg / mL). A trypan blue exclusion test was performed to exclude the possibility that the reduction in Cr uptake was due to cell death and a lack of membrane integrity. The results showed no significant difference between control cells and those incubated in the higher concentrations of tunicamycin. This suggested that the decreased Cr uptake was

indeed due to decreased *N*-linked glycosylation of the CrT, in contrast to the findings of a previous study [39]. This point is important, as tunicamycin has been shown to have apoptotic side-effects [39]. It has previously been shown that *N*-linked glycosylation plays a role in CrT trafficking to the plasma membrane, and also that the loss of either of the active glycans from the second extracellular loop of CrT impairs its Cr transport efficiency for Cr by a factor of two [39]. Studies on other members of the SLC6 family have shown similar results, with glycosylation-deficient mutants of the NET and DAT transporters showing similar deviations between surface presence and uptake efficiency [245 259 260].

5.5.3.Phosphorylation of the CrT

The treatment of CrT-HA with CIAP clearly showed the presence of phosphorylation in the CrT. In cell lysates treated with phosphatase inhibitors, CIAP-treated samples demonstrated a large shift in migration pattern, causing the predominant 70-80 kDa band to migrate with an apparent molecular mass of 62 kDa. The band also appeared less diffuse than in untreated lysate. The 58 kDa band was still present, but appeared reduced in intensity. Conversely, *in vitro* treatment with sodium orthovanadate did not have a pronounced affect on the migration of the CrT on SDS-PAGE, indicating that, under normal cell culture conditions, in the absence of additional Cr, the CrT is at least partially phosphorylated. Together, these results indicate the presence of phosphorylation in the CrT.

5.5.4. PKA- and PKC-mediated phosphorylation of the CrT

The migration of CrT-HA was studied following treatment with inhibitors of PKA and PKC, and it was established that inhibition of PKA has no noticeable effect. This implies either that any effect on the migration of the CrT is simply too small to be seen, or that PKA is not

constitutively active, and therefore its inhibition in the absence of prior external stimulation has no effect. A previous study found that activation of PKA, with 8-bromo-cyclic AMP, had no effect on Cr uptake, although these results were obtained from studies in *Xenopus* oocytes [9]. PKC inhibition with BIM also failed to cause a shift in the electrophoretic mobility of the CrT. Therefore, these results do not provide any evidence to suggest the involvement of *constitutive* PKA- or PKC-mediated phosphorylation of the CrT, though as outlined in the previous chapter, PKC-mediated phosphorylation has been shown to have a positive effect on CrT activity Stimulation of these pathways prior to western blotting may elucidate more, and would be a worthwhile experiment.

5.5.5. Creatine and its effects on post-translational modification of the CrT

Cells treated with Cr for 48 h prior to harvesting showed no changes to the migration of the CrT. Cr withdrawal also failed to have an effect. Although there was no noticeable shift in migration, this does not confirm that Cr has no effect on the phosphorylation of the CrT. It is possible that phosphorylation is altered, but that too few sites are affected to cause an electrophoretic shift noticeable by western blotting. An additional possibility is that the window during which Cr affects phosphorylation was missed. Future considerations for Cr incubation of these cells include 'optimisation' of the concentration of Cr included in incubation medium, enabling maintenance of intracellular [Cr] at a constant, physiological level. The shift observed in CrT electrophoretic mobility following CIAP treatment was substantial, and clearly visible on SDS-PAGE, but this would have involved dephosphorylation of all available sites. It is known that prolonged exposure to Cr reduces CrT activity [29 31]. However, if this effect is mediated by phosphorylation, it seems likely that a more sensitive method, such as LC / MS-MS or the use of phosphospecific antibodies would be required to detect it.

5.5.6. Attempts to identify phosphorylated CrT using phosphospecific antibodies

Initial attempts were made to identify the presence of serine and tyrosine phosphorylation on the CrT, using anti-phosphoserine (clone 4A4) and anti-phosphotyrosine (4G10) antibodies. These were used to probe the product of an IP performed against anti-HA (on 3T3-CrT-HA cell lysate), but no bands were detected in the resulting blots. Subsequently, 4G10, and an additional anti-phosphotyrosine antibody, PY99, were obtained from an alternative source. Optimisation of the antibodies on western blot, through pervanadate treatment, demonstrated that a good signal was obtained with the anti-PY99 antibody, and tyrosine phosphorylation was detected in the crude lysates of these treated cells. Subsequent immunoprecipitation of these lysates failed to detect any tyrosine-phosphorylated bands at the expected size for CrT. When the blots were stripped and re-probed with the anti-HA antibody, it was evident that CrT was present, indicating a genuine lack of tyrosine-phosphorylated protein. This was the case in the pervanadate-treated samples, as well as samples incubated in various concentrations of Cr. As such, it seems unlikely that the CrT is regulated by tyrosine phosphorylation. This is surprising, given the indication of putative tyrosine sites on the protein, and the publication of previous studies implicating tyrosine phosphorylation in the regulation of the CrT [235] [261]. However, as discussed briefly in the introduction to this chapter, the results obtained by Wang *et al* in these studies could have been compromised by the antibody used to immunoprecipitate the CrT. No details were given by the authors of the antibody used, and there has been no published follow-up study. Their western blots appeared different to what has been observed in the work performed in this thesis, and the laboratory in general (with both our anti-CrT and anti-HA antibodies). An additional point to note is, that of the 11 putative phosphorylation sites identified in Figure 5-1, only 2 are tyrosine (Y-11 and Y-135).

Further investigation utilising the ProQ Daimond phosphoprotein stain on immunoprecipitated CrT-HA did indicate the presence of a phosphoprotein, with a molecular mass of around 80 kDa. It is likely that this corresponds to the CrT, and indicates that, although tyrosine phosphorylation has been shown to be absent, there may be serine and / or threonine phosphorylation present in the CrT. Further investigation is required of these preliminary findings.

5.5.7. Immunoprecipitation and LC / MS-MS confirmation of CrT isoforms

With the exception of the 2 studies performed by Wang *et al* (detailed above) on tyrosine phosphorylation of the CrT in sepsis, there are no reports of CrT immunoprecipitation in the literature. This is likely due to the lack of a reliable antibody against the CrT. The creation of the 3T3-CrT-HA cell line over-expressing the HA-tagged CrT provided an excellent opportunity for immmunoprecipitation of the CrT with established anti-HA conjugated agarose. Having used this approach to confirm the presence of CrT in the various sized species that were observed on SDS-PAGE, it was hoped that the high sensitivity and accuracy of this method would enable the identification of post-translational modifications on the CrT using LC-MS / MS.

The immunoprecipitation protocol proved extremely difficult to optimise. While it was possible to purify small amounts of protein suitable for immunoblotting, there were difficulties precipitating enough pure protein to provide adequate samples for LC-MS / MS analysis. Silver staining the IP product separated on SDS-PAGE revealed the presence of multiple non-specific bands. Additional challenges were faced due to the use of an SDS lysis buffer for extraction of the CrT. Lysis buffer containing high levels of SDS has been required to successfully extract CrT, but owing to its detrimental effects on the efficacy of IPs, it was necessary to dilute cell

lysates 20-fold, to ensure the final concentration of SDS was below 0.1%. This resulted in large volumes of very dilute cell lysate, making the immunoprecipitation more challenging. Increasing the amount of starting material greatly (to several milligrams of cells) enabled the precipitation of enough protein to be detected by mass spectrometry, but persistent problems included contamination with other proteins (particularly keratin, a common contaminant of IP), and low sequence coverage of the CrT. Other proprietary lysis buffers have been used, but did not enable successful extraction of CrT. Only recently, a different lysis buffer, based on RIPA and used to extract protein for the phosphotyrosine blots, has been found to successfully extract CrT. This eliminates the need for the dilution of the cell lysates, as its SDS content is low enough so as not to interfere with the IP. Future large-scale immunoprecipitations will be performed using this RIPA- derived lysis buffer, and may enable a better yield of CrT, thus enhancing the ability to gain a high sequence coverage and possibly detect PTMs. Another approach to improving IP yield is the use of sub-cellular fractionation. This would allow greater purification of CrT (along with other membrane proteins) prior to performing IP, increasing the likelihood of a successful 'pulldown', due to (a) an increase in the concentration of CrT, and (b) a reduction in the presence of non-specific proteins which have proved problematic in the past.

Although the failure to obtain high sequence coverage by LC-MS / MS thus far is the most likely reason that it has not been possible to identify any PTMs on the CrT to date, the technique has provided adequate detail to enable confirmation of CrT in all bands shown in the results, with the exception of the 200 kDa species. The lack of detectable CrT in this sample could have been due simply to an inadequate amount of protein, as sequence coverage was low in all samples. The band was visible on an immunoblot of the IP product probed with anti-HA, suggesting that the protein was indeed present. In addition to the bands observed at 70-80 kDa and 58 kDa, a band of 150 kDa was routinely observed after IP, and this was confirmed as CrT

by LC-MS / MS. This is the first evidence to suggest a CrT species of this mass. It has been proposed that the band observed at 58 kDa is the native form of CrT, and that the slightly larger diffuse 70-80 kDa band is a CrT dimer, only present at the cell membrane [39]. Oligomerization has been shown to be involved in both the passage of protein through the quality control system of the ER (endoplasmic reticulum), as well as being involved in the transport of protein from the ER to the plasma membrane [262]. Another study that detected CrT with a calculated mass of 210 kDa by gel-filtration and 224 kDa by laser light scattering in decyl maltoside contradicted this theory, concluding that this large isoform could itself be a dimer [241]. If this were the case, it would be difficult to explain the presence of an additional species at 150 kDa. Oligomers of other members of the SLC6 family have been shown to exist by FRET (fluorescence resonance energy transfer) [262]. For example, the human SERT (serotonin transporter) and the rat GAT-1 (GABA transporter) [263], as well as the human DAT (dopamine transporter) [264] exist as oligomers. A dimerization motif, G(V/I)XXG(V/I)XX(A/T) has been identified in DAT, in TM6, and also exists in the CrT [262]. Additionally, a leucine heptad repeat is present, and highly conserved, in TM2 of members of the SLC6 family, including CrT [262]. These findings support the concept of the formation of dimers in the CrT. If the largest CrT isoform observed is a tetramer, it could be that the 150 kDa form is a trimer of CrT. Although no trimeric forms of SLC6 family members have been reported, EAATs (glutamate transporters) of the related SLC1 family do exist in trimeric form [265].

5.5.8. Conclusions and future work

This chapter has demonstrated the existence of several species of CrT with varying electrophoretic mobility. All of these have been verified with LC-MS / MS. Additionally, it was proved that the CrT is a glycoprotein, with replication of the results obtained by Straumann *et al*

[39], suggesting the involvement of 2 of the 3 potential glycosylation sites in the regulation of the CrT. The different sized species identified were similar to those reported in this paper, with the additional identification of a previously unreported 150 kDa band, which, upon analysis by LC-MS / MS was proved to be CrT. Thus, CrT (glycosylated and deglycosylated) was identified at band sizes of 43, 48, 58, 70-80, and 150 kDa, with a suspected band (identified by immunoblot but not LC-MS / MS) at 200 kDa. This is believed to be the first time that the presence of CrT has been confirmed in these different band sizes using mass spectrometry. In keeping with the literature, deglycosylation of the CrT was found to have an effect on its activity, possibly due to effects on intracellular location.

The use of IP as a tool to purify the CrT-HA protein has been valuable, enabling positive identification of various different sized species. Whilst the presence of phosphorylation in the CrT was confirmed by total dephosphorylation with CIAP, the purification of adequate levels of pure protein to provide significant sequence coverage and facilitate the identification of PTMs has not yet been possible. Alternative methods, such as site-directed mutagenesis, would be of limited benefit, as such a technique has been used in the investigation of *N*-linked glycosylation [39], and as such would provide little additional information. Owing to the large number of predicted phosphorylation sites (11), their investigation by site-directed mutagenesis would be a labourious process. Therefore, ways to enhance the detection by LC-MS / MS have been discussed, and are being pursued.

Chapter 6. Transcriptional regulation of the CrT: Work in progress and future directions

6.1. Introduction

6.1.1. Background and aims

This thesis has so far aimed to investigate the regulation of the CrT both *in vivo* and *in vitro*. Firstly, an *in vivo* model of CrT overexpression was attempted, as a means of manipulating cellular energetics. However, the expected phenotype of elevated myocardial [Cr] was not achieved. Subsequent *in vitro* work focussed on stably overexpressing CrT in a murine cell line, a valuable tool for studying CrT mRNA activity and regulation via post-translational modifications. The aspect of the transporter's regulation not yet discussed is that of transcriptional regulation. Little is known about the function of the 5' UTR of the *CrT* and its involvement in the regulation of Cr uptake. This is due perhaps in part to the challenging nature of studies on the promoter regions of genes.

It has previously been demonstrated that a degree of regulation of the CrT does occur at the transcriptional level. GAMT $^{-/-}$ hearts demonstrated a 7-fold increase in V_{max} of Cr uptake, that was accompanied by a 1.4-fold increase in CrT mRNA levels. These increases were both ablated when the knockout mice were fed a Cr- supplemented diet, indicating that Cr uptake is regulated at the transcriptional level by negative feedback [48]. Additionally, CrT-OE mice showed total CrT mRNA levels that correlated well with myocardial Cr content. These findings led the authors of this study to conclude that, although CrT transcription is not the main regulator of CrT activity, it is one of the factors involved in it [48]. Ireland *et al* showed an increase in CrT

mRNA expression in the prenatal spiny mouse brain between mid-pregnancy and term, and while they were unable to measure the resulting level of CrT protein (due to their lack of a reliable antibody), they hypothesised that this would lead to an increase in CrT numbers, coinciding with increased demand for Cr in the developing CNS, which synthesis within the CNS itself is unable to meet [47].

6.1.2. Experimental strategy and planning

The strategy undertaken in the preliminary work in this chapter was initially to amplify several lengths of up to 3 kb of the 5' UTR of the CrT by PCR, with a view to cloning different regions of this amplicon into a luciferase reporter vector, thus determining which regions are involved in driving gene expression. This strategy would involve the cloning of the full length 5' UTR, in addition to smaller regions, into the luciferase reporter vector pGL3-Basic, then transiently transfecting the construct into HL-1 cells *in vitro*, prior to treatment with various compounds-candidate regulators of the CrT. Any change in the luciferase activity following incubation with these candidate regulators would indicate a regulatory mechanism.

Latterly, a bioinformatics-guided approach was adopted, in order to seek candidate regulatory sites involved in *CrT* regulation. This strategy change was necessary due to the failure of the original PCR-based cloning strategy, primarily due to the technical challenges associated with the amplification a highly GC- rich region such as the 5' UTR. In an attempt to identify highly conserved putative sites on the 5' UTR upstream of *hCrT*, HEY1 was found to be a strong candidate. HEY1, a basic helix-loop-helix protein, is a member of the *Hey* genes subfamily of *hairy*- and *Enhancer of split* related genes known to be expressed during mouse embryogenesis [266]. These genes also play a role in the establishment and development of the atrioventricular

canal myocardial boundary [267]. HEY1 was identified as being of potential interest following the inspection of the ChIP-Seq results set stored on the UCSC genome browser, by Dr Richard Copley (University of Oxford). HEY1 was also identified as a candidate transcription factor following a set of predictions of the region up to 2.7 kb upstream of the CrT, using Transfac Position Weight Matrices, with a high scoring threshold (0.9) in order to reduce the number of false positives. Additionally, it exhibited a high degree of cross-species conservation. HEY1 has previously been identified as a *trans*-acting repressor of gene expression of the dopamine transporter (DAT1), in this instance through the 3' UTR [268]. For these reasons, it was selected as a potential regulator of CrT expression, and a strategy of short interfering RNA (siRNA) knockdown is underway to establish its involvement in the transcription of the CrT.

6.2. Methods and Results

6.2.1. Amplification of the CrT 5' UTR

A series of primers (listed in Appendix II) were designed against a region of 2-3 kb upstream of the human *CrT*, against transcripts SLC6A8-002 (ENST00000253122) and SLC6A8-005 (ENST00000430077), obtained from Ensembl (www.ensembl.org). All primers were designed using the NCBI 'Primer-BLAST' program, with sense primers incorporating a *Hind*III restriction site and GC clamp, and antisense primers incorporating a *Bgl*II restriction site, determined by their presence in the pGL3-Basic vector (Promega) and their absence from the 3 kb region of the 5' UTR of the CrT. The pGL3-Basic vector was chosen as a reporter vector into which the 5' UTR amplicons would be cloned.

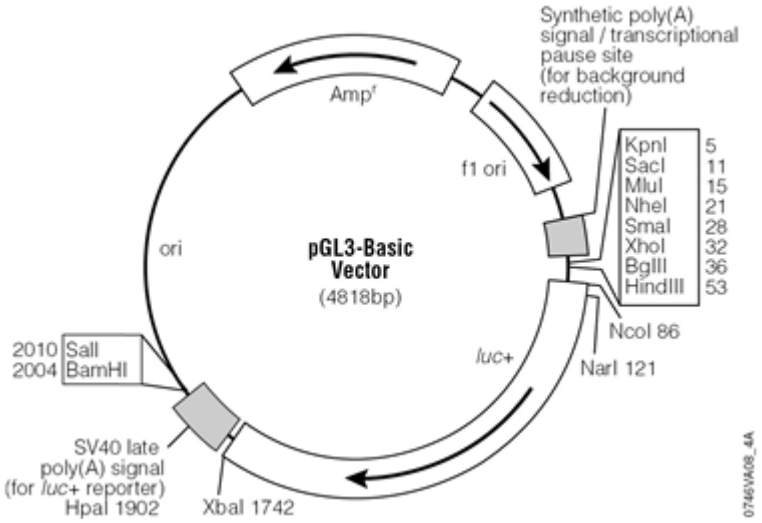


Figure 6-1. The pGL3 luciferase reporter vector (Promega).

Human genomic DNA from an intra-departmental source was used as the template for all PCR reactions, which were carried out using Phusion high-fidelity DNA polymerase (Finnzymes). Reactions were performed according to the manufacturer's protocol, with the addition of 3 % DMSO in order to aid amplification of the GC- rich template. PCR conditions are listed in Appendix II.

Numerous attempts to amplify regions of the 5' UTR proved unsuccessful, generally yielding multiple non-specific bands. Where bands of the expected size were amplified, DNA was purified from the gel and sequenced, as detailed in General Materials and Methods. Sequencing results confirmed that the correct product had not been amplified (data not shown). An example gel is shown in figure 6-2.

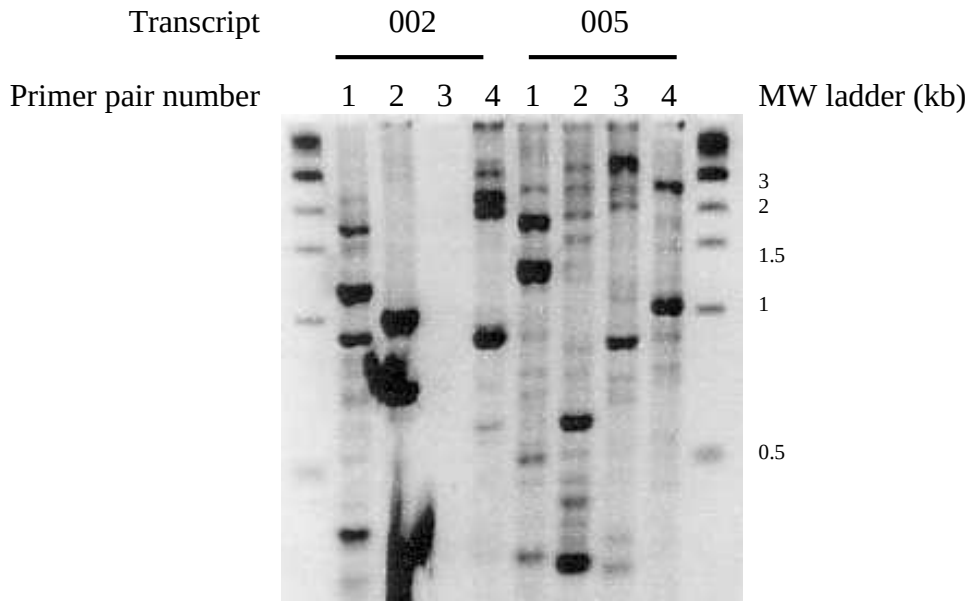


Figure 6.2. 1% agarose gel showing products of amplification of regions of the CrT 5' UTR, amplified using primers against transcripts 002 and 005 (Appendix II). Reactions were performed using Phusion DNA polymerase, with an annealing temperature of 57^{o} C, 1.5 mM $MgCl_2$ and 3% DMSO. Despite numerous products, sequencing showed that even those fragments of the expected size were not the desired product.

6.2.2. siRNA knockdown of *Hey1*

Following the unsuccessful attempt to amplify and isolate the 5' UTR of hCrT, a targeted approach was adopted, focussing on highly conserved transcription factors within the promoter region of the CrT. An siRNA protocol was used, in this case, to knock down *Hey1 in vitro*, and study any effects on CrT activity.

siRNAs are a class of double-stranded RNA molecules, typically around 20-25 nucleotides long with 2-nucleotide 3' overhangs on either end. They are known to play a role in the RNA interference (RNAi) pathway, and are formed by the processing of long double-stranded RNAs or short-hairpin RNAs by 'dicer' (an endoribonuclease) [269]. Since synthetic siRNAs were shown

to be able to induce RNAi in mammalian cells [270], they have been widely used in the investigation of the effects of gene function and regulation.

6.2.2.1. Initial siRNA transfections using standard transfection protocol

siRNA oligos against *Hey1* and *cyclophilin B* (mouse) were obtained from Dharmacon RNAi Technologies (Thermo Scientific, UK). (Sequences listed in Appendix II). HL-1 cells were used for all siRNA experiments, owing to the presence of the endogenous murine 5' UTR upstream of the CrT, unlike the 3T3-CrT-HA cells, in which the transgenic CrT cDNA is downstream of the TRE and the P_{CMV} minimal promoter. All transfections were performed in 6-well plates. Initially, HL-1 cells were transfected according to the method outlined in General Materials and Methods. A Cr uptake assay was performed (see General Materials and Methods), 48h post-transfection. Cells were transfected with siRNA at a final concentration of 25 nM, using 2 different ratios of siRNA to transfection reagent (5 μL and 10 μL of transfection reagent). Cr uptake was determined in the cells using 250 μM extracellular Cr, over a 1 h period, as described in General Materials and Methods. No change in Cr uptake was observed in the cells transfected under either condition (see figure 6-3).

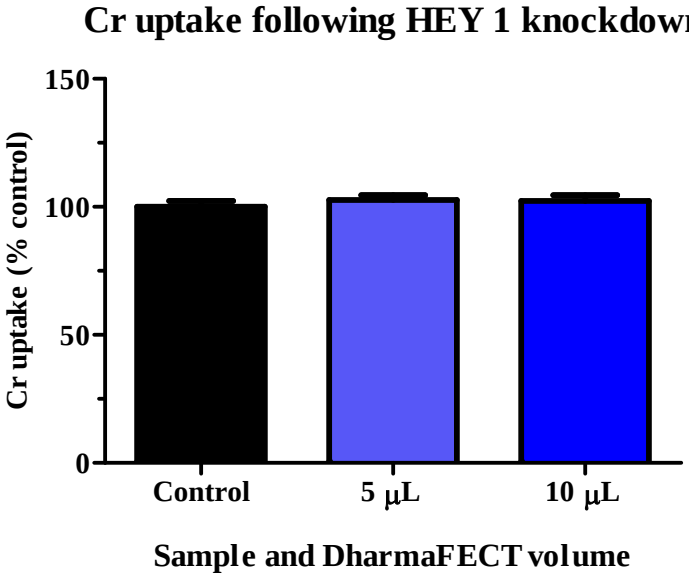


Figure 6-3. Results of Cr uptake assay following siRNa transfection of HL-1 cells using the standard transfection protocol. Neither transfection led to an alteration in Cr uptake 48 h post-transfection. Results in duplicate, error bars represent SEM.

6.2.2.2. Repeat siRNA knockdown of *Hey1* and *Cyclophilin B* using DharmaFECT optimised transfection protocol

Transfections of HL-1 cells were repeated, using an alternative transfection reagent optimised for the transfection of siRNA, DharmaFECT (Thermo Scientific Dharmacon, UK). The final concentration of siRNA used for both *cyclophilin B* and *Hey1* knockdown was 25 nM (10 µL of 5 µM stock siRNA). Two volumes of DharmaFECT were used, equivalent to either 5 µL or 10 µL final volume per well. The protocol was performed according to the manufacturer's instructions. The full details of reagents used are listed in table 6-1.

Tube 1: diluted siRNA (µL / well)		Tube 2: diluted transfection reagent (µL / well)			
Volume of 5 µM si RNA (µL)	**Serum-free medium (µL)**	**Volume of DharmaFECT transfection reagent (µL)**	**Serum-free medium (µL)**	**Complete medium (µL / well)**	**Total transfection volume (µL / well)**
10	190	5 or 10	195 or 190	1600	2000

Table 6-1. Detail of the volumes of reagents used to transfect HL-1 cells with siRNA. Two separate mixtures were prepared, in tube 1 and tube 2, then combined, prior to being added to each well of cells.

HL-1 cells were plated out in 6-well plates on day 1, at a density of 2.5 x 10^5 / well, in complete Claycomb medium (see General Materials and Methods). On day 2, the medium was changed. On day 3, prior to transfection, the medium was changed to antibiotic-free. On day 4, 24 h post-transfection, the medium was changed back to complete Claycomb, according to the DharmaFECT protocol and previous optimisations performed on HL-1 transfections in our lab. On day 5, a Cr uptake assay was performed. Additional treated cells were harvested and RNA was extracted ready to perform real time RT-PCR analyses (see General Materials and Methods).

6.2.2.3. Real-time RT-PCR results of *Hey1* and *cyclophilin B* knockdown

To confirm the efficiency of the siRNA knockdown in the transfected HL-1 cells, real-time RT-PCR was performed (see General Materials and Methods). Initially, RNA extracted from the cells transfected with *cyclophilin B* siRNA was tested, as a positive control and indicator of the efficiency of the siRNA knockdown. The results demonstrated a knockdown of *cyclophilin B* mRNA transcription of around 75% in the cells treated with the 10 µL DharmaFECT transfection reagent mix. This is close to the >80% knockdown figure quoted by Dharmacon as the highest expected level of efficiency (Figure 6.4). All real-time RT PCR results in this

chapter are normalised to the constitutive reference gene *36B4* (acidic ribosomal phosphoprotein P0, Primer Bank ID 6671569a1). [131 132].

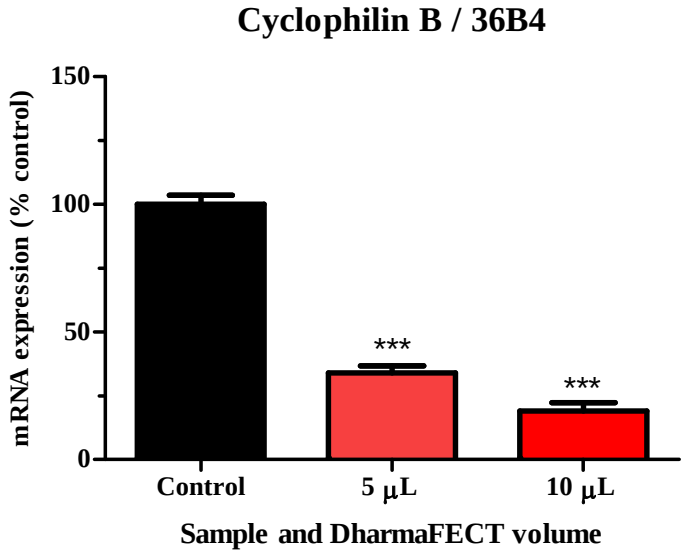


Figure 6-4. Real-time PCR results showing efficiency of *cyclophilin B* knockdown 48 h post-transfection with 25 nM *cyclophilin B* siRNA. Four control samples wells were compared to 2 wells each of the transfected samples. Of these, each individual sample was run in triplicate. Results are normalised to % untransfected control. Values are mean ± SEM. ***p< 0.001, compared to untreated control group (One-way ANOVA with Dunnett's multiple comparison test).

Having demonstrated a high knockdown efficiency, the experiment was repeated using the *Hey1* siRNA oligo. Conditions were exactly as detailed above. Once again, efficient knockdown of the target was observed, with the 5 µL and 10 µL DharmaFECT transfections yielding a 75% and 76% reduction in *Hey1* mRNA expression respectively.

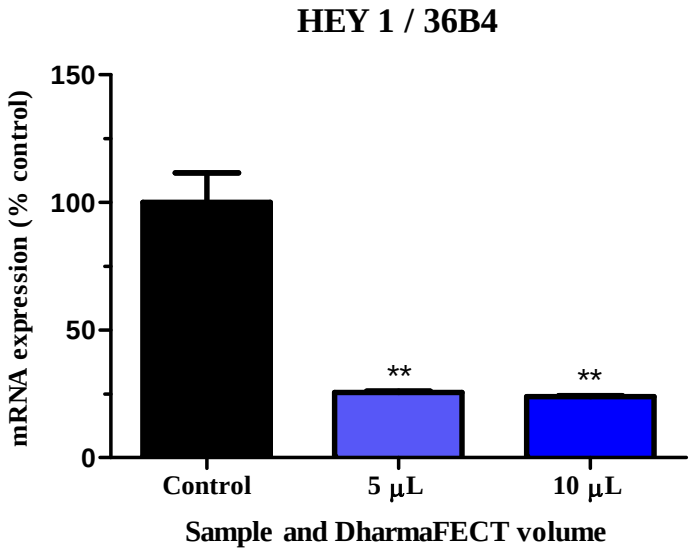


Figure 6-5. Real-time PCR results showing efficiency of *Hey1* knockdown 48 h post-transfection with *Hey1* siRNA. Four control samples wells were compared to 2 wells each of the transfected samples. Of these, each individual sample was run in triplicate. Results are normalised to % untransfected control. Values are mean ± SEM. **p< 0.01, compared to untreated control group (One-way ANOVA with Dunnett's multiple comparison test).

Expression of *CrT* was also measured in the samples treated with *Hey1* siRNA. Despite the 75% reduction observed in *Hey1* expression, there was no significant difference between the expression levels of CrT in transfected versus untransfected cells. Though a small decrease was observed, repeat experiments are needed to validate this effect.

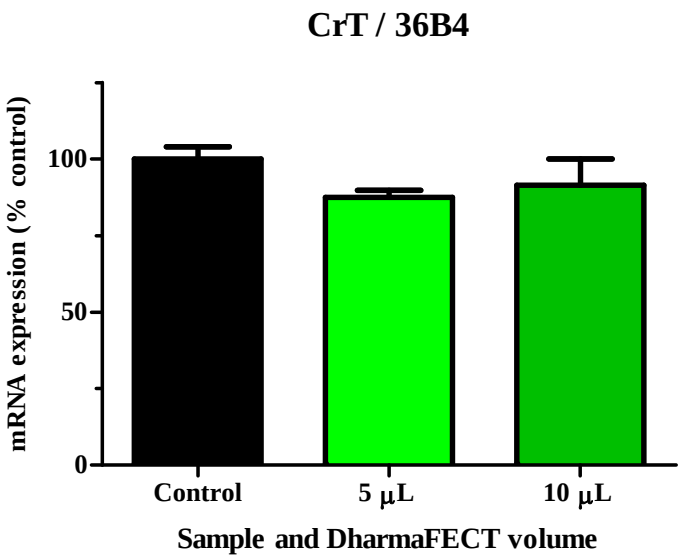


Figure 6-6. Real-time PCR results showing efficiency of CrT knockdown 48 h post-transfection with *Hey1* siRNA Four control samples wells were compared to 2 wells each of the transfected samples. Of these, each individual sample was run in triplicate. Results are normalised to % untransfected control. Error bars represent SEM. There was no significant difference between the untreated control group and treated groups (One-way ANOVA and Dunnett's multiple comparison test).

6.2.2.4. Creatine uptake following HEY1 knockdown

Creatine uptake was investigated once more, this time in the cells transfected using the optimised protocol, as detailed in section 6.2.2.2. Despite the lack of a reduction in the expression of *CrT* mRNA, as determined by real-time RT-PCR, a small reduction of ~13% in Cr uptake was observed in the 5 µL- treated cells, and of ~22% in the cells treated with the higher transfection reagent : siRNA ratio.

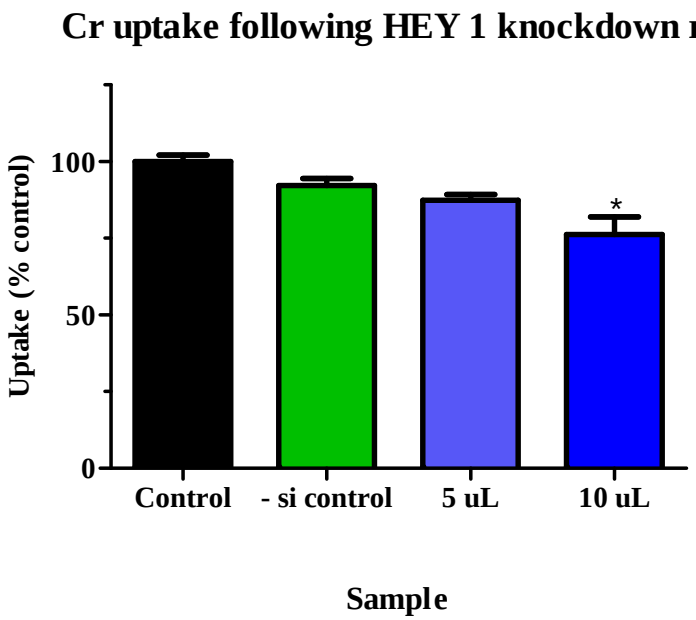


Figure 6-7. Results of Cr uptake assay following *Hey1* siRNA transfection of HL-1 cells using the modified transfection protocol with DharmaFECT transfection reagent. 5 µL- and 10 µL- transfected samples showed a 13% and 22% reduction in Cr uptake, respectively. Results in duplicate, normalised to % untransfected control. Results are normalised to % untransfected control. Error bars represent SEM. There was a significant difference between the untreated control group and 10 µL treated group (One-way ANOVA and Dunnett's multiple comparisons test).

6.3. Discussion

The initial approach taken to study the regulation of the *hCrT* did not yield the desired results. The use of extended length oligos (to increase specificity) still led to the amplification of a non-specific product. It is likely that the main cause of these difficulties is the highly GC- rich nature of the 5' UTR, which in turn led to many difficulties designing specific primers against this region, and also to technical issues regarding the actual PCR reaction. The use of the PCR buffer provided by Finnzymes for GC-rich templates did not help, and nor did the addition of DMSO to the PCR reaction. A variety of Mg^{2+} concentrations, in addition to a multitude of PCR conditions, including higher annealing temperatures of up to 69^{o}C, and the use of touchdown programs, also failed. It currently seems likely that, due to the very nature of the highly GC- rich template, it will not be possible to amplify regions of the 5' UTR as planned to study its

involvement in the regulation of the CrT. To date, there exist no other reports of studies on the CrT promoter region in the literature, and this may be a possible explanation.

The use of siRNA to begin studies into the effect of transcription factors identified in the 5' UTR has been started as an alternative strategy to establish more about the transcriptional regulation of the CrT. To date, a preliminary investigation into the role of HEY1 on CrT has been performed. HEY1 belongs to the HESR family of basic helix-loop-helix transcription factors, and its expression is induced by the Notch and c-Jun signal transduction pathways. Although the knockout of *Hey1* in mouse has not been shown to lead to a phenotype, mice lacking the closely related *Hey2* develop severe cardiac hypertrophy, whereas combined *Hey1/Hey2* deficiency in the mouse leads to severe vascular defects and embryonic lethality around embryonic day E9.5 [271]. More recently, the combined loss of *Hey1* and the third *Hey* family member, *HeyL*, has been demonstrated to lead to congenital heart defects due to impaired endothelial to mesenchymal transition [272].

Prior to *Hey1* knockdown, HL-1 cells had demonstrated high levels of expression of *Hey1* and, while *CrT* expression is known to be lower in these cells than in the overexpressing 3T3-CrT-HA line, it is readily detectable by real-time RT PCR. Additionally, the HL-1 line is known to express functional endogenous CrT (see Chapter 4). They also retain the cardiac milieu, as they are able to beat in culture. These factors make the HL-1 cell line a suitable system in which to test knockdown of *Hey1* and its effects on *CrT* expression.

Following optimisation of the knockdown transfection protocol, satisfactory levels of gene knockdown were achieved both with the positive control, *cyclophilin B*, and *Hey1* itself.

Despite a 75% reduction of the expression of *Hey1*, no difference was seen in the expression of CrT mRNA. However, these cells did demonstrate a small level of reduction in Cr uptake. Further experiments will be required to prove whether this decrease is a genuine effect of HEY1 regulating the CrT, although at this stage, two options seem possible.

1. Despite the absence of a reduction in the expression level of CrT mRNA following *Hey1* knockdown, it could still be involved in the regulation of the CrT. This could be due to a resultant decrease in CrT mRNA. It is known that without changes at the transcription level, mRNA steady-state levels can vary dramatically due to small changes in mRNA stability, which may be a key regulator in the expression of many proteins [273]. Again, further repeats of this knockdown would be required to determine whether this is indeed the cause of the reduced Cr uptake observed.
2. It is possible that the activity of CrT in its 'unstimulated' state is largely unaffected. There is a possibility that the effect observed would be different following upregulation of the CrT, for example with the PKC activators PMA and sapinotoxin D (as discussed in Chapter 4), or indeed in the presence of Cr. Repeats of the *Hey1* knockdown, following the stimulation of the CrT, will clarify this question.

6.4. Conclusions

The identification of potentially important transcription factors involved in the regulation of CrT function, and the use of siRNA oligos to target them, could prove a useful tool to elucidate more regarding the transcriptional regulation of the CrT. The determination of the level of mRNA, post-knockdown by real-time RT-PCR, in the presence and absence of compound-stimulation with known CrT activators, provides a straightforward method of identifying and quantifying

any effects caused on *CrT* transcription. Additionally, the use of radiolabelled-Cr uptake assays enables easy detection of the effect on CrT activity.

Chapter 7. General discussion

Intracellular Cr is depleted in the myocardium in heart failure. Previous literature explores the link between decreased Cr availability and deranged cardiac energetics, as extensively reviewed by Neubauer [83]. The current thesis outlines several different strategies that aim to modulate Cr levels, through molecular and pharmacological intervention, studying several routes of regulation of CrT. In particular, a novel mouse model for overexpressing CrT in a time-specific manner in the mature mouse heart following the onset of HF is described. The effects of post-translational modifications on CrT function are investigated, with a view to confirming the presence of predicted sites by sensitive LC-MS tools. The influence of a signalling pathway implicated in the regulation of CrT is studied using a highly relevant cardiac-derived cell line. Furthermore, preliminary work is performed on the regulation of the 5'UTR of mouse CrT, using a targeted siRNA knockdown strategy against potentially key putative transcription factor HEY1. These approaches complement one another by establishing more about the regulation and maintenance of cellular Cr levels, which is highly relevant in the study of high-energy phosphate metabolism in the heart.

Attempts were made to create a functioning mouse model for the inducible overexpression of the CrT. The aim of this strategy was to enable restoration of the depleted myocardial Cr levels associated with heart failure [87 88 89], whilst avoiding the pitfalls associated with long-term supra-normal myocardial [Cr], a phenotypic feature of a previous mouse model of CrT overexpression created by our group [97]. A construct was assembled containing *CrT* cDNA, with a C-terminal epitope tag, downstream of a tetracycline response element. This was flanked by *H19* insulating elements, shown to reduce the chance of positional effects from random integration [161].

Successful validation of the construct *in vitro*, using a stable cell line, showed expression of the transgenic CrT on the plasma membrane (and to a lesser degree, in the cytoplasm), and a doxycycline mediated response was confirmed. Ten viable founder mice were generated with this construct, of which 8 demonstrated normal germline transmission. Following the creation of double-transgenic mice, by breeding these 8 founders with the rtTA transactivator line, 7 of the double-transgenic lines completely failed to express the transgene in LV. However, one double-transgenic line showed limited success; of those animals tested, 1 alone overexpressed CrT, demonstrating an LV Cr concentration around 2.3-fold greater than WT following dox mediated induction. The lack of phenotype in the majority of the lines tested suggests that, in spite of the incorporation of insulating elements in the construct, position-dependent effects prevented expression of the transgene. Position-effect variegation could explain the one-off example of successful expression observed. Further work, to test whether the problem lay with the responder line, was carried out by the creation of a double-transgenic luciferase reporter line in which expression was driven by the same rtTA transactivator line as for the CrT-OE mice. All double-transgenic mice treated with doxycycline demonstrated high levels of luciferase activity in LV tissue. Although the generation of further founder lines for CrT OE using this approach may lead to success, a more suitable direction for the future would include the targeted insertion of the transgene via RMCE (recombinase-mediated cassette exchange) into the *Rosa26* locus.

It was then decided that suitable *in vitro* tools would assist in elucidating other mechanisms of CrT regulation. Previous studies on post-translational modifications of CrT suggested that *N*-linked glycosylation and phosphorylation may be regulators of CrT activity *in vitro* [48], with putative glycosylation and phosphorylation sites previously identified [39] [26]. The use of cells overexpressing the HA-tagged CrT enabled immunoprecipitation of the protein, through utilisation of the HA tag. Efficient immunoprecipitation of the CrT has not previously been

possible, owing to the lack of reliable anti-CrT antibodies. Numerous unsuccessful attempts to optimise commercially available or other custom-made anti-CrT antibodies led to the utilisation of the HA tag as a means of CrT isolation for protein studies. Immunopreciptitated CrT-HA enabled analysis by LC-MS / MS with a view to identifying PTMs on the protein. Whilst no PTMs were identified, due to inadequate sequence coverage of the CrT, the technique enabled confirmation of the presence of CrT in 5 different-sized species observed on SDS-PAGE. Some debate exists regarding the size and migratory patterns of these species [39] [241], and the use of LC-MS / MS conclusively demonstrated the existence of native bands at 58 kDa and 70-80 kDa. Additionally, the existence of a previously unreported species of 150 kDa was confirmed. Following deglycosylation, additional CrT species were observed at 48 kDa and 43 kDa, in keeping with the findings of Straumann and colleagues [39], but in contrast to West *et al* [241]. Phosphatase treatment of CrT-HA led to a marked decrease in the apparent size of the protein on SDS-PAGE, suggesting the presence of phosphorylation. However, attempts to identify the type of phosphorylation more accurately, through the use of phosphospecific antibodies, proved challenging. The anti-phosphotyrosine antibody, PY99, was successfully optimised to detect tyrosine phosphorylation. Its use demonstrated a lack of detectable tyrosine phosphorylation on the CrT following incubation of CrT overexpressing cells in the presence and absence of Cr, and also following Cr starvation after a prolonged period of exposure to Cr. Even following stimulation with pervanadate, no tyrosine phosphorylation was detected on the CrT, despite the prediction of 2. Tests with anti-phosphoserine antibodies proved unsuccessful. Work to identify the presence of PTMs by LC-MS / MS continues, and the refinement of the IP protocol, combined with the use of subcellular fractionation techniques, may improve the chances of their detection and identification.

Having demonstrated the presence of phosphorylation on the CrT, work in the following chapter concentrated on proving the role of a signalling pathway previously identified as a potential modulator of CrT activity [11], the IGF-1R pathway. Two cell lines were used throughout this study, including the HL-1 cardiac-derived line. This gave increased relevance to the results over many previous studies which often used artificial and potentially irrelevant cell systems, such as *Xenopus* oocytes. The confirmation of the role of insulin in mediating increased Cr uptake, in addition to the finding that GH causes a similar effect, strongly suggests the involvement of IGF-1R in the regulation of CrT. Furthermore, this insulin-mediated increase in uptake was blocked by the addition of the IGF-1R inhibitor, PPP. The case for the involvement of this pathway is strengthened by the finding that inhibition of PKA and PKC, both potentially downstream of IGF-1R, block the insulin and GH mediated response, whilst having little effect on Cr uptake in the absence of IGF-1R stimulation. In contrast to previous reports in the literature [9], stimulation of PKC with 2 different compounds was found to enhance Cr uptake. The use of rapamycin prior to Cr uptake assays suggested a role for mTOR in the CrT regulatory network; however, this aspect merits further clarification, as rapamycin inhibits the complex TORC1 only, and may also interfere with the cell cycle.

Additionally, the effects of the Na^+ K^+ - ATPase in the insulin-mediated stimulation of Cr uptake will be investigated, using the inhibitor oubain. Further trafficking experiments could be performed in order to test regulation of CrT localisation within HL1 cells. For example, PMA has been shown to change other Slc family transporter trafficking characteristics [274] via PKC dependent or independent pathways.

Our studies have been limited by a number of factors so far. Firstly, we have not been able to estimate baseline intracellular Cr levels in each *in vitro* experiment. Responses in 3T3-CrT-HA

cells in particular would have been better characterised if we had the cell line permanently exposed to physiological Cr levels (64nM) in order to compare to responses in cells grown in the absence of Cr. Secondly, no information is available on the rate of CrT recycling within the 3T3-CrT-HA cells, as this issue would be linked to regulation of CrT by its substrate and localisation of active CrT on the plasma membrane vs. cytoplasmic or lysosomal localisation. An attempt to clone hCrT into an mCHERRY construct using Gateway vector technology, for monitoring the transporter's recycling within the cell in the presence or absence of stimuli, has so far proved unsuccessful.

The final section of work in this thesis explored the involvement of a candidate transcription factor, HEY1, in CrT regulation at the transcriptional level. Initial attempts to amplify regions of the 5' UTR of CrT and follow up with luciferase reporter assays *in vitro* were hampered by the GC- rich nature of the sequence, which prevented the successful amplification of a specific product. No literature exists so far on isolation of the CrT promoter region for promoter studies. This necessitated a change to a more targeted approach. The revised approach focussed on the identification of transcription factors highly conserved between species in the 5' UTR of the CrT. HEY1 was selected as a strong candidate, and a strategy of siRNA knockdown was pursued *in vitro*, to determine the involvement of this transcription factor in the regulation of CrT. Although the knockdown of *Hey1* was successful, no statistically significant reduction of *CrT* mRNA was observed, despite a slight reduction. However, a minor reduction in Cr uptake was observed in treated cells, suggesting a potential regulatory role for HEY1. Clarification of the cause of this effect is required, in order to determine whether it is a direct consequence of a reduction in *CrT* mRNA transcription, or due to another factor, such as a reduction in mRNA stability [273]. These preliminary findings suggest a role for HEY1 in the transcriptional regulation of the CrT. In the future, the work on HEY1 could be further explored by additional

assessments intracellular Cr levels after siRNA knockdown experiments *in vitro*, in addition to testing the involvement of other highly conserved transcription factors, similarly to HEY1.

The approaches described within this thesis demonstrate that the regulation of Cr transport is highly complex and controlled at many different levels; by transcriptional means at the gene level and via signal transduction and post-translational modification at the protein level. The evidence collected provides an insight into a small part of a dynamic system required to maintain Cr homeostasis under a multitude of changing metabolic demands in both cardiac and skeletal muscle. Modulation of myocardial [Cr] is particularly relevant in the context of cardiac disease, with the discovery that moderately elevated Cr levels reduce myocardial injury following ischaemia and reperfusion *in vivo.* Whilst there remains a huge amount to explore in the regulation of the CrT, particularly with regard to tightly-controlled regulation in HF, it is clear that the modulation of myocardial [Cr] through manipulation of CrT remains a worthy path for further investigation.

References

1. Fitch CD, Shields RP. Creatine metabolism in skeletal muscle. I. Creatine movement across muscle membranes. *The Journal of Biological Chemistry*. 1966;**241**(15):3611-4.

2. Wyss M, Kaddurah-Daouk R. Creatine and creatinine metabolism. *Physiological Reviews*. 2000;**80**(3):1107-213.

3. Walker JB. Creatine: biosynthesis, regulation, and function. *Advances in Enzymology and Related Areas of Molecular Biology*. 1979;**50**:177-242.

4. Boroujerdi M, Mattocks AM. Metabolism of creatinine in vivo. *Clinical Chemistry*. 1983;**29**(7):1363-6.

5. Hultman E, Soderlund K, Timmons JA, Cederblad G, Greenhaff PL. Muscle creatine loading in men. *Journal of Applied Physiology*. 1996;**81**(1):232-7.

6. Harris RC, Soderlund K, Hultman E. Elevation of creatine in resting and exercised muscle of normal subjects by creatine supplementation. *Clinical Science*. 1992;**83**(3):367-74.

7. Loike JD, Somes M, Silverstein SC. Creatine uptake, metabolism, and efflux in human monocytes and macrophages. *The American Journal of Physiology*. 1986;**251**(1 Pt 1):C128-35.

8. Daly MM, Seifter S. Uptake of creatine by cultured cells. *Archives of Biochemistry and Biophysics*. 1980;**203**(1):317-24.

9. Dai W, Vinnakota S, Qian X, Kunze DL, Sarkar HK. Molecular characterization of the human CRT-1 creatine transporter expressed in Xenopus oocytes. *Archives of Biochemistry and Biophysics*. 1999;**361**(1):75-84.

10. Guimbal C, Kilimann MW. A Na(+)-dependent creatine transporter in rabbit brain, muscle, heart, and kidney. cDNA cloning and functional expression. *The Journal of Biological Chemistry*. 1993;**268**(12):8418-21.

11. Odoom JE, Kemp GJ, Radda GK. The regulation of total creatine content in a myoblast cell line. *Molecular and Cellular Biochemistry*. 1996;**158**(2):179-88.

12. Hoglund PJ, Adzic D, Scicluna SJ, Lindblom J, Fredriksson R. The repertoire of solute carriers of Family 6: identification of new human and rodent genes. *Biochemical and Biophysical Research Communications*. 2005;**336**(1):175-89.

13. Gregor P, Nash SR, Caron MG, Seldin MF, Warren ST. Assignment of the creatine transporter gene (SLC6A8) to human chromosome Xq28 telomeric to G6PD. *Genomics*. 1995;**25**(1):332-3.

14. Iyer GS, Krahe R, Goodwin LA, Doggett NA, Siciliano MJ, Funanage VL, Proujansky R. Identification of a testis-expressed creatine transporter gene at 16p11.2 and confirmation of the X-linked locus to Xq28. *Genomics*. 1996;**34**(1):143-6.

15. Sandoval N, Bauer D, Brenner V, Coy JF, Drescher B, Kioschis P, Korn B, Nyakatura G, Poustka A, Reichwald K, Rosenthal A, Platzer M. The genomic organization of a human creatine transporter (CRTR) gene located in Xq28. *Genomics*. 1996;**35**(2):383-5.

16. Saltarelli MD, Bauman AL, Moore KR, Bradley CC, Blakely RD. Expression of the rat brain creatine transporter in situ and in transfected HeLa cells. *Developmental Neuroscience*. 1996;**18**(5-6):524-34.

17. Hahn KA, Salomons GS, Tackels-Horne D, Wood TC, Taylor HA, Schroer RJ, Lubs HA, Jakobs C, Olson RL, Holden KR, Stevenson RE, Schwartz CE. X-linked mental retardation with seizures and carrier manifestations is caused by a mutation in the creatine-transporter gene (SLC6A8) located in Xq28. *American Journal of Human Genetics*. 2002;**70**(5):1349-56.

18. Salomons GS, van Dooren SJ, Verhoeven NM, Cecil KM, Ball WS, Degrauw TJ, Jakobs C. X-linked creatine-transporter gene (SLC6A8) defect: a new creatine-deficiency syndrome. *American Journal of Human Genetics*. 2001;**68**(6):1497-500.

19. Stockler S, Schutz PW, Salomons GS. Cerebral creatine deficiency syndromes: clinical aspects, treatment and pathophysiology. *Sub-cellular Biochemistry*. 2007;**46**:149-66.

20. Martinez-Munoz C, Rosenberg EH, Jakobs C, Salomons GS. Identification, characterization and cloning of SLC6A8C, a novel splice variant of the creatine transporter gene. *Gene*. 2008;**418**(1-2):53-9.

21. Eichler EE, Lu F, Shen Y, Antonacci R, Jurecic V, Doggett NA, Moyzis RK, Baldini A, Gibbs RA, Nelson DL. Duplication of a gene-rich cluster between 16p11.1 and Xq28: a novel pericentromeric-directed mechanism for paralogous genome evolution. *Human Molecular Genetics*. 1996;**5**(7):899-912.

22. Xu W, Liu L, Gorman PA, Sheer D, Emson PC. Assignment of the human creatine transporter type 2 (SLC6A10) to chromosome band 16p11.2 by in situ hybridization. *Cytogenetics and Cell Genetics*. 1997;**76**(1-2):19.

23. Broer S. The SLC6 orphans are forming a family of amino acid transporters. *Neurochemistry International*. 2006;**48**(6-7):559-67.

24. Betsalel OT, Rosenberg EH, Almeida LS, Kleefstra T, Schwartz CE, Valayannopoulos V, Abdul-Rahman O, Poplawski N, Vilarinho L, Wolf P, den Dunnen JT, Jakobs C, Salomons GS. Characterization of novel SLC6A8 variants with the use of splice-site analysis tools and implementation of a newly developed LOVD database. *European Journal of Human Genetics : EJHG*. 2011;**19**(1):56-63.

25. Dodd JR, Zheng T, Christie DL. Creatine accumulation and exchange by HEK293 cells stably expressing high levels of a creatine transporter. *Biochimica et Biophysica Acta*. 1999;**1472**(1-2):128-36.

26. Nash SR, Giros B, Kingsmore SF, Rochelle JM, Suter ST, Gregor P, Seldin MF, Caron MG. Cloning, pharmacological characterization, and genomic localization of the human creatine transporter. *Receptors & Channels*. 1994;**2**(2):165-74.

27. Sora I, Richman J, Santoro G, Wei H, Wang Y, Vanderah T, Horvath R, Nguyen M, Waite S, Roeske WR, et al. The cloning and expression of a human creatine transporter. *Biochemical and Biophysical Research Communications*. 1994;**204**(1):419-27.

28. Schloss P, Mayser W, Betz H. The putative rat choline transporter CHOT1 transports creatine and is highly expressed in neural and muscle-rich tissues. *Biochemical and Biophysical Research Communications*. 1994;**198**(2):637-45.

29. Guerrero-Ontiveros ML, Wallimann T. Creatine supplementation in health and disease. Effects of chronic creatine ingestion in vivo: down-regulation of the expression of creatine transporter isoforms in skeletal muscle. *Molecular and Cellular Biochemistry*. 1998;**184**(1-2):427-37.

30. Moller A, Hamprecht B. Creatine transport in cultured cells of rat and mouse brain. *Journal of Neurochemistry*. 1989;**52**(2):544-50.

31. Boehm E, Chan S, Monfared M, Wallimann T, Clarke K, Neubauer S. Creatine transporter activity and content in the rat heart supplemented by and depleted of creatine. *American Journal of Physiology Endocrinology and Metabolism*. 2003;**284**(2):E399-406.

32. Fischer A, Ten Hove M, Sebag-Montefiore L, Wagner H, Clarke K, Watkins H, Lygate CA, Neubauer S. Changes in creatine transporter function during cardiac maturation in the rat. *BMC Developmental Biology*. 2010;**10**:70.

33. Garcia-Delgado M, Peral MJ, Cano M, Calonge ML, Ilundain AA. Creatine transport in brush-border membrane vesicles isolated from rat kidney cortex. *Journal of the American Society of Nephrology : JASN*. 2001;**12**(9):1819-25.

34. Walzel B, Speer O, Boehm E, Kristiansen S, Chan S, Clarke K, Magyar JP, Richter EA, Wallimann T. New creatine transporter assay and identification of distinct creatine transporter isoforms in muscle. *American Journal of Physiology Endocrinology and metabolism*. 2002;**283**(2):E390-401.

35. Snow RJ, Murphy RM. Creatine and the creatine transporter: a review. *Molecular and Cellular Biochemistry*. 2001;**224**(1-2):169-81.

36. Marescau B, De Deyn P, Wiechert P, Van Gorp L, Lowenthal A. Comparative study of guanidino compounds in serum and brain of mouse, rat, rabbit, and man. *Journal of Neurochemistry*. 1986;**46**(3):717-20.

37. Murphy R, McConell G, Cameron-Smith D, Watt K, Ackland L, Walzel B, Wallimann T, Snow R. Creatine transporter protein content, localization, and gene expression in rat skeletal muscle. *American Journal of Physiology Cell Physiology*. 2001;**280**(3):C415-22.

38. Hemmer W, Riesinger I, Wallimann T, Eppenberger HM, Quest AF. Brain-type creatine kinase in photoreceptor cell outer segments: role of a phosphocreatine circuit in outer segment energy metabolism and phototransduction. *Journal of Cell Science*. 1993;**106 (Pt 2)**:671-83.

39. Straumann N, Wind A, Leuenberger T, Wallimann T. Effects of N-linked glycosylation on the creatine transporter. *Biochem J*. 2006;**393**(Pt 2):459-69.

40. Speer O, Neukomm LJ, Murphy RM, Zanolla E, Schlattner U, Henry H, Snow RJ, Wallimann T. Creatine transporters: a reappraisal. *Molecular and Cellular Biochemistry*. 2004;**256-257**(1-2):407-24.

41. Yamashita A, Singh SK, Kawate T, Jin Y, Gouaux E. Crystal structure of a bacterial homologue of Na+/Cl--dependent neurotransmitter transporters. *Nature*. 2005;**437**(7056):215-23.

42. Dodd JR, Christie DL. Cysteine 144 in the third transmembrane domain of the creatine transporter is located close to a substrate-binding site. *The Journal of Biological Chemistry*. 2001;**276**(50):46983-8.

43. Christie DL. Functional insights into the creatine transporter. *Sub-Cellular Biochemistry*. 2007;**46**:99-118.

44. Dodd JR, Christie DL. Substituted cysteine accessibility of the third transmembrane domain of the creatine transporter: defining a transport pathway. *The Journal of Biological Chemistry*. 2005;**280**(38):32649-54.

45. Blom N, Gammeltoft S, Brunak S. Sequence and structure-based prediction of eukaryotic protein phosphorylation sites. *J Mol Biol*. 1999;**294**(5):1351-62.

46. Corpet F. Multiple sequence alignment with hierarchical clustering. *Nucleic Acids Res*. 1988;**16**(22):10881-90.

47. Ireland Z, Russell AP, Wallimann T, Walker DW, Snow R. Developmental changes in the expression of creatine synthesizing enzymes and creatine transporter in a precocial rodent, the spiny mouse. *BMC Developmental Biology*. 2009;**9**:39.

48. ten Hove M, Makinen K, Sebag-Montefiore L, Hunyor I, Fischer A, Wallis J, Isbrandt D, Lygate C, Neubauer S. Creatine uptake in mouse hearts with genetically altered creatine levels. *Journal of Molecular and Cellular Cardiology*. 2008;**45**(3):453-9.

49. Kammermeier H, Schmidt P, Jungling E. Free energy change of ATP-hydrolysis: a causal factor of early hypoxic failure of the myocardium? *Journal of Molecular and Cellular Cardiology*. 1982;**14**(5):267-77.

50. Eppenberger HM, Dawson DM, Kaplan NO. The comparative enzymology of creatine kinases. I. Isolation and characterization from chicken and rabbit tissues. *The Journal of Biological Chemistry*. 1967;**242**(2):204-9.

51. Saupe KW, Spindler M, Tian R, Ingwall JS. Impaired cardiac energetics in mice lacking muscle-specific isoenzymes of creatine kinase. *Circ Res*. 1998;**82**(8):898-907.

52. Veksler VI, Kuznetsov AV, Anflous K, Mateo P, van Deursen J, Wieringa B, Ventura-Clapier R. Muscle creatine kinase-deficient mice. II. Cardiac and skeletal muscles exhibit tissue-specific adaptation of the mitochondrial function. *The Journal of Biological Chemistry*. 1995;**270**(34):19921-9.

53. Yoshizaki K, Watari H, Radda GK. Role of phosphocreatine in energy transport in skeletal muscle of bullfrog studied by 31P-NMR. *Biochimica et Biophysica Acta*. 1990;**1051**(2):144-50.

54. Wallimann T, Wyss M, Brdiczka D, Nicolay K, Eppenberger HM. Intracellular compartmentation, structure and function of creatine kinase isoenzymes in tissues with high and fluctuating energy demands: the 'phosphocreatine circuit' for cellular energy homeostasis. *Biochem J*. 1992;**281 (Pt 1)**:21-40.

55. Bessman SP, Geiger PJ. Transport of energy in muscle: the phosphorylcreatine shuttle. *Science*. 1981;**211**(4481):448-52.

56. Iyengar MR. Creatine kinase as an intracellular regulator. *Journal of Muscle Research and Cell Motility*. 1984;**5**(5):527-34.

57. Iyengar MR, Fluellen CE, Iyengar C. Creatine kinase from the bovine myometrium: purification and characterization. *Journal of Muscle Research and Cell Motility*. 1982;**3**(2):231-46.

58. Wyss M, Smeitink J, Wevers RA, Wallimann T. Mitochondrial creatine kinase: a key enzyme of aerobic energy metabolism. *Biochimica et Biophysica Acta*. 1992;**1102**(2):119-66.

59. Meyer RA, Sweeney HL, Kushmerick MJ. A simple analysis of the "phosphocreatine shuttle". *The American Journal of Physiology*. 1984;**246**(5 Pt 1):C365-77.

60. Saks VA, Chernousova GB, Gukovsky DE, Smirnov VN, Chazov EI. Studies of energy transport in heart cells. Mitochondrial isoenzyme of creatine phosphokinase: kinetic properties and regulatory action of $Mg2^{+}$ ions. *European Journal of Biochemistry / FEBS*. 1975;**57**(1):273-90.

61. Jacobus WE. Respiratory control and the integration of heart high-energy phosphate metabolism by mitochondrial creatine kinase. *Annual Review of Physiology*. 1985;**47**:707-25.

62. Saks VA, Khuchua ZA, Vasilyeva EV, Belikova O, Kuznetsov AV. Metabolic compartmentation and substrate channelling in muscle cells. Role of coupled creatine kinases in in vivo regulation of cellular respiration--a synthesis. *Molecular and Cellular Biochemistry*. 1994;**133-134**:155-92.

63. Ventura-Clapier R, Kuznetsov A, Veksler V, Boehm E, Anflous K. Functional coupling of creatine kinases in muscles: species and tissue specificity. *Molecular and Cellular Biochemistry*. 1998;**184**(1-2):231-47.

64. Wegmann G, Zanolla E, Eppenberger HM, Wallimann T. In situ compartmentation of creatine kinase in intact sarcomeric muscle: the acto-myosin overlap zone as a molecular sieve. *Journal of Muscle Research and Cell Motility*. 1992;**13**(4):420-35.

65. Dzeja PP, Terzic A. Phosphotransfer networks and cellular energetics. *The Journal of Experimental Biology*. 2003;**206**(Pt 12):2039-47.

66. Dzeja PP, Vitkevicius KT, Redfield MM, Burnett JC, Terzic A. Adenylate kinase-catalyzed phosphotransfer in the myocardium : increased contribution in heart failure. *Circ Res*. 1999;**84**(10):1137-43.

67. Van Rompay AR, Johansson M, Karlsson A. Identification of a novel human adenylate kinase. cDNA cloning, expression analysis, chromosome localization and characterization of the recombinant protein. *European Journal of Biochemistry / FEBS*. 1999;**261**(2):509-17.

68. Dzeja P, Terzic A. Adenylate kinase and AMP signaling networks: Metabolic monitoring, signal communication and body energy sensing. *International Journal of Molecular Sciences*. 2009;**10**(4):1729-72.

69. Tanabe T, Yamada M, Noma T, Kajii T, Nakazawa A. Tissue-specific and developmentally regulated expression of the genes encoding adenylate kinase isozymes. *Journal of Biochemistry*. 1993;**113**(2):200-7.

70. Carrasco AJ, Dzeja PP, Alekseev AE, Pucar D, Zingman LV, Abraham MR, Hodgson D, Bienengraeber M, Puceat M, Janssen E, Wieringa B, Terzic A. Adenylate kinase phosphotransfer communicates cellular energetic signals to ATP-sensitive potassium channels. *Proceedings of the National Academy of Sciences of the United States of America*. 2001;**98**(13):7623-8.

71. Dzeja PP, Zeleznikar RJ, Goldberg ND. Adenylate kinase: kinetic behavior in intact cells indicates it is integral to multiple cellular processes. *Molecular and Cellular Biochemistry*. 1998;**184**(1-2):169-82.

72. McMurray JJ, Pfeffer MA. Heart failure. *Lancet*. 2005;**365**(9474):1877-89.

73. Hunt SA, Abraham WT, Chin MH, Feldman AM, Francis GS, Ganiats TG, Jessup M, Konstam MA, Mancini DM, Michl K, Oates JA, Rahko PS, Silver MA, Stevenson LW, Yancy CW. 2009 focused update incorporated into the ACC/AHA 2005 Guidelines for the Diagnosis and Management of Heart Failure in Adults: a report of the American College of Cardiology Foundation/American Heart Association Task Force on Practice Guidelines: developed in collaboration with the International Society for Heart and Lung Transplantation. *Circulation*. 2009;**119**(14):e391-479.

74. Francis GS, Pierpont GL. Pathophysiology of congestive heart failure secondary to congestive and ischemic cardiomyopathy. *Cardiovascular Clinics*. 1988;**19**(1):57-74.

75. Kannel WB, Belanger AJ. Epidemiology of heart failure. *American Heart Journal*. 1991;**121**(3 Pt 1):951-7.

76. Murdoch DR, Love MP, Robb SD, McDonagh TA, Davie AP, Ford I, Capewell S, Morrison CE, McMurray JJ. Importance of heart failure as a cause of death. Changing contribution to overall mortality and coronary heart disease mortality in Scotland 1979-1992. *European Heart Journal*. 1998;**19**(12):1829-35.

77. Senni M, Tribouilloy CM, Rodeheffer RJ, Jacobsen SJ, Evans JM, Bailey KR, Redfield MM. Congestive heart failure in the community: trends in incidence and survival in a 10-year period. *Archives of Internal Medicine*. 1999;**159**(1):29-34.

78. Mendez GF, Cowie MR. The epidemiological features of heart failure in developing countries: a review of the literature. *International Journal of Cardiology*. 2001;**80**(2-3):213-9.

79. Dickstein K, Cohen-Solal A, Filippatos G, McMurray JJ, Ponikowski P, Poole-Wilson PA, Stromberg A, van Veldhuisen DJ, Atar D, Hoes AW, Keren A, Mebazaa A, Nieminen M, Priori SG, Swedberg K. ESC Guidelines for the diagnosis and treatment of acute and chronic heart failure 2008: the Task Force for the Diagnosis and Treatment of Acute and Chronic Heart Failure 2008 of the European Society of Cardiology. Developed in collaboration with the Heart Failure Association of the ESC (HFA) and endorsed by the European Society of Intensive Care Medicine (ESICM). *European Heart Journal*. 2008;**29**(19):2388-442.

80. Kelland NF, Webb DJ. Clinical trials of endothelin antagonists in heart failure: publication is good for the public health. *Heart*. 2007;**93**(1):2-4.

81. Ashrafian H, Frenneaux MP, Opie LH. Metabolic mechanisms in heart failure. *Circulation*. 2007;**116**(4):434-48.

82. Ingwall JS, Weiss RG. Is the failing heart energy starved? On using chemical energy to support cardiac function. *Circ Res*. 2004;**95**(2):135-45.

83. Neubauer S. The failing heart--an engine out of fuel. *The New England Journal of Medicine*. 2007;**356**(11):1140-51.

84. Smith CS, Bottomley PA, Schulman SP, Gerstenblith G, Weiss RG. Altered creatine kinase adenosine triphosphate kinetics in failing hypertrophied human myocardium. *Circulation*. 2006;**114**(11):1151-8.

85. Ventura-Clapier R, Garnier A, Veksler V. Energy metabolism in heart failure. *The Journal of Physiology*. 2004;**555**(Pt 1):1-13.

86. Ye Y, Gong G, Ochiai K, Liu J, Zhang J. High-energy phosphate metabolism and creatine kinase in failing hearts: a new porcine model. *Circulation*. 2001;**103**(11):1570-6.

87. Zhang J, Merkle H, Hendrich K, Garwood M, From AH, Ugurbil K, Bache RJ. Bioenergetic abnormalities associated with severe left ventricular hypertrophy. *The Journal of Clinical Investigation*. 1993;**92**(2):993-1003.

88. Markiewicz W, Wu SS, Parmley WW, Higgins CB, Sievers R, James TL, Wikman-Coffelt J, Jasmin G. Evaluation of the hereditary Syrian hamster cardiomyopathy by ^{31}P nuclear magnetic resonance spectroscopy: improvement after acute verapamil therapy. *Circ Res*. 1986;**59**(6):597-604.

89. Nascimben L, Friedrich J, Liao R, Pauletto P, Pessina AC, Ingwall JS. Enalapril treatment increases cardiac performance and energy reserve via the creatine kinase reaction in myocardium of Syrian myopathic hamsters with advanced heart failure. *Circulation*. 1995;**91**(6):1824-33.

90. Neubauer S, Horn M, Cramer M, Harre K, Newell JB, Peters W, Pabst T, Ertl G, Hahn D, Ingwall JS, Kochsiek K. Myocardial phosphocreatine-to-ATP ratio is a predictor of mortality in patients with dilated cardiomyopathy. *Circulation*. 1997;**96**(7):2190-6.

91. Neubauer S, Krahe T, Schindler R, Horn M, Hillenbrand H, Entzeroth C, Mader H, Kromer EP, Riegger GA, Lackner K, et al. ^{31}P magnetic resonance spectroscopy in dilated cardiomyopathy and coronary artery disease. Altered cardiac high-energy phosphate metabolism in heart failure. *Circulation*. 1992;**86**(6):1810-8.

92. Ten Hove M, Chan S, Lygate C, Monfared M, Boehm E, Hulbert K, Watkins H, Clarke K, Neubauer S. Mechanisms of creatine depletion in chronically failing rat heart. *Journal of Molecular and Cellular Cardiology*. 2005;**38**(2):309-13.

93. Neubauer S, Remkes H, Spindler M, Horn M, Wiesmann F, Prestle J, Walzel B, Ertl G, Hasenfuss G, Wallimann T. Downregulation of the Na(+)-creatine cotransporter in failing human myocardium and in experimental heart failure. *Circulation*. 1999;**100**(18):1847-50.

94. Wu F, Zhang J, Beard DA. Experimentally observed phenomena on cardiac energetics in heart failure emerge from simulations of cardiac metabolism. *Proceedings of the National Academy of Sciences of the United States of America*. 2009;**106**(17):7143-8.

95. Hardouin SN, Nagy A. Mouse models for human disease. *Clinical Genetics*. 2000;**57**(4):237-44.

96. Skelton MR, Schaefer TL, Graham DL, Degrauw TJ, Clark JF, Williams MT, Vorhees CV. Creatine transporter (CrT; Slc6a8) knockout mice as a model of human CrT deficiency. *PloS One*. 2011;**6**(1):e16187.

97. Wallis J, Lygate CA, Fischer A, ten Hove M, Schneider JE, Sebag-Montefiore L, Dawson D, Hulbert K, Zhang W, Zhang MH, Watkins H, Clarke K, Neubauer S. Supranormal myocardial creatine and phosphocreatine concentrations lead to cardiac hypertrophy and heart failure: insights from creatine transporter-overexpressing transgenic mice. *Circulation*. 2005;**112**(20):3131-9.

98. Schmidt A, Marescau B, Boehm EA, Renema WK, Peco R, Das A, Steinfeld R, Chan S, Wallis J, Davidoff M, Ullrich K, Waldschutz R, Heerschap A, De Deyn PP, Neubauer S, Isbrandt D. Severely altered guanidino compound levels, disturbed body weight homeostasis and impaired fertility in a mouse model of guanidinoacetate N-methyltransferase (GAMT) deficiency. *Human Molecular Genetics*. 2004;**13**(9):905-21.

99. Palmiter RD, Brinster RL. Transgenic mice. *Cell*. 1985;**41**(2):343-5.

100. Loike JD, Zalutsky DL, Kaback E, Miranda AF, Silverstein SC. Extracellular creatine regulates creatine transport in rat and human muscle cells. *Proceedings of the National Academy of Sciences of the United States of America*. 1988;**85**(3):807-11.

101. Liu J, Wang C, Murakami Y, Gong G, Ishibashi Y, Prody C, Ochiai K, Bache RJ, Godinot C, Zhang J. Mitochondrial ATPase and high-energy phosphates in failing hearts. *American Journal of Physiology Heart and Circulatory Physiology*. 2001;**281**(3):H1319-26.

102. Tian R, Nascimben L, Ingwall JS, Lorell BH. Failure to maintain a low ADP concentration impairs diastolic function in hypertrophied rat hearts. *Circulation*. 1997;**96**(4):1313-9.

103. Neubauer S. Cardiac magnetic resonance spectroscopy. *Current Cardiology Reports*. 2003;**5**(1):75-82.

104. Phillips D, Ten Hove M, Schneider JE, Wu CO, Sebag-Montefiore L, Aponte AM, Lygate CA, Wallis J, Clarke K, Watkins H, Balaban RS, Neubauer S. Mice over-expressing the myocardial creatine transporter develop progressive heart failure and show decreased glycolytic capacity. *Journal of Molecular and Cellular Cardiology*. 2010;**48**(4):582-90.

105. Glyn-Jones S, Song S, Black MA, Phillips AR, Choong SY, Cooper GJ. Transcriptomic analysis of the cardiac left ventricle in a rodent model of diabetic cardiomyopathy: molecular snapshot of a severe myocardial disease. *Physiological Genomics*. 2007;**28**(3):284-93.

106. Keller A, Rouzeau JD, Farhadian F, Wisnewsky C, Marotte F, Lamande N, Samuel JL, Schwartz K, Lazar M, Lucas M. Differential expression of alpha- and beta-enolase genes during rat heart development and hypertrophy. *The American Journal of Physiology*. 1995;**269**(6 Pt 2):H1843-51.

107. Saeedi R, Wambolt RB, Parsons H, Antler C, Leong HS, Keller A, Dunaway GA, Popov KM, Allard MF. Gender and post-ischemic recovery of hypertrophied rat hearts. *BMC Cardiovascular Disorders*. 2006;**6**:8.

108. Aasum E, Hafstad AD, Larsen TS. Changes in substrate metabolism in isolated mouse hearts following ischemia-reperfusion. *Molecular and Cellular Biochemistry*. 2003;**249**(1-2):97-103.

109. Neubauer S, Hu K, Horn M, Remkes H, Hoffmann KD, Schmidt C, Schmidt TJ, Schnackerz K, Ertl G. Functional and energetic consequences of chronic myocardial creatine depletion by beta-guanidinopropionate in perfused hearts and in intact rats. *Journal of Molecular and Cellular Cardiology*. 1999;**31**(10):1845-55.

110. Zweier JL, Jacobus WE, Korecky B, Brandejs-Barry Y. Bioenergetic consequences of cardiac phosphocreatine depletion induced by creatine analogue feeding. *The Journal of Biological Chemistry*. 1991;**266**(30):20296-304.

111. Kapelko VI, Saks VA, Novikova NA, Golikov MA, Kupriyanov VV, Popovich MI. Adaptation of cardiac contractile function to conditions of chronic energy deficiency. *Journal of Molecular and Cellular Cardiology*. 1989;**21 Suppl 1**:79-83.

112. Mekhfi H, Hoerter J, Lauer C, Wisnewsky C, Schwartz K, Ventura-Clapier R. Myocardial adaptation to creatine deficiency in rats fed with beta-guanidinopropionic acid, a creatine analogue. *The American Journal of Physiology*. 1990;**258**(4 Pt 2):H1151-8.

113. Shoubridge EA, Jeffry FM, Keogh JM, Radda GK, Seymour AM. Creatine kinase kinetics, ATP turnover, and cardiac performance in hearts depleted of creatine with the substrate analogue beta-guanidinopropionic acid. *Biochimica et Biophysica Acta*. 1985;**847**(1):25-32.

114. ten Hove M, Lygate CA, Fischer A, Schneider JE, Sang AE, Hulbert K, Sebag-Montefiore L, Watkins H, Clarke K, Isbrandt D, Wallis J, Neubauer S. Reduced inotropic reserve and increased susceptibility to cardiac ischemia/reperfusion injury in phosphocreatine-deficient guanidinoacetate-*N*-methyltransferase-knockout mice. *Circulation*. 2005;**111**(19):2477-85.

115. van Deursen J, Heerschap A, Oerlemans F, Ruitenbeek W, Jap P, ter Laak H, Wieringa B. Skeletal muscles of mice deficient in muscle creatine kinase lack burst activity. *Cell*. 1993;**74**(4):621-31.

116. Steeghs K, Heerschap A, de Haan A, Ruitenbeek W, Oerlemans F, van Deursen J, Perryman B, Pette D, Bruckwilder M, Koudijs J, Jap P, Wieringa B. Use of gene targeting for compromising energy homeostasis in neuro-muscular tissues: the role of sarcomeric mitochondrial creatine kinase. *Journal of Neuroscience Methods*. 1997;**71**(1):29-41.

117. Steeghs K, Benders A, Oerlemans F, de Haan A, Heerschap A, Ruitenbeek W, Jost C, van Deursen J, Perryman B, Pette D, Bruckwilder M, Koudijs J, Jap P, Veerkamp J, Wieringa B. Altered Ca^{2+} responses in muscles with combined mitochondrial and cytosolic creatine kinase deficiencies. *Cell*. 1997;**89**(1):93-103.

118. Momken I, Lechene P, Koulmann N, Fortin D, Mateo P, Doan BT, Hoerter J, Bigard X, Veksler V, Ventura-Clapier R. Impaired voluntary running capacity of creatine kinase-deficient mice. *The Journal of Physiology*. 2005;**565**(Pt 3):951-64.

119. Spindler M, Niebler R, Remkes H, Horn M, Lanz T, Neubauer S. Mitochondrial creatine kinase is critically necessary for normal myocardial high-energy phosphate metabolism. *American Journal of Physiology Heart and Circulatory Physiology*. 2002;**283**(2):H680-7.

120. Boehm E, Veksler V, Mateo P, Lenoble C, Wieringa B, Ventura-Clapier R. Maintained coupling of oxidative phosphorylation to creatine kinase activity in sarcomeric mitochondrial creatine kinase-deficient mice. *Journal of Molecular and Cellular Cardiology*. 1998;**30**(5):901-12.

121. Bonz AW, Kniesch S, Hofmann U, Kullmer S, Bauer L, Wagner H, Ertl G, Spindler M. Functional properties and [$Ca(^{2+})$](i) metabolism of creatine $kinase^{-/-}$KO mice myocardium. *Biochemical and Biophysical Research Communications*. 2002;**298**(1):163-8.

122. Spindler M, Meyer K, Stromer H, Leupold A, Boehm E, Wagner H, Neubauer S. Creatine kinase-deficient hearts exhibit increased susceptibility to ischemia-reperfusion injury and impaired calcium homeostasis. *American Journal of Physiology Heart and Circulatory Physiology*. 2004;**287**(3):H1039-45.

123. Nahrendorf M, Spindler M, Hu K, Bauer L, Ritter O, Nordbeck P, Quaschning T, Hiller KH, Wallis J, Ertl G, Bauer WR, Neubauer S. Creatine kinase knockout mice show left ventricular hypertrophy and dilatation, but unaltered remodeling post-myocardial infarction. *Cardiovascular Research*. 2005;**65**(2):419-27.

124. Boehm E, Ventura-Clapier R, Mateo P, Lechene P, Veksler V. Glycolysis supports calcium uptake by the sarcoplasmic reticulum in skinned ventricular fibres of mice deficient in mitochondrial and cytosolic creatine kinase. *Journal of Molecular and Cellular Cardiology*. 2000;**32**(6):891-902.

125. Gustafson LA, Van Beek JH. Activation time of myocardial oxidative phosphorylation in creatine kinase and adenylate kinase knockout mice. *American Journal of Physiology Heart and Circulatory Physiology*. 2002;**282**(6):H2259-64.

126. Lygate CA, Hunyor I, Medway D, de Bono JP, Dawson D, Wallis J, Sebag-Montefiore L, Neubauer S. Cardiac phenotype of mitochondrial creatine kinase knockout mice is modified on a pure C57BL/6 genetic background. *Journal of Molecular and Cellular Cardiology*. 2009;**46**(1):93-9.

127. Nahrendorf M, Streif JU, Hiller KH, Hu K, Nordbeck P, Ritter O, Sosnovik D, Bauer L, Neubauer S, Jakob PM, Ertl G, Spindler M, Bauer WR. Multimodal functional cardiac MRI in creatine kinase-deficient mice reveals subtle abnormalities in myocardial perfusion and mechanics. *American Journal of Physiology Heart and Circulatory Physiology*. 2006;**290**(6):H2516-21.

128. Dzeja PP, Hoyer K, Tian R, Zhang S, Nemutlu E, Spindler M, Ingwall JS. Rearrangement of energetic and substrate utilization networks compensate for chronic myocardial creatine kinase deficiency. *The Journal of Physiology*. 2011;**589**(Pt 21):5193-211.

129. Claycomb WC, Lanson NA, Jr., Stallworth BS, Egeland DB, Delcarpio JB, Bahinski A, Izzo NJ, Jr. HL-1 cells: a cardiac muscle cell line that contracts and retains phenotypic characteristics of the adult cardiomyocyte. *Proceedings of the National Academy of Sciences of the United States of America*. 1998;**95**(6):2979-84.

130. White SM, Constantin PE, Claycomb WC. Cardiac physiology at the cellular level: use of cultured HL-1 cardiomyocytes for studies of cardiac muscle cell structure and function. *American Journal of Physiology Heart and Circulatory Physiology*. 2004;**286**(3):H823-9.

131. Wang X, Seed B. A PCR primer bank for quantitative gene expression analysis. *Nucleic Acids Res*. 2003;**31**(24):e154.

132. Laborda J. 36B4 cDNA used as an estradiol-independent mRNA control is the cDNA for human acidic ribosomal phosphoprotein PO. *Nucleic Acids Res*. 1991;**19**(14):3998.

133. Church GM, Gilbert W. Genomic sequencing. *Proceedings of the National Academy of Sciences of the United States of America*. 1984;**81**(7):1991-5.

134. Lowry OH, Rosebrough NJ, Farr AL, Randall RJ. Protein measurement with the Folin phenol reagent. *The Journal of Biological Chemistry*. 1951;**193**(1):265-75.

135. O'Brien TX, Lee KJ, Chien KR. Positional specification of ventricular myosin light chain 2 expression in the primitive murine heart tube. *Proceedings of the National Academy of Sciences of the United States of America*. 1993;**90**(11):5157-61.

136. Feil R, Brocard J, Mascrez B, LeMeur M, Metzger D, Chambon P. Ligand-activated site-specific recombination in mice. *Proceedings of the National Academy of Sciences of the United States of America*. 1996;**93**(20):10887-90.

137. Petrich BG, Molkentin JD, Wang Y. Temporal activation of c-Jun N-terminal kinase in adult transgenic heart via cre-loxP-mediated DNA recombination. *The FASEB journal : official*

publication of the Federation of American Societies for Experimental Biology. 2003;**17**(6):749-51.

138. Koitabashi N, Bedja D, Zaiman AL, Pinto YM, Zhang M, Gabrielson KL, Takimoto E, Kass DA. Avoidance of transient cardiomyopathy in cardiomyocyte-targeted tamoxifen-induced MerCreMer gene deletion models. *Circ Res*. 2009;**105**(1):12-5.

139. Gossen M, Bujard H. Tight control of gene expression in mammalian cells by tetracycline-responsive promoters. *Proceedings of the National Academy of Sciences of the United States of America*. 1992;**89**(12):5547-51.

140. Baron U, Bujard H. Tet repressor-based system for regulated gene expression in eukaryotic cells: principles and advances. *Methods Enzymol*. 2000;**327**:401-21.

141. Gossen M, Freundlieb S, Bender G, Muller G, Hillen W, Bujard H. Transcriptional activation by tetracyclines in mammalian cells. *Science*. 1995;**268**(5218):1766-9.

142. Yutzey KE, Robbins J. Principles of genetic murine models for cardiac disease. *Circulation*. 2007;**115**(6):792-9.

143. Curci JA, Mao D, Bohner DG, Allen BT, Rubin BG, Reilly JM, Sicard GA, Thompson RW. Preoperative treatment with doxycycline reduces aortic wall expression and activation of matrix metalloproteinases in patients with abdominal aortic aneurysms. *Journal of Vascular Surgery : official publication, the Society for Vascular Surgery [and] International Society for Cardiovascular Surgery, North American Chapter*. 2000;**31**(2):325-42.

144. Vinet L, Rouet-Benzineb P, Marniquet X, Pellegrin N, Mangin L, Louedec L, Samuel JL, Mercadier JJ. Chronic doxycycline exposure accelerates left ventricular hypertrophy and progression to heart failure in mice after thoracic aorta constriction. *American Journal of Physiology Heart and Circulatory Physiology*. 2008;**295**(1):H352-60.

145. McCloskey DT, Turnbull L, Swigart PM, Zambon AC, Turcato S, Joho S, Grossman W, Conklin BR, Simpson PC, Baker AJ. Cardiac transgenesis with the tetracycline transactivator changes myocardial function and gene expression. *Physiol Genomics*. 2005;**22**(1):118-26.

146. Turnbull L, Zhou HZ, Swigart PM, Turcato S, Karliner JS, Conklin BR, Simpson PC, Baker AJ. Sustained preconditioning induced by cardiac transgenesis with the tetracycline transactivator. *American Journal of Physiology Heart and Circulatory Physiology*. 2006;**290**(3):H1103-9.

147. Sanbe A, Gulick J, Hanks MC, Liang Q, Osinska H, Robbins J. Reengineering inducible cardiac-specific transgenesis with an attenuated myosin heavy chain promoter. *Circ Res*. 2003;**92**(6):609-16.

148. Kistner A, Gossen M, Zimmermann F, Jerecic J, Ullmer C, Lubbert H, Bujard H. Doxycycline-mediated quantitative and tissue-specific control of gene expression in transgenic mice. *Proceedings of the National Academy of Sciences of the United States of America*. 1996;**93**(20):10933-8.

149. Hasan MT, Schonig K, Berger S, Graewe W, Bujard H. Long-term, noninvasive imaging of regulated gene expression in living mice. *Genesis*. 2001;**29**(3):116-22.

150. Pham DH, Moretti PA, Goodall GJ, Pitson SM. Attenuation of leakiness in doxycycline-inducible expression via incorporation of 3' AU-rich mRNA destabilizing elements. *Biotechniques*. 2008;**45**(2):155-6, 8, 60 passim.

151. Forster K, Helbl V, Lederer T, Urlinger S, Wittenburg N, Hillen W. Tetracycline-inducible expression systems with reduced basal activity in mammalian cells. *Nucleic Acids Res*. 1999;**27**(2):708-10.

152. Uchida S, Sakai S, Furuichi T, Hosoda H, Toyota K, Ishii T, Kitamoto A, Sekine M, Koike K, Masushige S, Murphy G, Silva AJ, Kida S. Tight regulation of transgene expression by tetracycline-dependent activator and repressor in brain. *Genes Brain Behav*. 2006;**5**(1):96-106.

153. Zhu Z, Zheng T, Lee CG, Homer RJ, Elias JA. Tetracycline-controlled transcriptional regulation systems: advances and application in transgenic animal modeling. *Semin Cell Dev Biol*. 2002;**13**(2):121-8.

154. Masui S, Shimosato D, Toyooka Y, Yagi R, Takahashi K, Niwa H. An efficient system to establish multiple embryonic stem cell lines carrying an inducible expression unit. *Nucleic Acids Res*. 2005;**33**(4):e43.

155. Qu Z, Thottassery JV, Van Ginkel S, Manuvakhova M, Westbrook L, Roland-Lazenby C, Hays S, Kern FG. Homogeneity and long-term stability of tetracycline-regulated gene expression with low basal activity by using the rtTA2S-M2 transactivator and insulator-flanked reporter vectors. *Gene*. 2004;**327**(1):61-73.

156. Premsrirut PK, Dow LE, Kim SY, Camiolo M, Malone CD, Miething C, Scuoppo C, Zuber J, Dickins RA, Kogan SC, Shroyer KR, Sordella R, Hannon GJ, Lowe SW. A rapid and scalable system for studying gene function in mice using conditional RNA interference. *Cell*. 2011;**145**(1):145-58.

157. Dorn R, Krauss V, Reuter G, Saumweber H. The enhancer of position-effect variegation of Drosophila, E(var)3-93D, codes for a chromatin protein containing a conserved domain common to several transcriptional regulators. *Proceedings of the National Academy of Sciences of the United States of America*. 1993;**90**(23):11376-80.

158. Eissenberg JC. Position effect variegation in Drosophila: towards a genetics of chromatin assembly. *BioEssays : News and Reviews in Molecular, Cellular and Developmental Biology*. 1989;**11**(1):14-7.

159. West AG, Gaszner M, Felsenfeld G. Insulators: many functions, many mechanisms. *Genes & Development*. 2002;**16**(3):271-88.

160. Giraldo P, Rival-Gervier S, Houdebine LM, Montoliu L. The potential benefits of insulators on heterologous constructs in transgenic animals. *Transgenic Research*. 2003;**12**(6):751-5.

161. Guglielmi L, Truffinet V, Carrion C, Le Bert M, Cogne N, Cogne M, Denizot Y. The 5'HS4 insulator element is an efficient tool to analyse the transient expression of an Em mu-GFP vector in a transgenic mouse model. *Transgenic Research*. 2005;**14**(4):361-4.

162. Kaffer CR, Srivastava M, Park KY, Ives E, Hsieh S, Batlle J, Grinberg A, Huang SP, Pfeifer K. A transcriptional insulator at the imprinted H19/Igf2 locus. *Genes & Development*. 2000;**14**(15):1908-19.

163. Bell AC, Felsenfeld G. Methylation of a CTCF-dependent boundary controls imprinted expression of the Igf2 gene. *Nature*. 2000;**405**(6785):482-5.

164. Potzner MR, Griffel C, Lutjen-Drecoll E, Bosl MR, Wegner M, Sock E. Prolonged Sox4 expression in oligodendrocytes interferes with normal myelination in the central nervous system. *Mol Cell Biol*. 2007;**27**(15):5316-26.

165. Wei BR, Martin PL, Hoover SB, Spehalski E, Kumar M, Hoenerhoff MJ, Rozenberg J, Vinson C, Simpson RM. Capacity for resolution of Ras-MAPK-initiated early pathogenic myocardial hypertrophy modeled in mice. *Comparative Medicine*. 2011;**61**(2):109-18.

166. Lu S, Crawford GL, Dore J, Anderson SA, Despres D, Horowits R. Cardiac-specific NRAP overexpression causes right ventricular dysfunction in mice. *Experimental Cell Research*. 2011;**317**(8):1226-37.

167. Redfern CH, Coward P, Degtyarev MY, Lee EK, Kwa AT, Hennighausen L, Bujard H, Fishman GI, Conklin BR. Conditional expression and signaling of a specifically designed Gi-coupled receptor in transgenic mice. *Nature Biotechnology*. 1999;**17**(2):165-9.

168. Dor Y, Djonov V, Abramovitch R, Itin A, Fishman GI, Carmeliet P, Goelman G, Keshet E. Conditional switching of VEGF provides new insights into adult neovascularization and pro-angiogenic therapy. *The EMBO Journal*. 2002;**21**(8):1939-47.

169. Yang LL, Gros R, Kabir MG, Sadi A, Gotlieb AI, Husain M, Stewart DJ. Conditional cardiac overexpression of endothelin-1 induces inflammation and dilated cardiomyopathy in mice. *Circulation*. 2004;**109**(2):255-61.

170. Yu Z, Redfern CS, Fishman GI. Conditional transgene expression in the heart. *Circ Res*. 1996;**79**(4):691-7.

171. Subramaniam A, Jones WK, Gulick J, Wert S, Neumann J, Robbins J. Tissue-specific regulation of the alpha-myosin heavy chain gene promoter in transgenic mice. *The Journal of Biological Chemistry*. 1991;**266**(36):24613-20.

172. Johnson JE, Wold BJ, Hauschka SD. Muscle creatine kinase sequence elements regulating skeletal and cardiac muscle expression in transgenic mice. *Mol Cell Biol*. 1989;**9**(8):3393-9.

173. Bruning JC, Michael MD, Winnay JN, Hayashi T, Horsch D, Accili D, Goodyear LJ, Kahn CR. A muscle-specific insulin receptor knockout exhibits features of the metabolic syndrome of NIDDM without altering glucose tolerance. *Molecular Cell*. 1998;**2**(5):559-69.

174. Wu B, Zhou B, Wang Y, Cheng HL, Hang CT, Pu WT, Chang CP. Inducible cardiomyocyte-specific gene disruption directed by the rat Tnnt2 promoter in the mouse. *Genesis*. 2010;**48**(1):63-72.

175. Ng WA, Grupp IL, Subramaniam A, Robbins J. Cardiac myosin heavy chain mRNA expression and myocardial function in the mouse heart. *Circ Res*. 1991;**68**(6):1742-50.

176. Lyons GE, Schiaffino S, Sassoon D, Barton P, Buckingham M. Developmental regulation of myosin gene expression in mouse cardiac muscle. *The Journal of Cell Biology*. 1990;**111**(6 Pt 1):2427-36.

177. Izumo S, Lompre AM, Matsuoka R, Koren G, Schwartz K, Nadal-Ginard B, Mahdavi V. Myosin heavy chain messenger RNA and protein isoform transitions during cardiac hypertrophy. Interaction between hemodynamic and thyroid hormone-induced signals. *The Journal of Clinical Investigation*. 1987;**79**(3):970-7.

178. Molkentin JD, Robbins J. With great power comes great responsibility: using mouse genetics to study cardiac hypertrophy and failure. *Journal of Molecular and Cellular Cardiology*. 2009;**46**(2):130-6.

179. Niman HL, Houghten RA, Walker LE, Reisfeld RA, Wilson IA, Hogle JM, Lerner RA. Generation of protein-reactive antibodies by short peptides is an event of high frequency: implications for the structural basis of immune recognition. *Proceedings of the National Academy of Sciences of the United States of America*. 1983;**80**(16):4949-53.

180. Coccaro E, Mraiche F, Malo M, Vandertol-Vanier H, Bullis B, Robertson M, Fliegel L. Expression and characterization of the Na^+/H^+ exchanger in the mammalian myocardium. *Molecular and Cellular Biochemistry*. 2007;**302**(1-2):145-55.

181. Fazakerley DJ, Lawrence SP, Lizunov VA, Cushman SW, Holman GD. A common trafficking route for GLUT4 in cardiomyocytes in response to insulin, contraction and energy-status signalling. *Journal of Cell Science*. 2009;**122**(Pt 5):727-34.

182. Valencik ML, McDonald JA. Codon optimization markedly improves doxycycline regulated gene expression in the mouse heart. *Transgenic Research*. 2001;**10**(3):269-75.

183. Schonig K, Schwenk F, Rajewsky K, Bujard H. Stringent doxycycline dependent control of CRE recombinase *in vivo*. *Nucleic Acids Res*. 2002;**30**(23):e134.

184. Manthorpe M, Cornefert-Jensen F, Hartikka J, Felgner J, Rundell A, Margalith M, Dwarki V. Gene therapy by intramuscular injection of plasmid DNA: studies on firefly luciferase gene expression in mice. *Human Gene Therapy*. 1993;**4**(4):419-31.

185. Robertson A, Perea J, Tolmachova T, Thomas PK, Huxley C. Effects of mouse strain, position of integration and tetracycline analogue on the tetracycline conditional system in transgenic mice. *Gene*. 2002;**282**(1-2):65-74.

186. Juhila J, Roozendaal R, Lassila M, Verbeek SJ, Holthofer H. Podocyte cell-specific expression of doxycycline inducible Cre recombinase in mice. *Journal of the American Society of Nephrology : JASN*. 2006;**17**(3):648-54.

187. Bowman JC, Steinberg SF, Jiang T, Geenen DL, Fishman GI, Buttrick PM. Expression of protein kinase C beta in the heart causes hypertrophy in adult mice and sudden death in neonates. *The Journal of Clinical Investigation*. 1997;**100**(9):2189-95.

188. Russell LK, Mansfield CM, Lehman JJ, Kovacs A, Courtois M, Saffitz JE, Medeiros DM, Valencik ML, McDonald JA, Kelly DP. Cardiac-specific induction of the transcriptional coactivator peroxisome proliferator-activated receptor γ coactivator-1α promotes mitochondrial biogenesis and reversible cardiomyopathy in a developmental stage-dependent manner. *Circ Res*. 2004;**94**(4):525-33.

189. Lee HG, Chen Q, Wolfram JA, Richardson SL, Liner A, Siedlak SL, Zhu X, Ziats NP, Fujioka H, Felsher DW, Castellani RJ, Valencik ML, McDonald JA, Hoit BD, Lesnefsky EJ, Smith MA. Cell cycle re-entry and mitochondrial defects in myc-mediated hypertrophic cardiomyopathy and heart failure. *PLoS One*. 2009;**4**(9):e7172.

190. Furth PA, St Onge L, Boger H, Gruss P, Gossen M, Kistner A, Bujard H, Hennighausen L. Temporal control of gene expression in transgenic mice by a tetracycline-responsive promoter. *Proceedings of the National Academy of Sciences of the United States of America*. 1994;**91**(20):9302-6.

191. Snow RJ, McKenna MJ, Carey MF, Hargreaves M. Sprint training attenuates plasma ammonia accumulation following maximal exercise. *Acta Physiologica Scandinavica*. 1992;**144**(3):395-6.

192. Fitch CD, Shields RP, Payne WF, Dacus JM. Creatine metabolism in skeletal muscle. 3. Specificity of the creatine entry process. *The Journal of Biological Chemistry*. 1968;**243**(8):2024-7.

193. Haugland RB, Chang DT. Insulin effect on creatine transport in skeletal muscle (38464). *Proceedings of the Society for Experimental Biology and Medicine Society for Experimental Biology and Medicine*. 1975;**148**(1):1-4.

194. Koszalka TR, Andrew CL, Brent RL. Effect of insulin on the uptake of creatine-1- ^{14}C by skeletal muscle in normal and x-irradiated rats. *Proceedings of the Society for Experimental Biology and Medicine Society for Experimental Biology and Medicine*. 1972;**139**(4):1265-71.

195. Steenge GR, Lambourne J, Casey A, Macdonald IA, Greenhaff PL. Stimulatory effect of insulin on creatine accumulation in human skeletal muscle. *The American Journal of Physiology*. 1998;**275**(6 Pt 1):E974-9.

196. Clausen T, Hansen O. Active Na-K transport and the rate of ouabain binding. The effect of insulin and other stimuli on skeletal muscle and adipocytes. *The Journal of Physiology*. 1977;**270**(2):415-30.

197. Clausen T, Flatman JA. The effect of catecholamines on Na-K transport and membrane potential in rat soleus muscle. *The Journal of Physiology*. 1977;**270**(2):383-414.

198. Clausen T. Clinical and therapeutic significance of the Na^+,K^+ pump*. *Clinical Science*. 1998;**95**(1):3-17.

199. Marette A, Krischer J, Lavoie L, Ackerley C, Carpentier JL, Klip A. Insulin increases the Na($^+$)-K($^+$)-ATPase alpha 2-subunit in the surface of rat skeletal muscle: morphological evidence. *The American Journal of Physiology*. 1993;**265**(6 Pt 1):C1716-22.

200. Humbel RE. Insulin-like growth factors I and II. *European Journal of Biochemistry / FEBS*. 1990;**190**(3):445-62.

201. Lang F, Bohmer C, Palmada M, Seebohm G, Strutz-Seebohm N, Vallon V. (Patho)physiological significance of the serum- and glucocorticoid-inducible kinase isoforms. *Physiological Reviews*. 2006;**86**(4):1151-78.

202. Shojaiefard M, Christie DL, Lang F. Stimulation of the creatine transporter SLC6A8 by the protein kinases SGK1 and SGK3. *Biochemical and Biophysical Research Communications*. 2005;**334**(3):742-6.

203. Waldegger S, Barth P, Raber G, Lang F. Cloning and characterization of a putative human serine/threonine protein kinase transcriptionally modified during anisotonic and isotonic alterations of cell volume. *Proceedings of the National Academy of Sciences of the United States of America*. 1997;**94**(9):4440-5.

204. Berwick DC, Dell GC, Welsh GI, Heesom KJ, Hers I, Fletcher LM, Cooke FT, Tavare JM. Protein kinase B phosphorylation of PIKfyve regulates the trafficking of GLUT4 vesicles. *Journal of Cell Science*. 2004;**117**(Pt 25):5985-93.

205. Strutz-Seebohm N, Shojaiefard M, Christie D, Tavare J, Seebohm G, Lang F. PIKfyve in the SGK1 mediated regulation of the creatine transporter SLC6A8. *Cellular Physiology and Biochemistry : International Journal of Experimental Cellular Physiology, Biochemistry, and Pharmacology*. 2007;**20**(6):729-34.

206. Brault JJ, Terjung RL. Creatine uptake and creatine transporter expression among rat skeletal muscle fiber types. *American Journal of Physiology Cell Physiology*. 2003;**284**(6):C1481-9.

207. Willott CA, Young ME, Leighton B, Kemp GJ, Boehm EA, Radda GK, Clarke K. Creatine uptake in isolated soleus muscle: kinetics and dependence on sodium, but not on insulin. *Acta Physiologica Scandinavica*. 1999;**166**(2):99-104.

208. Cittadini A, Grossman JD, Napoli R, Katz SE, Stromer H, Smith RJ, Clark R, Morgan JP, Douglas PS. Growth hormone attenuates early left ventricular remodeling and improves cardiac function in rats with large myocardial infarction. *Journal of the American College of Cardiology*. 1997;**29**(5):1109-16.

209. Kanashiro-Takeuchi RM, Tziomalos K, Takeuchi LM, Treuer AV, Lamirault G, Dulce R, Hurtado M, Song Y, Block NL, Rick F, Klukovits A, Hu Q, Varga JL, Schally AV, Hare JM. Cardioprotective effects of growth hormone-releasing hormone agonist after myocardial infarction. *Proceedings of the National Academy of Sciences of the United States of America*. 2010;**107**(6):2604-9.

210. Omerovic E, Bollano E, Lorentzon M, Walser M, Mattsson-Hulten L, Isgaard J. Growth hormone induces myocardial expression of creatine transporter and decreases plasma levels of IL-1β in rats during early postinfarct cardiac remodeling. *Growth hormone & IGF research : official journal of the Growth Hormone Research Society and the International IGF Research Society*. 2003;**13**(5):239-45.

211. Cittadini A, Ishiguro Y, Stromer H, Spindler M, Moses AC, Clark R, Douglas PS, Ingwall JS, Morgan JP. Insulin-like growth factor-1 but not growth hormone augments mammalian myocardial contractility by sensitizing the myofilament to $Ca2^{+}$ through a wortmannin-sensitive pathway: studies in rat and ferret isolated muscles. *Circ Res*. 1998;**83**(1):50-9.

212. Kontoleon PE, Anastasiou-Nana MI, Papapetrou PD, Alexopoulos G, Ktenas V, Rapti AC, Tsagalou EP, Nanas JN. Hormonal profile in patients with congestive heart failure. *International Journal of Cardiology*. 2003;**87**(2-3):179-83.

213. Fazio S, Sabatini D, Capaldo B, Vigorito C, Giordano A, Guida R, Pardo F, Biondi B, Sacca L. A preliminary study of growth hormone in the treatment of dilated cardiomyopathy. *The New England Journal of Medicine*. 1996;**334**(13):809-14.

214. Mayser W, Schloss P, Betz H. Primary structure and functional expression of a choline transporter expressed in the rat nervous system. *FEBS Letters*. 1992;**305**(1):31-6.

215. Balasubramanian S, Johnston RK, Moschella PC, Mani SK, Tuxworth WJ, Jr., Kuppuswamy D. mTOR in growth and protection of hypertrophying myocardium. *Cardiovascular & Hematological Agents in Medicinal Chemistry*. 2009;**7**(1):52-63.

216. Kurdi M, Booz GW. Three 4-letter words of hypertension-related cardiac hypertrophy: TRPC, mTOR, and HDAC. *Journal of Molecular and Cellular Cardiology*. 2011;**50**(6):964-71.

217. Shojaiefard M, Christie DL, Lang F. Stimulation of the creatine transporter SLC6A8 by the protein kinase mTOR. *Biochemical and Biophysical Research Communications*. 2006;**341**(4):945-9.

218. Shaw RJ, Bardeesy N, Manning BD, Lopez L, Kosmatka M, DePinho RA, Cantley LC. The LKB1 tumor suppressor negatively regulates mTOR signaling. *Cancer Cell*. 2004;**6**(1):91-9.

219. Darrabie MD, Arciniegas AJ, Mishra R, Bowles DE, Jacobs DO, Santacruz L. AMPK and substrate availability regulate creatine transport in cultured cardiomyocytes. *American Journal of Physiology Endocrinology and Metabolism*. 2011;**300**(5):E870-6.

220. Chijiwa T, Mishima A, Hagiwara M, Sano M, Hayashi K, Inoue T, Naito K, Toshioka T, Hidaka H. Inhibition of forskolin-induced neurite outgrowth and protein phosphorylation by a newly synthesized selective inhibitor of cyclic AMP-dependent protein kinase, N-[2-(p-bromocinnamylamino)ethyl]-5-isoquinolinesulfonamide (H-89), of PC12D pheochromocytoma cells. *The Journal of Biological Chemistry*. 1990;**265**(9):5267-72.

221. Martiny-Baron G, Kazanietz MG, Mischak H, Blumberg PM, Kochs G, Hug H, Marme D, Schachtele C. Selective inhibition of protein kinase C isozymes by the indolocarbazole Go 6976. *The Journal of Biological Chemistry*. 1993;**268**(13):9194-7.

222. Jorgensen K, Skrede M, Cruciani V, Mikalsen SO, Slipicevic A, Florenes VA. Phorbol ester phorbol-12-myristate-13-acetate promotes anchorage-independent growth and survival of melanomas through MEK-independent activation of ERK1/2. *Biochem Biophys Res Commun*. 2005;**329**(1):266-74.

223. Geiges D, Meyer T, Marte B, Vanek M, Weissgerber G, Stabel S, Pfeilschifter J, Fabbro D, Huwiler A. Activation of protein kinase C subtypes alpha, gamma, delta, epsilon, zeta, and eta by tumor-promoting and nontumor-promoting agents. *Biochemical Pharmacology*. 1997;**53**(6):865-75.

224. Leung-Pineda V, Ryan CE, Piwnica-Worms H. Phosphorylation of Chk1 by ATR is antagonized by a Chk1-regulated protein phosphatase 2A circuit. *Mol Cell Biol*. 2006;**26**(20):7529-38.

225. Shah BH, Olivares-Reyes JA, Catt KJ. The protein kinase C inhibitor Go6976 [12-(2-cyanoethyl)-6,7,12,13-tetrahydro-13-methyl-5-oxo-5H-indolo(2,3-a)pyrrolo(3 ,4-c)-carbazole] potentiates agonist-induced mitogen-activated protein kinase activation through tyrosine phosphorylation of the epidermal growth factor receptor. *Molecular Pharmacology*. 2005;**67**(1):184-94.

226. Swan JW, Walton C, Godsland IF, Clark AL, Coats AJ, Oliver MF. Insulin resistance in chronic heart failure. *European Heart Journal*. 1994;**15**(11):1528-32.

227. Paolisso G, De Riu S, Marrazzo G, Verza M, Varricchio M, D'Onofrio F. Insulin resistance and hyperinsulinemia in patients with chronic congestive heart failure. *Metabolism: Clinical and Experimental*. 1991;**40**(9):972-7.

228. Schulze PC, Biolo A, Gopal D, Shahzad K, Balog J, Fish M, Siwik D, Colucci WS. Dynamics in insulin resistance and plasma levels of adipokines in patients with acute decompensated and chronic stable heart failure. *Journal of Cardiac Failure*. 2011;**17**(12):1004-11.

229. Swan JW, Anker SD, Walton C, Godsland IF, Clark AL, Leyva F, Stevenson JC, Coats AJ. Insulin resistance in chronic heart failure: relation to severity and etiology of heart failure. *Journal of the American College of Cardiology*. 1997;**30**(2):527-32.

230. Pi Y, Goldenthal MJ, Marin-Garcia J. Mitochondrial involvement in IGF-1 induced protection of cardiomyocytes against hypoxia/reoxygenation injury. *Molecular and Cellular Biochemistry*. 2007;**301**(1-2):181-9.

231. Vinciguerra M, Santini MP, Claycomb WC, Ladurner AG, Rosenthal N. Local IGF-1 isoform protects cardiomyocytes from hypertrophic and oxidative stresses via SirT1 activity. *Aging*. 2010;**2**(1):43-62.

232. Menu E, Jernberg-Wiklund H, Stromberg T, De Raeve H, Girnita L, Larsson O, Axelson M, Asosingh K, Nilsson K, Van Camp B, Vanderkerken K. Inhibiting the IGF-1 receptor tyrosine kinase with the cyclolignan PPP: an in vitro and in vivo study in the 5T33MM mouse model. *Blood*. 2006;**107**(2):655-60.

233. Stromberg T, Ekman S, Girnita L, Dimberg LY, Larsson O, Axelson M, Lennartsson J, Hellman U, Carlson K, Osterborg A, Vanderkerken K, Nilsson K, Jernberg-Wiklund H. IGF-1 receptor tyrosine kinase inhibition by the cyclolignan PPP induces G2/M-phase accumulation and apoptosis in multiple myeloma cells. *Blood*. 2006;**107**(2):669-78.

234. Vasilcanu R, Vasilcanu D, Rosengren L, Natalishvili N, Sehat B, Yin S, Girnita A, Axelson M, Girnita L, Larsson O. Picropodophyllin induces downregulation of the insulin-like growth factor 1 receptor: potential mechanistic involvement of Mdm2 and beta-arrestin1. *Oncogene*. 2008;**27**(11):1629-38.

235. Wang W, Jobst MA, Bell B, Zhao CR, Shang LH, Jacobs DO. Cr supplementation decreases tyrosine phosphorylation of the CreaT in skeletal muscle during sepsis. *American Journal of Physiology Endocrinology and metabolism*. 2002;**282**(5):E1046-54.

236. Law RM, Stafford A, Quick MW. Functional regulation of gamma-aminobutyric acid transporters by direct tyrosine phosphorylation. *The Journal of Biological Chemistry*. 2000;**275**(31):23986-91.

237. Hers I, Tavare JM, Denton RM. The protein kinase C inhibitors bisindolylmaleimide I (GF 109203x) and IX (Ro 31-8220) are potent inhibitors of glycogen synthase kinase-3 activity. *FEBS Letters*. 1999;**460**(3):433-6.

238. Deldicque L, Theisen D, Bertrand L, Hespel P, Hue L, Francaux M. Creatine enhances differentiation of myogenic C2C12 cells by activating both p38 and Akt/PKB pathways. *American Journal of Physiology Cell Physiology*. 2007;**293**(4):C1263-71.

239. Wang QJ. PKD at the crossroads of DAG and PKC signaling. *Trends in Pharmacological Sciences*. 2006;**27**(6):317-23.

240. Fox TE, Young MM, Pedersen MM, Giambuzzi-Tussey S, Kester M, Gardner TW. Insulin signaling in retinal neurons is regulated within cholesterol-enriched membrane microdomains. *American Journal of Physiology Endocrinology and Metabolism*. 2011;**300**(3):E600-9.

241. West M, Park D, Dodd JR, Kistler J, Christie DL. Purification and characterization of the creatine transporter expressed at high levels in HEK293 cells. *Protein Expression and Purification*. 2005;**41**(2):393-401.

242. Bennett ER, Kanner BI. The membrane topology of GAT-1, a (Na^+ + Cl^-)-coupled gamma-aminobutyric acid transporter from rat brain. *The Journal of Biological Chemistry*. 1997;**272**(2):1203-10.

243. Melikian HE, McDonald JK, Gu H, Rudnick G, Moore KR, Blakely RD. Human norepinephrine transporter. Biosynthetic studies using a site-directed polyclonal antibody. *The Journal of Biological Chemistry*. 1994;**269**(16):12290-7.

244. Tate CG, Blakely RD. The effect of N-linked glycosylation on activity of the Na(+)- and Cl(-)-dependent serotonin transporter expressed using recombinant baculovirus in insect cells. *The Journal of Biological Chemistry*. 1994;**269**(42):26303-10.

245. Li LB, Chen N, Ramamoorthy S, Chi L, Cui XN, Wang LC, Reith ME. The role of *N*-glycosylation in function and surface trafficking of the human dopamine transporter. *The Journal of Biological Chemistry*. 2004;**279**(20):21012-20.

246. Peral MJ, Garcia-Delgado M, Calonge ML, Duran JM, De La Horra MC, Wallimann T, Speer O, Ilundain A. Human, rat and chicken small intestinal Na^+ - Cl^- -creatine transporter: functional, molecular characterization and localization. *The Journal of Physiology*. 2002;**545**(Pt 1):133-44.

247. Tarnopolsky M, Parise G, Fu MH, Brose A, Parshad A, Speer O, Wallimann T. Acute and moderate-term creatine monohydrate supplementation does not affect creatine transporter mRNA or protein content in either young or elderly humans. *Molecular and Cellular Biochemistry*. 2003;**244**(1-2):159-66.

248. Zhao CR, Shang L, Wang W, Jacobs DO. Myocellular creatine and creatine transporter serine phosphorylation after starvation. *The Journal of Surgical Research*. 2002;**105**(1):10-6.

249. Quick MW, Corey JL, Davidson N, Lester HA. Second messengers, trafficking-related proteins, and amino acid residues that contribute to the functional regulation of the rat brain GABA transporter GAT1. *The Journal of Neuroscience : the official journal of the Society for Neuroscience*. 1997;**17**(9):2967-79.

250. Beckman ML, Quick MW. Neurotransmitter transporters: regulators of function and functional regulation. *The Journal of Membrane Biology*. 1998;**164**(1):1-10.

251. Brewer JW, Hendershot LM, Sherr CJ, Diehl JA. Mammalian unfolded protein response inhibits cyclin D1 translation and cell-cycle progression. *Proceedings of the National Academy of Sciences of the United States of America*. 1999;**96**(15):8505-10.

252. Elbein AD. Inhibitors of the biosynthesis and processing of *N*-linked oligosaccharides. *CRC Critical Reviews in Biochemistry*. 1984;**16**(1):21-49.

253. Buckley BJ, Whorton AR. Tunicamycin increases intracellular calcium levels in bovine aortic endothelial cells. *The American Journal of Physiology*. 1997;**273**(4 Pt 1):C1298-305.

254. Reiland J, Ott VL, Lebakken CS, Yeaman C, McCarthy J, Rapraeger AC. Pervanadate activation of intracellular kinases leads to tyrosine phosphorylation and shedding of syndecan-1. *Biochem J*. 1996;**319 (Pt 1)**:39-47.

255. Imbert V, Peyron JF, Farahi Far D, Mari B, Auberger P, Rossi B. Induction of tyrosine phosphorylation and T-cell activation by vanadate peroxide, an inhibitor of protein tyrosine phosphatases. *Biochem J*. 1994;**297 (Pt 1)**:163-73.

256. Mikalsen SO, Kaalhus O. Properties of pervanadate and permolybdate. Connexin43, phosphatase inhibition, and thiol reactivity as model systems. *The Journal of Biological Chemistry*. 1998;**273**(16):10036-45.

257. Radian R, Bendahan A, Kanner BI. Purification and identification of the functional sodium- and chloride-coupled gamma-aminobutyric acid transport glycoprotein from rat brain. *The Journal of Biological Chemistry*. 1986;**261**(33):15437-41.

258. Burton LD, Kippenberger AG, Lingen B, Bruss M, Bonisch H, Christie DL. A variant of the bovine noradrenaline transporter reveals the importance of the C-terminal region for correct targeting to the membrane and functional expression. *Biochem J*. 1998;**330 (Pt 2)**:909-14.

259. Melikian HE, Ramamoorthy S, Tate CG, Blakely RD. Inability to *N*-glycosylate the human norepinephrine transporter reduces protein stability, surface trafficking, and transport activity but not ligand recognition. *Molecular Pharmacology*. 1996;**50**(2):266-76.

260. Nguyen TT, Amara SG. N-linked oligosaccharides are required for cell surface expression of the norepinephrine transporter but do not influence substrate or inhibitor recognition. *Journal of Neurochemistry*. 1996;**67**(2):645-55.

261. Wang W, Shang LH, Jacobs DO. Complement regulatory protein CD59 involves c-SRC related tyrosine phosphorylation of the creatine transporter in skeletal muscle during sepsis. *Surgery*. 2002;**132**(2):334-40.

262. Sitte HH, Farhan H, Javitch JA. Sodium-dependent neurotransmitter transporters: oligomerization as a determinant of transporter function and trafficking. *Molecular Interventions*. 2004;**4**(1):38-47.

263. Schmid JA, Scholze P, Kudlacek O, Freissmuth M, Singer EA, Sitte HH. Oligomerization of the human serotonin transporter and of the rat GABA transporter 1 visualized by fluorescence resonance energy transfer microscopy in living cells. *The Journal of Biological Chemistry*. 2001;**276**(6):3805-10.

264. Sorkina T, Doolen S, Galperin E, Zahniser NR, Sorkin A. Oligomerization of dopamine transporters visualized in living cells by fluorescence resonance energy transfer microscopy. *The Journal of Biological Chemistry*. 2003;**278**(30):28274-83.

265. Jiang J, Shrivastava IH, Watts SD, Bahar I, Amara SG. Large collective motions regulate the functional properties of glutamate transporter trimers. *Proceedings of the National Academy of Sciences of the United States of America*. 2011;**108**(37):15141-6.

266. Leimeister C, Externbrink A, Klamt B, Gessler M. Hey genes: a novel subfamily of hairy- and Enhancer of split related genes specifically expressed during mouse embryogenesis. *Mechanisms of Development*. 1999;**85**(1-2):173-7.

267. Niessen K, Karsan A. Notch signaling in cardiac development. *Circ Res*. 2008;**102**(10):1169-81.

268. Kanno K, Ishiura S. Differential effects of the HESR/HEY transcription factor family on dopamine transporter reporter gene expression via variable number of tandem repeats. *Journal of Neuroscience Research*. 2011;**89**(4):562-75.

269. Bernstein E, Caudy AA, Hammond SM, Hannon GJ. Role for a bidentate ribonuclease in the initiation step of RNA interference. *Nature*. 2001;**409**(6818):363-6.

270. Elbashir SM, Harborth J, Lendeckel W, Yalcin A, Weber K, Tuschl T. Duplexes of 21-nucleotide RNAs mediate RNA interference in cultured mammalian cells. *Nature*. 2001;**411**(6836):494-8.

271. Fischer A, Klattig J, Kneitz B, Diez H, Maier M, Holtmann B, Englert C, Gessler M. Hey basic helix-loop-helix transcription factors are repressors of GATA4 and GATA6 and restrict expression of the GATA target gene ANF in fetal hearts. *Mol Cell Biol*. 2005;**25**(20):8960-70.

272. Fischer A, Steidl C, Wagner TU, Lang E, Jakob PM, Friedl P, Knobeloch KP, Gessler M. Combined loss of Hey1 and HeyL causes congenital heart defects because of impaired epithelial to mesenchymal transition. *Circ Res*. 2007;**100**(6):856-63.

273. Cheneval D, Kastelic T, Fuerst P, Parker CN. A review of methods to monitor the modulation of mRNA stability: a novel approach to drug discovery and therapeutic intervention. *Journal of Biomolecular Screening*. 2010;**15**(6):609-22.

274. Fornes A, Nunez E, Alonso-Torres P, Aragon C, Lopez-Corcuera B. Trafficking properties and activity regulation of the neuronal glycine transporter GLYT2 by protein kinase C. *Biochem J*. 2008;**412**(3):495-506.

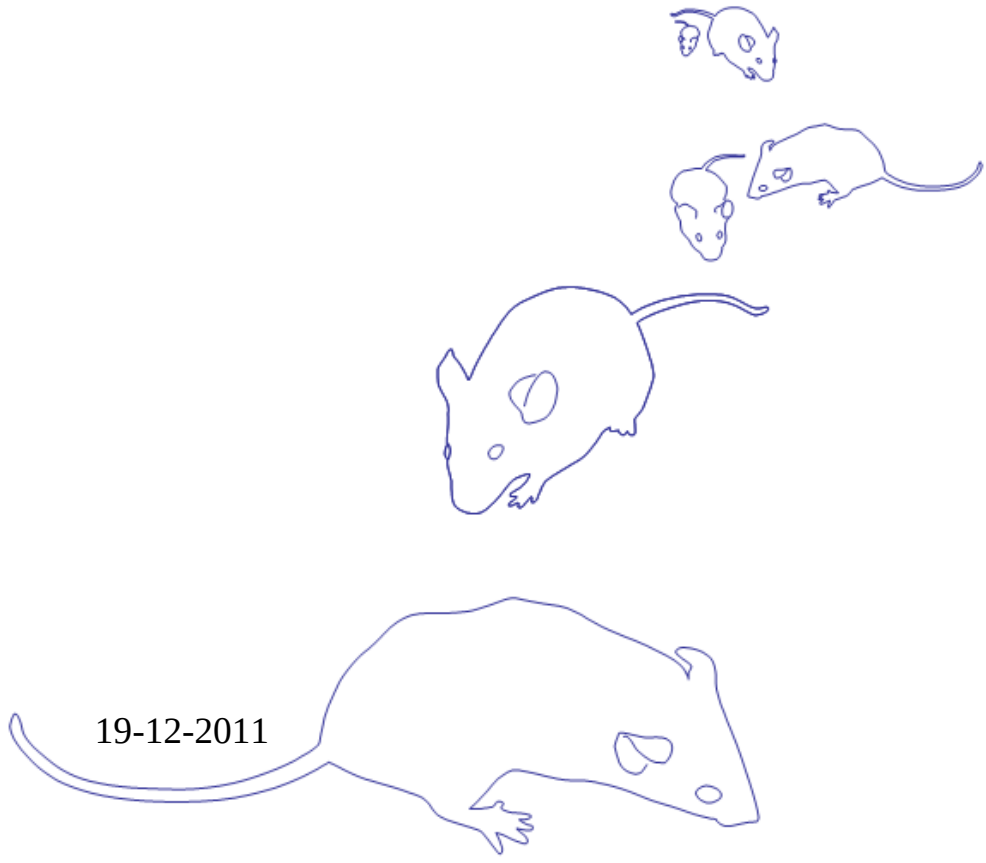
Appendix I

Documentation

A C G G G C T G A A A T G T T T T C A G T A A C A C A G T C T A A T G G C G G T C A G T A A C A

Generation of a transgenic mouse model expressing the CrT gene under the control of a tetracycline inducible promoter

Update of the previous report (12/05/2008)



Date: 19-12-2011

Summary

The transgenic construct pWTT1-CrT-HA, containing the tetracycline inducible pTIGHT promoter and a HA-tagged rabbit CrT (*Slc6a8*) cDNA cassette, flanked by two H19 insulators, was injected into the male pronucleus of fertilized oocytes. Following overnight cultivation, the surviving two-cell embryos were transplanted into pseudo-pregnant foster mothers. The resulting pups were genotyped and transgenic founder mice were identified using PCR.

Purification of the transgenic construct

The transgenic construct was isolated from the plasmid pWTT1-CrT-HA via PacI digestion (figure 1A). The ~7 kb fragment was isolated, purified, filtered using a micro-filtration unit (millipore) and diluted to a concentration of 5 ng/ µl in microinjection buffer (10 mM Tris-HCl pH 7.4, 1 mM EDTA). The construct purity and the concentration were verified by agarose gel electrophoresis (figure 1B).

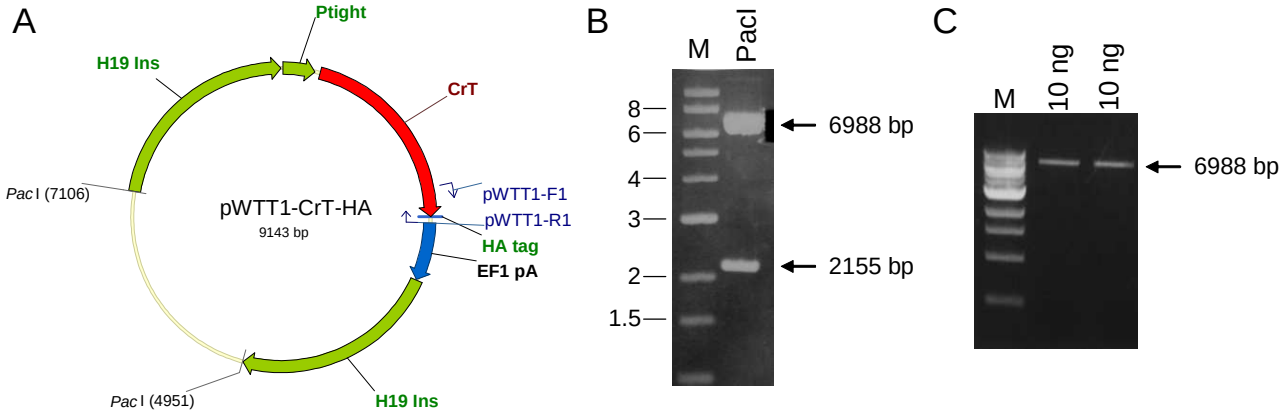


Fig. 1: (A) Plasmid map of the transgenic construct showing the presence of the pTIGHT promoter, the H19 insulators, the CrT cDNA, the HA tag and the EF1 poly adenylation signal. The primers used for genotyping are shown in blue. (B) PacI digest of pWTT1-CrT-HA. (C) 10 ng aliquot of the isolated transgenic construct. M: 1kb Ladder (NEB)

Establishing the screening PCR

To establish the PCR screening for the genotyping of the generated transgenic mice, two primers were designed amplifying a specific PCR product of 372 bp from the pWTT1-CrT-HA DNA (see fig. 2). The forward primer pWTT1-F1 binds specifically within the CrT cDNA and the reverse primer pWTT1-R1 binds within the 5'-end of the EF1 polyadenylation sequence. To confirm that the screening PCR is sufficiently sensitive at the level of genomic DNA, the transgenic vector DNA was serially diluted with wild-type genomic DNA. The primer sequences and the optimised PCR conditions are listed in table 1. Figure 2 shows the result of the sensitivity screen.

Table 1: PCR conditions of the Screening PCR

Name	Sequence
WTT1-F1	5'- CGT GTA CTA CAA GCC GCT GGT C -3'
WTT1-R1	5'- GGT GGC AGG TAT TAG GGA TAA TGC -3'

Reaction Mix		Reaction conditions			
(pWTT1-CrT-HA)	(0.01-10.0 pg)	**Step**	**Temp.**	**Time**	**Cycles**
genomic Mouse DNA	100.0 ng	Denaturing	94°C	300s	1x
Primers	10 pmol	Denaturing	94°C	60s	
dNTPs	0.16 mM	Annealing	65°C	60s	35x
Reaction Buffer	0.1 Vol	Extension	72°C	30s	
MgCl2	3 mM	Completion	72°C	420s	1x
Taq Polymerase (Immolase)	1.0 U		4°C	-	
Reaction Volume	20.0 µl				

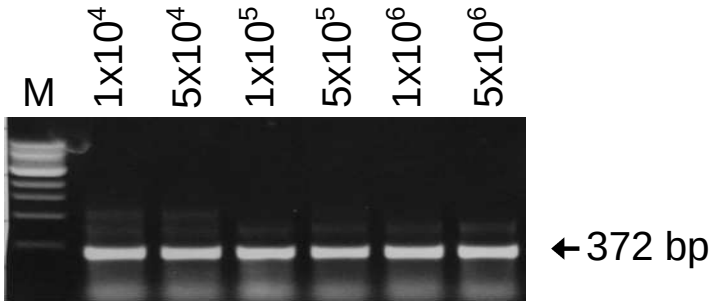


Fig. 2: Testing the sensitivity of the screening PCR. The optimised PCR screen was conducted using serial dilutions of the pWTT1-CrT-HA construct in genomic wild-type DNA (100 ng per reaction). Dilution factors are shown. PCR amplification of the transgenic DNA with the primer pair WTT1-F1 / WTT1-R1 yielded a ~ 372 bp product. M: 1 kb ladder (NEB)

The pWTT1-CrT-HA DNA was also still detectable at a dilution of 5 x 10^6 in 100 ng of genomic DNA, confirming the PCR screen is sufficiently sensitive to detect an integration event. The primers were also checked against wild-type genomic DNA which failed to yield an amplification product

Pronucleus microinjection

3 week old female FVB/NCrl mice were superovulated and mated with male FVB/NCrl mice. The resulting fertilized oocytes were collected from the oviduct of plugged female mice and cultured until two clear pronuclei were visible.

The purified transgenic construct was microinjected into the male pronucleus (figure 3) and injected embryos were cultivated overnight to the two-cell stage.

Two-cell embryos were then reimplanted into the oviduct of pseudopregnant CD1 foster mothers at 0.5 days post-coitum.

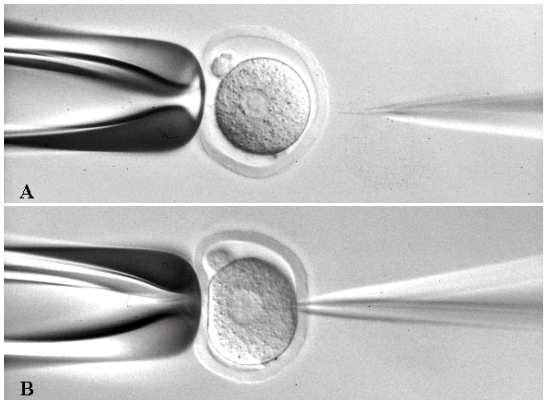


Fig. 3: (A) Oocyte before injection. The male pronucleus is clearly visible. (B) Oocyte after injection. The male pronucleus is clearly enlarged, demonstrating the successful injection.

Between 18 and 19 days later, pups were born from the foster mothers. Table 1 summarizes the DNA microinjections performed.

Table 1 and 2: Summary of the microinjections performed to date

Injection Date	Embryos transferred	Date of Birth	No. of Males	No. of Females	Total born
29.02.08	52	/	0	0	0
07.03.08	24	26.03.08	0	2	2
14.03.08	48	02.04.08	8	10	18
19.03.08	66	07.04.08	3	4	7
Total	190		11	16	27

Injection Date	Embryos transferred	Date of Birth	No. of Males	No. of Females	Total born
15.07.09	78	06.08.09	5	4	9
29.05.09	42	/	0	0	0
10.07.09	24	30.07.09	1	1	2
14.10.09	78	03.11.09	11	3	14
21.10.20	56	10.11.09	8	9	17
Total	278		25	17	42

Screening for transgenic founders

In total, 69 mice were born. Tail / ear biopsies from weaned pups were prepared and DNA was extracted using an E.Z.N.A DNA tissue extraction kit (Omega). The individual DNAs prepared from the tail biopsies were then genotyped by PCR using the primer pair shown in table 1. A specific 372 bp PCR product was obtained when the transgenic construct had integrated into the host genome. In addition, a second PCR was performed specific for a control DNA to ensure that the DNA prepared from the biopsy was of sufficient quality. Figure 4, shows an example of the screening methodology.

Figure 4 shows an example of the PCR screening.

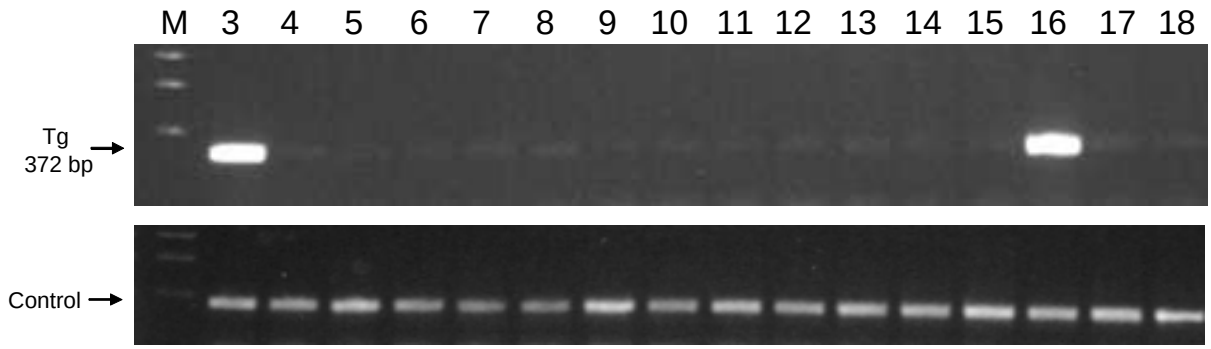


Fig. 4: Screening for founders. PCR with the primers WTT1-F1 and WTT1-R1 (transgene PCR) was performed with genomic DNA from the F0-generation (top panel). Control PCR was performed to confirm the integrity of the DNA sample (bottom panel) M: DNA-Ladder Mix (GeneRuler; MBI)

A total of 11 independent founders were identified and passed to the Neubauer group for further breeding and analysis

Appendix

Table 3: Summary table of the transgenic founders

FVB/NCrl-*Tg (H19-TRE-Slc6a8-H19)*				
ID No.	**Generation**	**Date of Birth**	**Sex**	**Genotype**
F0-3	F0, Founder	02.04.2008	♀	TG/+
F0-16	F0, Founder	02.04.2008	♂	TG/+
F0-722	F0, Founder	08.09.2009	♂	TG/+
F0-758	F0, Founder	03.11.2009	♂	TG/+
F0-760	F0, Founder	03.11.2009	♂	TG/+
F0-765	F0, Founder	03.11.2009	♀	TG/+
F0-769	F0, Founder	10.11.2009	♂	TG/+
F0-771	F0, Founder	10.11.2009	♀	TG/+
F0-773	F0, Founder	10.11.2009	♀	TG/+
F0-774	F0, Founder	10.11.2009	♂	TG/+
F0-784	F0, Founder	10.11.2009	♀	TG/+

Appendix II

PCR conditions for genotyping RCT, rtTA and ICT mice

Reaction Mix		**Reaction conditions**			
Genomic mouse DNA	100 ng/rxn	**Step**	**Temp**	**Time (min)**	**Cycles**
Primers	0.3 µM				
dNTPs	0.2 mM	Denaturing	96 °C	10:00	1x
10 x Reaction Buffer	0.1 Vol	Denaturing	94 °C	1:00	35x
$MgCl_2$	1.5 mM	Annealing	67 °C	1:00	
Taq Polymerase	1.0 U	Extension	72 °C	2.00	
Reaction Volume	20.0 µL	Completion	72 °C	10:00	1x

Real-time PCR conditions (SYBR green)

Reaction conditions			
Step	**Temp**	**Time (min)**	**Cycles**
Reverse transcription	50 °C	30:00	
Initial denaturation	95 °C	15:00	
Denaturation	95 °C	0:15	40x
Annealing	56 °C	0:20	
Extension	72 °C	0:20	
Completion	60 °C	0:15	
Melt	60 – 99 °C	0:05, +1 °C per cycle	x 30

Allelic discrimination of rtTA mice using qPCR

The protocol below, adapted from the Jackson Laboratory (USA) was used for determination of zygosity of rtTA mice, using the delta Ct method. Delta CT values of each sample are compared against known homozygous and heterozygous controls. Delta Ct is the difference between the ct value of the transgene and that of the endogenous control.

Reaction mix		**Reaction conditions**			
Genomic mouse DNA	10 µL	**Step**	**Temp**	**Time (min)**	**Cycles**
Primers	0.4 µM				

Probes	0.15 µM	AmpErase uracil-N-glycosylase (UNG) incubation	50 °C	2:00	1x
2 x Universal Master Mix*	10 µL				
Reaction volume	25.0 µL	Amplitaq Gold Activation	95 °C	10:00	
		Denaturing	95 °C	0:05	40x
		Annealing/ Extension	60 °C	1:00	

* is 2x Universal Master Mix- Taqman Universal PCR Master Mix, Catalogue #4304437 (Applied Biosystems, UK)

Primers designed against the CrT 5' UTR

Name	Transcript	Sequence
CrT pr F1	002	5'-GCG CGC AAG CTT CCC ATC ACA CTC CAT CTC GT-3'
CrT pr R1	002	5'-GCG CGC AGA TCT CAG TCC ACG AAG CAC TTG AA-3'
CrT pr F2	002	5'-GCG CGC AAG CTT GAG GTC GTG GGA GTC AGG TA-
CrT pr R2	002	5'-GCG CGC AGA TCT CAG TCA GAA GCA GTC CAC ACG A-3'
CrT pr F3	002	5'- GCG CGC AAG CTT GTG GCA GCC ATT CTG GAC-3'
CrT pr R3	002	5'- GCG CGC AGA TCT CAG TCC ACG AAG CAC TTG AA-3'
CrT pr F4	002	5'-GCG CGC AAG CTT CTC TGC TTT CTC TCC CTT CC-3'
CrT pr R4	002	5'- GCG CGC AGA TCT CAG TCA GAA GCA GTC CAC GA-3'
CrT pr R5	002	GCG CGC AGA TCT GGC CTCC GGC GGG CCG CAC GGC-3'
CrT pr R6	002	5'- GCG CGC AGA TCT TGA GCC TGA AGA ATC TCA TGT G-3'
CrT pr F7	002	5'- GCG CGC AAG CTT AGG GGC TGG TAG TGG GTG CA-3'
CrT pr R7	002	5'- GCG CGC AGA TCT GCG CAG TCA GAA GCA GTC CA-3'
CrT pr F8	002	5'- GCG CGC AAG CTT GGG GTC CAG ACC AGC TGG GG-3'
CrT pr R8	002	5'- GCG CGC AGA TCT GGC GGC GCA GTC AGA AGC AGT-3'
CrT pr F9	002	5'- GCG CGC AAG CTT GTG TGG GAA GGG GTG GCT GC -3'
CrT pr R9	002	5'- GCG CGC AGA TCT GCG GCG CAG TCA GAA GCA GT-3'
CrT tr 002 F1	002	5' GCGCGCAAGCTTCTGGAGAAGAGCCCAGTTCCAGGAG-3'
CrT tr 002 R1	002	5'- GCGCGCAGATCTTCTTGTAGCACAGGTAGGGGAAGCG-3'
CrT tr 002 F2	002	5'- GCGCGCAAGCTTGAGAAGAGCCCAGTTCCAGGAGGTC-3'
CrT tr 002 R2	002	5'- GCGCGCAGATCTTATAGATGCCGTTCTCGGCGCTCTT-3'
CrT tr 002 F3	002	5'- GCGCGCAAGCTTGGGGCTGGTCAGATTTGTGCTTCAG-3'
CrT tr 002 R3	002	5'- GCGCGCAGATCTCCACGCACGACATGATGAAGTCCAT-3'
CrT tr 002 F4	002	5'- GCGCGCAAGCTTCTTTGCCTTTGTTCCCCCAACTGCT-3'
CrT tr 002 R4	002	5'- GCGCGCAGATCT

		CCGGACACGCTATAGATGCCGTTCT-3’
CrT tr 005 F1	005	5’ GCGCGCAAGCTTGAGCCTACTTCACCGGGTCCTCTTC-3’
CrT tr 005 R1	005	5’-GCGCGCAGATCTCCCCAGTGCTGTTTTGTAGTCACAGG-3’
CrT tr 005 F2	005	5’-GCGCGCAAGCTTTCTTCCCTCTGTCCTGGGTCCTTGA-3’
CrT tr 005 R2	005	5’-GCGCGCAGATCTACCCCAGTGCTGTTTTGTAGTCACA-3’
CrT tr 005 F3	005	5’-GCGCGCAAGCTTTCTCAAAGGCAATGGGGTTTGCCTG-3’
CrT tr 005 R3	005	5’-GCGCGCAGATCTACCCCAGTGCTGTTTTGTAGTCACAG-3’
CrT tr 005 F4	005	5’-GCGCGCAAGCTTGCCTACTTCACCGGGTCCTCTTCTT-3’
CrT tr 005 R4	005	5’-GCGCGCAGATCTCCCAGTGCTGTTTTGTAGTCACAGG-3’

Solutions and media

Bacterial Media

L-agar

1 % (w/v) Bactotryptone,
0.5 % (w/v) Yeast Extract,
0.5 % (w/v) NaCl,
0.1 % (w/v) Glucose,
1.5 % Bactoagar

L-broth

1 % (w/v) Bactotryptone,
0.5 % (w/v) Yeast Extract,
0.5 % (w/v) NaCl,
0.1 % (w/v) Glucose

Antibiotic concentrations for bacterial & mammalian cell culture

The following concentrations used unless otherwise specified:
Ampicillin 100 µg/mL
Chloramphenicol 25 µg/mL
Doxycycline 100 µg/mL
Geneticin, G418 200 µg/mL
Penicillin 100 U/mL
Puromycin 2 µg/mL
Streptomycin 100 µg/mL

Ear-notch lysis buffer

100 mM EDTA
50 mM Tris HCl, pH 8
1 % SDS
200 mM NaCl

Tail lysis buffer

5 mM EDTA
100 mM Tris HCl, pH 8.5

0.5% Tween-20
200 mM NaCl

TE
10 mM Tris,
1 mM EDTA
pH 8.0

T0.1E
10 mM Tris,
0.1 mM EDTA
pH 8.0

50 X TAE
2.0 M Tris Acetate
100 mM Na_2EDTA

10 X TBE
0.89 M Tris Borate pH8.3
20 mM Na_2EDTA

1X Gel Loading Dye, Blue (6X):

2.5 % Ficoll 400

11 mM EDTA

3.3 mM Tris-HCl

0.017 % SDS

0.015 % Bromophenol Blue

pH 8.0 @ 25° C

2% Western blot extraction buffer

50 mM Tris pH 7.5

150 mM NaCl

2 % SDS

1 mM DTT

1 mM PMSF

1 x Protease Inhibitor Cocktail (Roche, Germany)

RIPA extraction buffer

0.1% SDS

0.5% deoxycholate

1% Triton-X

100 mM NaCl

1 mM EDTA

20 mM Tris HCl pH 7.5

Western blot loading (Laemmli) buffer (4 x)

0.25 M Tris HCl, pH 6.8

6 % SDS

40 % glycerol

20 % 2-mercaptoethanol

0.04 % Bromophenol blue

Tris-glycine SDS-Polyacrylamide gels (SDS-PAGE)

Pre-cast 12% SDS-PAGE were purchased from Thermo Scientific (UK) and used for all blots unless stated otherwise.

Western running buffer

(20X) MOPS/SDS running buffer:

1 M MOPS
1 M Tris, pH 7.7
69.3 mM SDS
20.5 mM EDTA

SDS transfer buffer
0.039 M Glycine
0.048 M Tris-base
0.0375 % SDS
20 % Methanol

Southern blotting solutions

Modified Gilbert & Church buffer
7 % SDS
0.5 M Phosphate buffer, pH 7.2 (Na_2HPO_4)
10 mM EDTA

20x SSC
3 M NaCl
0.3 M Sodium Citrate, pH 7.0

Low stringency wash buffer
2X SSC/0.1 % SDS

Medium stringency wash buffer
1X SSC/0.1 % SDS

High stringency wash buffer
0.5X SSC/0.1 % SDS